



**Assessing Floor Vibration Performance in Cross-Laminated Timber
(CLT) Flooring Systems: An Experimental Study across Various Test
Methods**

Yan GAO

A thesis submitted in partial fulfilment of the requirements for the degree of
Doctor of Philosophy

The University of Sheffield
Faculty of School of Architecture

April 2024

Abstract

This research examined the measurement, analysis, and computation of vibration characteristics in cross-laminated timber (CLT) floors. The serviceability performance of CLT floors under human-induced loads was evaluated according to four key standards (ISO 2631, BS 6841, BS 6472, and revised Eurocode5), using weighted acceleration to measure human response to vibration.

Experimental research was conducted on eight floors at three sites, the vibration performance of CLT floors was investigated using various test methods. Detailed technical descriptions of the test methods were provided under the guidance of two testing standards (ISO 18324 and BS EN 16929), addressing testing details not fully covered by the standards.

The effectiveness of three different testing methods—modal shaker, impact hammer, and heel drop—was compared. The results indicated that modal shaker testing yielded the highest accuracy in acquiring dynamic parameters, making it particularly suitable for assessing floor structures within the critical frequency range of 0-20 Hz. While the impact hammer method is also applicable within this frequency range, it is prone to interference from noise signals between 0-10 Hz, which can lead to misinterpretations of the structural parameters. The heel drop test, though the most straightforward and cost-effective approach, allows for quick identification of fundamental frequencies but may introduce significant errors in the estimation of damping parameters.

The experimental modal analysis (EMA) of the test data was performed using MATLAB, enabling the extraction of modal parameters of the tested structures, such as frequency, damping, and mode shapes. For CLT floors supported by glulam beams, the fundamental frequency ranged from 8 to 10 Hz, with damping between 1.5% and 3.5%. Steel-CLT composite floors exhibited a fundamental frequency between 8 to 12 Hz, with a recommended damping of 3% to 5%. CLT floors supported by CLT walls showed fundamental frequencies around 7 Hz, with a higher damping ratio of around 7%. Furthermore, relatively simple and effective beam-slab-column finite element models were established using ANSYS for preliminary analysis, allowing for further validation of the experimental data through frequency and mode shape comparisons.

Acknowledgements

I would like to express my sincere gratitude to my supervisor, Dr. Wen-shao Chang, for his valuable advice, insightful discussions, interest, and unwavering encouragement throughout this project. I would also like to extend my thanks to Dr. Jim Uttley from the department, whose patient and meticulous guidance greatly supported me throughout my doctoral journey.

I am also thankful to my past and present colleagues in architecture and landscape for their enthusiasm, support, and for fostering such an enjoyable working environment.

I owe special gratitude to my friend Liwen Zhang for the mutual support we provided each other throughout our Ph.D. journey. Thanks to Yi Yang, Deniz Kesici and Esti A Nurdiah for their timely assistance during crucial moments. A special note of appreciation goes to Chunyi Wu for her unwavering patience, guidance, and support. I am privileged to have had the support of such remarkable colleagues throughout my Ph.D. experience.

I am deeply grateful to the China Scholarship Council and University of Sheffield for the financial support that made my PhD studies possible.

Finally, I extend my heartfelt thanks to my family—my mother, father, grandmother, and brother—for their love, patience, and support, particularly during the final stages of this work. Their encouragement has been invaluable in completing this thesis.

Table of Contents

Abstract	ii
Acknowledgements.....	iii
Table of Contents	iv
List of Tables	vii
List of Figures	viii
1. Introduction.....	1
1.1 Background	1
1.2 The Research Problem.....	1
1.3 Scope of Research	2
1.4 Thesis Outline	3
2. Literature Review	4
2.1 Timber Flooring Systems	4
2.1.1 Timber as the Future of Construction	4
2.1.2 Cross Laminated Timber (CLT).....	7
2.1.3 CLT Floor and Hybrid CLT Floor	9
2.1.3.1 CLT Floor.....	9
2.1.3.2 CLT-concrete Floor.....	11
2.1.3.3 Steel-CLT Floor.....	12
2.1.4 Dynamic Properties of CLT Floors	13
2.2 Human Induced Vibration Issues	16
2.2.1 Floor Vibration due to Human Activity.....	16
2.2.2 Source of Vibration: Human Activities	17
2.2.2.1 Walking and Running Pattern.....	18
2.2.2.2 Load Models for Walking and Running.....	19
2.2.2.3 Deterministic Load Model, Probabilistic Load Model and Group Effect	22
2.2.3 Transmission Path: Floor Properties	24
2.2.3.1 Transient and Steady-state vibration	24
2.2.3.2 High Frequency Floor and Low Frequency Floors.....	25
2.2.4 Receivers: Floor and Human Response	26
2.2.4.1. Floor structures as vibration receiver.....	26
2.2.4.2. Human Occupants as vibration receiver.....	27
2.3 Serviceability Criteria	29
2.3.1 Serviceability and Codification	29
2.3.2 Design Code and Evaluation Standards.....	29
2.3.3 ‘Good Code’	30
2.3.4 Design Code for Timber.....	31
2.3.4.1 Current Eurocode 5 (EC5): Design of Timber Structures	31
2.3.4.2 Revised Eurocode 5 (rEC5) Draft	33
2.3.5 Evaluation Standards for Timber.....	35
2.3.5.1 International Standard 2631: Evaluation of human exposure to whole-body vibration (1-80 Hz)	35
2.3.5.2 BS 6841 (1987): Measurement and evaluation of human exposure to whole-body mechanical vibration and repeated shock (0.5 to 80 Hz).....	37
2.3.5.3 BS 6472 (2008): Guide to the evaluation of human exposure to vibration in buildings (0.5 to 80 Hz)....	40
2.4 Floor Vibration Experimental Testing and Finite Element Modeling.....	42

2.5 Summary	44
3. Floor Testing Methods and Experimental Modal Analysis	47
3.1 Standards for Timber Floor Test Methods	47
3.1.1 ISO 18324 (2016): Timber structures - Test methods - Floor vibration performance.....	47
3.1.2 BS EN 16929(2018): Test methods - Timber floors -Determination of vibration properties	48
3.2. Experimental modal testing	49
3.2.1 The Role of Modal Testing in Experimental Investigation.....	49
3.2.2 Modal Testing Theory.....	50
3.3. Measurement of vibration	51
3.3.1 Modal testing Using Modal Shaker	51
3.3.2 Modal Testing Using Impact Hammer	53
3.3.3 Heel Drop Test.....	55
3.3.4 Walking and Running Test.....	57
3.4. Model Analysis Process in MATLAB	59
3.4.1 FRF Data	59
3.4.2 Preliminary Check of FRF Data	60
3.4.3 Pre-processing of time streamed data in MATLAB	61
3.4.4 Modal Parameter Extraction (Curve-fitting) Methods	62
3.4.4.1 Non-Linear Least-Squares (NLLS) Method.....	62
3.4.4.2 Complex Exponential (CE) Method.....	64
3.4.5 Modal Parameter Extraction from FRF in MATLAB	65
4. Experimental Work	69
4.1. Introduction to the Experimental Work	69
4.2. Description of the Testing CLT Floors	70
4.2.1 Site 1.....	70
4.2.2 Site 2.....	71
4.2.3 Site 3.....	72
4.3. Test Grid and Test point	73
4.4 Test Results	77
4.4.1 Input Signal Analysis.....	77
4.4.1.1 Site 1.....	77
4.4.1.2 Site 2.....	79
4.4.1.3 Site 3.....	80
4.4.2 FRF Results of Frequency and Damping	81
4.4.2.1 Site 1.....	81
4.4.2.2 Site 2.....	83
4.4.2.3 Site 3.....	85
4.4.3 Heel drop results of frequency and damping.....	88
4.4.3.1 Site 1.....	89
4.4.3.2 Site 2.....	90
4.4.3.3 Site 3.....	91
4.4.4 Mode Shape and Modal Assurance Criteria (MAC) value	95
4.4.4.1 Site 1.....	96
4.4.4.2 Site 2.....	98
4.4.4.3 Site 3.....	100
4.5 Acceleration and R-factor	102
4.6 Summary of the Comparison between Sites and Various Test Methods	105
4.6.1 Investigated Buildings	105
4.6.2 Experiments	106

4.6.2.1 The location of the exciter and sensors.....	106
4.6.2.2 The input signal of the field test.....	107
4.6.2.3 The analysis method.....	110
4.6.3 Experimental Results and Conclusions.....	111
4.6.3.1 The natural frequency and damping ratio of Site 1.....	111
4.6.3.2 The natural frequency and damping ratio of Site 2.....	113
4.6.3.3 The natural frequency and damping ratio of Site 3- 3rd Floor and CLT Extension.....	114
4.6.4 Conclusions and Recommendations	118
5. Computational work.....	121
5.1 Introduction to the Computational Work	121
5.1.1 Mode Participation Factor and Effective Mass in ANSYS	121
5.1.2 Bonded Contact in ANSYS	121
5.2 Floor models of Site 1.....	122
5.2.1 Model 1- Small Floor	122
5.2.2 Modal 2- Large Floor	125
5.3 Floor models of Site 2.....	128
5.3.1 Model 3- Small Floor	129
5.3.2 Model 4- Large Floor	132
5.4 Floor Models of Site 3.....	134
5.4.1 Model 5- Area 1 and Area 2	134
5.4.2 Model 6, Model 7 and Model 8- CLT Extensions.....	137
5.5 Comparison between the Experimental and Computational Results.....	143
5.5.1 Site 1- Small Floor and Large Floor.....	143
5.5.3 Site 2-Small Floor and Large Floor.....	145
5.5.4 Site 3- Area 1, Area 2 and CLT Extensions	147
5.6 Summary of Conclusions from FE Analysis	150
6. Conclusions and Related Further Work	153
6.1 Conclusions	153
6.1.1 Field Test Results of CLT Flooring Systems.....	154
6.1.2 Guidelines and Standards Check Results.....	155
6.1.3 Different Test Methods for Measuring Design Parameters	155
6.1.4 Post-processing in MATLAB.....	157
6.2 Recommendations for Future Research	157
References	159

List of Tables

Table 2. 1: Mass, Frequency and Damping of CLT Compared to Other Floor Material (Hu, 2013)	10
Table 2. 2: Frequency Ranges of Human Activities	18
Table 2. 3: Single Pedestrian Vertical Walking/Running Load Models Proposed by Different Authors	20
Table 2. 4: Cut-off Frequency between Low- and High-frequency Floors by Different Researchers	25
Table 3. 1: Heel Drop Test Used by Different Researchers	57
Table 3. 2: Important Commands and Explanations for Modal Identification in MATLAB	67
Table 4. 1: Summary of the Testing Floors	70
Table 4. 2: Modal Identification Results of Site 1	83
Table 4. 3: Modal Identification Results of Site 2	85
Table 4. 4: Modal Identification Results of Area 1 and Area 2 (Site3)	86
Table 4. 5: Modal Identification Results of Extension Area (Site 3)	87
Table 4. 6: Comparison between Heel Drop Results on Site 1	89
Table 4. 7: Comparison between Heel Drop Results on Site 2	90
Table 4. 8: Comparison between Heel-drop 1-9 on Area 1 and Area 2 (Site 3)	93
Table 4. 9: Comparison between Heel-drops on the 1st, 2nd and 3rd CLT Extension Floor (Site 3)	95
Table 4. 10: The RMS Acceleration and R-factor Results from Walking and Running	103
Table 4. 11: Comparison between Heel Drop and Modal Shaker Results on Site 1	112
Table 4. 12: Comparison between Heel drop and Modal shaker Results on Site 2	114
Table 4. 13: Comparison between Heel Drop and Modal Shaker Results on Site 3 (Area 1 and Area 2)	115
Table 4. 14: Comparison between Heel Drop and Modal Shaker Results on Site 3- Extension	117
Table 5. 1: The Material Properties of the CLT and Glulam (Site 1)	124
Table 5. 2: Frequency and Mass Participation (Site 1: Small Floor)	125
Table 5. 3: Frequency and Mass Participation (Site 1: Large Floor)	126
Table 5. 4: The Material Properties of the CLT and Glulam (Site 2)	129
Table 5. 5: Frequency and Mass Participation (Site 2: Small Floor)	131
Table 5. 6: Frequency and Mass Participation (Site 2: Large Floor)	133
Table 5. 7: The Material Properties of the Model 5-8 (Site 3)	134
Table 5. 8: Frequency and Mass Participation of model 5 (Site 3)	136
Table 5. 9: Frequency and Mass Participation of Model 6 (Site 3)	140
Table 5. 10: Frequency and mass participation of model 7 (Site 3)	140
Table 5. 11: Frequency and Mass Participation of Model 8 (Site 3)	142
Table 5. 12: Comparison of Frequencies between Measurements and FE Results of Model 1	144
Table 5. 13: Comparison of Frequencies between Measurements and FE Results of Model 2	144
Table 5. 14: Comparison of Frequencies between Measurements and FE Results of Model 3	146
Table 5. 15: Comparison of Frequencies between Measurements and FE Results of Model 4	147
Table 5. 16: Comparison between Measurements and FE Results of Site 3- Area 1	147
Table 5. 17: Comparison of Frequencies between Measurements and FE Results of Site 3-Area 2	148
Table 5. 18: Comparison between Measurements and FE Results of Site 3 - CLT Extensions	149

List of Figures

Figure 2. 1: Number of Publications per Year on Timber Floor Vibration from Scopus (Total: 226)	5
Figure 2. 2: Pie Chart of Floor Types in 226 Selected Documents	6
Figure 2. 3: Results of Literature Analysis: Number of Documents Published per Year on Floor vibration Research.....	6
Figure 2. 4: CLT Panel (TRADA Website)	7
Figure 2. 5: TRADA CLT Properties (TRADA Sheet 61, 2009).....	8
Figure 2. 6: Location of the Majority of CLT Producers (https://www.timber-online.net).....	9
Figure 2. 7: Murray Grove, the ‘Pure CLT’ Building in London.....	10
Figure 2. 8: CLT Floor System and Conventional Joisted Floor System.....	10
Figure 2. 9: Typical TCC Flooring System (Dackermann et al., 2016).....	11
Figure 2. 10: Types of Shear Connectors (Setragian and Chandra, 2018).....	12
Figure 2. 11: Steel-CLT Hybrid Floor	12
Figure 2. 12: Steel-CLT Connection	12
Figure 2. 13: Factors Affecting the Acceptability of Building Vibration	16
Figure 2. 14: Comparison of the Phases of the Walking and Running Cycles.....	19
Figure 2. 15: A Portion of a Continuously Measured Ground Reaction Force (GRF) due to Walking (Racic and Brownjohn, 2011)	19
Figure 2. 16: Simulated Walking Load Time Histories of 8 Different Models at $f_p=2.0$ Hz.....	21
Figure 2. 17: Load Models Comparison: (A) Simulated Walking Load Time Histories of Four Different Models at $f_p = 2.0$ Hz; (B) Simulated Running Load Time Histories of Three Different Models at $f_p = 2.0$ Hz	22
Figure 2. 18: DLF for the First Harmonic of the Walking Force as a Function of Number of People and Walking Frequency (Ebrahimpour et al., 1996)	23
Figure 2. 19: Floor Characteristics: (a) Series of Transient Vibrations Due to Impacts on A “Stiffer” Floor, (b) Steady-State Solution Due to Continuous Excitation Force on A “Softer” Floor	24
Figure 2. 20: Acceleration Compared to Acceptability (Toratti and Talja, 2006).....	28
Figure 2. 21: Floor Vibration and the Frequency Range of the Body’s Internal Organs	28
Figure 2. 22: Statistical Model for a Design Code (Leicester, 1993)	30
Figure 2. 23: Illustration of the Design Process for Timber Floors according to EC5 (Schirén and Swahn, 2019)	32
Figure 2. 24: Floor Vibration Criteria according to the Floor Performance Level in rEC5.....	33
Figure 2. 25: Illustration of the Design Process for Timber Floors according to the rEC5 Draft (Schirén and Swahn, 2019)	35
Figure 2. 26: Frequency Weighting w_k	36
Figure 2. 27: Multiplying Factors for ‘Base Curve’ with Respect to Human Response (ISO 10137:2007)	37
Figure 2. 28: Building Vibration Z-axis ‘Base Curve’ for Vibration (Foot-to-head Vibration Direction)	37
Figure 2. 29: Basicentric Axes of the Human Body	39
Figure 2. 30: Moduli of the Frequency Weightings with Band-limiting Filters	39
Figure 2. 31: Root-mean-square Acceleration Magnitudes Corresponding to Vibration Dose Values from $1.9 \text{ m}\cdot\text{s}^{-1.75}$ to $60 \text{ m}\cdot\text{s}^{-1.75}$ for Vibration Exposure Periods from 1 s to 24 h	40
Figure 2. 32: Frequency Weighting Curve for Vertical Vibration and Horizontal Vibration.....	41
Figure 2. 33: VDV Ranges which Might Result in Various Probabilities of Adverse Comment within Residential Buildings (BS 6472-1, 2008)	42
Figure 2. 34: Proportion of Researcher Methods in Timber Vibration	42
Figure 3. 1: Single-degree-of-freedom (SDOF) System	50
Figure 3. 2: Transfer Function Block Diagram.....	51
Figure 3. 3: Modal Shaking System and Accelerometers Used.....	52
Figure 3. 4: Laptops for Data Monitoring	52
Figure 3. 5: Shaker Testing Setup.....	53
Figure 3. 6: Roving Sensor Test Method	53
Figure 3. 7: Impact Hammer Used in Testing.....	54
Figure 3. 8: Typical Impact Force Pulse and Spectrum	54
Figure 3. 9: Force Spectrum of Different Hammer Tips.....	55
Figure 3. 10: Hammer Test Setup	55
Figure 3. 11: Heel Drop Test	56
Figure 3. 12: Acceleration Response and Spectrum of Heel-Drop Test.....	57

Figure 3. 13: Acceleration Response and Spectrum of Walking at 1.5 Hz	58
Figure 3. 14: Acceleration Response and Spectrum of Walking at 2.0 Hz	58
Figure 3. 15: Acceleration Response and Spectrum of Running at 2.89 Hz	58
Figure 3. 16: Bode plot of FRFs	59
Figure 3. 17: Schematic Overview of FRF from Time Streamed Data	60
Figure 3. 18: A Good FRF Measurement and a Bad FRF Measurement.....	61
Figure 3. 19: Data Pre-processing in MATLAB	61
Figure 3. 20: Experimental Time Streamed Data of Output and Input: (a) Raw data (b) Averaged data	62
Figure 3. 21: Fit between Data and Model using NLLS Method	63
Figure 3. 22: Fitted Time History using CE Method	65
Figure 3. 23: Curve-fitting Diagram for the FRFs from the State-Space Model	66
Figure 3. 24: Roadmap of Modal Identification in MATLAB	66
Figure 3. 25: Stability Diagram for the FRFs from the State-Space Model	67
Figure 4. 1: The Roadmap of Chapter 4	69
Figure 4. 2: Modal Testing on the Bare CLT Floors at Site 1	71
Figure 4. 3: Raised Access Flooring System: Support System and Removable Panels.....	71
Figure 4. 4: Modal Testing on the Raised Access CLT Floors at Site 2.....	72
Figure 4. 5: Modal Testing on the Raised Access CLT Floors at Site 3.....	72
Figure 4. 6: Impact Hammer Testing on Side Extension Raised Access CLT Floors at Site 3.....	73
Figure 4. 7: The Boundary Conditions and Elevation of the Side Extension CLT Floors.....	73
Figure 4. 8: The Location of the Reference Point, Test Points and Modal Testing Order on Small Floor (Site 1).....	74
Figure 4. 9: The Location of the Reference Point, Test Points and Modal Testing Order on Large Floor (Site 1).....	74
Figure 4. 10: The Location of the Reference Point, Test Points and Modal Testing Order on Small Floor (Site 2).....	75
Figure 4. 11: The Location of the Reference Point, Test Points and Modal Testing Order on Large Floor (Site 2)	75
Figure 4. 12: The Location of the Reference Point, Test Points and Modal Testing Order on Area 1 (Site 3)	76
Figure 4. 13: The Location of the Reference Point, Test Points and Modal Testing Order on Area 2 (Site 3)	76
Figure 4. 14: Impact hammer test on Site 3: the location of the reference point, test points and modal testing order ...	77
Figure 4. 15: Time History Data and Frequency Domain Data of Shaker Test at Site 1: (a) Small Floor; (b) Small Bare Floor; (c) Large Bare Floor	78
Figure 4. 16: Coherence Function from Shaker Test at Site 1: (a) Small Floor; (b) Small Bare Floor; (c) Large Bare Floor.	79
Figure 4. 17: Time History Data and Frequency Domain Data of Shaker Test at Site 2: (a) Small Floor; (b) Large Floor....	79
Figure 4. 18: Coherence Function from Shaker Test at Site 2: (a) Small Floor; (b) Large Bare Floor	80
Figure 4. 19: Time History Data and Frequency Domain Data of Shaker Test at Site 3: Area 1 and Area 2	80
Figure 4. 20: Coherence Function from Shaker Test at Site 3: (a) Area 1; (b) Area 2	81
Figure 4. 21: Curve fitted FRF and Stabilization Diagram of Small Bare Floor (Site 1).....	82
Figure 4. 22: Curve fitted FRF and Stabilization Diagram of Small Raised Access Floor (Site 1)	82
Figure 4. 23: Curve fitted FRF and Stabilization Diagram of Large Bare Floor (Site 1).....	83
Figure 4. 24: Curve fitted FRF and Stabilization Diagram of Small Raised Access Floor (Site 2)	84
Figure 4. 25: Curve fitted FRF and Stabilization Diagram of Large Raised Access Floor (Site 2)	84
Figure 4. 26: Curve fitted FRF and Stabilization Diagram of Area 1 (Site 3).....	86
Figure 4. 27: Curve fitted FRF and Stabilization Diagram of Area 2 (Site 3).....	86
Figure 4. 28: Curve fitted FRF and Stabilization Diagrams of the Side Extension-1st CLT Floor	88
Figure 4. 29: Curve fitted FRF and Stabilization Diagrams of the Side Extension-2nd CLT Floor.....	88
Figure 4. 30: Curve fitted FRF and Diagrams of the Side Extension-3rd CLT Floor	88
Figure 4. 31: FFT results of Heel-drop Test on Site 1	89
Figure 4. 32: FFT results of Heel Drop Test on the Small floor (Site 2)	90
Figure 4. 33: FFT results of Heel Drop Test on the Large floor (Site 2)	90
Figure 4. 34: Heel Drop Area on Site 3.....	91
Figure 4. 35: FFT Results of Heel-drop 1-9 on HTS floors (Site 3)	92
Figure 4. 36: FFT Results of Heel-drops on the 1st, 2nd and 3rd CLT Extension Floor (Site 3)	94
Figure 4. 37: Mode shapes of Small Bare floor and Small Raised Floor of Site 1.....	96
Figure 4. 38: Mode shapes of Large Bare Floor of Site 1	97
Figure 4. 39: MAC Values of Site 1: Small Bare floor and Small Raised Floor	97
Figure 4. 40: MAC Values of Site 1: Large Bare Floor.....	98
Figure 4. 41: Mode Shape and MAC Values of Small Floor (Site 2)	99

Figure 4. 42: Mode Shape and MAC Values of Large Floor (Site 2)	99
Figure 4. 43: Mode Shape and MAC Values of Area 1 (Site 3)	100
Figure 4. 44: Mode Shape and MAC Values of Area 2 (Site 3)	101
Figure 4. 45: Mode Shape and MAC Values of 1st CLT Extension (Site 3)	101
Figure 4. 46: Mode Shape and MAC Values of 2nd CLT Extension (Site 3)	102
Figure 4. 47: Mode Shape and MAC Values of 3rd CLT Extension (Site 3)	102
Figure 4. 48: Acceleration Compared with Criteria Response Factor R Recommended in Revised Eurocode 5	104
Figure 4. 49: The Layout of the Eight Tested Floors	105
Figure 4. 50: The Test Grid and Location of the Sensors and Exciter	107
Figure 4. 51: Output and Input Time History Data from the Field Test	108
Figure 4. 52: The Tested 6m×6m Floor and the Frequency Response	109
Figure 4. 53: The tested 6m×6m floor and Coherence Function	110
Figure 4. 54: Performing a Heel Drop Test on the Load Cell and the Coherence Determined by Instrumented Heel Drop Test (Blakeborough and Williams, 2003)	110
Figure 4. 55: The Fit between FRF Data and Refined Model of the Large Floor on Site 2	111
Figure 4. 56: CE Method in Time Domain for Identification	111
Figure 4. 57: Illustrated Frequency and Damping Data of Table 1	113
Figure 4. 58: Illustrated Frequency and Damping Data of Table 4.12	114
Figure 4. 59: Illustrated Frequency and Damping Data of Table 4.13	116
Figure 4. 60: Illustrated Frequency and Damping Data of Table 4.14	118
Figure 5. 1: Bonded Contact	122
Figure 5. 2: Test Areas and CLT Panel Material (Site 1)	123
Figure 5. 3: Support conditions of floors (Site 1)	123
Figure 5. 4: Model Settings of the Small Floor (Site 1)	124
Figure 5. 5: Comparison between mode shapes of the Small Floor built in 3 models (Site 1)	125
Figure 5. 6 Model Settings of the Large Floor (Site 1)	126
Figure 5. 7: The Mode Shape of the One and Half Bay Model	127
Figure 5. 8: The Mode Shape of the Two Bay Model	128
Figure 5. 9: Site 2 Test Areas and CLT Panel Material	128
Figure 5. 10: Support Conditions of Floors (Site 2)	129
Figure 5. 11: Model Settings of the Small Floor (Site 2)	130
Figure 5. 12: Model Settings of the Small Floor (Site 2)	131
Figure 5. 13: Model Settings of the Small Floor (Site 2)	132
Figure 5. 14: Model Settings of the Small Floor (Site 2)	133
Figure 5. 15: Support Conditions of Floors (Site 3)	134
Figure 5. 16: The Partitioning of the Test Area on the Third Floor of Site 3	135
Figure 5. 17: Model Settings of Area 1 and Area 2 (Site 3)	135
Figure 5. 18: Mode Shape of Model 5 (Site 3)	137
Figure 5. 19: Test Areas of Extension CLT Floors (Site 3)	138
Figure 5. 20: Support Conditions of Extension CLT Floors (Site 3)	138
Figure 5. 21: Model Settings of CLT Extensions (Site 3)	139
Figure 5. 22: Mode Shapes from Model 6 (Site 3)	140
Figure 5. 23: Mode Shapes from Model 7 (Site 3)	141
Figure 5. 24: Mode Shapes from Model 8 (Site 3)	143
Figure 5. 25: Small Floor (Site 1) - Comparison of the Mode Shapes between Measurements and FE Results of Model 1	144
Figure 5. 26: Large Floor (Site 1) - Comparison of the Mode Shapes between Measurements and FE Results of Model 2	145
Figure 5. 27: Small Floor (Site 2) - Comparison of the Mode Shapes between Measurements and FE Results of Model 3	146
Figure 5. 28: Large Floor (Site 2) - Comparison of the Mode Shapes Measurements and FE Results of Model 4	147
Figure 5. 29: Area 1 (Site 3) - Comparison of the Mode Shapes between the FE Model and Measurement	148
Figure 5. 30: Area 2 (Site 3) - Comparison of the Mode Shapes between the FE Model and Measurement	149
Figure 5. 31: CLT Extensions (Site 3) - Comparison of the Mode Shapes between the FE Model and c Measurement ...	150

1. Introduction

1.1 Background

Cross-Laminated Timber (CLT), an environmentally friendly material, addresses the limitations of conventional wood in terms of lightweight and high strength when used as a floor structure. As a result, CLT is widely used in Europe today in various buildings, such as open-plan offices and structures with steel or reinforced concrete (RC) frameworks. Modern building trends toward open-plan designs with longer spans have reduced the mass, stiffness, and damping of floor structures (Ussher et al., 2017). This reduction has increased the likelihood of resonance between the natural frequencies of the floors and human activities, prompting extensive research into floor vibration discomfort.

Researchers have extensively studied floor vibrational behavior, proposing design parameters that assess vibration performance. These evaluations include simplified calculations, laboratory studies, field studies, and finite element methods. Among these, researchers often prioritize experimental investigations over simulations due to their ability to generate intricate data analyses and the availability of necessary funding and testing equipment. Consequently, many design codes are derived from experimental studies.

Research into the vibrational behavior of CLT floors, and timber structures in general, builds on the knowledge established for concrete and steel structures. However, further refinement is needed to adapt the standards borrowed from these materials to fit the unique properties of CLT. There is a growing need for comprehensive guidance on measuring and assessing floor vibrations in buildings. Standardizing design methodologies and testing procedures, including the instruments used, is essential for comparing results across studies. Without consistent measurement procedures, the current standardized ratings for acceptable vibration levels and associated multiplying factors remain inadequate for practical application.

1.2 The Research Problem

The study of vibration in Cross-Laminated Timber (CLT) floors holds significant potential, but current research is limited in scope, particularly in standardizing methods for assessing human-induced vibrations. A key debate among researchers revolves around the use of the Response-factor, a measure of vibration severity, versus the Vibration Dose Value (VDV) method, which assesses the cumulative impact of vibration on human comfort. Additionally, the current Eurocode 5 falls short of

adequately addressing the design requirements for CLT flooring, and the feasibility of the revised version of Eurocode 5 still requires verification through real-world applications and feedback from engineers and researchers.

Existing test standards for timber floors, such as BS EN 16929 and ISO 18324, provide parameters to assess floor vibration performance, including frequency, damping, deflection, and acceleration. Although only four parameters are typically considered, various studies (e.g., Ohlsson, 1982; Smith and Chui, 1988; H et al., 2001) have proposed a wide range of suggested values. Researchers often employ different testing methods and select varying measurement parameters, resulting in a lack of repeatability and transparency in published studies. Moreover, design codes face similar challenges. For example, Eurocode 5 has been criticized for its use of velocity under unit impulse (1 Ns), which some professionals argue that this parameter is difficult to apply in practice.

Upon examining the standards that govern floor vibration design, it becomes evident that differences in controlled parameters often stem from variations in both laboratory and field test methods. These discrepancies can be attributed to two primary factors: the type of testing equipment used and the analysis methods applied to process the raw test data. ‘Clean’ test floor is rare and most testing in the literature were doubt for the test quality, as they often lack critical details regarding the testing and analysis processes.

1.3 Scope of Research

The purpose of this study is to investigate the vibration behavior of Cross-Laminated Timber (CLT) floor systems in office buildings. To achieve this, field tests are expected to be conducted on relatively "clean" CLT floor slabs—those free from occupants, building materials, and office furniture. The dynamic properties of the floors are obtained through high-quality on-site modal measurements, processed using a self-developed, fully transparent, non-commercial modal analysis program. The primary goals of this research are as follows:

- Develop a system to ensure efficient on-site data collection. This includes creating MATLAB signal processing and analysis programs specifically for Single-Input Multiple-Output (SIMO) test purposes. Build finite element models of the tested floors for modal analysis.
- Conduct experimental dynamic testing of in-situ multi-bay Cross-laminated timber (CLT) office floors using an electrodynamic shaker, process the testing data using MATLAB programs to determine dynamic characteristics such as frequency, damping, and modal shapes. Perform walking and running tests to observe the response of CLT floors under

human-induced loads and evaluate their vibration performance according to relevant standards.

- Identify and summarize the best practices in dynamic testing of in-situ floor systems, including insights on equipment, experimental techniques, and measurement analysis. Evaluate the test quality of dynamic properties in CLT floors using various testing methods. Provide recommendations on the appropriate selection of testing methods according to specific requirements.

1.4 Thesis Outline

Chapter 2 provides a comprehensive literature review on CLT flooring systems and their structural dynamic properties, emphasizing the pressing need for research in this area, particularly concerning human-induced vibrations. It examines floor vibrations from three perspectives: sources, transmission, and receivers. The chapter also discusses mainstream timber floor design and vibration serviceability assessment standards, while summarizing key experimental and finite element studies conducted by various researchers on CLT floor vibrations. **Chapter 3** explores experimental testing methods, including common approaches such as shaker tests, impact hammer tests, heel drops, and walking tests. Each method is presented with detailed protocols, followed by a thorough explanation of the analytical techniques employed to extract dynamic parameters from the floor systems. **Chapter 4** focuses on the analysis of experimental results, providing insights into the dynamic properties of CLT floors, such as frequency, damping, and modal behavior. **Chapter 5** compares the results from finite element modeling with the experimental findings, highlighting areas of convergence and divergence between simulated and actual behavior. **Chapter 6** concludes the study by summarizing the key findings, offering insights into the implications for the design of CLT floors, and proposing recommendations for future research in this field.

2. Literature Review

2.1 Timber Flooring Systems

2.1.1 Timber as the Future of Construction

The construction industry is a significant contributor to greenhouse gas emissions on a global scale, placing high demand on natural resources (European Commission, 2019; Zhao et al., 2023). Currently, the sector is responsible for approximately 40% of global carbon dioxide (CO₂) emissions and consumes about 35% of the world's total energy (Zhao et al., 2023). The Paris Agreement (2015) aims to reduce worldwide CO₂ emissions by 45% by 2030, reaching net-zero emissions by 2050 to limit global temperature rise below 1.5°C. Given the annual rise in CO₂ emissions, mitigating the climate impacts of the construction industry is crucial in achieving these targets. To address this, two main strategies are employed: (i) adopting eco-friendly construction materials (Ekhaese and Ndimako, 2023), and (ii) optimizing energy usage throughout the operational lifespan of buildings (Liu et al., 2022).

Given the urgency to reduce emissions from the construction industry, sustainable materials such as timber provide a viable solution due to their minimal carbon footprint. Timber, as the world's oldest construction material, boasts an unrivalled low carbon footprint due to its renewable nature and ability to sequester carbon during its lifecycle. A building's carbon footprint refers to the total greenhouse gases produced during its operations, a factor that affects both new constructions and existing structures, emphasizing the need for sustainable practices across the industry. Engineered wood products (EWPs) exhibit superior environmental attributes compared to conventional non-renewable materials such as steel and concrete. (Singh et al., 2022; Sikkema et al., 2023; De Araujo et al., 2023).

As the construction industry continues to evolve, the integration of sustainable materials and the reduction of energy consumption are critical steps toward meeting global climate targets. In buildings, flooring systems serve multiple functions, including providing a horizontal platform for movement, separating vertical spaces, and distributing structural forces. Initially, flooring systems were predominantly constructed from concrete due to its low cost. As materials and construction techniques developed, concrete flooring became widely popular for its affordability. Subsequently, steel flooring systems were introduced to accommodate the demand for faster construction and taller buildings.

More recently, timber flooring systems have been developed in response to increasing environmental sustainability requirements. According to Lehmann (2012), replacing steel floor joists with engineered wood joists, which weigh approximately one metric ton, can reduce carbon dioxide (CO₂) emissions by about 10 tonnes. Similarly, the use of wood flooring in place of concrete slab flooring has been shown to lower CO₂ emissions to 3.5 tonnes for every ton of wood utilized. For comparison, total greenhouse gas emissions from food consumption alone are estimated at 2.2 tonnes of CO₂ equivalent per person per year (Liu et al., 2022).

In light of these environmental advantages, recent research has increasingly focused on the structural performance of timber flooring systems, particularly concerning vibration issues. A search using the keywords "timber" AND "floor" AND "vibration" within the Scopus database, conducted in March 2024, yielded 226 relevant documents. As illustrated in Figure 2.1, there has been a significant increase in research addressing vibration concerns associated with timber floors, especially in the last three years (2021–2023). This analysis provides valuable insights into emerging trends and highlights the growing academic interest in addressing the technical challenges of timber flooring systems.

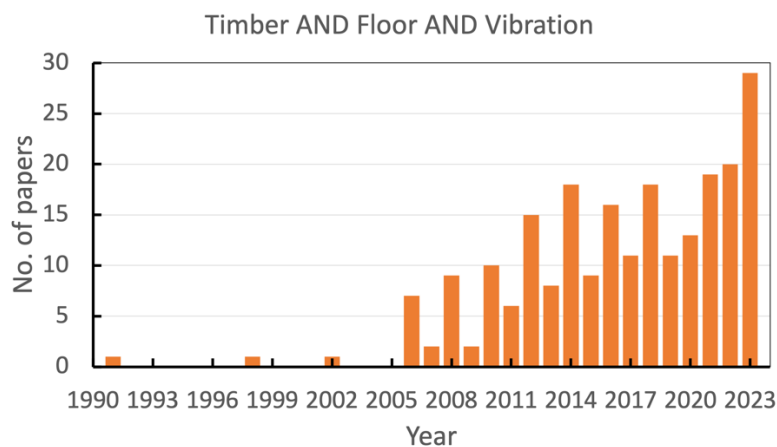


Figure 2. 1: Number of Publications per Year on Timer Floor Vibration from Scopus (Total: 226)

The analysis of the 226 documents provides important insights into the distribution of research across different types of timber floors. Figure 2.2 illustrates the classification and distribution of various floor types examined in these studies. Of the studies reviewed, 57.5% focus on traditional timber floors, underscoring the widespread concern over vibration issues. The exploration of CLT floors, which constitutes 17.3% of the research, reflects a growing interest in this novel solution due to its increased adoption in recent years. The anticipated release of new European specifications governing CLT floor slabs in 2025 is expected to further accelerate this trend. Additionally, 18.1% of the studies focus on timber-concrete composite floors, while 7.1% concentrate on steel-timber composite floors, highlighting the growing popularity of hybrid flooring systems. Notably, many

studies within both categories examine composite floors integrating concrete and steel with CLT, signaling a shift towards more sustainable and efficient hybrid flooring solutions.

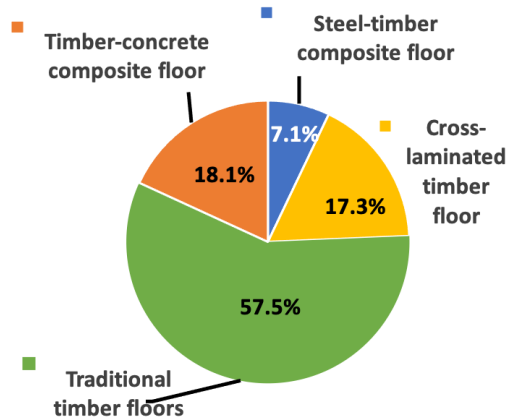


Figure 2. 2: Pie Chart of Floor Types in 226 Selected Documents

Despite growing interest and significant research efforts, studies on timber floors remain limited compared to those on other materials. To further investigate this research gap, additional searches were conducted in Scopus using the following keyword sets: (1) steel AND floor AND vibration, and (2) concrete AND floor AND vibration. The first search yielded 294 documents published between 1960 and 2023, while the second search yielded 470 documents from the same period. The decision to start from 1960 is based on historical developments in building materials, as the post-war construction boom, particularly in the late 1960s, marked a significant increase in the use of steel and concrete in housing construction. Figure 2.3 shows that research on timber floors was relatively sparse before 2010, with fewer documents on timber structures compared to those on steel and concrete. These findings are consistent with the conclusions of Aloisio et al. (2023), suggesting that research on timber floors is still emerging compared to more established materials.

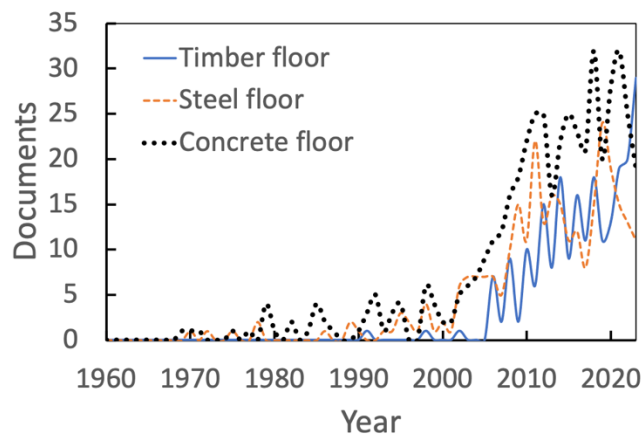


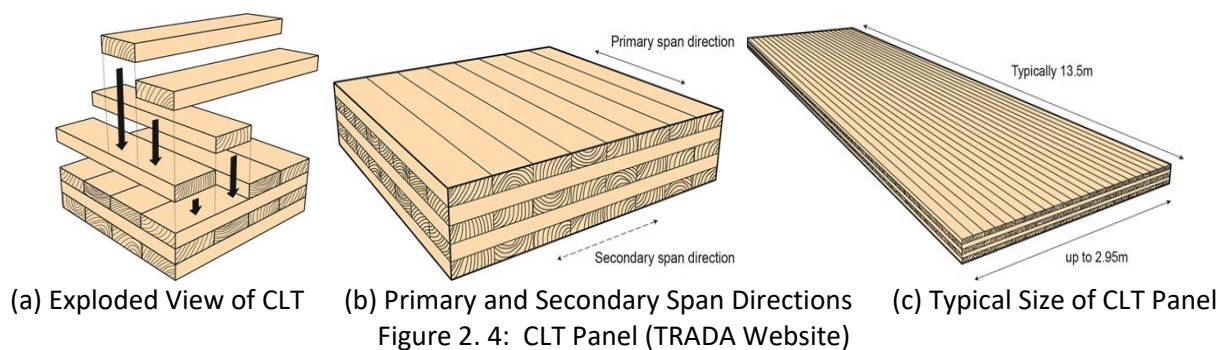
Figure 2. 3: Results of Literature Analysis: Number of Documents Published per Year on Floor vibration Research

2.1.2 Cross Laminated Timber (CLT)

Engineered wood products (EWPs) are manufactured from veneers, strands, or flakes obtained through peeling, chipping, or slicing processes. These components are then arranged for structural applications and bonded together using adhesives under controlled heat and pressure to create panels or shaped structural products.

Among the various engineered wood products (EWPs), cross-laminated timber (CLT) has emerged as a key innovation, especially in Central Europe, where it is increasingly used as a substitute for reinforced concrete slabs in construction (Brandner et al., 2016). CLT panels consist of multiple layers of wood laminates, typically spruce. These layers are placed at right angles to each other to form a stable, strong composite structure. Figure 2.4 (a) illustrates the orthogonal arrangement of wood laminates, which contributes to the structural strength of CLT panels. Figure 2.4 (b) shows the primary and secondary span directions, which are critical for load-bearing calculations. After assembling the layers, the resulting CLT panels vary in thickness, typically ranging from 60 mm to 300 mm. Panel sizes depend on the manufacturer, but transportation limitations often reduce the maximum sizes to 13.5 meters by 2.95 meters (see Figure 2.4 (c)).

According to the Timber Research and Development Association (TRADA), the mechanical properties of CLT, listed in Sheet 61 (2009), show that a 150 mm layer of C24 CLT has an average density of 530 kg/m³ (see Figure 2.5). These characteristics, along with the growing adoption of CLT, demonstrate its potential as a sustainable alternative to traditional concrete construction.



CLT Properties:		
CLT Depth/Manufacturer:	125	c24
Bending perp to plane, parallel to grain $f_k =$	24.0	N/mm ²
Bending in the plane, parallel to grain $f_k =$	0.0	N/mm ²
Tension in the plane, l el to grain, $f_{t,0,k}$	14.0	N/mm ²
Compression in the plane, l el to grain, $f_{c,0,k}$	21.0	N/mm ²
Compression perp to grain $f_{c,90,k}$	2.5	N/mm ²
Shear perp to plane, l el to grain, $f_{v,k}$	2.5	N/mm ²
Rolling Shear perp to plane, perp to grain, $f_{r,v,k}$	0.0	N/mm ²
Shear in the plane, l el to grain, $f_{v,k}$	2.5	N/mm ²
MOE _{mean} - perp to plane, parallel to grain, $E_{0,mean}$	11000	N/mm ²
MOE _{mean} - perp to plane, perp to grain, $E_{90,mean}$	370.0	N/mm ²
MOE _{mean} - perp to plane, parallel to grain, $E_{0,min}$	7400.0	N/mm ²
MOE _{mean} - in the plane, parallel to grain, $E_{0,mean}$	6100.0	N/mm ²
Shear modulus, parallel to grain, G_{mean}	690	N/mm ²
Rolling Shear modulus, perp to grain, $G_{R,mean}$	69	N/mm ²
Characteristic density	350	kg/cu.m
Average density	530	kg/cu.m

Figure 2. 5: TRADA CLT Properties (TRADA Sheet 61, 2009)

CLT was first developed in Europe in the early 1990s, with Austria and Germany pioneering its introduction (Karacabeyli and Douglas, 2013). As a wood paneling system, CLT offers a cost-effective and wood-based alternative to traditional construction materials, such as concrete, masonry, and steel. Its potential to complement existing light-frame and heavy-timber building systems further demonstrates its versatility.

Though the adoption of CLT was initially slow, its use in construction gained momentum in the early 2000s, driven by the rise of the green building movement and improvements in efficiency, product approvals, and marketing strategies. Another key factor contributing to its growing popularity is the perception that CLT, like masonry and concrete, represents a robust and durable construction system (Karacabeyli and Douglas, 2013).

The growing demand for CLT in regions such as Austria, Germany, Scandinavia, as well as Canada and Japan, has led to the rise of several key suppliers. Europe remains the largest producer of cross-laminated timber globally, with high demand for CLT-based buildings in both North America and Europe. According to a 2023 market research report by MarketsandMarkets, leading companies in the CLT sector include Stora Enso (Finland), KLH Massivholz GmbH (Austria), Mayr-Melnhof Holz (Austria), Binderholz GmbH (Austria), Eugen Decker Holzindustrie KG (Germany), Hasslacher Holding GmbH (Austria), Schilliger Holz AG (Switzerland), Structurlam Mass Timber Corporation (Canada), and XLam NZ Limited (New Zealand). Figure 2.6 provides a visual representation of the geographic locations of these major CLT producers.

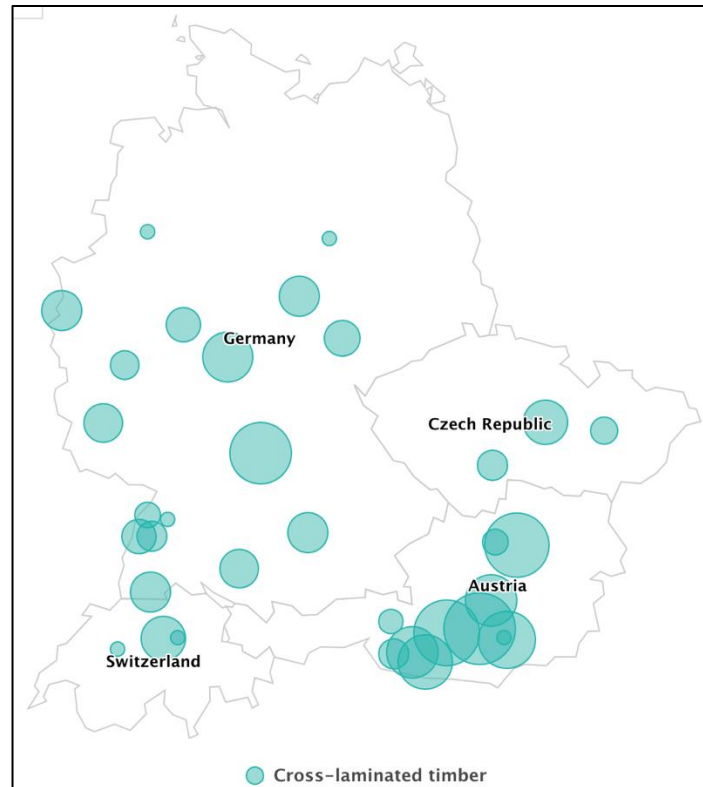


Figure 2. 6: Location of the Majority of CLT Producers (<https://www.timber-online.net>)

2.1.3 CLT Floor and Hybrid CLT Floor

Cross-Laminated Timber (CLT) products can be utilized as standalone flooring systems or in combination with glued-laminated beams and I-joists. Additionally, composite structures incorporating steel or concrete beams are employed in some applications. However, true composite construction is less frequently used in the UK due to the high stresses in the vicinity of shear connectors and the increased complexity it introduces into otherwise straightforward construction methods. In cases where large, open floor plans are required, the use of internal load-bearing panel walls may be too restrictive. In such scenarios, a structural system combining CLT with glulam, steel, or concrete framing elements may be a more suitable solution.

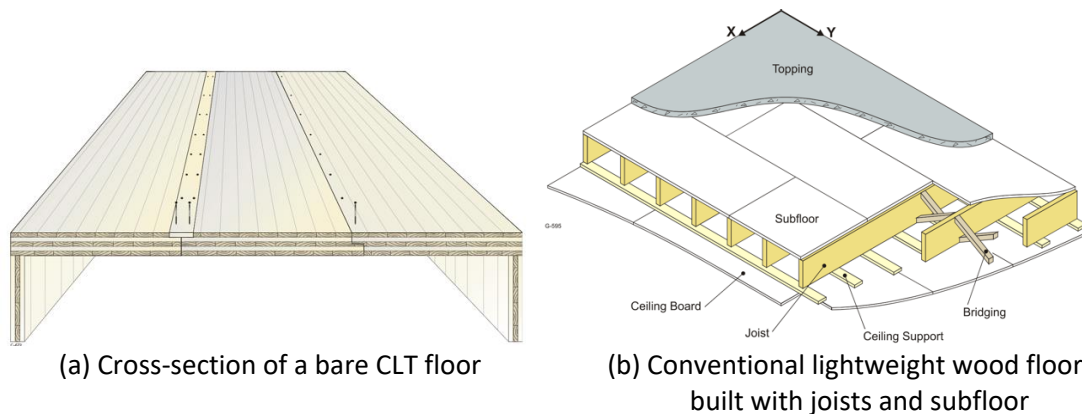
2.1.3.1 CLT Floor

Murray Grove, completed in 2009, represents the first tall urban housing project constructed entirely from prefabricated solid timber. This nine-storey superstructure extensively utilizes Cross-Laminated Timber (CLT) for its load-bearing walls, floor slabs, and stair and lift cores (see Figures 2.7(b) and 2.7(c)). Externally, the building does not appear to be constructed from timber, as its exterior panels are composed of 70% wood pulp mixed with fiber cement (Figure 2.7(a)).



(a) Murray Grove in Hackney, London (b) Structures (c) Floor slabs are also made of CLT
 Figure 2. 7: Murray Grove, the 'Pure CLT' Building in London

Unlike conventional lightweight joisted wood flooring systems, CLT floors consist of solid wood slabs and are typically constructed without joists (Figure 2.8). In comparison to joisted wood floors of equivalent span and vibration performance, CLT floors are generally shallower. For instance, a CLT floor with a 6.5 m span can be constructed with 0.23 m thick panels, whereas traditional joisted wood floors of the same span require joists at least 0.3 m deep (Hu, 2013).



(a) Cross-section of a bare CLT floor (b) Conventional lightweight wood floor built with joists and subfloor
 Figure 2. 8: CLT Floor System and Conventional Joisted Floor System

A comprehensive review of existing literature (Hu, 2013) is presented in Table 2.1, which summarizes the distinctive material properties of bare CLT floors in comparison to traditional lightweight joisted floors and heavy concrete slab floors. One notable limitation of bare CLT floors is their low damping ratio, which can negatively impact their vibrational performance. Enhancing the damping characteristics of CLT floors through construction detailing could mitigate these effects and improve overall performance.

Table 2. 1: Mass, Frequency and Damping of CLT Compared to Other Floor Material (Hu, 2013)

Floor material	Area mass	Fundamental frequency	Damping ratio
Lightweight joisted floors without topping	15-30 kg/m ²	> 15 Hz	3%
Bare CLT floors	30-150 kg/m ²	> 9 Hz	1%
Heavy concrete floors	>150 kg/m ²	< 9 Hz	2-5%

2.1.3.2 CLT-concrete Floor

Aloisio et al. (2023) emphasized the potential of hybrid timber floors, particularly those combining timber and concrete, in mitigating vibration levels. Figure 2.9 illustrates a typical Timber-Concrete Composite (TCC) flooring system.

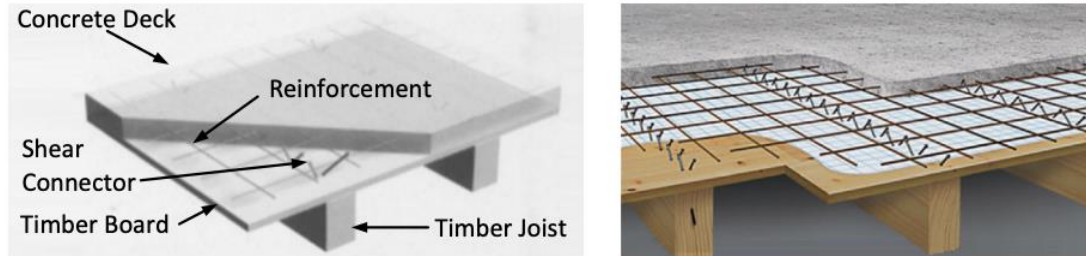


Figure 2. 9: Typical TCC Flooring System (Dackermann et al., 2016)

While CLT has certain limitations—such as low bending strength, limited global stability, and susceptibility to vibrations in floor systems (Jiang and Crocetti, 2019; Yeoh et al., 2011)—the integration of concrete layers within CLT systems significantly enhances structural performance. These composite floor systems improve stiffness, resistance to bending and deflection, load-bearing capacity, durability, and dynamic resilience (Siddika et al., 2021). Additionally, the inclusion of a concrete layer reduces vibration under service loads by increasing flexural capacity (Negrão et al., 2010). Mai's (2018) experimental studies demonstrated that CLT-concrete composite floors have a bending capacity three to five times greater than that of standard CLT floors designed for typical office use, highlighting the potential of these systems for long-span, high-rise buildings.

Setragian and Chandra (2018) further explored the use of CLT-concrete composite slabs for spans ranging from 6 to 12 meters. The total height of these slabs is optimized by a 60:40 distribution ratio between the CLT and concrete layers. Effective interaction between the two materials requires the use of shear connectors, with various types available depending on cost and efficiency. Figure 2.10 illustrates common shear connector types. Siddika et al. (2021) expands on this by identifying a range of connection methods, including glue, metal fasteners, notches, and shear keys, selected based on specific structural requirements. Furthermore, Siddika provided a summary of the performance of common CLT-concrete composite floor systems, emphasizing their suitability for various structural applications.

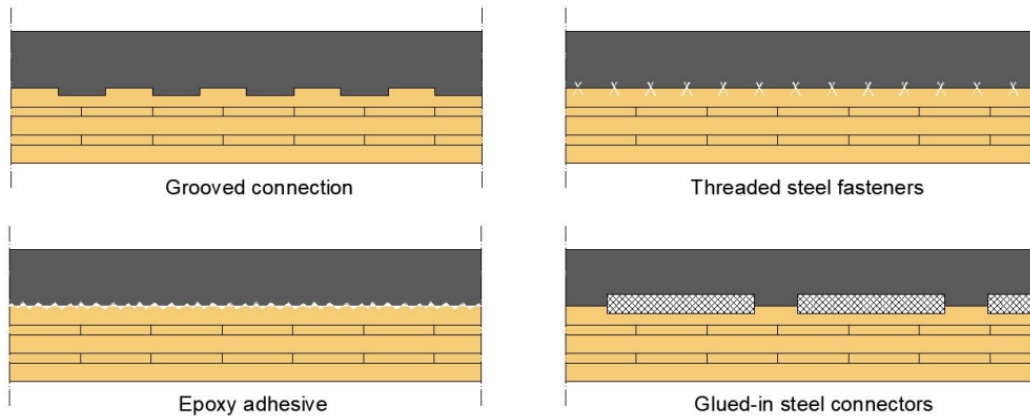


Figure 2. 10: Types of Shear Connectors (Setragian and Chandra, 2018)

2.1.3.3 Steel-CLT Floor

The hybrid steel-timber composite (STC) floors consist of prefabricated CLT panels and steel beams, which are connected using various types of shear connectors. Screws and bolts are installed through pre-drilled holes in the top flange of the steel beam and the CLT slabs (Hassanieh et al., 2017). A typical Steel-CLT hybrid floor is shown in Figure 2.11, with the connections between the CLT plate and steel joist detailed in Figure 2.12.



Figure 2. 11: Steel-CLT Hybrid Floor

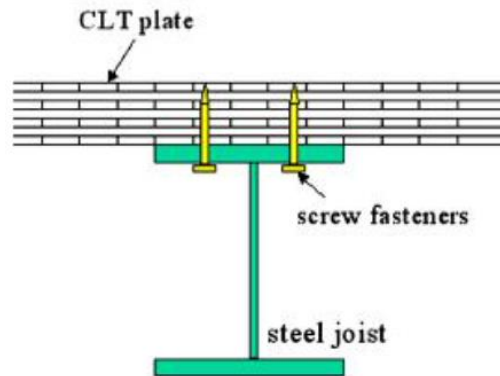


Figure 2. 12: Steel-CLT Connection

Steel-CLT hybrid floors have proven effective as structural solutions, particularly due to their high strength-to-weight ratio. Research on these floors largely focuses on performance simulation and experimental investigations of the connection systems. These research includes examining the mechanical behavior of steel-timber composite connections, with a specific focus on strength and stiffness properties determined through experimental tests.

Loss et al. (2014, 2016a, 2016b) explored the performance of steel-timber hybrid prefabricated buildings, integrating CLT panels with a range of steel profiles, including hot-rolled, cold-formed, and welded steel. These studies involved extensive testing of both steel-wood and wood-wood connections, illustrating the capability of Steel-CLT hybrid systems to support adaptable and sustainable building designs.

In particular, Loss (2016a) highlighted several key benefits of CLT-steel combinations compared to traditional timber-timber and timber-concrete systems. He noted that “hybrid systems with steel frames and CLT wood-based panels are typically as light as timber–timber mixed construction systems. However, they can take advantage both of the intrinsic deformation capacity of the steel elements and the use of mechanical fastening devices. Furthermore, since steel–timber hybrid structures are joined using special dry devices, they do not require either casting concrete on site or the on-site completion of precast concrete elements, as commonly required by heavy hybrid timber–concrete construction systems.”

2.1.4 Dynamic Properties of CLT Floors

Understanding the core principles of vibration is crucial for effective floor design. While mathematical models of vibration systems are well-documented in the literature, this section focuses on two fundamental formulas that encompass all relevant parameters. Thus, the analysis of vibration primarily revolves around these key dynamic parameters.

The simplest structure in dynamic analysis is the single-degree-of-freedom (SDOF) system, which forms the basis for multi-degree-of-freedom analysis. An SDOF linear system is described by key quantities such as displacement, mass, viscous damping ratio, and stiffness. The free vibration of such a system is governed by the homogeneous differential equation of motion:

$$m\ddot{x} + c\dot{x} + kx = 0 \quad (2.1)$$

The solution to this equation is strongly dependent on the mass (m), stiffness (k) and damping coefficients (c). Damping primarily affects the decay of vibration but has a relatively minor influence on the vibration frequency, which is negligible in most cases of structural vibration. Although damping in real structures is often nonlinear, an equivalent viscous damping coefficient can typically yield satisfactory results.

In engineering and theoretical research, natural frequency (f_n) is often used to measure the speed of structural vibration, and it is determined by the equation:

$$f_n = \frac{1}{2\pi} \sqrt{\frac{k}{m}} \text{ [Hz]} \quad (2.2)$$

The most critical parameters for assessing the dynamic behavior of a structural frame include natural frequency (influenced by mass and stiffness), damping, and effective mass. Below is an explanation of these parameters in the context of CLT flooring systems:

- Mass and Modal Mass

Wood-based floors are generally lightweight. Composite CLT floor slabs, particularly those combined with concrete or steel, increase the overall floor mass. In a real structure, the concrete layer and gypsum layer on the top of the floor slab are usually used for fire protection and sound insulation, which is typically required in most residential buildings (Heikki, 2014). Therefore, the additional mass should be estimated properly.

Modal mass refers to the mass that contributes to a particular mode of vibration. It is a key parameter for assessing the vibrational significance of a mode. To ensure effective vibration analysis, the total effective modal mass should represent at least 90% of the actual system mass (Irvine, 2015). Eurocode 5 specifies that wood flooring should account for the first 40 modes of vibration relevant to structural performance. However, a gap exists in the literature regarding the number of modes necessary for cross-laminated timber (CLT) vibration design, as well as the exact percentage of each mode in the total modal mass. It is crucial to note that the mode with a higher proportion of modal mass relative to the total mass of the structure significantly influences its response.

- Stiffness

The greater the stiffness of a floor slab, the higher the frequency and the smaller the deflection, which improves the serviceability of the floor. Stiffness is largely determined by the properties of the physical components, including boards, panels, nails, and screws (Piazza et al., 2008; Brignola et al., 2012). The stiffness of the diaphragms can be enhanced by screwing the CLT panels along the main floor grid, such as on the main beams or lateral beams of the frame. Experimental tests indicate that CLT connections play a crucial role in determining the effective shear stiffness of the diaphragm, contributing more than 50% to its overall stiffness (Loss and Frangi, 2017).

Previous research has shown that boundary conditions significantly affect the dynamic behavior of the floor (Jarnérö et al., 2015; Weckendorf et al., 2015; Huang, 2020). The number of supports, whether on two or four sides, impacts the natural frequency of the structure (Glisovic and Stevanovic, 2010). When the floor is fixed to the wall, the clamping effect increases the floor's rigidity, raising the natural frequency of the system. If the floor is supported on elastic beams, its natural frequency differs from that of a single slab unit (Hamm et al., 2010). Changes to edge support conditions can significantly impact modal mass and stiffness, thereby altering the dynamic behavior of the floor system (Ussher et al., 2014). For instance, in the scenario of a single panel with fully fixed ends, there is an approximately 84% increase in fundamental frequencies compared to a single panel with hinge support. From a structural engineering perspective, the connection characteristics must be carefully considered, as they influence both the static and dynamic responses of complete floor systems (Ussher et al., 2014).

- Damping Ratio

Damping refers to the characteristic of a material or structure that reduces vibrational energy, eventually stopping the motion. For floor systems, higher damping is always preferable as it minimizes unwanted vibrations. However, accurately estimating damping is challenging (Jarnérö et al., 2015) due to the complex interplay of material damping, structural damping, and frictional damping. Each material used in construction possesses its own intrinsic damping properties, and the total damping effect results from the combined influence of these factors.

The damping ratio is influenced by the type of timber structure, the assembly of the structural components, and the support conditions. Additional factors, such as partitions, raised floors, suspended ceilings, and furnishings, can further affect damping. Damping ratios also vary between different modes of vibration, as energy dissipation depends on the internal friction and damping characteristics of each mode (Jarnérö, 2014).

Timber-framed structures generally exhibit higher damping compared to steel or concrete-framed structures. Fitz's research indicates that the damping of CLT floor plates, with or without light or heavy top flooring, varies between 2% and 4%, depending on whether the floor is supported on two or four sides. Eurocode 5 recommends a damping ratio of 1% for general floors, while the British Annex suggests a 2% damping ratio for CLT floors.

2.2 Human Induced Vibration Issues

2.2.1 Floor Vibration due to Human Activity

Vibration disturbances in buildings can originate from both external and internal sources. External sources include vibrations transmitted through the ground from industrial machinery or vehicles, which can propagate through the building structure and affect its occupants. In some cases, the vibration originates from within the building itself, caused by domestic equipment, ventilation systems, door banging, or footfalls. The perception of vibration in a building may be considered unacceptable not only because of the sensation it produces but also due to the potential for building damage or visible movement of objects. Occupants' attitudes toward vibration will depend on several factors, including what they feel, hear, and see, their expectations, and whether they believe any measures could be taken to reduce the vibrations. Additionally, occupants may consider whether expressing their dissatisfaction could lead to improvements or financial compensation (Griffin, 2012). The entire process by which occupants perceive vibrations and are affected by them is illustrated in Figure 2.13.

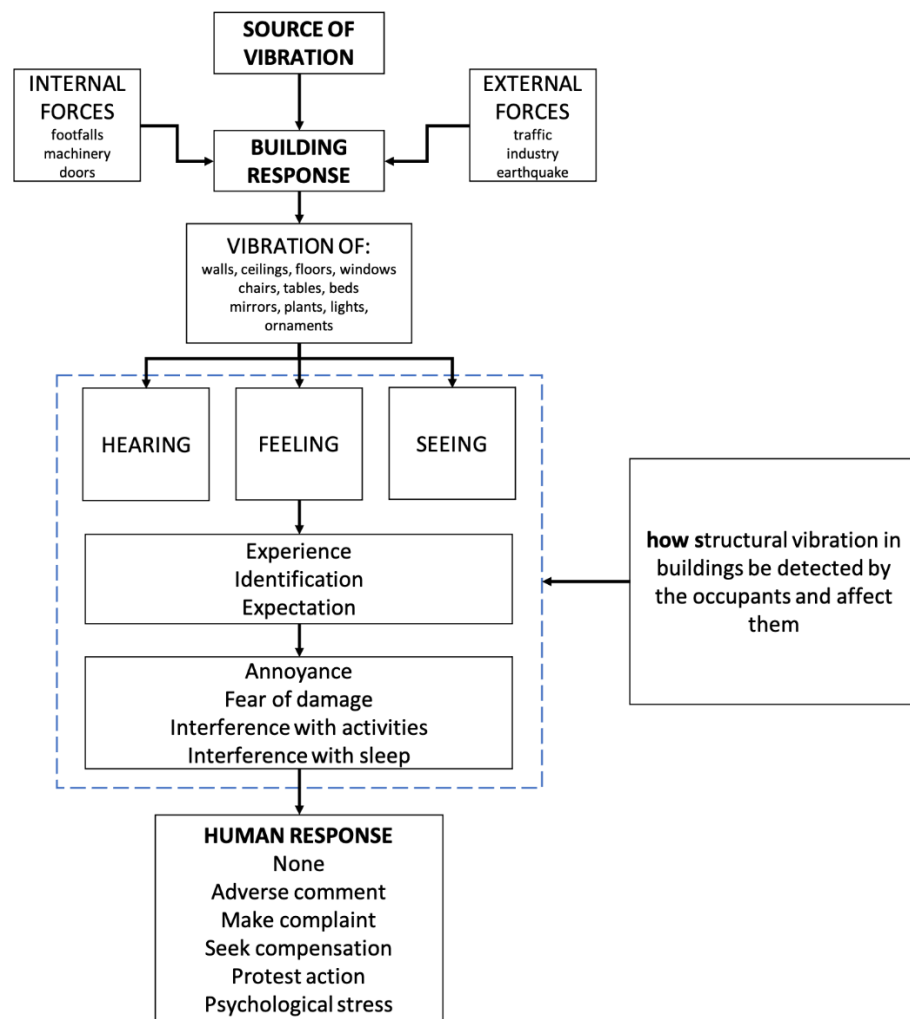


Figure 2. 13: Factors Affecting the Acceptability of Building Vibration

Floor vibration is not a new phenomenon. The 'live' feel of timber floors under pedestrian loading is well-established. Among the structural components in direct contact with occupants, floors are the most affected by human activities, which often lead to unavoidable vibrations. Research has demonstrated that certain human movements can induce floor resonance, causing significant discomfort for other occupants and raising concerns about structural security (Ljunggren, 2006).

However, not all floors experience vibration problems caused by human activity. Whether a particular type of activity leads to discomfort depends on the frequency relationship between the activity and the floor. Wooden floor slabs, such as those made of Cross-Laminated Timber (CLT), are particularly prone to vibration due to their low stiffness and mass. The frequency of vibrations in CLT floor slabs typically falls within the range of 7-12 Hz, with a significant overlap in the 4-8 Hz range. This lower frequency range corresponds to the resonant frequency of the body's internal organs and is approximately 2-4 times higher than the frequency of walking (1-2 Hz). This alignment can lead to resonance, resulting in serious structural discomfort and, in extreme cases, safety concerns.

This research focuses on office buildings, specifically examining common activities such as running and walking. In accordance with the International Organization for Standardization (ISO) 10137:2007, evaluating vibrations in buildings involves considering three key factors: the vibration source, the transmission path, and the receiver. The vibration source produces dynamic forces or actions, while the structure or medium between the source and the receiver constitutes the transmission path. The resulting vibrations at the receiver must then be evaluated according to the criteria for the serviceability limit state. Together, these three characteristics encompass all aspects relevant to human-induced vibration issues being investigated.

2.2.2 Source of Vibration: Human Activities

In the early 1990s, it became widely established that walking is a periodic function and that low-frequency floors could resonate when excited by the harmonics of the pedestrian pacing rate (Reynolds, 2000). Butz et al. (2006) in their report, and Smith (2009) in the SCI P354 guide, both addressed the walking phenomenon and proposed models for calculating walking loads.

The reliable prediction of floor vibration response to human activity depends on the accuracy of walking load models (Aloisio et al., 2023). Several design guidelines specify these models, including works by Willford and Young (2006), Butz et al. (2006), Smith et al. (2009), Feldmann et al. (2009),

and Murray et al. (2016). In these guidelines, continuous walking is modeled as a perfect periodic process and is mathematically described using Fourier series.

Accurate modeling of walking loads plays a critical role in designing structures that mitigate excessive vibrations, ensuring both occupant comfort and structural integrity.

2.2.2.1 Walking and Running Pattern

Walking and running are the most common human activities within buildings, both of which have well-established frequency ranges that can be accurately measured through experimental methods. These ranges are detailed in Table 2.2. Numerous researchers, such as Bachmann (1995), have performed regression analyses on large datasets to control for variability between individuals, thereby achieving consistent and reliable results.

Table 2. 2: Frequency Ranges of Human Activities

Representative types of activity			Range of applicability	
Designation	Description	Design rate (Hz)	Actual activities	Activity rate (Hz)
Walking	Walking with continuous ground contact	1.6 to 2.4	<ul style="list-style-type: none"> • Slow walking • Normal walking • Fast, brisk walking 	<ul style="list-style-type: none"> ~ 1.7 ~ 2.0 ~ 2.3
Running	Running with discontinuous ground contact	2.0 to 3.5	<ul style="list-style-type: none"> • Slow running • Normal running • Fast running 	<ul style="list-style-type: none"> ~ 2.1 ~ 2.5 > 3.0

Figure 2.14 illustrates the gait cycles for both walking and running. These cycles can be divided into three phases: stance, swing, and float. The primary distinction between running and walking loads lies in the shorter ground contact time and the increased force associated with running.

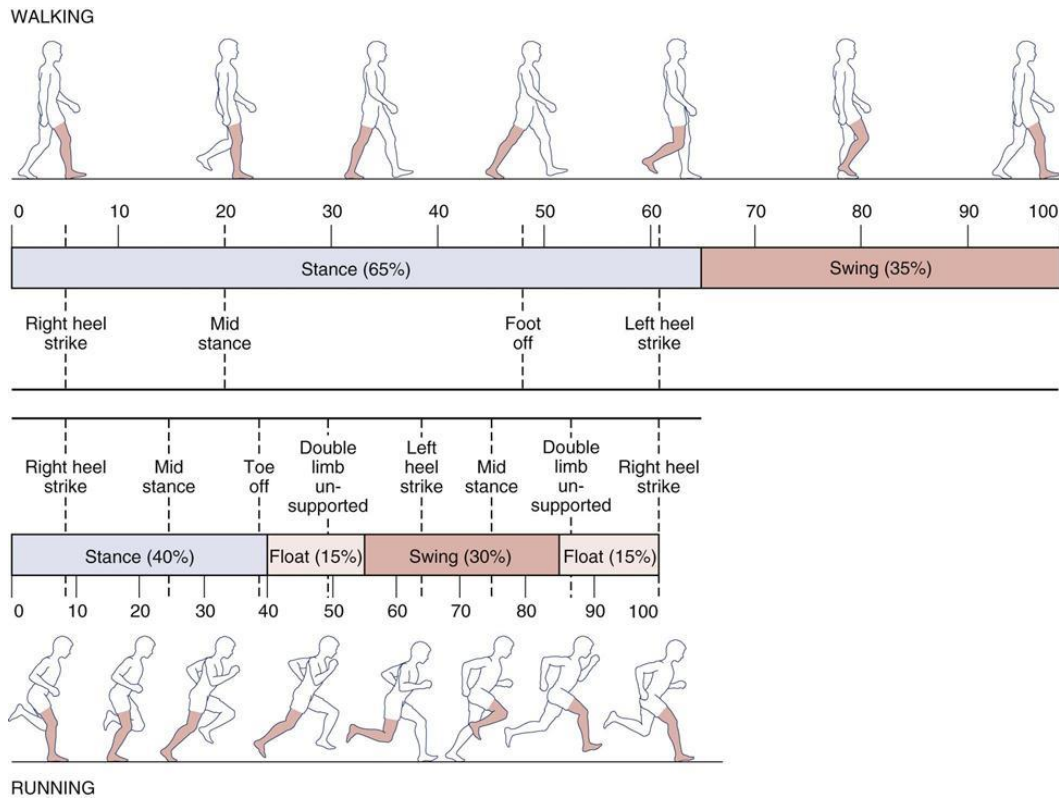


Figure 2. 14: Comparison of the Phases of the Walking and Running Cycles

2.2.2.2 Load Models for Walking and Running

Researchers typically use force plates to measure the shape and magnitude of forces applied to the ground during walking (Racic et al., 2009). Figure 2.15 illustrates the force and resultant force (normalized by body weight) for the left and right feet of a walking individual.

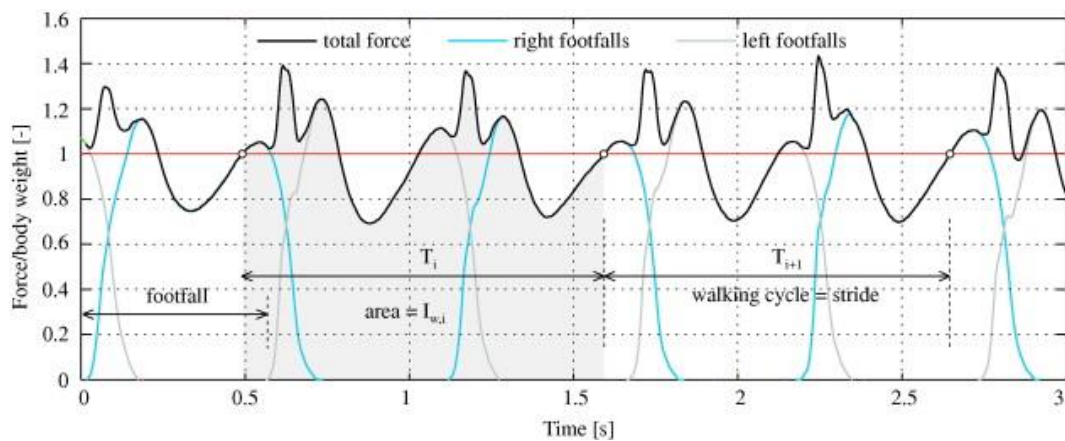


Figure 2. 15: A Portion of a Continuously Measured Ground Reaction Force (GRF) due to Walking (Racic and Brownjohn, 2011)

Assuming that an individual generates identical and perfectly repeatable footfalls with a period T , the vertical walking force can be represented in the time domain as a sum of Fourier harmonic components (Rainer et al., 1988; Bachmann et al., 1995):

$$F_p(t) = G + G \sum_{i=1}^n \lambda_i \sin(2i\pi f_p t - \varphi_i) \quad (2.3)$$

where G is the pedestrian's static weight, f_p is the walking frequency, φ_i is the phase angle for the i^{th} harmonic, and λ_i is the i^{th} Fourier coefficient, generally known as the dynamic loading factor (DLF), which is a key parameter in load modeling. Numerous single-person walking load models have been developed based on experimental data.

Mathematical load models can be divided into two categories: deterministic and probabilistic. The deterministic model assumes a fixed frequency and disregards variability within and between subjects. In contrast, the probabilistic model incorporates this variability, making it more complex mathematically (Živanović et al., 2007).

In deterministic models, each step is considered identical, with cycles repeated uniformly, neglecting random fluctuations in walking patterns. Various researchers have proposed deterministic models for both walking and running loads, as shown in Table 2.3, where the dynamic loading factor is largely dependent on step frequency.

Table 2. 3: Single Pedestrian Vertical Walking/Running Load Models Proposed by Different Authors

Walking load models						
No.	Authors	Year	DLFs	Phase angles	Pedestrian weight	Walking frequency
1	Bachmann	1987	$\lambda_1=0.4-0.5$ (2 Hz is 0.4), $\lambda_2=\lambda_3=0.1$	$\varphi_2=\varphi_3=\frac{\pi}{2}$	/	2.0-2.4 Hz
2	Rainer et al.	1988	curve	/	735 N	1.7-2.3 Hz
3	Allen& Murray	1993	$\lambda_1=0.5, \lambda_2=0.2,$ $\lambda_3=0.1, \lambda_4=0.005$	/	700 N	1.6-2.2 Hz
4	Kerr	1999	$\lambda_1=-0.265f_3+1.32f_2-1.760f$ $+0.761$ $\lambda_2=0.2, \lambda_3=0.1$	/	/	1.6-2.2 Hz
5	Young (Arup)	2001	$\lambda_1=0.41 (f_p-0.95)\leq 0.56,$ $\lambda_2=0.069+0.0056 (2f_p),$ $\lambda_3=0.033+0.0064 (3f_p),$	/	/	1-2.8 Hz

			$\lambda_4=0.013+0.0065(4f_p)$			
6	ISO 10137	2007	$\lambda_1=0.37(f_p - 1.0)$, $\lambda_2=0.1, \lambda_3=0.06$ $\lambda_4=0.06, \lambda_5=0.06$	$\varphi_i=\frac{\pi}{2} (f_n > f_p)$ $\varphi_i=0 (f_n \leq f_p)$	750 N	1.2-2.4 Hz
7	Smith (SCI P354)	2009	$\lambda_1=0.436(f_p - 0.95)$, $\lambda_2=0.006(2f_p + 12.3)$, $\lambda_3=0.007(3f_p + 5.2)$, $\lambda_4=0.007(4f_p + 2.0)$	$\varphi_1=0$ $\varphi_2=-\frac{\pi}{2}$, $\varphi_3=\pi$, $\varphi_4=\frac{\pi}{2}$	746 N	1.8-2.2 Hz
8	Chen et al.	2014	$\lambda_1=-0.2358f_p - 0.2010$, $\lambda_2=0.0949, \lambda_3=0.0523$, $\lambda_4=0.0461, \lambda_5=0.0339$	$\varphi_1=-\pi/4$ $\varphi_4 =\pi/4$ $\varphi_5 =\pi/2$	/	1.2-3.0 Hz

Running load models						
No.	Authors	Year	DLFs	Phase angles	Pedestrian weight	Walking frequency
1	Rainer et al.	1988	Curve, $\lambda_1=1.4$ (2.8-4.0 Hz)	/	735 N	1.6-4.0 Hz
2	Bachmann	1995	$\lambda_1=1.6, \lambda_2=0.7, \lambda_3=0.2$	/	/	2.0-3.0 Hz
3	ISO 10137	2007	$\lambda_1=1.4, \lambda_2=0.4, \lambda_3=0.1$	$\varphi_i=\frac{\pi}{2} (f_n > f_p)$ $\varphi_i=0 (f_n \leq f_p)$	750 N	2.0-4.0 Hz

A review of eight walking load models (Table 2.3) reveals significant differences in both amplitude and phase, as illustrated in Figure 2.16. For further comparative analysis, models with similar characteristics were selected.

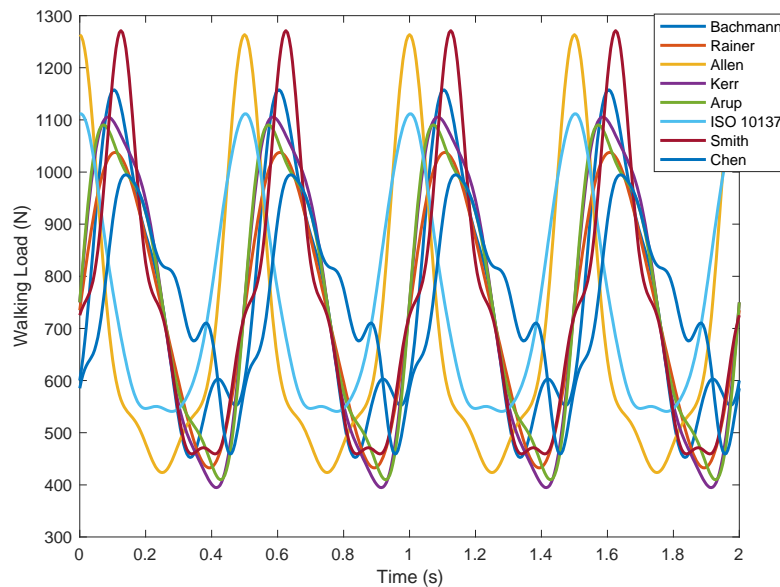


Figure 2. 16: Simulated Walking Load Time Histories of 8 Different Models at $f_p=2.0$ Hz

Figure 2.17(a) shows that the walking load curves proposed by Kerr (1999), Arup (Young, 2001), and ISO 10137 (2007) exhibit similar amplitudes, with the primary differences found in their phase angles. This study employs the walking load model developed by Arup due to its suitability for floor vibration calculations and its consideration of statistical probability distributions. Regarding running loads, frequencies below 3 Hz are influenced primarily by the first-order dynamic loading factor, while higher-order factors become significant at frequencies above 3 Hz (Živanović et al., 2005). Both the Bachmann (1995) and ISO 10137 (2007) models are appropriate for designing floor structures; however, this study adopts the ISO 10137 method due to its specific phase angle and its accurate representation of running loads (Figure 2.17(b)).

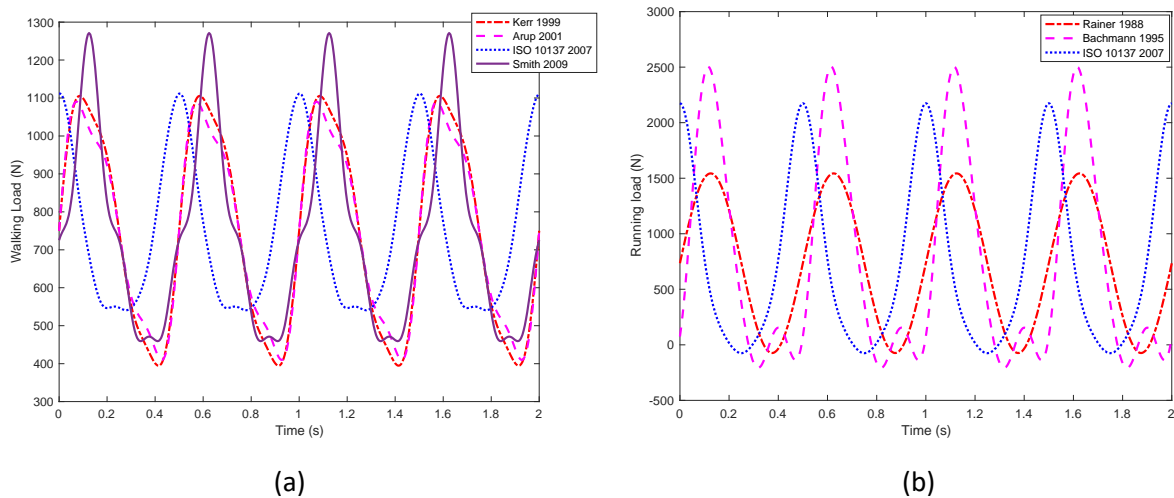


Figure 2. 17: Load Models Comparison: (A) Simulated Walking Load Time Histories of Four Different Models at $f_p = 2.0$ Hz; (B) Simulated Running Load Time Histories of Three Different Models at $f_p = 2.0$ Hz

2.2.2.3 Deterministic Load Model, Probabilistic Load Model and Group Effect

There are two fundamental models for analyzing individual pedestrian loads: deterministic and probabilistic (Pavic, 1998). The deterministic model assumes uniformity in each step and repetitive cycles, disregarding the inherent variability in walking. Various researchers have developed deterministic load models for walking and running, summarized in Table 2.3.

However, the deterministic approach cannot account for the inherent variability in human walking, including inter- and intra-subject differences, which are well-documented in current literature. Probabilistic models address these limitations by incorporating randomness into the walking

patterns, representing parameters such as speed, frequency, and weight through experimental probability distributions (Aloisio, 2023).

Zivanovic (2006) introduced a probability-based framework for predicting the vertical vibration response of footbridges to pedestrian excitation. Her model integrates multiple gait parameters, accounting for variability in walking frequency, step length, and amplitude. This model was developed using walking force time histories from three subjects measured on a treadmill, specifically a 65 kg male researcher, a 62 kg male student, and a 46 kg female student (Brownjohn et al., 2004).

Racic and Brownjohn (2011) collected vertical walking force data from 80 volunteers, generating 824 time series across ten walking speeds. This data was used to develop a mathematical algorithm for modeling dynamic loads from pedestrian walking.

Research on probabilistic modeling reveals a clear methodology. It involves gathering extensive time-varying load records and utilizing them to advance walking models for stochastic dynamic calculations.

Studies on group dynamics are limited. Ellingwood and Tallin (1984) found that dynamic forces from randomly walking groups seldom cause serviceability issues unless walking in sync. Pernica (1990) and Ebrahimpour et al. (1996) observed that dynamic load factors decrease with increasing group size (see Figure 2.18). Ellis (2000, 2003) further examined floor responses to crowd loading, noting that while the response increased with group size, the dynamic load factors decreased.

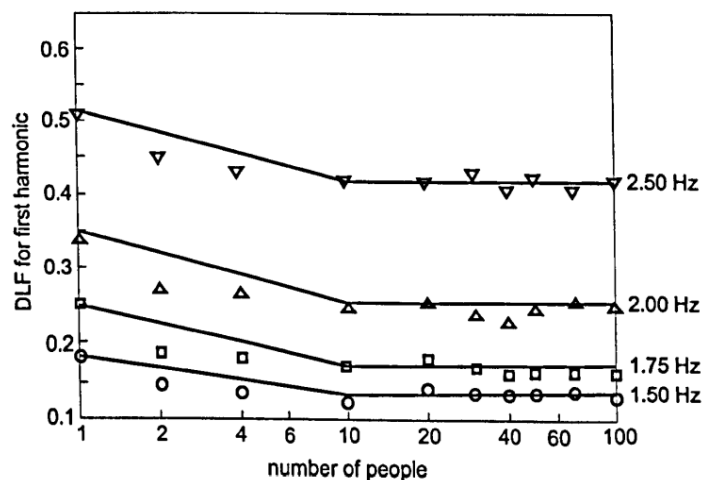


Figure 2. 18: DLF for the First Harmonic of the Walking Force as a Function of Number of People and Walking Frequency (Ebrahimpour et al., 1996)

2.2.3 Transmission Path: Floor Properties

2.2.3.1 Transient and Steady-state vibration

The dynamic properties of CLT floors are detailed in section 2.1.4. The response of a system to forced vibration consists of two parts: transient and steady-state (Willford and Young, 2006; Smith et al., 2009). The floor's response to footfalls may exhibit two distinct behaviors. Figures 2.19(a) and 2.19(b) illustrate these distinctions between transient and steady-state vibrations. For stiff structures, where the dominant vertical mode frequency is four times greater than the walking frequency, the transient solution dominates as vibrations rapidly decay between steps due to high stiffness and damping. In such cases, the excitation is modeled as a series of impacts (Figure 2.19a). Conversely, for softer structures, resonance occurs when the walking frequency or one of its harmonics coincides with an eigenfrequency. In this scenario, the steady-state solution prevails, with vibrations reaching a constant amplitude over time (Figure 2.19b).

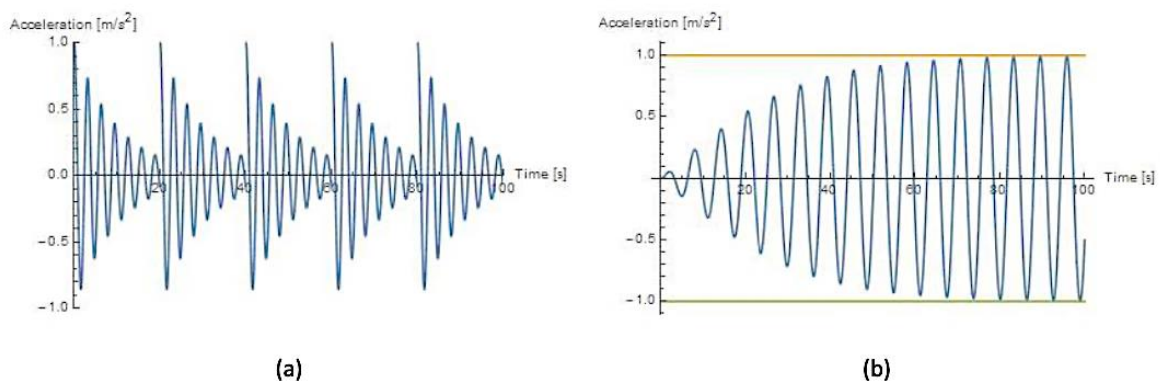


Figure 2. 19: Floor Characteristics: (a) Series of Transient Vibrations Due to Impacts on A “Stiffer” Floor, (b) Steady-State Solution Due to Continuous Excitation Force on A “Softer” Floor

Floors are prone to vibration when occupied (Bachmann, 1995). Therefore, both resonant and transient vibrations must be considered in the design process. Transient vibrations, caused by sudden movements such as walking or dropping objects, attenuate proportionally to the structure's damping, as seen in short-duration impacts that decay over time. In contrast, steady-state vibrations arise from repetitive cyclic activities such as dancing or machine operation. These distinctions are illustrated in Figure 2.19, aiding in the initial assessment of structural characteristics and indirectly reflecting external force features.

Several factors contribute to whether a floor slab exhibits greater stiffness or flexibility. These include material properties such as span, beam height, and support stiffness. Additionally, the

construction method, whether joisted or trussed, and the sheathing type are crucial. Longer spans tend to produce more vibrations due to larger deflections compared to shorter spans. The depth of the floor structure is also relevant, as shallow joists typically deflect more and generate more vibrations than deeper joists. Support stiffness is another critical factor, as any deflection in the supports can lead to increased floor vibrations. Finally, the placement of furniture, particularly between trusses, can influence whether the floor behaves more rigidly or flexibly.

2.2.3.2 High Frequency Floor and Low Frequency Floors

Floors are typically categorized into low-frequency and high-frequency types based on their fundamental frequencies (Mohammed et al., 2018). Low-frequency floors, characterized by fundamental frequencies below 8-10Hz, predominantly respond to walking-induced resonance, which can be sustained by continuous motion. In contrast, high-frequency floors, with fundamental frequencies above 8-10Hz, exhibit transient vibration responses to each heel strike during walking. These transient responses may interact, depending on factors such as the spacing between successive impacts and the level of vibration damping. Table 2.4 presents the cut-off frequencies for different floor types, as specified by various authors and design guidelines.

Table 2. 4: Cut-off Frequency between Low- and High-frequency Floors by Different Researchers

Author	Cut-off frequency	Floor type
Ohlsson (Eurocode 5)	8 Hz	timber joisted floors
Revised Eurocode 5 (draft)	4.5 Hz	all types of timber floor
Murray & Allen (DG11)	9-10Hz	wood deck on light metal joists
The Steel Construction Institute P354	10 Hz	general floors, open plan offices etc. in steel-framed buildings
	8 Hz	enclosed spaces, e.g., operating theatre, residential
Feldmann (JRC Report)	9-10 Hz	Concrete-steel composite floor
Willford (The Concrete Centre)	10 Hz	Concrete

Murray et al. (2016) noted that low-frequency floors are particularly susceptible to problematic vibrations, often resonating due to walking and causing accelerations that exceed human comfort levels. Guigrand (1971) emphasized that high frequencies are not necessarily associated with significant structural responses indicative of danger, highlighting the importance of low frequencies in assessing floor vibration serviceability.

Ji and Ellis (1994) suggested that resonance problems can be avoided by designing floors with sufficiently high fundamental frequencies. The most effective approach is to ensure that the lowest

and most energetic structural frequencies exceed the excitation frequency and its first one or two harmonics, a technique referred to as high-frequency tuning (Thelandersson and Larsen, 2003). Although this method is effective, it is often only achieved by adding extra material or reducing spans. Consequently, it is unsurprising that reports of vibration problems in structures have increased, as efforts to reduce material usage have generally led to lower stiffness-to-mass ratios. Increasing the strength-to-weight ratio of construction materials is typically easier than increasing their stiffness-to-mass ratio.

2.2.4 Receivers: Floor and Human Response

In the context of building vibration assessment, ISO 10137 defines the receiver of vibrations as the entity for which the vibration effects are to be evaluated. This definition encompasses not only the building structure and its components, such as beams, slabs, walls, and windows, but also the building's contents, including instruments and machinery, as well as its human occupants.

2.2.4.1. Floor structures as vibration receiver

The response characteristics of a structure play a critical role in determining the comfort level of a floor. Historically, various structural parameters, including mid-span deflection, velocity, and root mean square (RMS) velocity, have been used as key references for assessing floor comfort. Once a building is constructed, its structural elements are generally fixed, and human perceptions of vibration discomfort may vary. These parameters are crucial for both measurement and observation of potential vibration issues.

- Deflection limits

Early efforts to control floor vibration primarily focused on limiting static deflection under a specific uniform distributed load (UDL), ensuring that the floor had sufficient stiffness. For instance, when a timber floor was designed with a deflection limit of $L/360$ under UDL, occupants still reported excessive vibration. In response, Onysko (1986) conducted field measurements on over 300 residential floors, using resident surveys, performance testing, and simulations. His research found that static deflection under a concentrated load was the best predictive parameter, leading to the adoption of a static deflection limit under a 1 kN concentrated load at the floor's center in Canadian regulations.

While some vibrations can be mitigated using static response parameters, satisfactory performance is not always guaranteed. Hu et al. (2001) highlighted these limitations, prompting a shift toward investigating dynamic parameters. Ohlsson (1982) was the first to propose a floor design based on dynamic criteria.

- Fundamental frequency, unit impulse velocity, and acceleration limits

Ohlsson (1982) conducted tests on floors made of steel and timber, developing design criteria that included a recommended fundamental frequency below 8 Hz. He also combined this with an evaluation of the unit impulse velocity response, based on the response generated by a 1 Ns impulse applied at any point on the floor. These findings formed the basis of the current Eurocode 5, which employs three key criteria to regulate floor vibrations: frequency limits, deflection limits, and impulse velocity control.

Smith and Chui (1988) proposed a design method using the first eigenfrequency and RMS velocity. The frequency-weighting method applies a weighting factor to different frequency components, emphasizing those most relevant to human perception. In this context, they suggested that acceptable floors should have a maximum frequency-weighted acceleration of less than 0.45 m/s^2 under a heel-drop impact.

A Canadian research team, FPInnovations, later developed a simplified method for assessing the vibration performance of cross-laminated timber (CLT) floors, published in the CLT Handbook (Hu & Gagnon, 2011). This criterion provides an inequality based on the floor's fundamental frequency and effective stiffness under a unit load.

2.2.4.2. Human Occupants as vibration receiver

In human-induced floor vibration scenarios, it is essential to acknowledge that the vibration response of a floor does not fully represent the experience of individuals on that floor. Perception of floor vibrations varies from person to person. Research by Toratti and Talja (2006) revealed a phenomenon where floor acceleration responses outside specified limits did not elicit complaints from occupants, while some acceleration responses within the limits did cause discomfort (Figure 2.20). Therefore, the vibration experienced by occupants cannot be fully assessed using the structural parameter limits discussed in section 2.2.4.1.

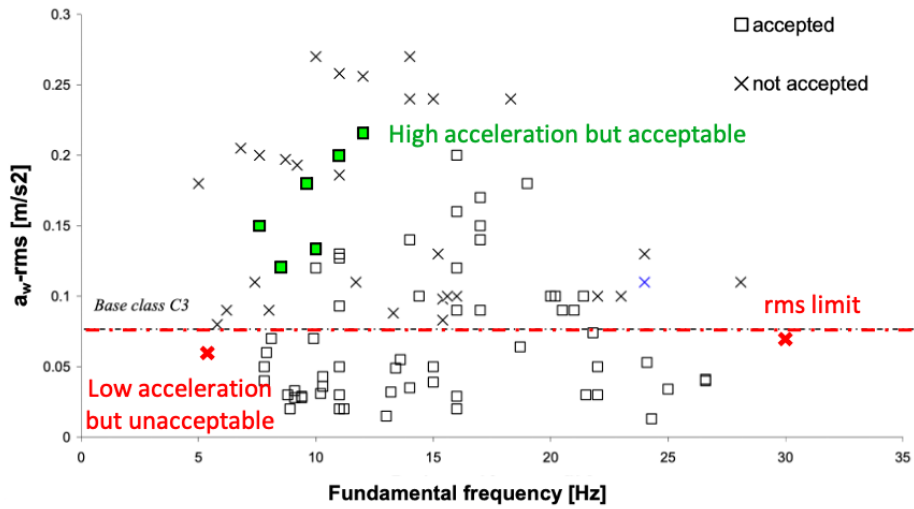


Figure 2. 20: Acceleration Compared to Acceptability (Toratti and Talja, 2006)

As shown in Figure 2.21, lightweight floor slab vibrations may cause annoyance to occupants. Humans are particularly sensitive to vibrations in the 4-8 Hz frequency range, as this range corresponds to the resonant frequency of the body's internal organs (Griffin, 2012; Hassanieh et al., 2019; Karampour et al., 2023). Consequently, researchers agree that structural frequencies within this range are undesirable.

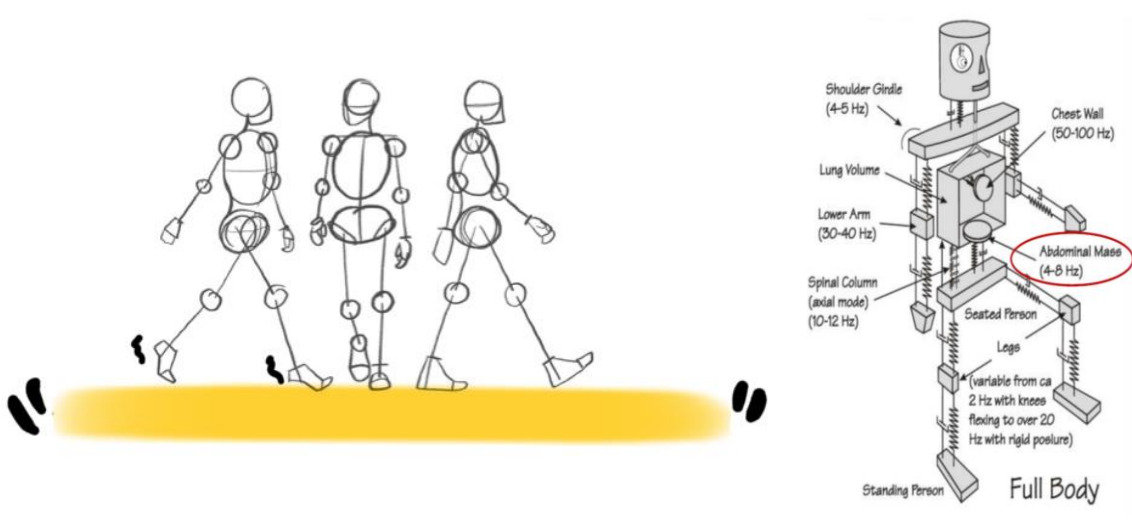


Figure 2. 21: Floor Vibration and the Frequency Range of the Body's Internal Organs

An individual's sensitivity to vibration is closely related to their activity level, a relationship first identified by Griffin (2012). When sitting or lying down, individuals are more sensitive to vibrations than when walking or engaging in physical activities. During rhythmic activities, such as running or aerobics, people are less sensitive to floor vibrations. Similarly, when walking across a floor, individuals tolerate much larger amplitude vibrations than when sitting quietly. The duration of the

disturbance is another significant factor in human perception of vibration; short-duration, heavily damped vibrations of high amplitude are more tolerable than continuous vibrations (Griffin, 2012).

One of the first laboratory studies on human vibration perception was conducted by Reiher and Meister in 1931 (Pavic & Reynolds, 2002). Their research established thresholds for vibration perception, ranging from 'imperceptible' to 'painful,' which has greatly influenced subsequent studies. Later researchers combined factors such as sensitive frequency ranges, body position, and vibration duration to develop two widely used evaluation methods for more complex vibrations: the weighted root mean square (RMS) method and the vibration dose value (VDV) method. Detailed explanations of these methods will be provided in Section 2.3.5.

2.3 Serviceability Criteria

2.3.1 Serviceability and Codification

According to Leicester (1993), the term 'serviceability' refers to all structural behaviors, excluding structural collapse, that render a building or construction unfit for its intended use. The lack of fitness may pertain to human reactions, including aesthetic, physiological, or psychological responses, which can range from minor discomfort and annoyance to significant medical conditions. Additionally, serviceability concerns may involve factors that hinder the efficient operation of both humans and equipment.

For the purpose of codification, serviceability criteria are often translated into a finite set of design decisions. Each design is associated with an effective cost, and code recommendations are typically based on minimizing these costs while ensuring the building meets serviceability requirements.

2.3.2 Design Code and Evaluation Standards

Because serviceability involves human actions and responses, two types of codes should generally be considered: the design code and the assessment standard. The design code focuses on the building's vibration characteristics and its dynamic response, while the assessment standard addresses human perception of the building's behavior.

The design code is typically optimized from the perspective of the building owner. Leicester (1993) refers to the statistical model developed by Leicester and Beresford (1977), as depicted in Figure 2.22. This model assumes that a building has a serviceability parameter, such as crack width, denoted

as \bar{T} , and a client's tolerance level or complaint threshold, denoted as \bar{U} . When \bar{T} exceeds \bar{U} , additional costs may be incurred. These costs could involve remedial expenses, indirect costs from negative publicity (such as with the London Millennium Bridge), or even the loss of tenants.

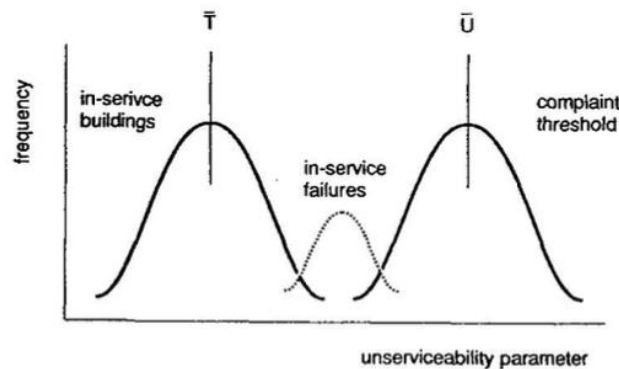


Figure 2. 22: Statistical Model for a Design Code (Leicester, 1993)

Evaluation standards, on the other hand, are optimized from both the building owner's and builder's cost perspectives. Building owners tend to focus on the maximum value at which residents begin to complain (the client's tolerance level), since complaints can lead to increased costs. However, builders are primarily concerned with the maximum unserviceability parameter in in-service buildings, which is typically below the client's complaint threshold. This margin allows for a buffer before complaints arise. This difference may explain why, in some cases, design specifications are met but evaluation standards are not satisfied if the unserviceability parameter approaches the failure curve for in-service buildings.

For floor vibrations, the unserviceability parameters related to human response to vibration have included various functions of displacement, velocity, acceleration, frequency, and damping. These parameters, while complex, provide useful criteria for assessing the serviceability of building floors from both technical and human-centric perspectives.

2.3.3 'Good Code'

What is the role of building codes, and how do they contribute to the design and construction process? Building codes serve three main functions: (1) they define the duties and responsibilities in the design and production of a building; (2) they provide a framework for collecting data from research and feedback from field experience; and (3) codifying design procedures allows engineers with varying levels of experience to competently design conventional structures.

To fulfill these functions, it is essential that the intent of a design code is transparent. A major challenge in applying modern codes is the ambiguity surrounding whether deformation limits are intended for aesthetic or structural damage considerations. Ideally, a comprehensive framework should be provided, including a description of the relevant failure mode and the corresponding range of remedial actions.

A key aspect of evaluation standards is that they specify performance in terms of measurable parameters, particularly in the event of a dispute. For instance, crack width is a useful parameter, while lateral sway of a building in a 50-year return wind is not as easily measured or applied.

The impact of unserviceability parameters on humans is influenced by several nonstructural factors, such as architectural features, audible and visual stimuli, building usage, and occupant behavior. Consequently, serviceability limits for both design codes and evaluation standards should not be specified as single values. Instead, these limits should be defined as a range of acceptable values, allowing designers and building owners the flexibility to choose limits that match specific building conditions and quality expectations.

2.3.4 Design Code for Timber

2.3.4.1 Current Eurocode 5 (EC5): Design of Timber Structures

Ohlsson (1982) proposed criteria to assess floor vibrations and their impact on human discomfort, which led to the development of a Swedish design guide on floor vibrations. These methods later formed the basis for the vibrational serviceability criteria in Eurocode 5 (EC5) and BS EN 1995-1-1:2004. Eurocode 5 was established as a pan-European standard, providing harmonized design criteria across member countries to create a common framework for design, research, and development (Weckendorf, 2009).

Eurocode 5 (2004) governs the design of timber buildings in civil engineering structures, including various forms of timber, such as solid timber, glued laminated timber, and wood-based structural products like Laminated Veneer Lumber (LVL). However, it does not include the latest material, Cross Laminated Timber (CLT).

The code sets out principles and requirements to ensure the safety and serviceability of structures. In terms of vibration, the relevant serviceability limit states are discussed in Section 7. These involve measurements and calculations that account for the expected stiffness of the structure and the

modal damping ratio. For floors, a modal damping ratio of $\zeta = 0.01$ (1%) is assumed unless proven otherwise. In contrast, the UK National Annex (2014) specifies a damping ratio of $\zeta = 0.02$ (2%) for typical UK floors.

Floor vibrational behavior is typically assessed using three criteria: natural frequency (frequency criteria), deflection or stiffness under a specified load (stiffness criteria), and velocity resulting from an impulse (velocity criteria). A detailed procedure, including calculation formulas, is provided in Figure 2.23.

It is important to note that the design section on serviceability limit states applies only to residential flooring systems with spans shorter than 6 meters and adopting a joist-type structure. Eurocode 5 suggests that the floor frequency should exceed 8 Hz to avoid falling within the 4-8 Hz range, which is known to cause discomfort for occupants. If the floor frequency falls below 8 Hz, the code does not provide explicit guidance but recommends conducting a special investigation to address potential issues.

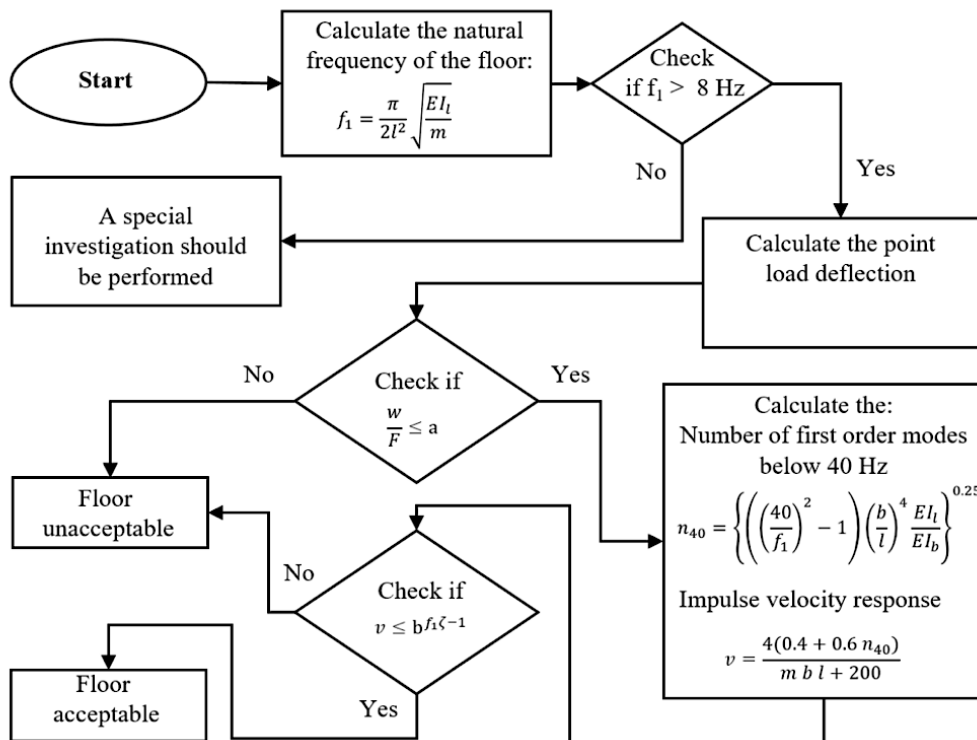


Figure 2. 23: Illustration of the Design Process for Timber Floors according to EC5 (Schirén and Swahn, 2019)

2.3.4.2 Revised Eurocode 5 (rEC5) Draft

Significant progress has been made in predicting floor vibrations, leading to the inclusion of modified serviceability criteria and evaluation methods for timber floors in the revised Eurocode 5 (rEC5) draft. Unlike EC5, which is primarily designed for joisted floors, rEC5 applies to a wider range of floor types, including slab-type systems. These include floors supported by plate structures such as cross-laminated timber (CLT), laminated veneer lumber (LVL), glue-laminated veneer lumber (GLVL), nailed laminated slabs, and cross-laminated timber-concrete composite slabs.

The revised Eurocode 5 draft, as depicted in Figure 2.24, categorizes floor performance levels from Level I (highest) to Level VI (lowest). The stiffness criterion evaluates deflection under a point load, while the response factor (R) corresponds to different performance levels. These serviceability requirements are defined by threshold values based on the response factor, which acts as a multiplier applied to the base curve value. This multiplier represents the degree of vibration perceived by an average person. Distinct performance levels are characterized by various R -values, such as 4, 8, and 48, as shown in Figure 2.24.

Criteria	Floor performance levels					
	Level I	Level II	Level III	Level IV	Level V	Level VI
Response factor R	4	8	12	24	36	48
Upper deflection limit $w_{lim,max}$ [mm]	0,25		0,5	1,0	1,5	2,0
<u>Stiffness criteria</u> for all floors w_{1kN} [mm] \leq	w_{lim} calculated with [Formula (9.18)]					
<u>Frequency criteria</u> for all floors f_1 [Hz] \geq	4,5					
<u>Acceleration criteria</u> for resonant vibration ($f_1 < f_{1,lim}$) design situations a_{rms} [m/s^2] \leq	0,005 R					
<u>Velocity criteria</u> for all floors v_{rms} [m/s] \leq	0,0001 R					

Figure 2. 24: Floor Vibration Criteria according to the Floor Performance Level in rEC5

It is important to note that these guidelines apply exclusively to wooden floors with a natural frequency greater than 4.5 Hz. Furthermore, the R -factor is only valid for human-induced vibrations in timber floors, where the walking frequency falls within a narrow range of 1.5 to 2.5 Hz. This limitation highlights the specific application of the R -factor in evaluating the perceptibility of vibrations caused by human activity.

The basis for this revised code includes ISO 2631-1 (1997), which provides general requirements for evaluating human exposure to whole-body vibration, and ISO 2631-2 (2003), which addresses vibration in buildings within a frequency range of 1 Hz to 80 Hz. Notably, these standards cover a wider vibration design frequency range compared to the narrow walking frequency addressed by the revised Eurocode 5 guidelines.

Figure 2.25 illustrates a flowchart for floor service design, based on the rEC5 draft, which outlines standardized procedural steps and associated mathematical formulas. First, the deflection under a point load is assessed to ensure compliance with stiffness requirements. Next, the natural frequency of the floor is calculated using a specified formula. If the frequency is below 4.5 Hz, the method is not applicable. For frequencies between 4.5 Hz and 8 Hz, the floor performance level is determined by calculating the response factor (R). For frequencies above 8 Hz, performance is evaluated based on peak velocity and the R factor.

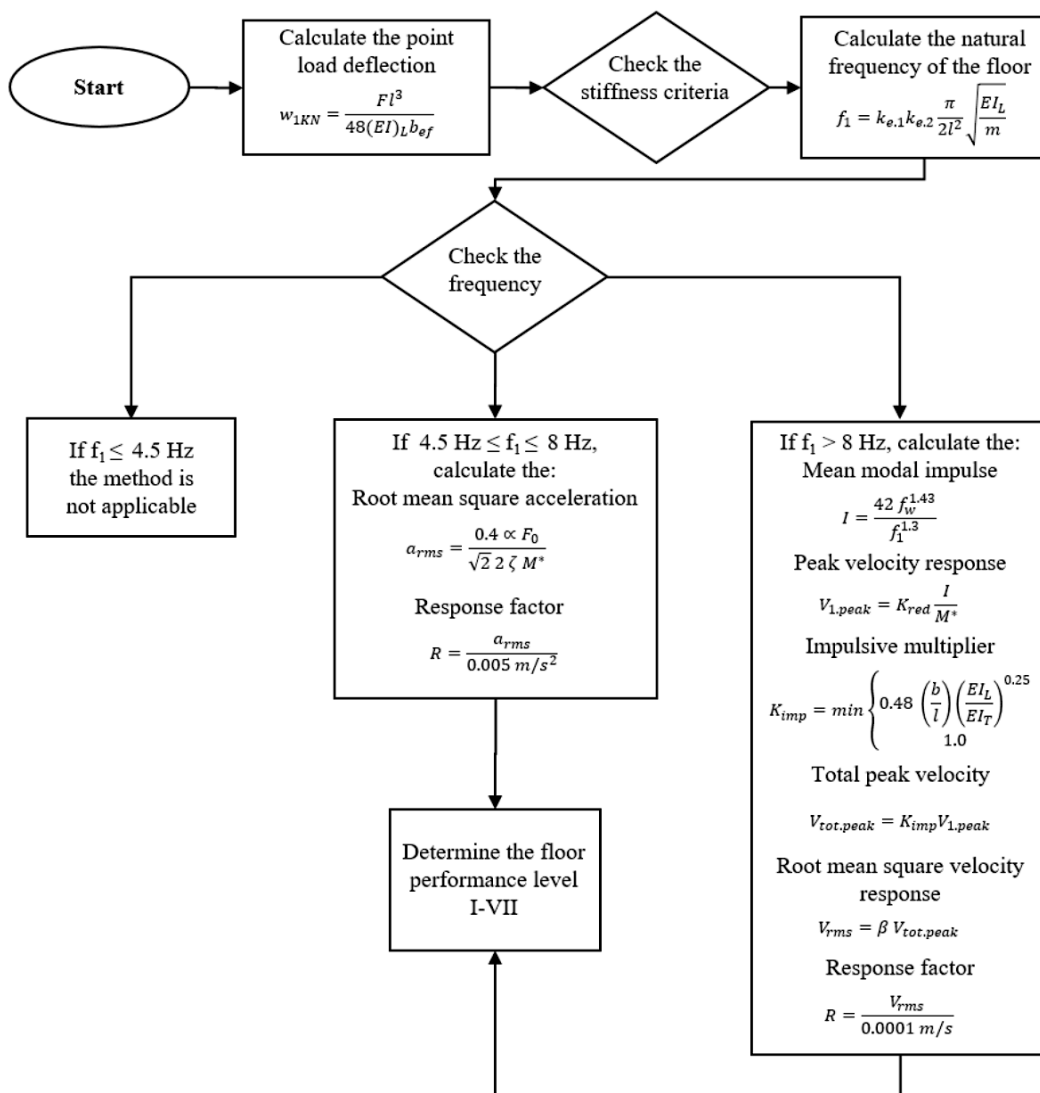


Figure 2. 25: Illustration of the Design Process for Timber Floors according to the rEC5 Draft
(Schirén and Swahn, 2019)

When adopting EC5 or rEC5 for floor serviceability design, the determination of 'acceptable' or 'unacceptable' outcomes may differ. This difference stems from two key factors: First, rEC5 accounts for lower-frequency floors, applicable down to 4.5 Hz, while EC5 only assesses floors with frequencies above 8 Hz. Additionally, rEC5 incorporates parameters for multi-span configurations. Second, the criteria for acceptability differ between the two codes. EC5 focuses on point load deflection and impulse velocity, whereas rEC5 evaluates the root mean square (RMS) acceleration (for frequencies between 4.5 and 8 Hz) and the RMS velocity (for frequencies above 8 Hz).

Unlike the binary 'acceptable' or 'unacceptable' results in EC5, rEC5 offers more detailed performance levels for engineers to choose from during the design process. However, further research is needed to assess the accuracy and practical usability of these performance levels in real-world applications.

2.3.5 Evaluation Standards for Timber

2.3.5.1 International Standard 2631: Evaluation of human exposure to whole-body vibration (1-80 Hz)

ISO 2631-1:1997, established by the International Organization for Standardization (ISO), provides a framework for assessing human exposure to whole-body vibration. Unlike traditional rating methods, this assessment relies on frequency weighting of the root mean square (r.m.s.) acceleration, expressed in metres per second squared (m/s^2) for translational vibration. The weighted r.m.s. acceleration, calculated using Equation 1, is based on the measurement duration 'T' in seconds.

$$a_{w,rms} = \left[\frac{1}{T} \int_0^T a_w^2(t) dt \right]^{\frac{1}{2}} [m/s^2] \quad (2.4)$$

When the basic evaluation method is insufficient, an additional approach called the fourth power vibration dose method can be used. This method is more sensitive to vibration peaks by employing the fourth power, instead of the second power, of the acceleration time history for averaging. The fourth power vibration dose value (VDV), measured in meters per second to the power of 1.75 ($m/s^{1.75}$), provides an alternative means of assessing vibration:

$$\text{VDV} = \left\{ \int_0^T [a_w(t)]^4 dt \right\}^{\frac{1}{4}} \quad [\text{m/s}^{1.75}] \quad (2.5)$$

For comfort and discomfort reactions to vibrations in residential and commercial buildings, ISO 2631-2:2003 should be referenced. This standard focuses on evaluating vibrations with respect to comfort and annoyance. It emphasizes overall weighted values, calculated with the appropriate frequency weighting, to assess the suitability of specific locations within buildings. The applicable frequency range for z-axis vibrations is 1 Hz to 80 Hz, and the frequency weighting w_k can be determined through a transfer function. A schematic illustration of the magnitude w_k is provided in Figure 2.26.

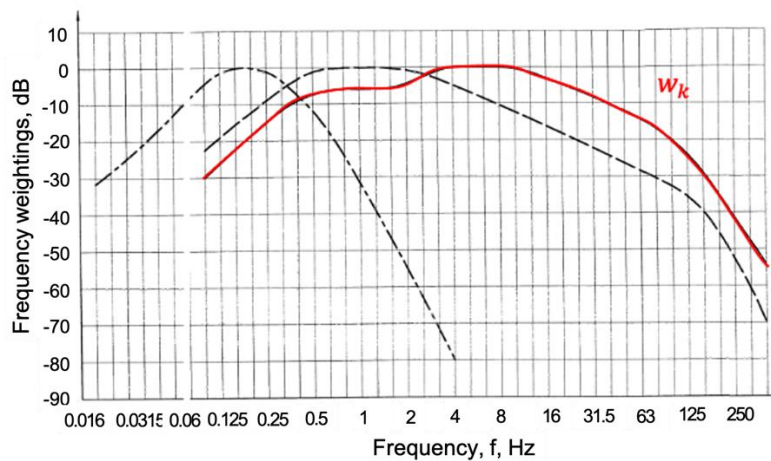


Figure 2. 26: Frequency Weighting w_k

The 'Baseline curve' approach used in ISO 2631-2:1989 related vibration magnitudes to multiples of the base curve. However, this standard was revised in 2003, and ISO 2631-2:2003 no longer provides explicit guidance on acceptance criteria due to the wide range of potential applications. Despite the withdrawal of ISO 2631-2:1989, portions of the earlier standard remain relevant for evaluating building vibrations. These criteria have been revised and reproduced in Table C.1 (Figure 2.27), as referenced in ISO 10137:2007. Multiplying factors for r.m.s. acceleration are applied to the base curves shown in Figures 2.28. For z-axis vibrations, the base magnitude is 0.005 m/s^2 r.m.s. for vibrations within the 4-8 Hz range.

Table C.1 — Multiplying factors used in several countries to specify satisfactory magnitudes of building vibration with respect to human response

Place	Time	Multiplying factors to base curve (Figures C.1, C.2 and C.3) ^a	
		Continuous vibration and intermittent vibration ^b	Impulsive vibration excitation with several occurrences per day
Critical working areas (e.g. some hospital operating-theatres, some precision laboratories, etc.)	Day	1	1
	Night	1	1 ^c
Residential (e.g. flats, homes, hospitals)	Day	2 to 4 ^d	30 to 90 ^{d, e, f}
	Night	1,4	1,4 to 20
Quiet office, open plan	Day	2	60 to 128 ^g
	Night	2	60 to 128
General office (e.g. schools, offices)	Day	4	60 to 128 ^g
	Night	4	60 to 128
Workshops ^h	Day	8	90 to 128 ^g
	Night	8	90 to 128

NOTE 1 For evaluating the effects of a vibration signal containing two or more discrete frequency components, the root-mean-quad (r.m.q.) method can be employed (see ISO 2631-2:1989, Annex B).

NOTE 2 This Table has been adapted from ISO 2631-2:1989, Annex A.

Figure 2. 27: Multiplying Factors for ‘Base Curve’ with Respect to Human Response (ISO 10137:2007)

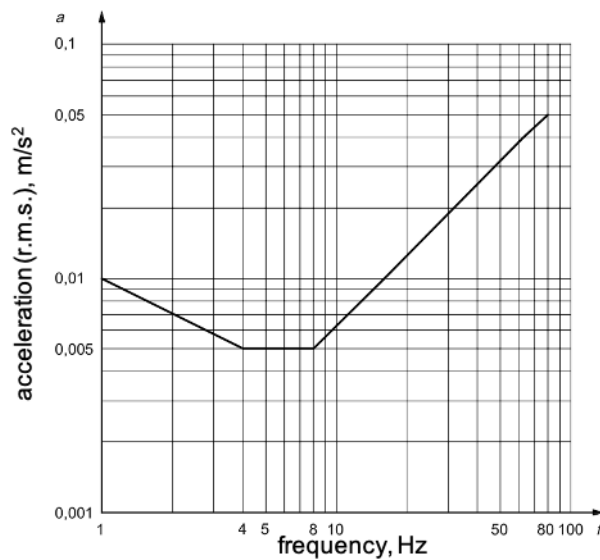


Figure 2. 28: Building Vibration Z-axis ‘Base Curve’ for Vibration (Foot-to-head Vibration Direction)

2.3.5.2 BS 6841 (1987): Measurement and evaluation of human exposure to whole-body mechanical vibration and repeated shock (0.5 to 80 Hz)

BS 6841 was prepared during the period when international agreement on the revision of ISO 2631-1:1997 had not yet been completed. ISO 2631-1:1985 has limitations, notably that it does not provide an adequate or widely accepted procedure for measuring vibration exposures and specifies vibration limits that are not generally accepted.

The primary differences between BS 6841 and ISO 2631-1:1985 include BS 6841's provision of a more comprehensive and clearly defined evaluation procedure, which does not specify vibration limits. BS 6841 also eliminates the complexity of time-dependency and introduces a method for assessing repeated shocks and intermittent vibration, known as the vibration dose value (VDV). Additionally, it offers a more detailed definition of the necessary frequency weightings.

The preferred method for assessing vibration exposure, the vibration dose value (VDV), can be applied to all types of vibration, including intermittent exposures and repeated shocks, as well as exposures consisting of vibrations at varying magnitudes. The VDV is calculated using the fourth root of the integral of the fourth power of the frequency-weighted acceleration:

$$VDV = \left(\int_0^T a^4(t) dt \right)^{\frac{1}{4}} \left[\frac{m}{s^{1.75}} \right] \quad (2.6)$$

When vibration conditions are constant or regularly repeated throughout the day, only one representative period (denoted as t_1) needs to be measured. The total vibration dose value for the day is then given by the fourth root of the fourth power of the VDV_1 (for the period t_1), multiplied by t_0/t_1 , where t_0 represents the total duration of vibration exposure:

$$VDV = \left(\frac{t_0}{t_1} \times VDV_1^4 \right)^{\frac{1}{4}} \left[\frac{m}{s^{1.75}} \right] \quad (2.7)$$

For days with multiple periods of varying durations (N periods), each with a measured or estimated vibration dose value (VDV_n), the total vibration dose value for the day is the fourth root of the sum of the fourth powers of the individual VDV's:

$$VDV = \left(\sum_{n=1}^{n=N} VDV_n^4 \right)^{\frac{1}{4}} \left[\frac{m}{s^{1.75}} \right] \quad (2.8)$$

Vibration should be measured according to a coordinate system centered at the interface with the body. The principal basicentric systems relevant to this are depicted in Figure 2.29.

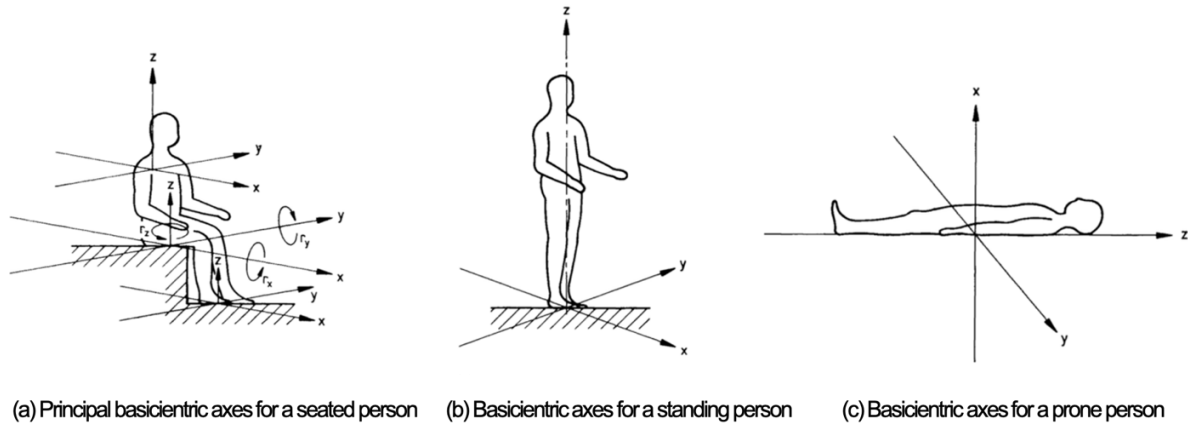


Figure 2. 29: Basicentric Axes of the Human Body

Frequency weightings, using band-limiting filters, can be applied through either analogue or digital methods. These are defined in a mathematical format familiar to filter designers and can be easily implemented using software such as MATLAB. For assessing vibration in relation to its impact on activities, BS 6841 (1987) recommends frequency weightings W_b for z-axis floor vibrations and W_d for x- and y-axis floor vibrations (as shown in Figure 2.30).

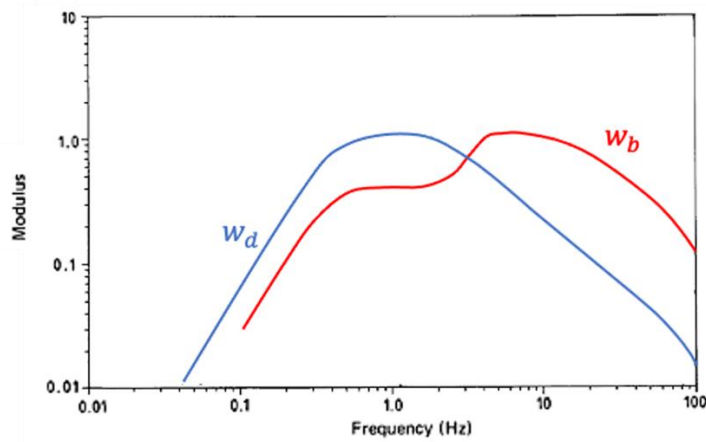


Figure 2 — Moduli of the frequency weightings with band-limiting filters

Figure 2. 30: Moduli of the Frequency Weightings with Band-limiting Filters

An alternative method for estimating VDV, known as the estimated vibration dose value (eVDV), is also provided. By applying a correction factor of 1.4 to the VDV, the total VDV for the day can be calculated using the fourth root of the fourth power of 1.4 times the measured weighted r.m.s. value, multiplied by the total duration, t_0 (in seconds), of vibration exposure:

$$eVDV = [(1.4 \times a)^4 \times t_0]^{1/4} \left[\frac{m}{s^{1.75}} \right] \quad (2.9)$$

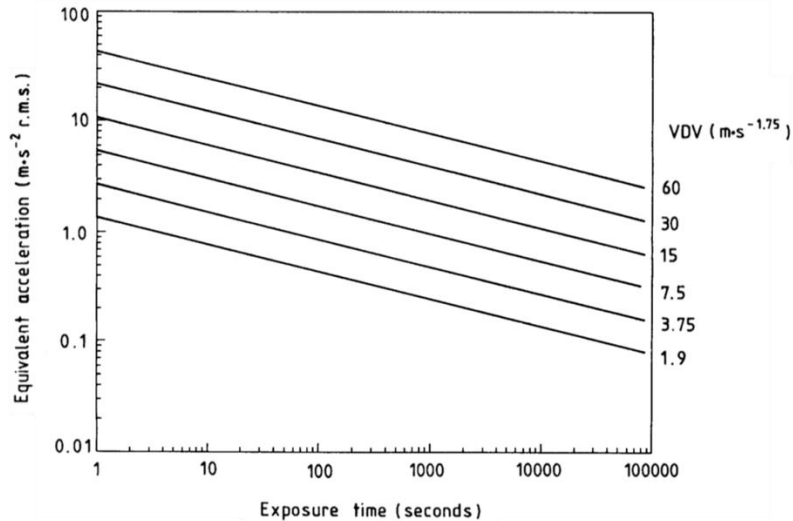


Figure 2. 31: Root-mean-square Acceleration Magnitudes Corresponding to Vibration Dose Values from $1.9 \text{ m}\cdot\text{s}^{-1.75}$ to $60 \text{ m}\cdot\text{s}^{-1.75}$ for Vibration Exposure Periods from 1 s to 24 h

2.3.5.3 BS 6472 (2008): Guide to the evaluation of human exposure to vibration in buildings (0.5 to 80 Hz)

Before the establishment of ISO 2631-2:2003, the slow progress toward developing an international standard for evaluating human reactions to building vibrations led the British Standards Institution to publish BS 6472:1992. This standard incorporated guidance from ISO 2631-2:1989 and was a simplified document. BS 6472:2008 has now superseded BS 6472:1992 and serves as the current standard, aligning with BS 6841:1987.

Figure 1(a) shows the weighting curve modulus for vertical acceleration, which demonstrates maximum sensitivity in the frequency range of 4 Hz to 12.5 Hz. A different weighting curve applies to horizontal vibrations, and its modulus is depicted in Figure 1(b), with sensitivity peaking between 1 Hz and 2 Hz. These weightings (for vertical motion) and (for horizontal motion) are defined similarly in BS 6841.

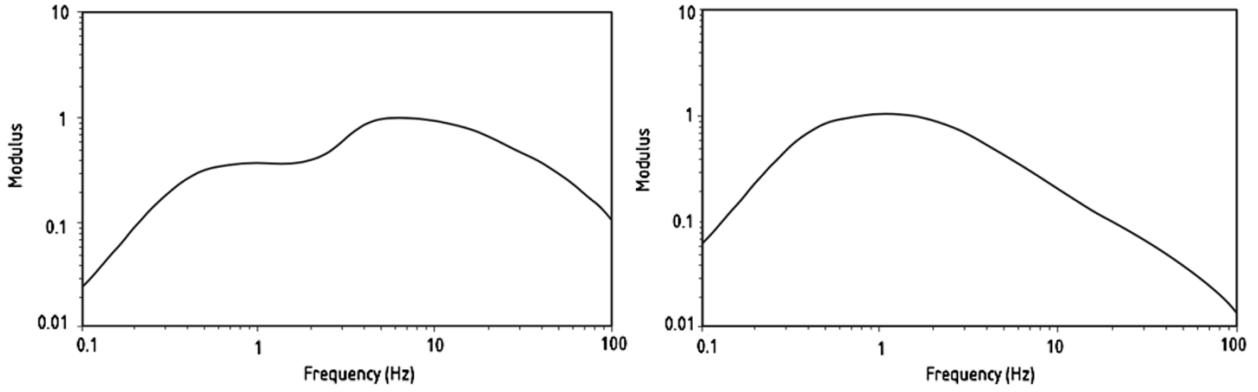
(a) W_b appropriate for vertical vibration(b) W_d appropriate for horizontal vibration

Figure 2.32: Frequency Weighting Curve for Vertical Vibration and Horizontal Vibration

The most significant difference between BS 6472:2008 and BS 6841:1987 lies in the time scale used for calculating the vibration dose value (VDV). While BS 6841 uses seconds as the unit of measurement, BS 6472 categorizes time into day (16 hours, from 7:00 to 23:00) and night (8 hours, from 23:00 to 7:00 the following day), depending on the occupancy of people in the building. The VDV calculation is based on vibration dose summation, where T represents the total duration (in seconds) of the day or night period during which vibration occurs:

$$\text{VDV}_{b/d, \text{ day/night}} = \left(\int_0^T a^4(t) dt \right)^{\frac{1}{4}} \left[\frac{\text{m}}{\text{s}^{1.75}} \right] \quad (2.10)$$

When vibration conditions are constant or regularly repeated throughout the day, only one representative sample, lasting τ seconds, needs to be measured. If the vibration dose value during this sample period is $\text{VDV}_{b/d, \tau}$, the total vibration dose value for the day ($\text{VDV}_{b/d, \text{ day}}$) is given by the equation:

$$\text{VDV}_{b/d, \text{ day}} = \left(\frac{t_{\text{day}}}{t_{\tau}} \right)^{\frac{1}{4}} \times \text{VDV}_{b/d, \tau} \left[\frac{\text{m}}{\text{s}^{1.75}} \right] \quad (2.11)$$

If there are multiple episodes of vibration during the assessment period, totaling N , each with a different duration (t_n) and corresponding vibration dose value ($\text{VDV}_{b/d, t_n}$), the total VDV for the day or night period is calculated by summing the fourth powers of the individual V DVs:

$$\text{VDV}_{b/d, \text{ day/night}} = \left(\sum_{n=1}^{n=N} \text{VDV}_{b/d, t_n}^4 \right)^{\frac{1}{4}} \left[\frac{\text{m}}{\text{s}^{1.75}} \right] \quad (2.12)$$

Once the appropriately-weighted vibration measurements have been obtained, the VDV for either the 16-hour daytime or the 8-hour nighttime period can be derived. Table 2.33 (Figure 2.33) provides a guide for interpreting these values in terms of human response. This table represents the best available judgments and applies to both vertical and horizontal vibrations, when the correct weightings are used.

Place and time	Low probability of adverse comment	Adverse comment possible	Adverse comment probable
Residential buildings 16 h day	0.2 to 0.4	0.4 to 0.8	0.8 to 1.6
Residential buildings 8 h night	0.1 to 0.2	0.2 to 0.4	0.4 to 0.8

"Note: For offices and workshops, multiplying factors of 2 and 4 respectively should be applied to the above vibration dose value ranges for a 16 h day." (BS 6472-1:2008)

Figure 2. 33: VDV Ranges which Might Result in Various Probabilities of Adverse Comment within Residential Buildings (BS 6472-1, 2008)

2.4 Floor Vibration Experimental Testing and Finite Element Modeling

Aloisio et al. (2023) found that researchers often favor experimental studies over finite element simulations when analyzing wooden structures. This preference arises due to the uncertainties associated with predicting the behavior of such materials, making experimental approaches more reliable. In timber vibration research, approximately 43% of studies are experimental, 11.7% are numerical, 25.1% combine both methods, and only 2.9% are purely theoretical (see Figure 2.34). The remaining research involves a combination of these methodologies.

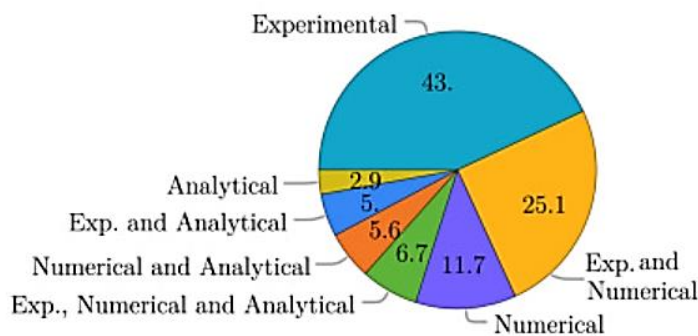


Figure 2. 34: Proportion of Researcher Methods in Timber Vibration

According to Aloisio et al. (2013), field monitoring and verification offer valuable data for validating numerical models and design methods. Consequently, there is a need for more field studies to assess

the actual dynamic response of composite flooring under real-life conditions and to compare it with predictions derived from analytical models.

Many studies primarily rely on acceleration response time histories from unreferenced heel drop, bouncing, and walking excitations. However, most of these lack sufficient field data and verified finite element models. Modal testing using high-cost equipment, such as an electrodynamic shaker, has been proven to yield high-quality data. For instance, Pavic and Reynolds (1999) assessed office floors through modal testing, comparing impact hammer excitation with shaker excitation while establishing quality assurance procedures. Their work was later extended by Reynolds and Pavic (2000a, 2000b) through further exploration of modal testing on building floors. Building on these findings, Hanagan et al. (2003) applied varied modal testing techniques and quality control procedures to a steel composite laboratory floor to determine optimal testing methods and provide guidelines for future research.

Barrett (2006) conducted high-quality dynamic tests on multi-bay steel composite office floors, offering detailed insights into both the equipment and experimental modal analysis methods. A full-scale model of the structure was constructed using SAP2000 software, and the experimental data from shaker testing was used to refine and update the model. Barrett emphasized that many finite element (FE) models, despite appearing sophisticated, often fail to fully utilize the available experimental data, impacting the accuracy of the models. He proposed a classification system for measurements: low objective tests, such as walking or heel drop, focus on frequency estimation, while high objective tests aim to develop detailed models for extensive use in simulations. Reliable FE modeling requires experience, sound assumptions, and accurate parameters, validated by high-quality experimental data.

Hu (2013) conducted laboratory studies on CLT floor slabs to investigate the effects of factors such as inter-slab connections, spans, support boundaries, ceilings, and toppings. Her research employed modal testing and subjective evaluations to assess natural frequency, damping ratio, and stiffness (measured as static deflection of 1.0 kN), along with human perception of vibration performance. Using a 2.5 kg hammer for impact excitation and sensitive accelerometers, Hu's findings showed that the damping of bare CLT floors was around 1%, significantly lower than the 3% damping found in traditional joisted wood floors. She also found that the span had a major influence on vibration, with shorter spans increasing frequency and reducing both acceleration and static deflection. Connections between CLT slabs, however, did not affect vibration parameters. Hu's study also found

that boundary supports increased structural frequency by 1 Hz, while ceilings added mass but not stiffness.

Casagrande et al. (2018) employed analytical, numerical, and experimental methods to assess the vibration performance of timber-concrete composite (TCC) and cross-laminated timber (CLT) floors. Using ISO 10137 and BS 6472, they simulated human walking to calculate vibration dose values (VDV). Both modal and walking tests were performed in the lab, with a 5.5 kg impact hammer used for floor excitation. Modal testing results indicated natural frequencies, mode shapes, and damping ratios, while the walking tests recorded acceleration responses. Field tests corroborated these findings, revealing consistent results between laboratory and on-site tests. The study confirmed that laboratory-based testing, when carefully replicated in the field, can provide accurate insights into the dynamic behavior of timber floors under human excitation.

Karampour et al. (2023) focused on modal testing of a CLT floor panel, collecting vibration responses at 24 positions using a modal hammer and accelerometer. Data acquisition was performed via LabVIEW, and the frequency response functions (FRF) were analyzed using MATLAB. For comparison, finite element modeling of the floor was conducted using ANSYS, with a 15% difference in fundamental frequency observed between the simulation and test. This discrepancy was reduced to 5% with finer meshing. The study also included walking tests on a lightweight joisted floor, comparing single and two-person walking paths. The root-mean-square (RMS) acceleration data revealed that, while unacceptable under ISO 2631 standards, the results were acceptable based on the VDV standard.

In summary, these studies highlight the importance of combining experimental, numerical, and analytical methods to validate finite element models and improve the accuracy of vibration predictions in timber and composite floor systems. The reviewed works emphasize the need for high-quality experimental data and appropriate modal testing techniques, as well as the value of integrating field studies with laboratory research to refine predictive models and methodologies.

2.5 Summary

Overview of Research on CLT Flooring and Vibration Serviceability

This chapter provides an overview of past research in the area of floor vibration serviceability prediction and assessment, emphasizing the necessity of field testing to better understand the vibrational performance of cross-laminated timber (CLT) flooring systems. The literature highlights

the current widespread use of CLT flooring and the existing research focus on their key characteristics, such as stiffness and damping.

Historical Context and Vibration Performance

Section 2.1 reviewed the history of CLT material application and its promotion, exploring the vibration performance of CLT floors. The aim is to encourage broader market adoption and reduce environmental impact. Despite the lightweight and high-strength properties of timber floors, concerns about vibration discomfort remain a major barrier to their widespread use.

Challenges in Addressing Vibration Discomfort

Resident complaints regarding vibration discomfort are common, as discussed in Section 2.2. The structure's characteristics and human perception of vibration are considered critical factors in addressing these discomfort issues. In assessing human perception of structural discomfort, two primary methods are commonly referenced: the acceleration-based Vibration Dose Value (VDV) method and the R-factor method. Although both methods have been widely adopted, ongoing debate persists within the industry and academia regarding which approach is more accurate and suitable for practical use.

Guidelines and Standards

Both Eurocode 5 (EC5) and its revisions (rEC5) offer key guidelines on timber structure characteristics, particularly concerning vibration performance. However, significant differences exist between older and newer specifications, which require further validation through practical application and testing by engineers and researchers.

Measuring Design Parameters

Although design standards such as EC5 provide parameters for assessing structural comfort, accurately measuring these parameters in real floors remains a persistent challenge. Discrepancies between measured data and the values provided in the specifications have generated significant interest among researchers. Diverse experimental setups, testing methods, and analytical techniques have led to various proposed control parameters and limits.

Gaps in Current Research

There is a clear gap in the literature, as few studies have developed calibrated finite element models (FEM) for CLT flooring systems based on high-quality modal test data. More specifically, the extent

of the discrepancy between the actual vibration characteristics of wooden floors and established evaluation standards remains unclear. Resolving this discrepancy requires the precise measurement of structural parameters as outlined in the specifications and bridging the gap between field test results and numerical simulations by refining correction standards. Collecting empirical data to validate and improve the standards outlined in the specifications is essential for ensuring their accuracy and relevance.

3. Floor Testing Methods and Experimental Modal Analysis

3.1 Standards for Timber Floor Test Methods

3.1.1 ISO 18324 (2016): Timber structures - Test methods - Floor vibration performance

This International Standard specifies procedures for measuring natural frequencies, modal damping ratios, and static deflection under concentrated loads for both joisted floors and plate-like timber slab floors, such as cross-laminated timber (CLT) floors, in laboratory or field settings.

Key Aspects of the Shaker Test:

- **Test Equipment:** Modal testing requires three essential components: a shaker to induce vibration, transducers to measure the excitation force and vibration response, and a signal analyzer to record and process the signals, extracting relevant information.
- **Selection of Excitation Location:** The exciter should not be placed at nodal points of the modes of interest and should be positioned near the floor's center to ensure excitation of the first natural frequency. For plate-like timber slab floors (e.g., CLT), accelerometers must be placed at the center of each timber panel and at the joints between adjacent panels along equally spaced rows.
- **Excitation Signal and Response Recording Requirements:** Random excitation should be applied to the test floor. To prevent signal leakage, the Hanning window is recommended for processing the response signals. Typically, averaging at least five frequency response function (FRF) measurements is sufficient to remove background noise. The measurements should be validated using the coherence function.
- **Sampling Frequency and Resolution:** To ensure accurate measurement of natural frequencies, the setup must be configured to ensure that the frequency resolution (ΔF) is no greater than 1% of the lowest natural frequency of interest. The sampling frequency should be at least twice the highest frequency of interest to capture all target frequencies of the test floor.

Key Aspects of the Impact Test:

- **Excitation:** Impact excitation can be generated using various methods, including hammer, ball drop, or heel drop. A rectangular window should be applied to the impact force signal to reduce noise in the analysis.

- **Response Signals:** An exponential window should be applied to the transient response signals to prevent truncation errors during FFT processing and to reduce the effects of leakage and noise in frequency response measurements. Any damping in the measured response signals due to the exponential window must be corrected.

3.1.2 BS EN 16929(2018): Test methods - Timber floors - Determination of vibration properties

This document specifies test methods for determining natural frequencies, damping ratios, unit point load deflection, and floor acceleration in sawn timber, engineered wood products, and mass timber beams or slabs (e.g., cross-laminated timber [CLT], glued laminated timber [GL], nail-laminated timber). The methods apply to floors with or without concrete screeds, as well as to timber-concrete composite floors.

The primary distinction between ISO 18324:2016 and BS EN 16929:2018 lies in their structural organization. While BS EN 16929:2018 is structured around laboratory and in-situ testing, ISO 18324:2016 classifies tests by shaker and impact methods. Some aspects of in-situ testing overlap with indoor tests. The parameters to be tested for in-situ testing include the following:

Determination of Natural Frequency:

An impact load can be applied using an impact hammer, heel drop, or rubber ball drop. The load should be applied at a location where the largest deformations are expected to ensure that the first natural frequency is excited. Accelerometers should be positioned 300–500 mm away from the point of impact. Test data should be continuously recorded for at least 10 seconds after impact, with a minimum sampling rate of 500 Hz. The individual fundamental frequencies and the average frequency for each test case must be reported.

Determination of Damping Ratio:

The floor should be excited either by a mechanical exciter or a stepping person. The damping ratio can then be calculated based on the exponentially decreasing amplitude. In some cases, an exponential window may need to be applied to the time-domain signal.

Determination of Floor Acceleration:

Acceleration response can be measured using either an exciter or a stepping person.

- **Method 1:** The exciter should be positioned at the mid-span of the floor for single-span floors or at the location where the largest accelerations are expected. The exciter must not be placed at or near nodal points, as these points exhibit minimal vibration. The exciter should generate a sinusoidal wave signal, with an excitation force typically ranging from 50 N to 200 N.
- **Method 2:** A metronome should be used to maintain a consistent step frequency. The test person should stand at the geometrical center of the floor for single-span floors or at the location where the largest accelerations are expected. The individual should step for at least 10 seconds to reach steady-state vibration and remain still during the decay period. A two-second period, during which the highest vibration is observed, should be selected for analysis. The data is filtered into third-octave bands, and the results are weighted according to the frequency weighting factors (w_k) outlined in ISO 2631-1:2003.

3.2. Experimental modal testing

3.2.1 The Role of Modal Testing in Experimental Investigation

The experimental study of structural dynamics has long made significant contributions to our understanding and control of various vibration phenomena encountered in practice (Ewins, 2009).

The necessity of experimental research can be categorized into the following three areas:

- Determining the nature and extent of vibration response levels exhibited by structures under real operating conditions;
- Verifying theoretical or computational models and their underlying assumptions;
- Measuring material and structural properties under dynamic loading, including material damping, natural frequency, and mode shapes.

Modal testing is crucial for obtaining comprehensive insights into a system's structural properties, such as natural frequencies, damping ratios, and mode shapes. As a method for data acquisition in modal analysis, experimental modal testing has become widely accepted in fields such as mechanical and structural engineering, with applications ranging from design and optimization to validation (Fu and He, 2001). Its use extends across various industries, including automotive, civil engineering, aerospace, power generation, and even musical instrument design.

Experimental modal analysis (EMA) consists of two primary stages: data measurement and analysis. The measurement phase refers to the acquisition of Frequency Response Function (FRF) data, while

the analysis phase involves applying curve-fitting techniques to construct the models necessary for modal parameter identification (Sehgal and Kumar, 2016).

3.2.2 Modal Testing Theory

A review of the theoretical foundation of structural vibration is essential, as it forms the basis for subsequent studies in measurement techniques, signal processing, and data analysis. The theory of modal testing and analysis has been extensively documented by Ewins (2009). Although few practical structures can realistically be modeled as single-degree-of-freedom (SDOF) systems, understanding the properties of such systems remains crucial. This is because complex multi-degree-of-freedom (MDOF) systems can often be represented as a linear superposition of SDOF characteristics (Edwin, 2019). Figure 3.1 illustrates a typical SDOF system.

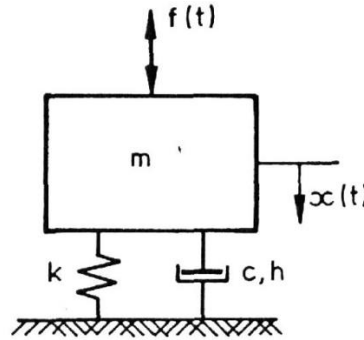


Figure 3. 1: Single-degree-of-freedom (SDOF) System

In this model, the force and displacement response are represented by $f(t)$ and $x(t)$, respectively. The system comprises a mass m , a spring k , and a viscous damper c , if damping is considered. The governing equation of motion is as follows:

$$m\ddot{x} + c\dot{x} + kx = f(t) \quad (3.1)$$

To analyze forced response, we consider excitation of the form $f(t) = Fe^{i\omega t}$ and assume a solution of the form $x(t) = Xe^{i\omega t}$, where X and F are complex quantities representing both amplitude and phase. The receptance frequency response function (FRF), which is the ratio of harmonic displacement to harmonic force, can be similarly defined for acceleration, a parameter often measured in tests. This FRF parameter is known as accelerance.

$$k - \omega^2 m + i(\omega c) = 0 \quad (3.2)$$

$$H(\omega) = \frac{X}{F} = \frac{1}{k - \omega^2 m + i(\omega c)} \quad (3.3)$$

In this case, $[M]$, $[C]$, and $[K]$ represent the mass, damping, and stiffness matrices, while $\{x\}$ and $\{f\}$ are the displacement and force vectors. The damped system's eigenvalues and eigenvectors describe the mode shapes and critical damping ratios.

$$[M]\{\ddot{x}(t)\} + [C]\{\dot{x}\} + [K]\{x\} = \{f\} \quad (3.4)$$

The usual definition of proportional damping is that the damping matrix $[C]$ should be of the form:

$$[C] = \beta[K] + \gamma[M] \quad (3.5)$$

In this case, the damped system will have eigenvalues and eigenvectors as follows:

$$\omega'_r = \bar{\omega}_r \sqrt{1 - \zeta_r^2} \quad ; \quad \zeta_r = \frac{\beta \bar{\omega}_r}{2} + \frac{\gamma}{2\bar{\omega}_r} \quad (3.6)$$

and

$$[\Psi_{damped}] \quad (3.7)$$

where $\bar{\omega}_r$ is the r^{th} mode eigenvalue, ζ_r is the r^{th} mode critical damping ratio and $\{\Psi_r\}$ is a description of the corresponding mode shape.

Consider a linear system, as illustrated in Figure 3.2. The transfer function, no matter how complex, acts as a 'black box' that relates the external force to the corresponding structural response. Modal analysis aims to extract dynamic parameters from this 'black box,' including mass, stiffness, damping, frequency, and mode shape.

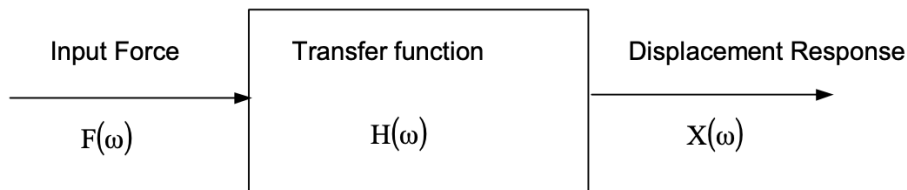


Figure 3. 2: Transfer Function Block Diagram

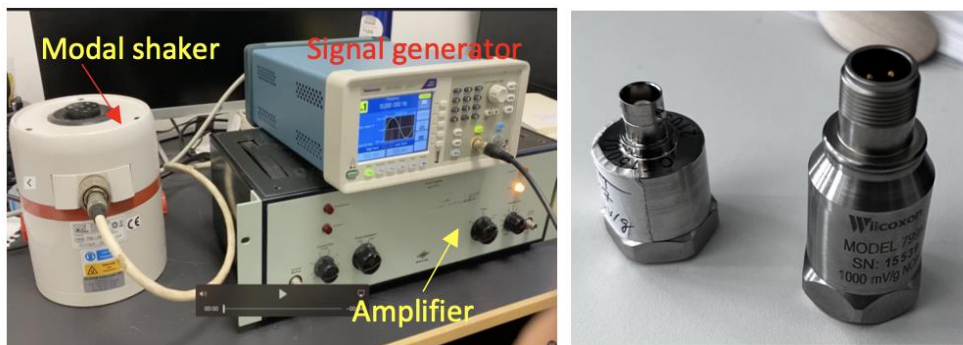
3.3. Measurement of vibration

3.3.1 Modal testing Using Modal Shaker

Shakers provide controlled and measurable vibration input into test structures and are essential for accurate modal testing. In this research, modal testing was conducted using a Brüel & Kjær (B&K) high-force LDS V406 permanent magnet shaker, as shown in Figure 3.3(a). The shaker has a body mass of 14.1 kg and was securely fastened to the floor to prevent any accidental movement, which could damage both the structure and the shaker.

An amplifier and signal generator (Figure 3.3(a)) were connected to the shaker to generate a sweep sine signal, with the excitation signal sweeping from 0 to 30 Hz. It is critical to ensure that the amplifier covers the full frequency range of the shaker and is compatible with the shaker’s impedance, which, for electrodynamic shakers, is typically around 2.5 Ω .

The response was measured using ICP accelerometers (Figure 3.3(b)), with a measurement range of 0-10g and a sensitivity of 100 mV/g. Two WebDAQ data loggers, each with 4 channels, were connected to the shaker and accelerometers, forming the data acquisition system. Additionally, the WebDAQ 504 data logger was connected to two standard laptop computers for real-time recording and analysis of test data (Figure 3.4). This setup allowed continuous monitoring of data quality during testing.



(a) shaker, amplifier and signal generator (b) sensors

Figure 3. 3: Modal Shaking System and Accelerometers Used



Figure 3. 4: Laptops for Data Monitoring

A complete modal shaker setup includes several key components, as illustrated in Figure 3.5. These components consist of the shaker, transducers, accelerometers, shaker amplifier, and signal generator, as well as various electronic devices integral to the data acquisition system. During testing,

the accelerometers mounted on the structure transmitted data through signal conditioning, which is now built into modern data loggers.

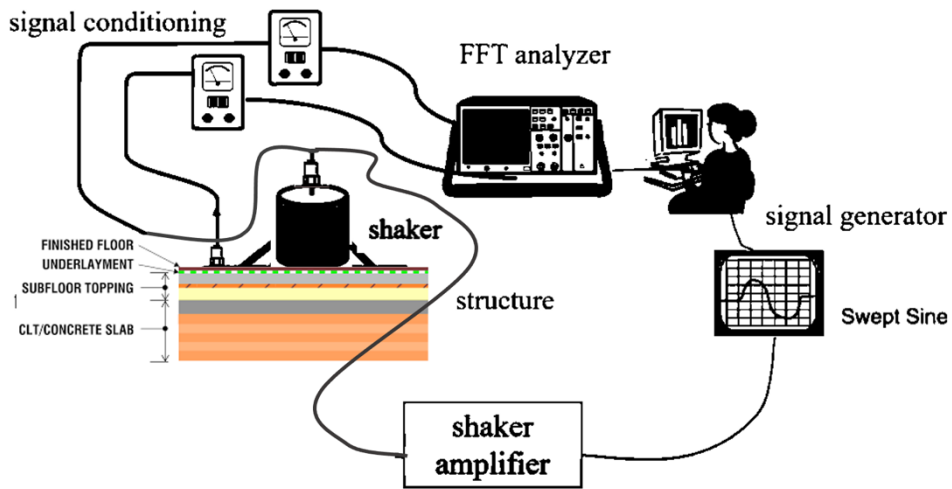


Figure 3. 5: Shaker Testing Setup

Due to the limited number of accelerometers available, the roving accelerometer method was employed (Figure 3.6). This method involves moving the accelerometer between different test points on the structure to gather data from multiple locations, while ensuring that the shaker or hammer impacts the structure at the same fixed point.

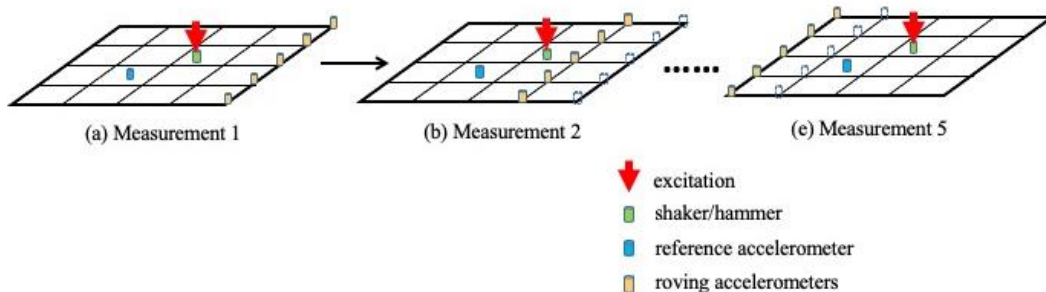


Figure 3. 6: Roving Sensor Test Method

This experimental setup ensures precise control of vibration inputs and accurate measurement of dynamic responses, facilitating detailed modal analysis of the test structure.

3.3.2 Modal Testing Using Impact Hammer

An alternative method of excitation commonly employed is the use of an impact hammer, which provides a relatively simple means of exciting a structure into vibration (Figure 3.7). In this research, a 0.16 kg ICP[®] instrumented impact hammer was used, and a heavier hammer tip was required to ensure sufficient force to excite the desired modes of the floor. The magnitude of the impact is

determined by the mass of the hammer head and the velocity at which it strikes the structure. Care must be taken to avoid missing a response from certain modes, particularly when ensuring that the stationary hammer input is not placed at a nodal point where the response would be minimal.



Figure 3. 7: Impact Hammer Used in Testing

When the hammer tip impacts the test structure, the structure experiences a force pulse, typically in the form of a half-sine wave, with a duration denoted as T_c (Figure 3.8a). The corresponding frequency content of this pulse is illustrated in Figure 3.8(b), showing a relatively flat spectrum up to a cut-off frequency (f_c), after which the signal diminishes and becomes uncertain.

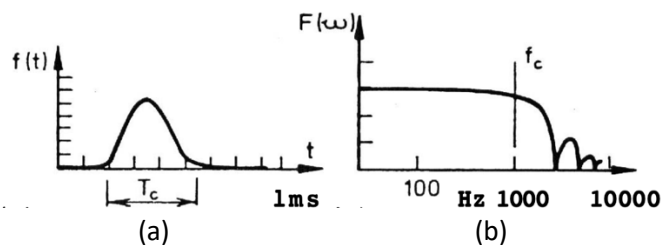


Figure 3. 8: Typical Impact Force Pulse and Spectrum

The stiffness of the test surface affects the pulse duration (T_c) and the frequency range (f_c) covered by the impact. A stiffer surface leads to a shorter pulse duration and a higher frequency range. Conversely, softer hammer tips increase the effective frequency range. Therefore, selecting the appropriate hammer tip is critical, depending on the frequency range of interest. A set of different hammer tips (Figure 3.8) can be used to ensure optimal excitation within the desired frequency range.



Figure 3.8: Modal impact hammers come with a variety of tips (rubbers, plastic, and metal)

The selection of proper hammer tips can be guided by the force spectrum shown in Figure 3.9. A significant drop in the input spectrum indicates that the tip may be too soft. If the hammer is too

hard, it may excite frequencies beyond the range of interest, potentially wasting energy on irrelevant modes.

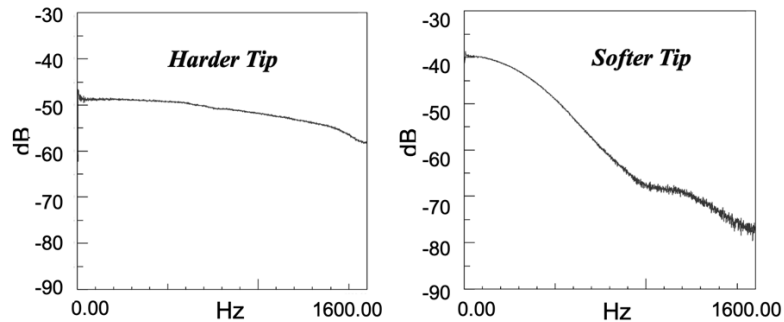


Figure 3. 9: Force Spectrum of Different Hammer Tips

The impact hammer testing procedure, as illustrated in Figure 3.10, can be summarized as follows:

1. Attach the hammer and roving accelerometer to the multi-channel DAQ device.
2. Configure the data acquisition equipment, including setting the sample rate and performing the necessary calibration to ensure the recorded signal units match the hardware setup.
3. Wait for the trigger signal and then impact the floor with the hammer at least 10 times, ensuring a minimum interval of 10 seconds between impacts.
4. Assess the quality of each impact to identify any double impacts, which are common during hammer testing and can distort the excitation spectrum.
5. Repeat the roving process across the test area to ensure sufficient data is collected from multiple locations.

This process allows for accurate excitation of the test structure and ensures that the desired frequency range is covered efficiently.

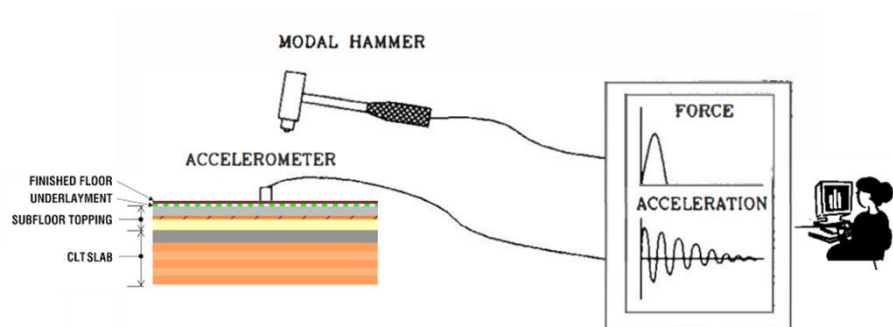


Figure 3. 10: Hammer Test Setup

3.3.3 Heel Drop Test

Heel impact testing is performed to determine the dynamic properties of a floor system. This method has been widely utilized over the past three decades and is incorporated into many proposed design procedures (Allen, 1974; Murray, 1975; Blakeborough, 2003; Azaman et al., 2018). The primary

advantage of the heel drop method is its simplicity, as it requires no expensive equipment. However, a limitation of this method is that it is an output-only test, meaning that only the floor's response is measured, without providing direct input force data. The test is performed by an individual rising onto their toes and then dropping their heels to strike the floor.

In the heel drop test depicted in Figure 3.11, the same participant stood at the location of maximum estimated floor displacement response. To ensure accurate measurements, it is important to position the sensor at an appropriate distance from the impact point to maximize the recorded response while avoiding interference with the sensor's operation. During the test, the participant raised their heels to a specific height before executing the drop. Although some literature suggests a height limit of 64 mm (Allen and Rainer, 1976), maintaining this exact height consistently during practical testing is challenging. Consequently, in this study, the participant was instructed to exert maximum effort to ensure consistent stimulation with each heel drop.

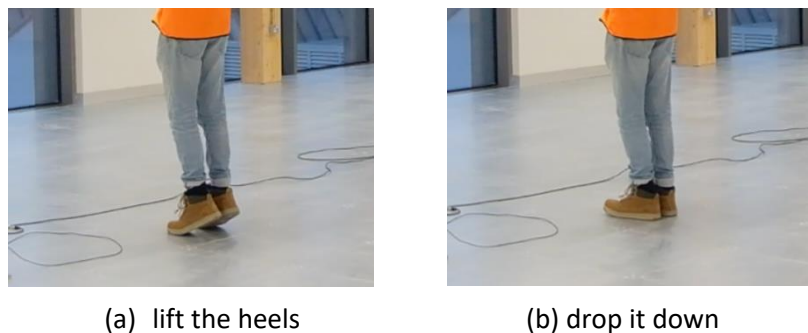


Figure 3. 11: Heel Drop Test

The heel drop was performed by a participant weighing 66 kg, followed by a 10-second interval to allow the response to decay fully. To ensure data accuracy, a minimum of eight measurements were conducted (Figure 3.12 (a)). The analysis of response signals indicated that the initial and final phases of the heel drop should be disregarded for averaging purposes, as these phases are less stable. Instead, the stable signals from the middle phase of the response were selected for averaging. The spectral analysis (Figure 3.12 (b)) showed that the heel drop method effectively excites the frequency structure of interest within the 0 to 30 Hz range.

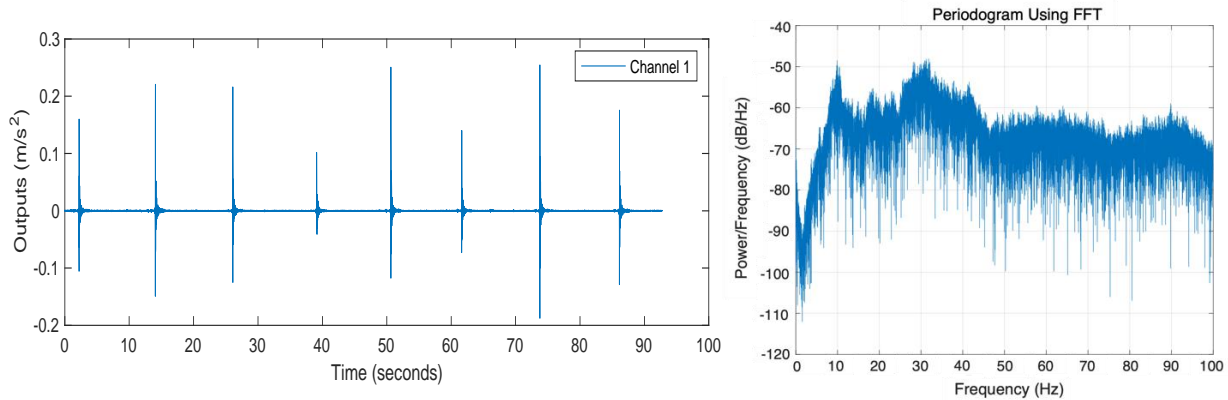


Figure 3. 12: Acceleration Response and Spectrum of Heel-Drop Test

Some researchers have developed force plates to measure the force generated by heel drops. However, results may vary due to differences in the performance of individuals conducting the test. Based on a review of the relevant literature, the key parameters of the heel drop test are summarized in Table 3.1.

Table 3. 1: Heel Drop Test Used by Different Researchers

Author	Heel drop force	Individual weight	Heel drop point	Times repeat	Duration for each heel drop
Azaman, 2018	Measured without method	75 kg	100mm from the centre point	10 times	1s
Zhou et al., 2016	Not measured	70 & 57 kg	at the centre of the test floor	3 times	8s
Blakeborough and Williams, 2002	Measured with a built load cell plate: four load cells sandwiched between aluminium alloy plate	75 kg	In the middle of the floor	10 times	4s
Hanagan and Murray, 1997	Measured with a force plate, constructed of four load cells supporting a 406mm square steel plate	86.1kg	at the centre of the test floor	Not mention	8s
This research, 2023	Not measured	66 kg	At centre of the test floor	8 times	10s

3.3.4 Walking and Running Test

Walking and running tests were conducted to determine acceleration levels across the floor. The participant, weighing 66 kg, as in the heel drop test, was instructed to walk at specified paces using a metronome. Two walking frequencies were tested: 1.5 Hz and 2 Hz. Frequency domain analysis revealed that the running frequency was approximately 2.89 Hz. The participant walked back and forth near the center of the floor, parallel to the span direction. The duration of each walk varied depending on the floor span within the testing range, typically requiring at least one round trip. As

shown in Figures 3.13, 3.14, and 3.15, the participant completed two round trips when walking at 1.5 Hz, more than two when walking briskly at 2.0 Hz, and four round trips while running. The spectrograms indicate that both walking and running activities effectively excited multiple modes in the test floor area within the frequency range of 0 to 30 Hz.

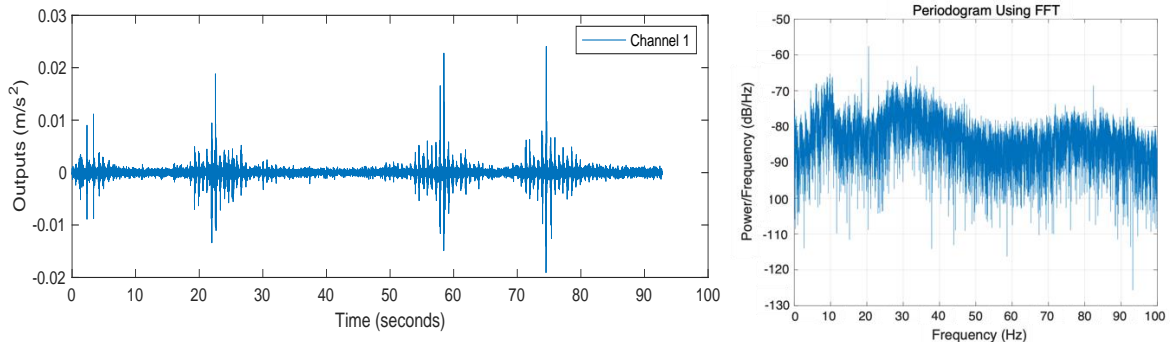


Figure 3. 13: Acceleration Response and Spectrum of Walking at 1.5 Hz

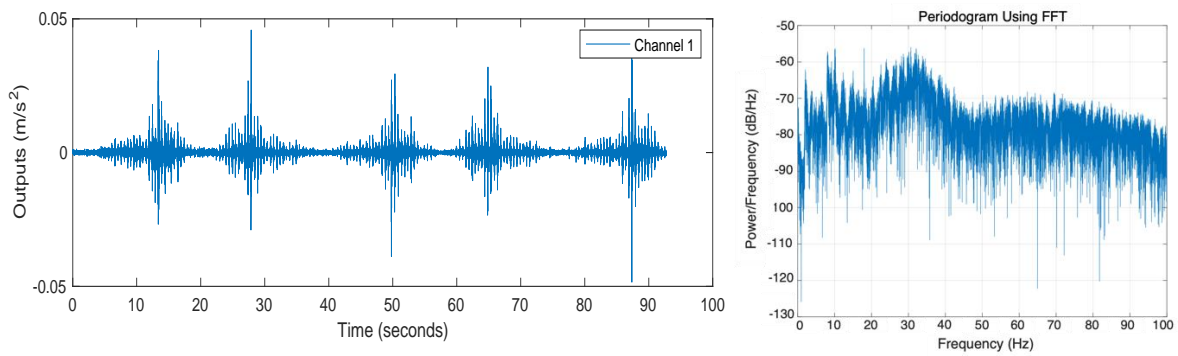


Figure 3. 14: Acceleration Response and Spectrum of Walking at 2.0 Hz

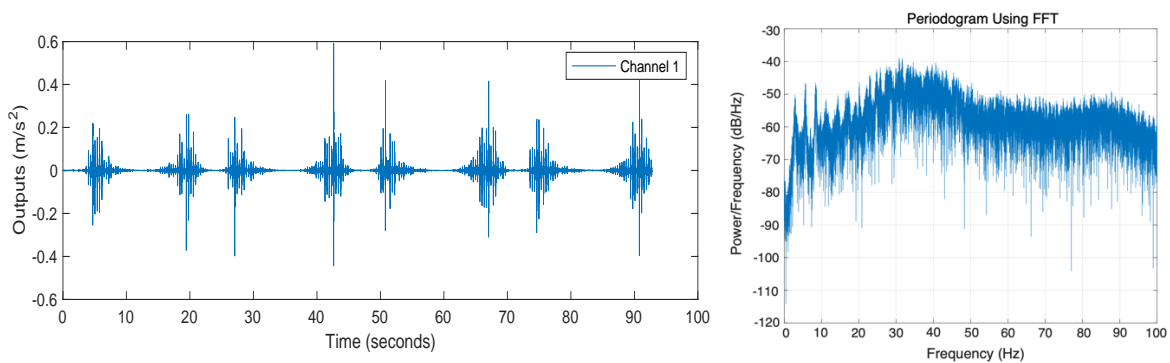


Figure 3. 15: Acceleration Response and Spectrum of Running at 2.89 Hz

The choice of walking path is an important factor in the study of floor vibrations (Hicks and Smith, 2011). The selected path can traverse several mode amplitudes of a modal shape, potentially leading to a resonant or near-resonant response (Muhammad et al., 2018). Hicks (2014) observed that the selection of the walking path might depend on which mode requires excitation. Reynolds and Pavic

(2003) investigated possible corridor layouts and future floor uses to explore potential walking paths. Ideally, selecting a path through the center of the floor maximizes excitation of the first and second vibration modes. However, in practical on-site measurements, the walking path may need to be adjusted to avoid obstacles such as equipment or construction materials. As a result, the chosen path may not always intersect with the middle of the floor area under test.

3.4. Model Analysis Process in MATLAB

3.4.1 FRF Data

A **frequency response function (FRF)**, also known as a transfer function, is defined as the ratio of output to input data in a system. In experimental investigations, FRF serves two main purposes:

- **Identifying the resonant frequencies, damping, and mode shapes** of a physical structure.
- **Describing the relationship** between the input (x) and output (y) of a linear, time-invariant system.

The mathematical formulation of FRF, $H(\omega) = X/F$, is presented using a Bode plot in Figure 3.16, which illustrates the separation of peak values in an ideal FRF. It is important to note that field tests may not always produce ideal results, particularly when compared to in-situ tests, due to environmental factors such as noise and unexpected events.

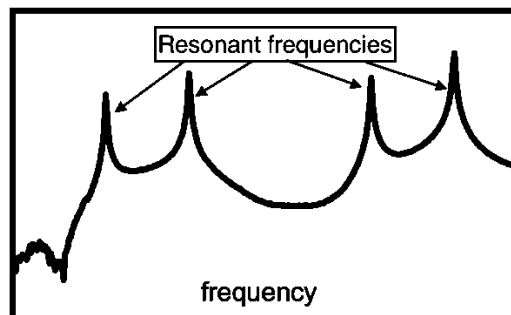


Figure 3. 16: Bode plot of FRFs

FRF is calculated using time-domain data, as illustrated in Figure 3.17, which outlines the full process of generating an FRF from time-streamed data. In this experimental investigation, field tests were conducted on various CLT floor areas. Time-domain data from both the input and output were recorded simultaneously. To minimize signal aliasing and noise, windows and averaging techniques were applied. The data were then transformed into the frequency domain, and the resulting spectrum was used to calculate the final FRF and coherence functions.

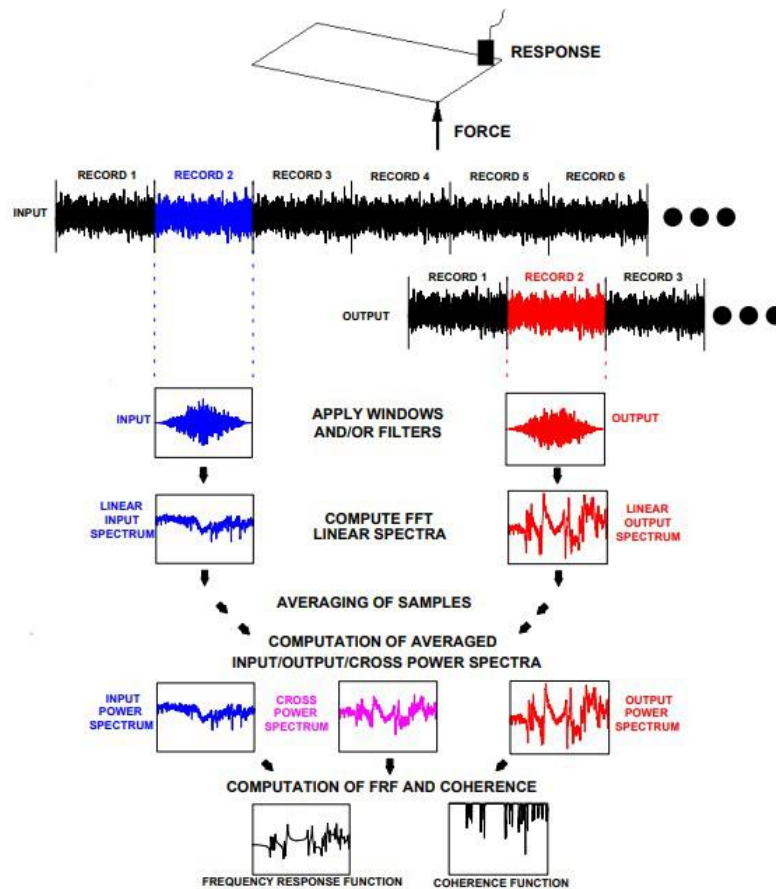


Figure 3. 17: Schematic Overview of FRF from Time Streamed Data

3.4.2 Preliminary Check of FRF Data

The **coherence function** is a critical tool used to ensure the quality of data collected during FRF measurements. It indicates how much of the output response is attributable to the input excitation, thereby serving as a measure of the quality of the FRF. The coherence function (Figure 3.18) takes values between 0 and 1, where:

- A coherence value of 1 at a specific frequency indicates a high-quality measurement or FRF.
- A value of 0 at a specific frequency suggests poor measurement quality.
- A coherence value above 0.8 is generally considered indicative of reliable, high-quality data.

As shown in the coherence function diagram below, the quality of the FRF across the entire frequency range can be assessed by examining the coherence values. When the amplitude of the FRF is very low, such as at anti-resonance, the coherence tends to be close to 0. This is expected, as little or no output is excited by the input at the anti-node. Conversely, at resonance, the coherence value will typically approach 1, indicating that the input excitation is effectively driving the system.

In Figure 3.18, the left diagram represents a high-quality FRF measurement, with coherence values close to 1, while the right diagram illustrates a poor-quality FRF, characterized by noisy data and low coherence values.

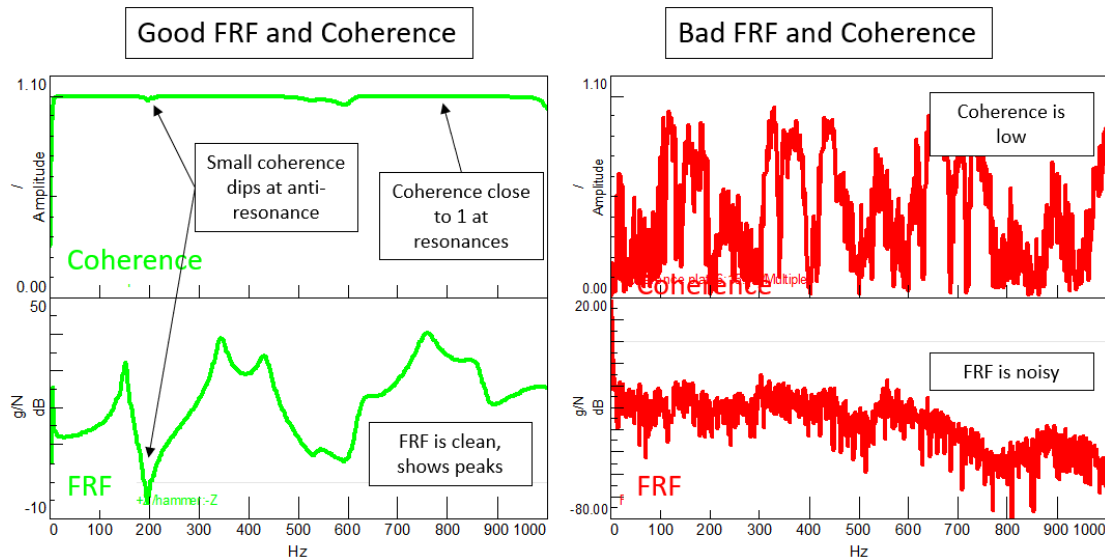


Figure 3. 18: A Good FRF Measurement and a Bad FRF Measurement

3.4.3 Pre-processing of time streamed data in MATLAB

After collecting the testing data from all test floors, the time-streamed data was classified into labeled fields (Exp1, Exp2..., ExpN), where each label corresponds to a specific test floor (Figure 3.19). Each experiment label (Exp1 to ExpN) contains a structure with vectors yyy and uuu, representing the measured responses and the corresponding input force data, respectively.

```
Data =
Time domain data set containing 4 experiments.

Experiment   Samples      Sample Time
Exp1         600000      0.000488281
Exp2         600000      0.000488281
Exp3         600000      0.000488281
Exp4         600000      0.000488281

Outputs      Unit (if specified)
y1
y2
y3

Inputs      Unit (if specified)
u1
```

Figure 3. 19: Data Pre-processing in MATLAB

As illustrated in Figure 3.20, the input signal from the modal shaker was repeated 10 times, with each period lasting 30 seconds, resulting in a total testing duration of 300 seconds (10 x 30). To calculate the average response, nine segments of the input excitation were used, with the first

segment excluded due to its irregularities. This approach helps to minimize noise in the averaged signal and ensures more accurate results.

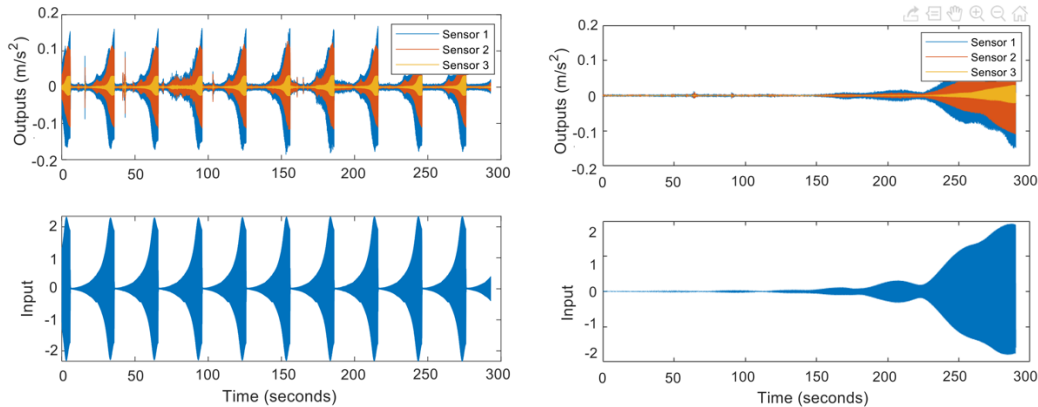


Figure 3.20: Experimental Time Streamed Data of Output and Input: (a) Raw data (b) Averaged data

3.4.4 Modal Parameter Extraction (Curve-fitting) Methods

Curve fitting methods can be categorized based on the form of data they use: frequency-domain methods, which analyze frequency response functions, and time-domain methods. Additionally, modal analysis can be classified by the number of modes extracted at once—either a Single Degree of Freedom (SDOF) or Multiple Degrees of Freedom (MDOF) approach.

This research primarily utilized the MDOF method to address the challenge of identifying adjacent modes, which occurs when structures exhibit closely spaced natural frequencies or, in some cases, identical modes. To accurately resolve these modes, it is necessary not only to apply the MDOF method (which extracts multiple modes simultaneously) but also to perform multi-curve analysis, allowing for a more comprehensive comparison of modal responses.

3.4.4.1 Non-Linear Least-Squares (NLLS) Method

The least squares method is a classical multi-degree-of-freedom (MDOF) modal analysis approach that numerically fits measured frequency response function (FRF) data using analytical expressions. It minimizes the least squares error to achieve the best fit between the test data and the mathematical model.

Principles of MDOF Curve-Fitting:

In MDOF curve fitting, individual FRF measurement data is collected, while the corresponding theoretical values are represented by unknown coefficients. An individual error is calculated at each frequency point of interest, and a weighting factor can be applied to increase generality. The curve-

fitting process aims to determine the values of the unknown coefficients that minimize the total error. This is accomplished by differentiating the error expression with respect to each unknown, resulting in a set of equations equal to the number of unknowns. Most solution methods rely on iterative solving, with some methods linearizing the expressions to simplify the problem. Almost all methods depend on an accurate initial estimate.

Example:

Consider a simple model equation, $y(t) = A_1 \exp(r_1 t) + A_2 \exp(r_2 t)$, where A_1 , A_2 , r_1 , and r_2 are unknown parameters, y is the response, and t represents time. Given data points for time (t_1, t_2, \dots, t_n) and noisy response measurements (y_1, y_2, \dots, y_n), the goal is to find the values of A and r that minimize the squared error $\sum (y(t) - y_{data})^2$.

Modal Curve-Fitting in MATLAB:

Modal curve fitting is based on measured FRF data, and various methods in MATLAB's toolbox are applied to construct a mathematical function that best fits the data points. MATLAB commands such as `n4sid` and `ssest` can be used to solve more complex versions of this problem, as shown in Figure 3.21. The primary advantage of the frequency-domain method is its intuitive nature. The distribution of the modes and rough estimates of modal parameters can be directly observed from the measured FRF curves.

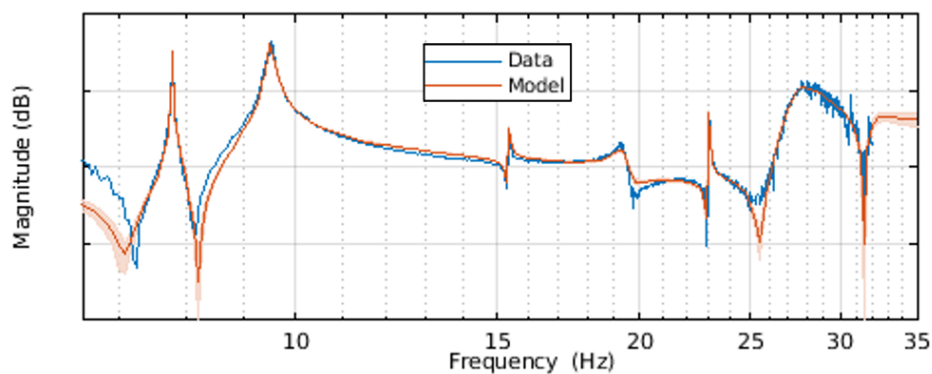


Figure 3. 21: Fit between Data and Model using NLLS Method

However, the key issue in identifying modal parameters using this method lies in the quality of the measured FRF data. High-quality data ensures accurate identification of modal parameters, regardless of the identification method used. Conversely, if the measured FRF data is poor, even the best identification methods will yield inaccurate results.

3.4.4.2 Complex Exponential (CE) Method

The complex exponential (CE) method is a time-domain method that uses system response data to estimate modal parameters. This method is derived from the 'complex exponential' technique, with several refinements introduced to enhance computational efficiency, particularly for smaller computer systems. One of the key advantages of the CE method is that it does not require initial estimates of the modal parameters, making it more robust. However, its primary drawback is the need for multiple iterations to accurately identify the correct modal order, a process that can be time-consuming.

The CE method is grounded in the principle that the free vibration response or impulse response function of a structure can be expressed as a sum of complex exponential functions. The unknown parameters of the system can then be determined using linear methods. The core idea involves establishing a relationship between the dynamic response and the modal parameters, based on the principle of modal superposition in the vibration equation. The impulse response function is then fitted to extract the complete set of modal parameters, yielding accurate results.

The complex exponential (CE) method is typically applied as follows. First, an initial estimate of the number of degrees of freedom (DOF) is determined, and the corresponding modal analysis is performed. The modal properties obtained from this analysis are then used to formulate the receptance frequency response function (FRF). A regenerated FRF curve is computed and compared to the original measured data, allowing the deviation or error between the two curves to be calculated.

The process is repeated with different assumed values for the number of degrees of freedom (e.g., $2N$), and the error is recalculated. As the correct number of degrees of freedom is approached, a significant reduction in the error should be observed. Figure 3.22 illustrates the fitted response generated using the CE method in this research.

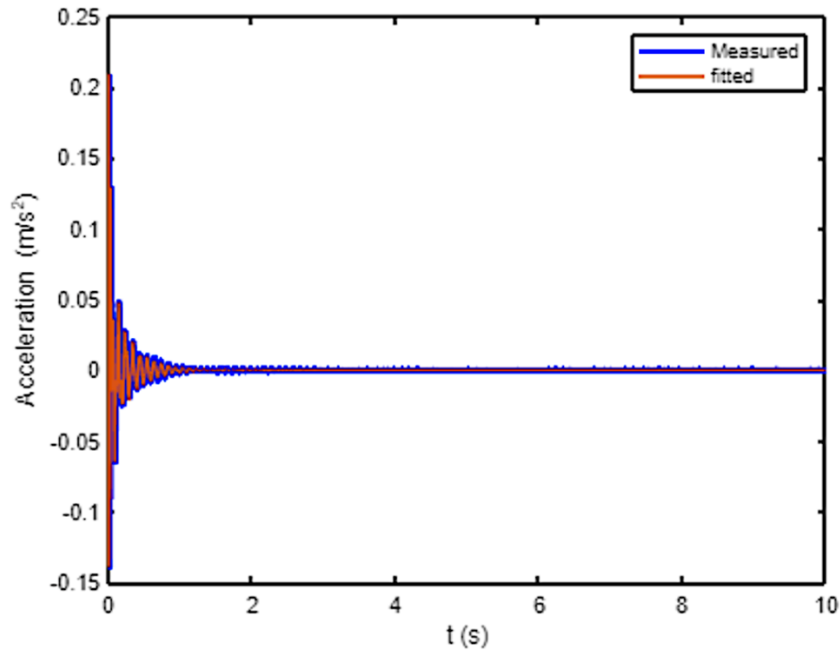


Figure 3. 22: Fitted Time History using CE Method

3.4.5 Modal Parameter Extraction from FRF in MATLAB

The modal analysis process consists of two key stages: first, identifying the appropriate type of model, and second, determining the approximate parameters of the chosen model. The majority of effort is devoted to the second stage. Modal identification, which includes modal curve fitting and modal parameter estimation, is a methodology for constructing mathematical models of dynamic systems based on input and output signal measurements. The process of modal identification involves the following steps:

- Estimating values for adjustable parameters in the selected model structure using an appropriate estimation method.
- Evaluating the estimated model for adequacy. Using a Stabilization Diagram as a guide, the optimal mathematical model—describing the system's frequencies, damping, and mode shapes—can be identified from the FRF data set.

The labeled and averaged input and output data from the pre-processing phase are subsequently used for further FRF analysis. Once the FRF curves are acquired, they are analyzed to identify modal frequencies, damping ratios, and mode shapes, a process known as modal curve fitting. Modal curve fitting is based on the measured FRF curves, and various curve fitting methods available in MATLAB's Toolbox are applied to construct a mathematical function that best fits the time-streamed data points, as shown in Figure 3.23.

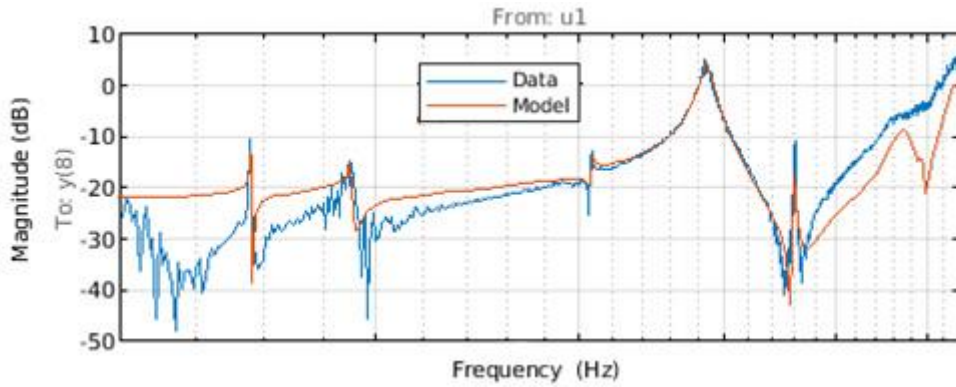


Figure 3. 23: Curve-fitting Diagram for the FRFs from the State-Space Model

To match the FRF of the mathematical model as closely as possible to that of the actual test system, key steps in MATLAB are outlined in Figure 3.24. The initial step involves converting the measured time-domain data into frequency response data using the empirical transfer function estimation (etfe) command. The estimated FRF is then used to identify a state-space model of the floor’s vibration response. The analysis focuses on a frequency span of 7-30 Hz, where the most critical bending modes of the floor are located, reducing the FRF to this specific frequency range.

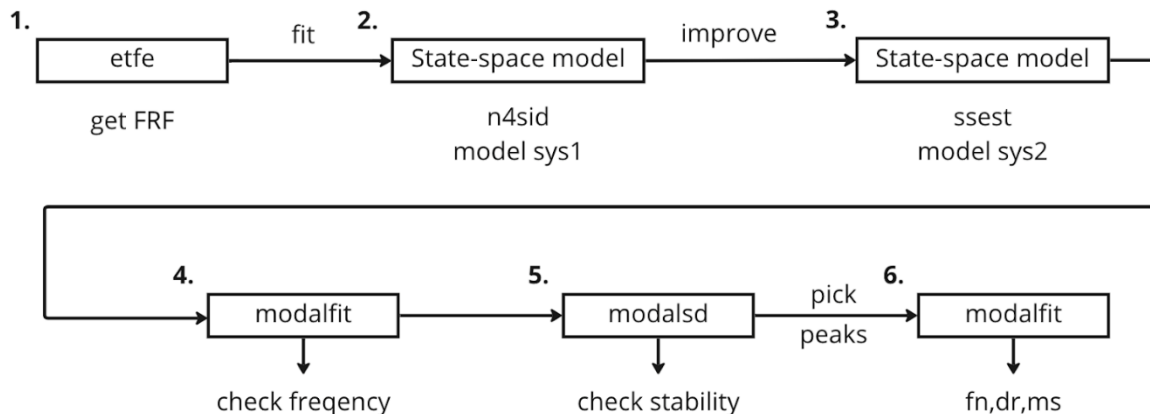


Figure 3. 24: Roadmap of Modal Identification in MATLAB

After narrowing the FRF to the desired frequency span, the next step is to identify a state-space model to fit the FRF across all measurement locations. Using the n4sid command, a 24th-order model is selected after several trials with various orders, followed by evaluation of the model's fit to the FRF. To ensure both low and high amplitudes receive equal emphasis, a custom weighting scheme is applied, varying inversely with the square root of the response.

After achieving a better fit with model sys2 using the iterative nonlinear least-squares refinement function (lsrf) via the ssest command, the natural frequencies of the modes can be extracted. This is

done using the modalfit command, which identifies the peaks on the sys2 curve corresponding to potential natural frequencies.

With the sys2 model, modal parameters, including natural frequencies, can be extracted. Peaks on the sys2 curve reveal these frequencies. To further verify this assessment, the modalsd command is employed to assess the stability of modal parameters as the model order changes.

Figure 3.25 illustrates a Stability Diagram generated in MATLAB, where the stability of FRFs identified from the state-space model at different frequencies is evaluated. A higher concentration of "+" symbols in a column suggests greater stability, and different poles are distinguished using a tolerance of 1% for frequency and 5% for damping.

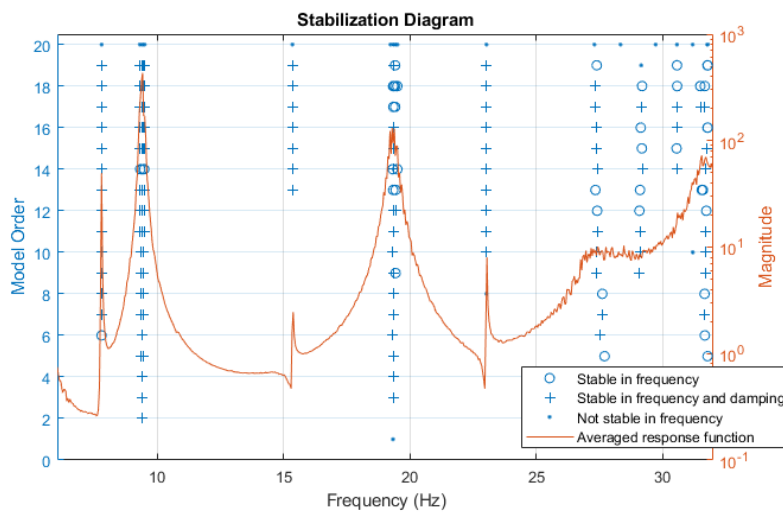


Figure 3. 25: Stability Diagram for the FRFs from the State-Space Model

A list of important MATLAB commands used to extract modal parameters and check the quality of the measured data is provided in Table 3.2. Control indexes for each command and key points for proper usage are highlighted.

Table 3. 2: Important Commands and Explanations for Modal Identification in MATLAB

Command	Control parameters	Highlight
etfe (frequency-response model)	They have different functions: <ul style="list-style-type: none"> • M-frequency resolution • N-frequency spacing 	functions <ul style="list-style-type: none"> • Generate FRF functions • periodograms
n4sid (state-space model)	<ul style="list-style-type: none"> • nx-order of the model • weighting-loss function 	<ul style="list-style-type: none"> • Noniterative, subspace method • Faster than SSEST algorithm

ssrest (state-space model)	<ul style="list-style-type: none"> • InitializeMethod- Least-squares rational function (lsrf)estimation-based approach • SearchMethod-Levenberg-Marquardt(lm) 	<ul style="list-style-type: none"> • Iterative method that uses Prediction error minimization algorithm • higher-accuracy results
ssregest (state-space model)	<ul style="list-style-type: none"> • nx-order of the model • Focus- simulation error to be minimized • SearchMethod- Trust-region-reflective constrained minimizer (fmincon) 	<ul style="list-style-type: none"> • Noniterative method. • Used on discrete time/frequency domain data • improved accuracy on short, noisy data sets
modalfit	<ul style="list-style-type: none"> • fn-returns the frequencies • dr-retuens the damping ratios • ms-returns to the mode-shape vectors • ofrf-returns a reconstructed frf 	<ul style="list-style-type: none"> • [fn,dr,ms,ofrf] = modalfit(____) also returns a reconstructed frequency-response function array based on the estimated modal parameters.
modalsd	<ul style="list-style-type: none"> • frf- from subspace model 	<ul style="list-style-type: none"> • fn = modalsd(____) returns a cell array of natural frequencies, fn, identified as being stable between consecutive model orders. The ith element contains a length-i vector of natural frequencies of stable poles. Poles that are not stable are returned as NaNs. This syntax accepts any combination of inputs from previous syntaxes.

4. Experimental Work

4.1. Introduction to the Experimental Work

The roadmap for this chapter, illustrated in Figure 4.1, builds on the background knowledge of test-based vibration research established in Chapter 3. Field experiments were conducted across 10 CLT floor slab test areas located at three different sites, referred to as Site 1, Site 2, and Site 3 for data protection purposes. These tests include modal testing, heel drop tests, as well as walking and running trials. The results of these tests were analyzed using MATLAB R2020a software.

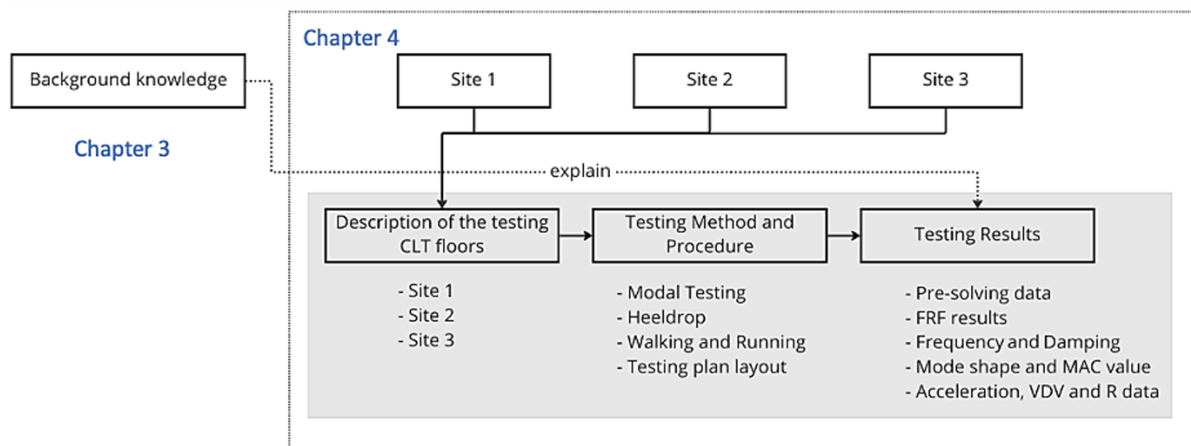


Figure 4. 1: The Roadmap of Chapter 4

This chapter focuses on explaining the experimental results from the three office buildings, named Site 1, Site 2, and Site 3. Each field test result includes the following components:

- Photos of the in-site conditions;
- Diagrams showing the location of exciters and sensors, as well as the test layout;
- Tables summarizing modal identification results and updates;
- A summary of key findings.

This chapter summarizes the most important data and the key principles underlying them. It provides an overview of the dynamic parameters of CLT floors in office buildings, including frequency, damping ratio, and mode shapes. Additionally, insights are provided into how different test methods influence the final frequency and damping results. The experimental techniques are described in detail to account for the case-specific nature of field-based studies, as results may vary depending on the context.

Table 4.1 summarized all tests conducted at the three sites. All three sites were equipped with raised access floor systems, providing 'clean' test areas. Different size of floors were specifically selected as test locations due to their spacious office design, constructed entirely from CLT panels and supported by long-span steel beams, glulam beams, or CLT walls. This selection facilitates the investigation of different support boundary conditions on CLT floors.

Table 4. 1: Summary of the Testing Floors

Site 1								
Total	Storey	Size	Heel-drop	Walking 1.5Hz	Walking 2Hz	Running	Modal shaker	Impact hammer
2 floors	3 rd floor	Area 1: Bare floor 6x6.6m	✓	✓	✓	✓	✓	✗
		Area 2: Bare floor 9x7.8m	✓	✓	✓	✓	✓	✗
		Area 2: Raised access floor 9x7.8m	✓	✓	✓	✓	✗	✗
Site 2								
2 floors	4 th floor	Small floor (9+9) x6.6 m	✓	✓	✓	✓	✓	✗
		Large floor (9+9+9) x6m	✓	✓	✓	✓	✓	✗
Site 3								
6 floors	3 rd floor	Floor (ABC) 3x4.5m	✓	✗	✗	✗	✓	✗
		Floor (DEF) 3x4.5m	✓	✓	✓	✓	✓	✗
		Floor (GHI) 3x4.5m	✓	✓	✓	✓	✗	✗
		Extension CLT floor	✓	✓	✓	✓	✓	✗
	2 nd floor	Extension CLT floor	✓	✓	✓	✓	✗	✓
	1 st floor	Extension CLT floor	✓	✓	✓	✓	✗	✓

4.2. Description of the Testing CLT Floors

4.2.1 Site 1

Site 1, a CLT building in London, was selected as one of the test buildings. The test area at Site 1 includes two floors of different sizes on the same storey level. The smaller floor, as shown in Figure 4.2(a), is located between four glulam columns and covers an area of 6m x 6.6m. It is a two-span floor, supported by five glulam beams. The larger floor, illustrated in Figure 4.2(b), spans three sections, supported by six glulam beams and four columns, with dimensions of 9m x 7.8m.

During testing, the effect of the raised access floor system was investigated. In addition to testing the floor with the raised access panels in place, several panels were removed to measure the response of the bare CLT floors, as indicated by the black squares in Figure 4.2.



Figure 4. 2: Modal Testing on the Bare CLT Floors at Site 1

A raised access floor system is an elevated floor installed above a sub-floor, leaving a void between the two. Raised floors not only preserve the visibility of the exposed wooden structure but also offer the potential to reduce sound transmission, thus enhancing acoustic performance.

As shown in Figure 4.3, the raised access floor panels measure 600mm x 600mm x 31mm, with a nominal system weight of 36kg/m³. The pedestals are bonded to the CLT floor using epoxy resin adhesive (Figure 4.3). Stringers, which are horizontal steel bars, connect the pedestal grid to improve the performance of the raised access floor system and provide lateral stability during installation.



Figure 4. 3: Raised Access Flooring System: Support System and Removable Panels

4.2.2 Site 2

Site 2 was selected to assess the condition of floor systems under construction. It is part of a new canal-side commercial development, which includes a mix of refurbished, extended, and newly built contemporary office spaces. The construction plan for Site 2 features a steel transfer deck above the existing roof slab, supported by a new glulam frame, with CLT floors spanning secondary beams.

The layout for modal testing of both the smaller and larger floor areas is shown in Figure 4.4. The entire floor area is finished using a raised access floor system. This system consists of 600mm x 600mm panels with a nominal weight of 36kg/m³. The raised access flooring not only allows for the concealment of services and cables but also affects the dynamic response of the structure, which is a key factor in the modal testing.

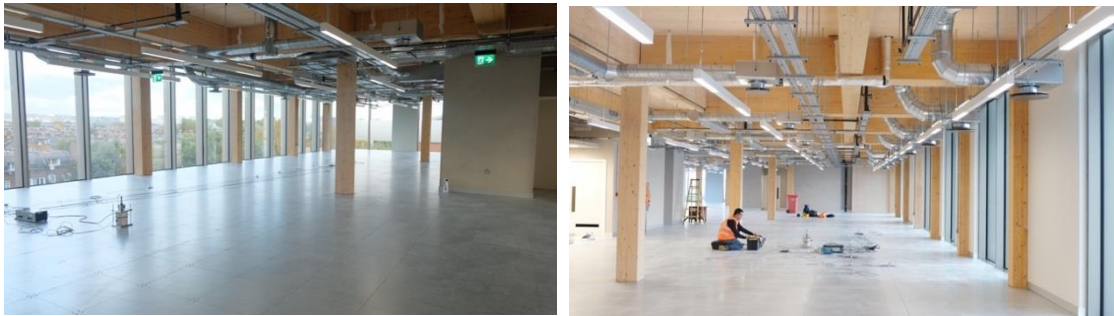


Figure 4. 4: Modal Testing on the Raised Access CLT Floors at Site 2

4.2.3 Site 3

Site 3 is a significant project involving the refurbishment and extension of an office building. This project employs a combination of CLT panels, steel beams, concrete beams, and glulam beams to expand both beyond and alongside the original brick and concrete structure. The third floor was selected as the primary test location due to its spacious office layout, constructed entirely from CLT panels and supported by long-span steel beams. The location of the shaker used for modal testing is shown in Figure 4.5. A raised access floor, covered with 8mm of acoustic resin, was installed on top of the CLT floor system, which was constructed using 140-5s thick CLT panels.



Figure 4. 5: Modal Testing on the Raised Access CLT Floors at Site 3

Additionally, the new side extension, which includes three CLT floors, was selected to investigate the effects of different support boundary conditions. The first and second storeys use a steel-wood raised floor system over the CLT panels, while the third floor is covered with resin material, as shown

in Figure 4.6. This configuration was chosen to fulfill different architectural and functional requirements for the workspace.



Figure 4. 6: Impact Hammer Testing on Side Extension Raised Access CLT Floors at Site 3

Modal testing was conducted using an impact hammer, striking the same fixed point while roving sensors collected the floor's response signal. The boundary conditions for each floor are detailed in Figure 4.7. The first floor is supported on all four edges, with two sides resting on a 250mm thick reinforced concrete (RC) core wall, one side fixed to the existing masonry wall with an L-shaped steel bracket, and the fourth side attached to the glulam frame on the glazed wall. The second and third floors share similar boundary conditions, supported on three sides: two resting on a 100mm thick CLT wall and one side on the glulam frame attached to the glazed wall. The primary difference lies in the fourth side, where the second floor is supported by an L steel bracket fixed to the masonry wall, while the third floor is supported by an RC capping beam that tops the masonry wall.

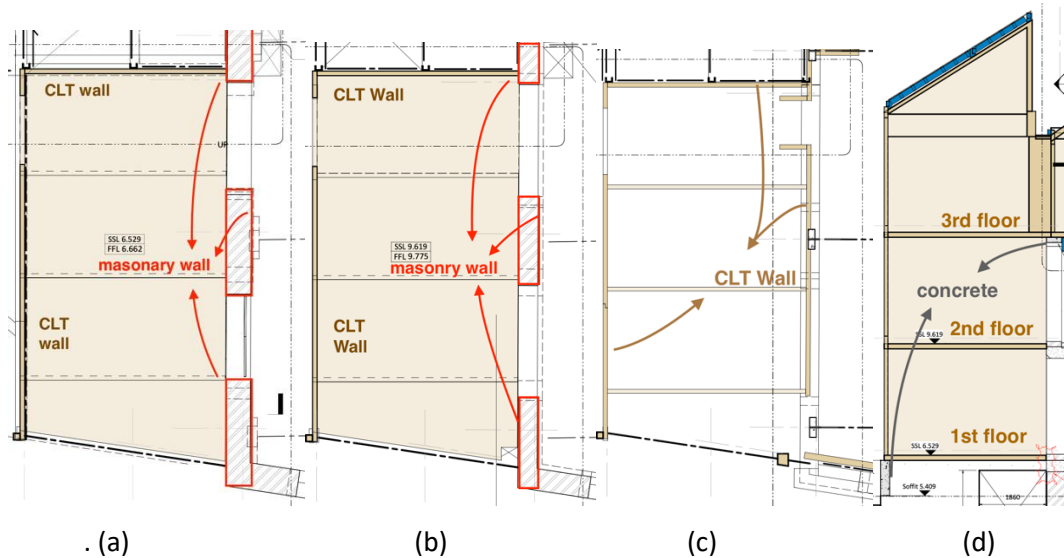


Figure 4. 7: The Boundary Conditions and Elevation of the Side Extension CLT Floors

4.3. Test Grid and Test point

The testing grid size was set at 0.6m, matching the dimensions of the raised access floor panels, which measure 600 x 600 x 31mm. Testing points were evenly distributed across these grids, as

shown in the figures below. Four sensors were used for modal testing at Site 1, while up to eight sensors were employed at Sites 2 and 3. The input signal was designated as Channel 0 (Ch0), while the output signals were assigned to Channels 1 through 8. The testing followed a “W” pattern.

For Site 1, modal testing was conducted on the bare CLT floor after several raised access panels were removed. The testing location, reference points, and procedures are shown in Figures 4.8 and 4.9. The smaller floor at Site 1 underwent four tests, covering nine points in the grid (Figure 4.8). One fixed accelerometer served as the reference point, while two additional accelerometers were roved across the remaining points. For the larger floor (Figure 4.9), six tests were conducted to cover the 9 x 7.8m area, using three accelerometers: one reference and two roving sensors, covering a total of 12 points.

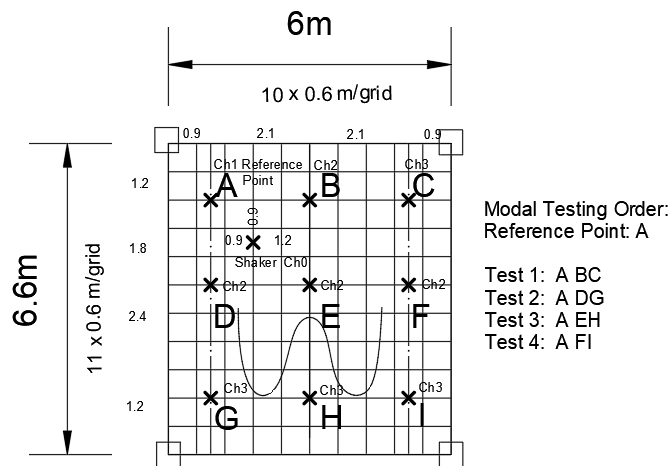


Figure 4. 8: The Location of the Reference Point, Test Points and Modal Testing Order on Small Floor (Site 1)

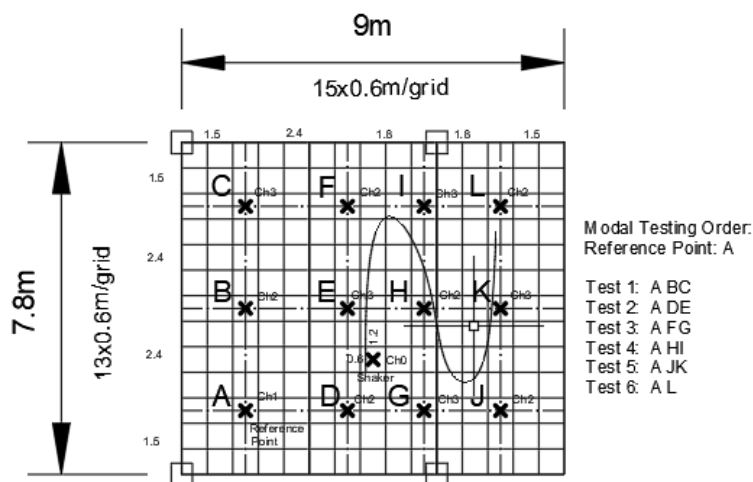


Figure 4. 9: The Location of the Reference Point, Test Points and Modal Testing Order on Large Floor (Site 1)

At Site 2, the small floor, a two-span CLT structure measuring 9 x 6.6m (Figure 4.10), was tested using a fixed reference point that transmitted the signal to Channel 1, while six roving sensors covered the floor surface. A total of six tests were conducted. For the larger floor, measuring 27 x 6.6m (Figure 4.11) and comprising three spans, three additional tests were necessary to cover the third span, resulting in a total of nine tests.

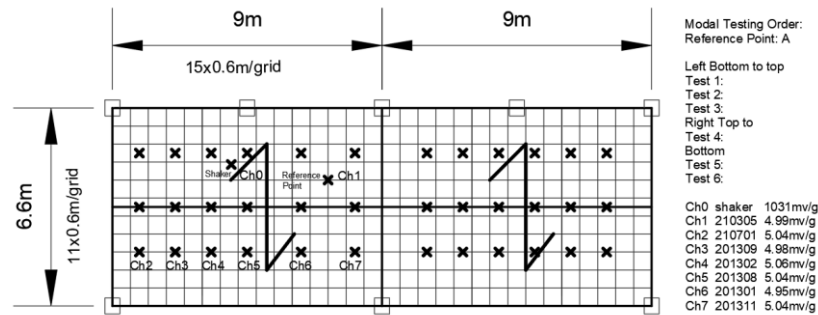


Figure 4. 10: The Location of the Reference Point, Test Points and Modal Testing Order on Small Floor (Site 2)

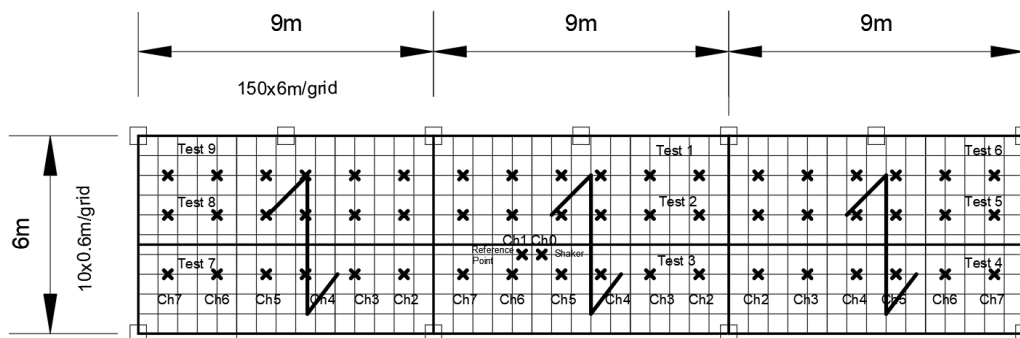


Figure 4. 11: The Location of the Reference Point, Test Points and Modal Testing Order on Large Floor (Site 2)

For Site 3, two areas were selected for testing due to sensor limitations. In Area 1, fourteen modal tests were conducted using two roving sensors, while thirteen tests were conducted in Area 2. The test grid was set at 1.5m, with sensor placement shown in Figures 4.12 and 4.13.

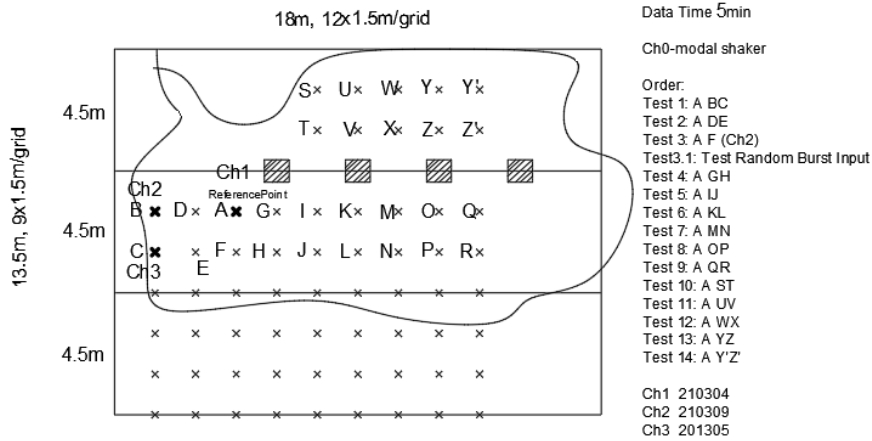


Figure 4. 12: The Location of the Reference Point, Test Points and Modal Testing Order on Area 1 (Site 3)

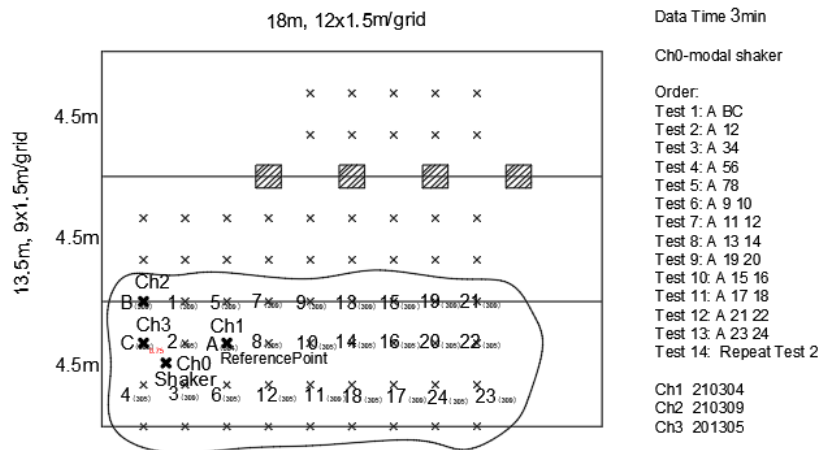


Figure 4. 13: The Location of the Reference Point, Test Points and Modal Testing Order on Area 2 (Site 3)

Impact hammer tests were conducted exclusively on the side extension cross-laminated timber (CLT) floor at Site 3. The side extension area is used as a meeting space, where three stories of the building are occupied by long, heavy tables and chairs, making it challenging to free up space for testing. Therefore, conducting shaker tests was not convenient, and impact hammer tests were performed on the three stories of the side extension at Site 3.

The impact magnitude was determined by both the hammer head's mass and the velocity of the strike. To avoid missing responses at modal nodes, care was taken to ensure that the stationary hammer impact at the reference point did not coincide with a modal node. The test grid measured sensor placed near the middle of the floor, as shown in Figure 4.14.

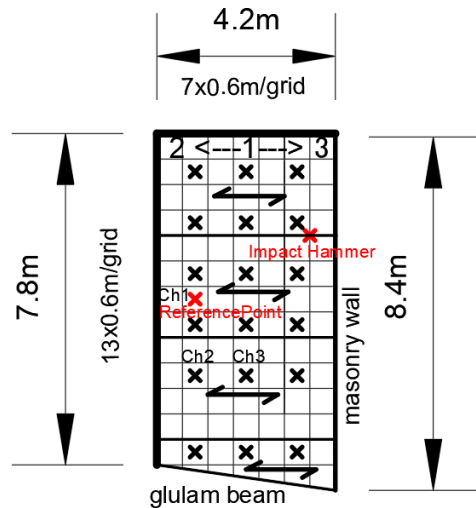


Figure 4. 14: Impact hammer test on Site 3: the location of the reference point, test points and modal testing order

4.4 Test Results

4.4.1 Input Signal Analysis

The Fast Fourier Transform (FFT) is one of the most efficient methods used in vibration research. Vibration data is typically collected in the time domain. However, transforming this data into the frequency domain can reveal important patterns, such as resonant frequencies, that may not be immediately apparent in the time domain. To minimize noise interference, time-domain averaging is performed before applying the FFT.

4.4.1.1 Site 1

Figure 4.15 illustrated the time history and frequency domain data (input spectra) of the sine sweep signal used in this experiment, which showed a significant peak around 27 Hz. Data from the three floors tested at Site 1 revealed the same peak value, with the position of frequency-domain spikes varying based on the sweep speed.

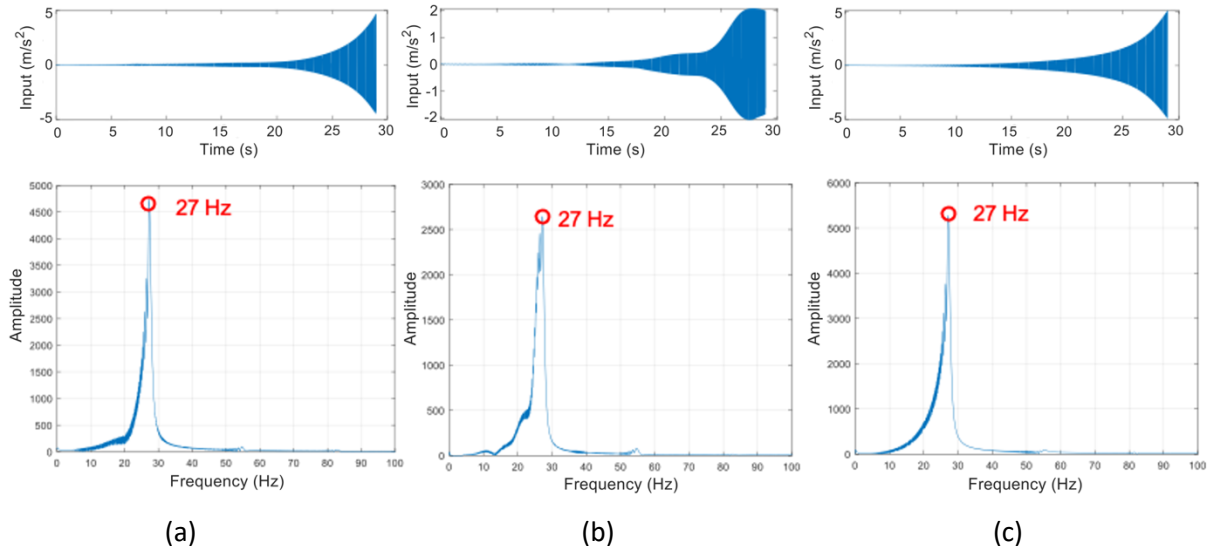
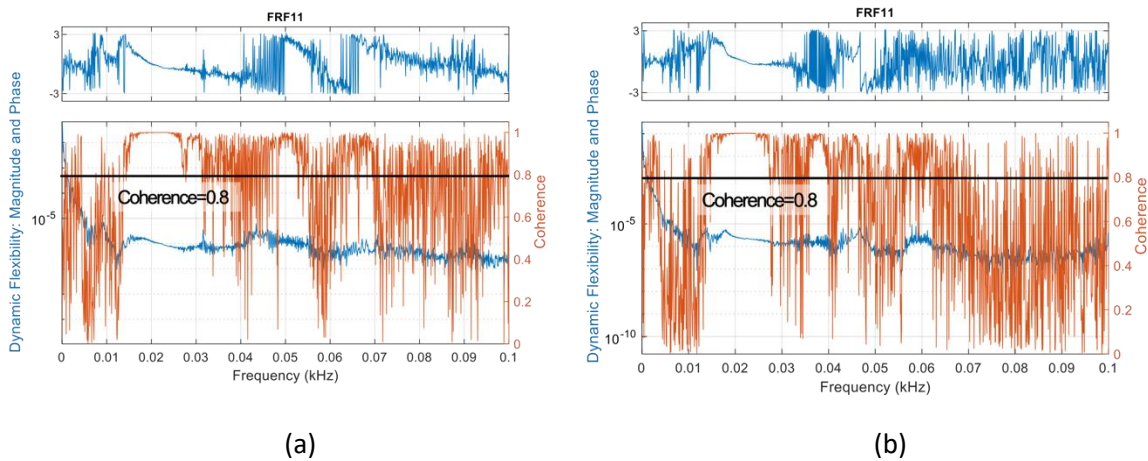
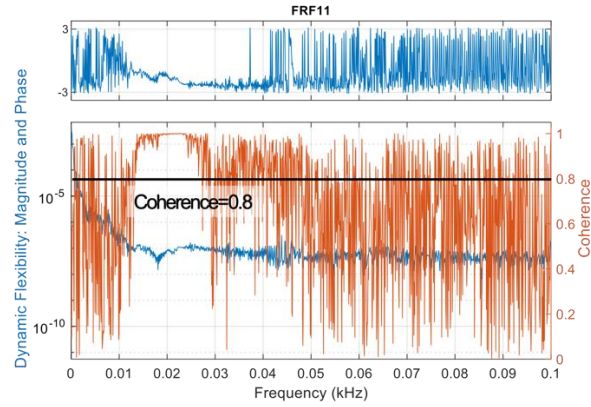


Figure 4. 15: Time History Data and Frequency Domain Data of Shaker Test at Site 1: (a) Small Floor; (b) Small Bare Floor; (c) Large Bare Floor

Coherence is represented by the orange-colored curve in Figure 4.16, shown in the Bode plots of the frequency response function (FRF). Coherence results from the FRF data of the three test floors at Site 1 indicated satisfactory test quality within the 15 to 30 Hz range, as evidenced by a high amplitude (>0.8). However, unwanted noise was detected in the 7-15 Hz range, suggesting the need for improvements in future testing to minimize interference. This issue is particularly important because the first natural frequency of the CLT floor falls within the 7-10 Hz range.



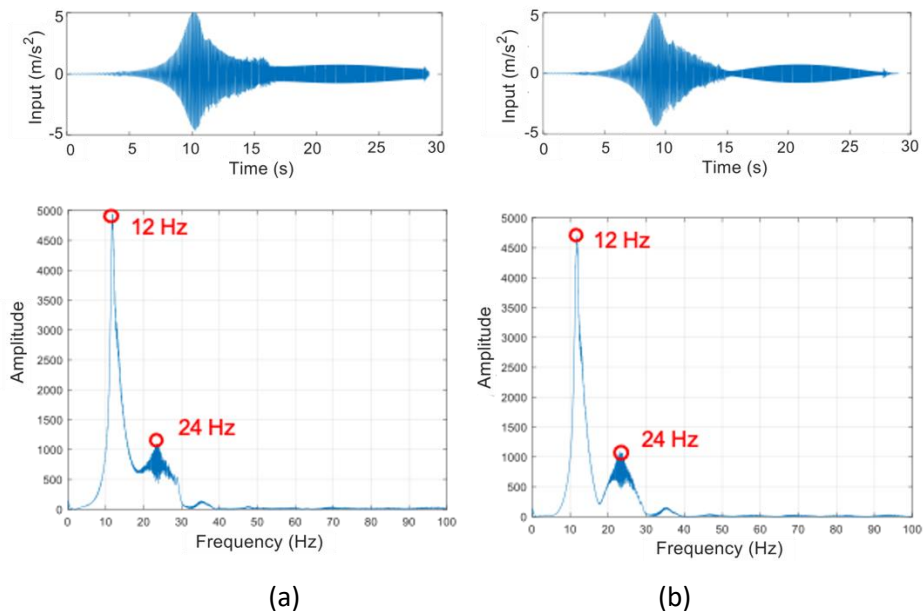


(c)

Figure 4. 16: Coherence Function from Shaker Test at Site 1: (a) Small Floor; (b) Small Bare Floor; (c) Large Bare Floor

4.4.1.2 Site 2

Figure 4.17 shows a frequency distribution concentrated in the 0-30 Hz sine sweep range, with notable peaks at 12 Hz and 24 Hz. This indicates a high energy level in the frequency sweep at these two frequencies. Structures with frequency components near these values are more likely to be identified accurately compared to other frequencies.



(a)

(b)

Figure 4. 17: Time History Data and Frequency Domain Data of Shaker Test at Site 2: (a) Small Floor; (b) Large Floor

Analysis of the input signal from Site 2 reveals the highest sweep drive efficiency and input-output quality among the three sites. As shown in Figure 4.18, the small floor exhibits strong coherence in the 10-25 Hz frequency range. For the large floor, coherence exceeds 0.8 between 8 Hz and 17 Hz and again between 20 Hz and 25 Hz. These results suggest that the testing conducted on Site 2 yielded high-quality data within these frequency ranges, providing valuable insights into the performance of the floor systems.

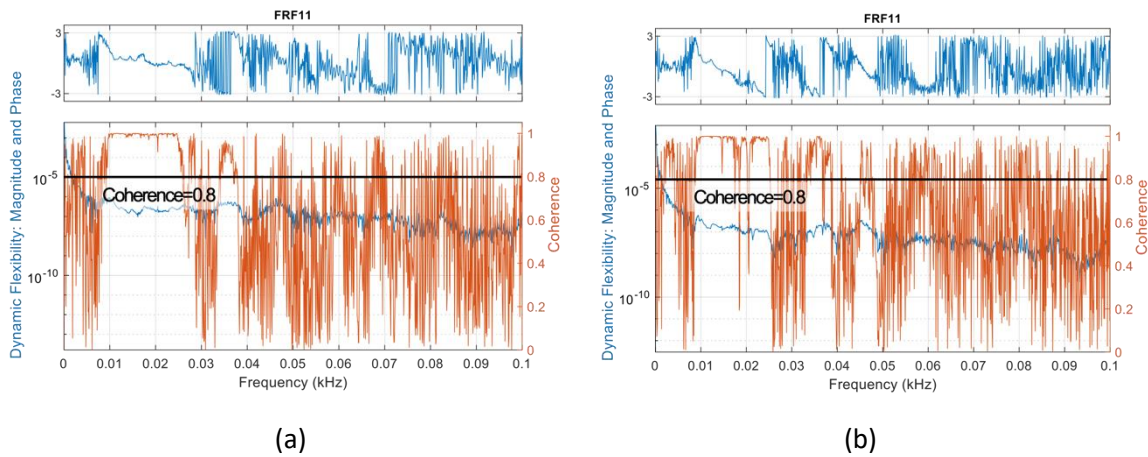


Figure 4. 18: Coherence Function from Shaker Test at Site 2: (a) Small Floor; (b) Large Bare Floor

4.4.1.3 Site 3

As shown in Figure 4.19, the excitation energy is concentrated near 29 Hz when the shaker at Site 3 executes a sine sweep signal ranging from 0 to 30 Hz. To capture structural responses at frequencies below 10 Hz more effectively, slower scan speeds are recommended.

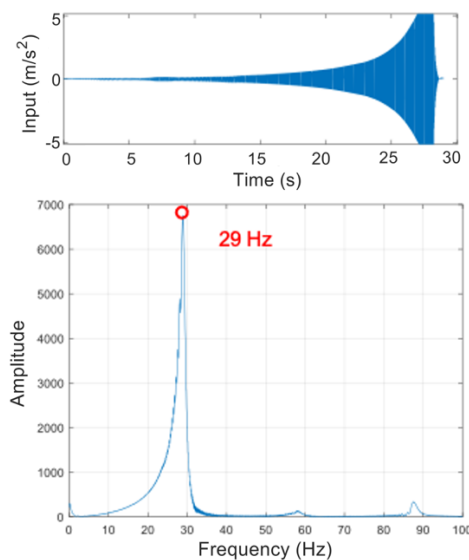


Figure 4. 19: Time History Data and Frequency Domain Data of Shaker Test at Site 3: Area 1 and Area 2

The coherence function, shown in Figure 4.20, serves as the basis for evaluating the quality of the measured FRFs at Site 3. In Area 1, coherence exceeds 0.8 between 15-28 Hz, indicating high FRF quality. Similarly, in Area 2, coherence surpasses 0.8 within the 20-28 Hz range, demonstrating reliable test performance.

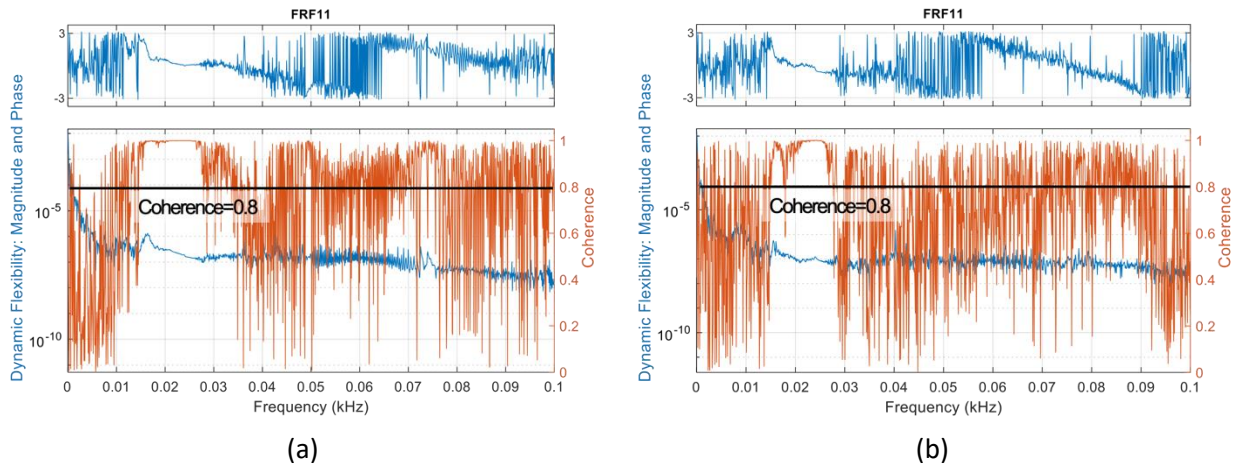


Figure 4. 20: Coherence Function from Shaker Test at Site 3: (a) Area 1; (b) Area 2

4.4.2 FRF Results of Frequency and Damping

A Frequency Response Function (FRF) is a complex function typically illustrated by a Bode plot. A Bode plot consists of two components: amplitude (the ratio of the input force to the response) and phase (expressed in degrees, indicating whether the response is in or out of phase with the input). Amplitude peaks correspond to the natural frequencies or resonances of the test object, facilitating the identification of the test structure's frequencies.

In the Stabilization diagram, markers represent the stability of the solutions, with the "+" marker indicating the highest stability in frequency and damping ratio. Unfortunately, no stable "+" poles appear within the target frequency range of 0 to 30 Hz; however, some "+" markers provide rough estimates. The low quality of the Stabilization diagram may be attributed to excessive noise during the testing procedure or an inappropriate input signal for the test structure.

4.4.2.1 Site 1

The FRF magnitude of the small bare floor, as shown in Figure 4.21, reveals peaks at approximately 9 Hz, 13 Hz, 18 Hz, and 25 Hz. Based on the Stabilization diagram, the most stable frequencies occur at 9 Hz, 13 Hz, 18 Hz, and 25 Hz, with damping stability observed only at 18 Hz and 25 Hz.

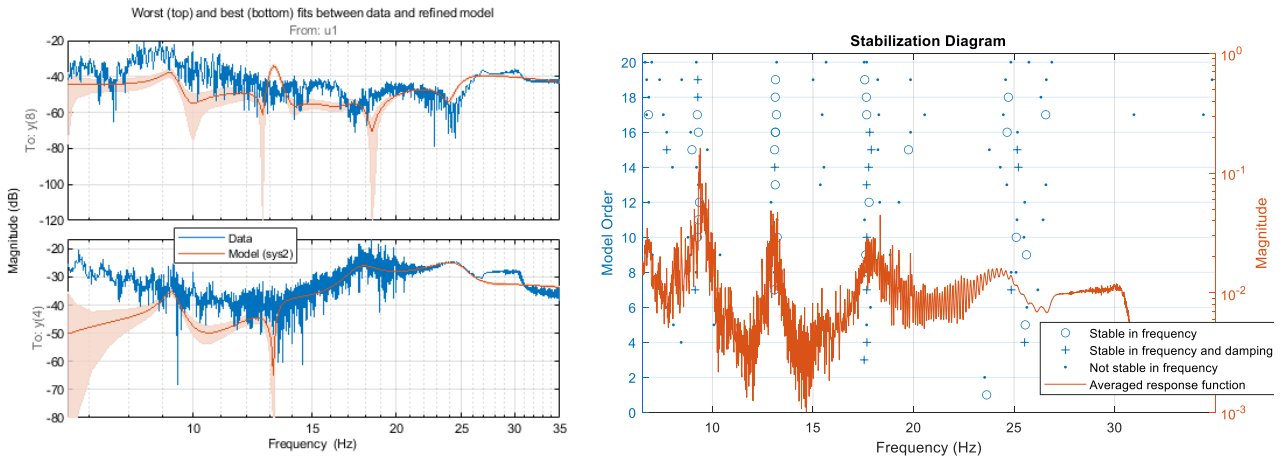


Figure 4. 21: Curve fitted FRF and Stabilization Diagram of Small Bare Floor (Site 1)

In the small raised access floor, stable frequencies are observed around 9 Hz, 17 Hz, and 24 Hz, with stable damping identified only at 25 Hz, as shown in Figure 4.22.

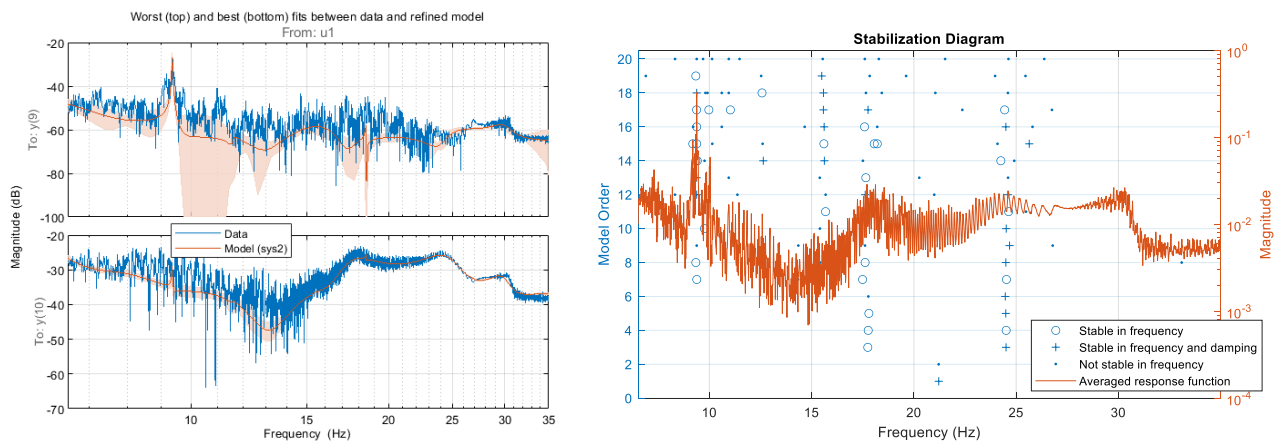


Figure 4. 22: Curve fitted FRF and Stabilization Diagram of Small Raised Access Floor (Site 1)

The frequency of the large bare floor is inferred from the FRF magnitude peaks, which are approximately 7.5 Hz, 8 Hz, 11 Hz, and 26 Hz. According to the Stabilization diagram (Figure 4.23), stable frequency and damping for the large bare floor are observed around 25 Hz.

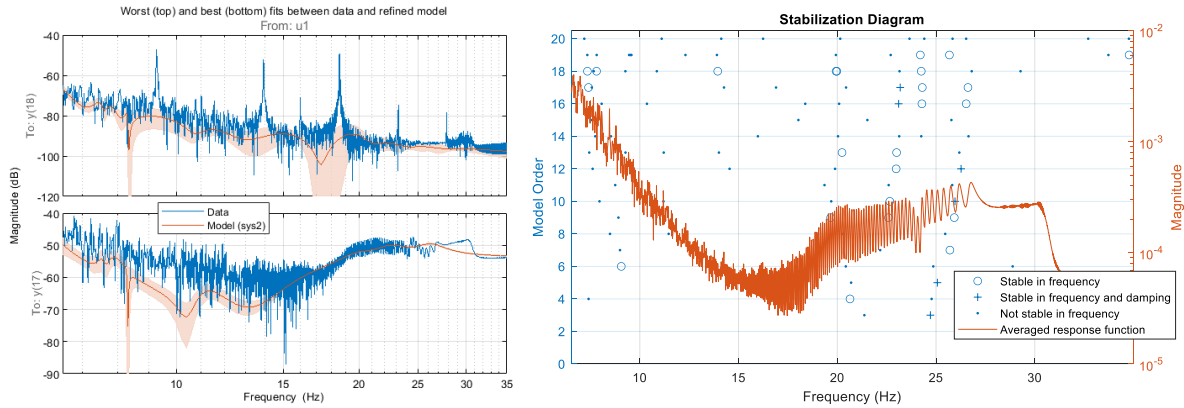


Figure 4. 23: Curve fitted FRF and Stabilization Diagram of Large Bare Floor (Site 1)

By combining the FRF magnitude and Stabilization diagram results, the potential frequency and damping values are summarized in Table 4.2. The first natural frequency of the CLT floors in a span of 6m x 6.6m (1 bay) at Site 1 is approximately 9.30 Hz. The stable damping ratio of the small bare floor ranges from 1.52% to 4.83% across four modes. The large bare floor, which shares the same structural configuration as the small bare floor but with an additional span, has a stable damping ratio ranging from 1.63% to 5.70% across eight modes. Therefore, for the bare CLT floor, the first damping ratio is approximately 1.52%. The difference in damping ratios between the small bare and raised floors, based on modal identification, is 1.61% (6.44% - 4.83%), which may be attributed to the damping contribution from the raised access floor structure or other construction elements.

Table 4. 2: Modal Identification Results of Site 1

Mode	small bare floor		small raised access floor		large bare floor	
	frequency	damping	frequency	damping	frequency	damping
1	9.30	1.52%	9.37	0.10%	7.54	1.63%
2	12.97	1.93%	15.99	10.05%	7.81	2.50%
3	17.89	3.30%	17.37	8.73%	11.00	6.96%
4	24.62	4.83%	24.64	6.44%	15.93	19.90%
5	/				16.85	32.02%
6					19.91	7.73%
7					22.33	7.17%
8					26.11	5.70%

* Bold damping is stable

4.4.2.2 Site 2

The FRF data from six modal experiments using roving sensors were analyzed for the small floor of Site 2. Figure 4.21 illustrates the curve-fitting results, showing both the best and worst fits between the data and the refined mathematical model. The red curve demonstrates a strong correlation with

the blue data curve, indicating a high degree of alignment. Notably, all fit percentages exceed 80%, and similar conclusions are drawn for the large raised access floor.

The stabilization diagrams in Figures 4.24 and 4.25 depict the stable frequencies observed at Site 2. For the small floor, stable frequencies are identified at approximately 9 Hz, 10 Hz, 28 Hz, and 30 Hz, with corresponding damping stability observed at 9 Hz, 25 Hz, 28 Hz, and 30 Hz. Similarly, for the large floor, stable frequencies are found around 10 Hz, 20 Hz, 25 Hz, and 30 Hz, while stable damping is evident at 9 Hz, 25 Hz, and 30 Hz.

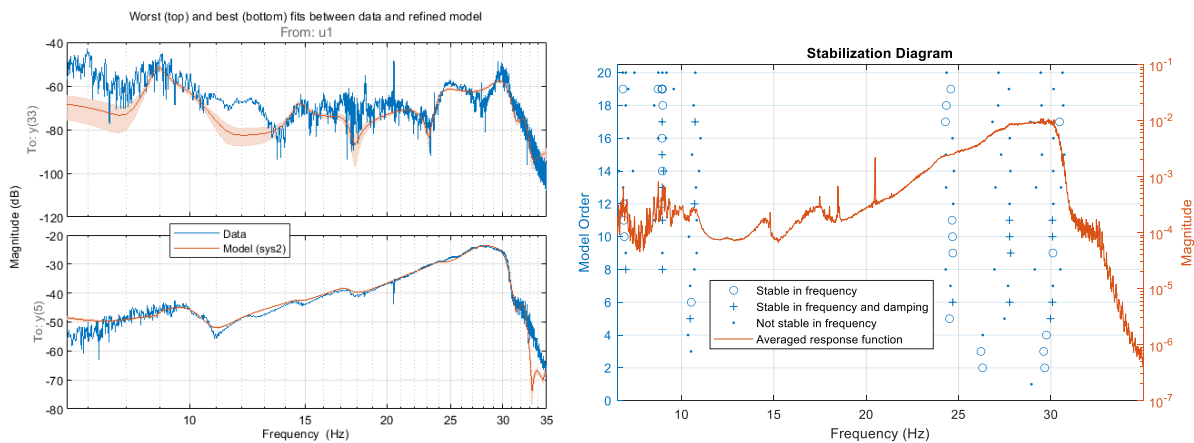


Figure 4. 24: Curve fitted FRF and Stabilization Diagram of Small Raised Access Floor (Site 2)

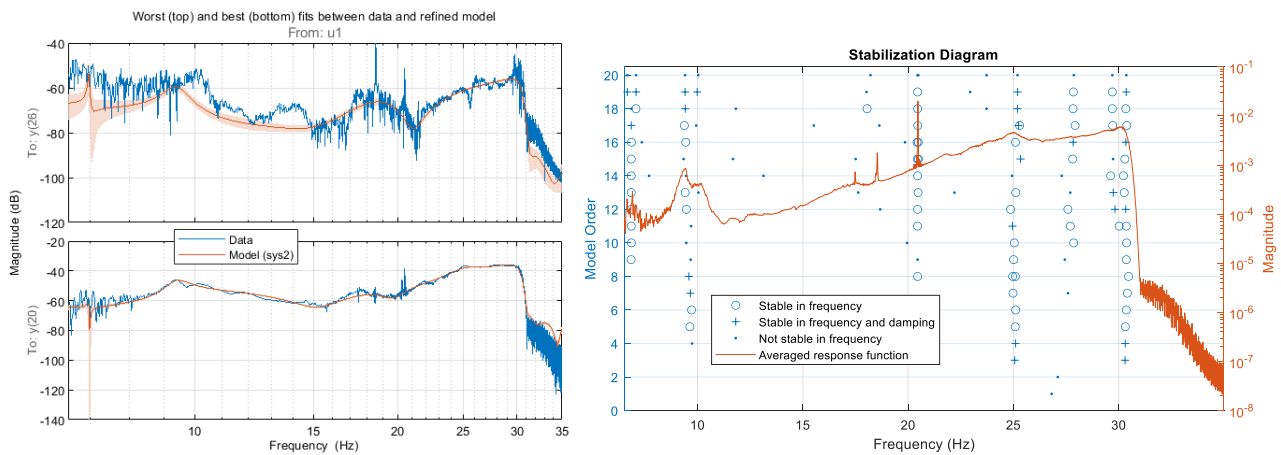


Figure 4. 25: Curve fitted FRF and Stabilization Diagram of Large Raised Access Floor (Site 2)

By combining the FRF magnitude data and stabilization diagrams, potential frequency and damping values can be determined, as shown in Table 4.3. The first natural frequency of the CLT floors in a 9m x 6.6m span (1 bay) at Site 1 is approximately 8.93 Hz. In contrast, the first natural frequency of the large floor, with a 9m x 6.6m bay, is 9.40 Hz. This slightly higher value can be attributed to reduced stiffness from smaller support columns. The stable damping ratio for the small floor ranges between 2.02% and 7.76% across eight modes, while the large floor, with a similar configuration but

an additional span, shows stable damping ratios ranging from 3.48% to 9.48%. The damping ratios for the first mode, 2.02% for the small floor and 3.48% for the large floor, are higher than those recorded at Site 1 (1.52% and 1.63%, respectively). This difference may be due to the raised access flooring systems and the thicker CLT floors at Site 2 (140mm versus 120mm at Site 1).

Table 4. 3: Modal Identification Results of Site 2

Mode	small floor		large floor	
	natural frequencies	damping ratio	natural frequencies	damping ratio
1	8.93 Hz	2.02%	9.40 Hz	3.48%
2	10.08 Hz	8.53%	10.50 Hz	44.86%
3	14.68 Hz	2.23%	19.00 Hz	10.00%
4	17.40 Hz	3.78%	22.09 Hz	16.76%
5	24.13 Hz	3.40%	23.96 Hz	38.98%
6	27.83 Hz	7.76%	25.23 Hz	5.37%
7	29.80 Hz	15.90%	28.70 Hz	9.48%
8	30.44 Hz	3.58%	30.46 Hz	1.35%
9	32.36 Hz	1.49%		

* Bold damping is stable

According to EC5, the recommended damping ratio for CLT buildings is approximately 1%, while the UK annex suggests a value of 2%. SCI_P354 recommends a damping ratio of 3% for fully fitted-out and furnished floors in regular use. The discrepancy between these guidelines remains unclear. However, research by K. Jarnerö (2015) has shown that in-situ conditions significantly impact damping ratios, often leading to higher values than those suggested in design codes.

4.4.2.3 Site 3

Due to constraints related to the sensor wire lengths, the entire third floor of the building at Site 3 was divided into test Areas 1 and 2. Both areas were tested using a modal shaker. Curve-fitting results for these areas show improved correlation between 15 Hz and 30 Hz. According to the stability diagrams in Figures 4.26 and 4.27, the stable frequencies and damping for Area 1 are found around 12 Hz, 14 Hz, 16 Hz, 24 Hz, and 29 Hz. In Area 2, stable frequencies and damping are identified at 8 Hz, 11 Hz, 14 Hz, 16 Hz, 25 Hz, 28 Hz, and 30 Hz.

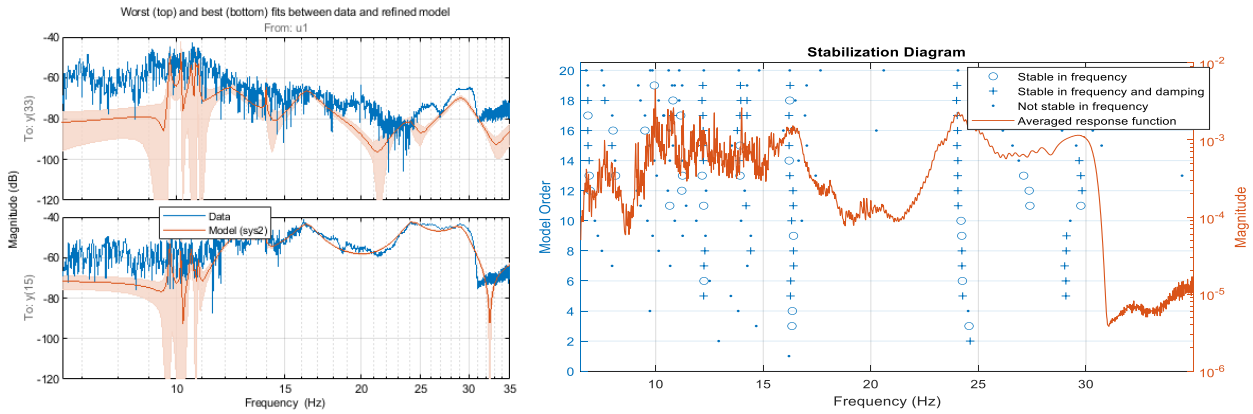


Figure 4. 26: Curve fitted FRF and Stabilization Diagram of Area 1 (Site 3)

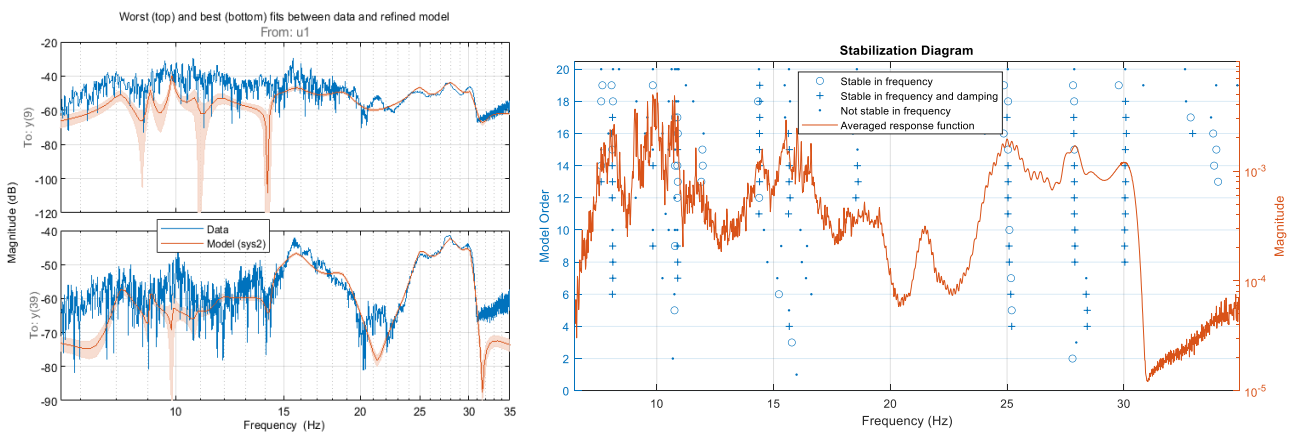


Figure 4. 27: Curve fitted FRF and Stabilization Diagram of Area 2 (Site 3)

The frequency and damping results are presented in Table 4.4. Most damping results are stable, as indicated in the table. In Area 1, the damping extracted from FRF curve fitting varies from 2.35% to 4.49%. In Area 2, a higher number of modes were identified, with stable damping ranging from 1.19% to 4.23%. Since Areas 1 and 2 represent the same physical testing area, similar damping results would be expected. However, the difference in damping may be attributed to the presence of furniture (such as a kitchen) and partition walls in Area 1, which could contribute an additional damping ratio between 1% and 2%.

Table 4. 4: Modal Identification Results of Area 1 and Area 2 (Site3)

Mode	Area 1		Area 2	
	natural frequencies	damping ratio	natural frequencies	damping ratio
1	12.25	4.49%	8.16	2.67%
2	14.04	2.35%	10.77	1.19%
3	16.29	3.29%	11.75	3.53%
4	24.16	3.36%	14.37	1.81%
5	29.15	3.09%	15.75	4.23%
6			18.77	3.97%
7			24.96	2.39%

8			28.00	2.61%
9			30.15	1.29%

* Bold damping is stable

The modal identification results for three extension CLT floors are shown in Table 4.5. The 1st and 2nd floors feature the same raised access floor system, while the 3rd floor uses raised access floor tiles with an Altro Flexiflow 8mm resin. This difference is reflected in the modal identification results, with the 1st CLT floor exhibiting the highest natural frequencies, followed by the 3rd floor, and then the 2nd floor.

A similar trend is observed for the damping ratios. The 1st floor shows the highest damping, ranging from 2.00% to 26.14%. Notably, the difference in damping between the 1st and 2nd floors (ranging from 0.08% to 23.23%) is larger than that between the 3rd and 2nd floors (ranging from 0.09% to 11.94%). This suggests that the construction details of the 2nd and 3rd floors are more similar compared to the 1st floor.

Table 4. 5: Modal Identification Results of Extension Area (Site 3)

Mode	1st CLT		2nd CLT		3rd CLT	
	natural frequencies	damping ratio	natural frequencies	damping ratio	natural frequencies	damping ratio
1	7.16	6.80%	7.12	6.77%	7.08	7.17%
2	14.55	4.84%	14.83	4.23%	14.88	3.16%
3	18.56	8.81%	18.08	3.28%	17.90	2.63%
4	30.32	2.12%	30.32	2.09%	30.30	1.99%

* Bold damping is stable

From the fitted FRF curves and stability diagrams (Figure 4.28), the stable frequencies and damping characteristics of the 1st CLT floor occur around 7 Hz, 15 Hz, 18 Hz, and 30 Hz. Similarly, the 2nd CLT floor shows stable frequencies at 7 Hz, 15 Hz, 18 Hz, and 30 Hz, but its stable damping is less discernible (Figure 4.29). As illustrated in Figure 4.30, the 3rd CLT floor exhibits greater stability in both frequency and damping, with stable results clearly identified around 7 Hz, 15 Hz, 18 Hz, and 30 Hz.

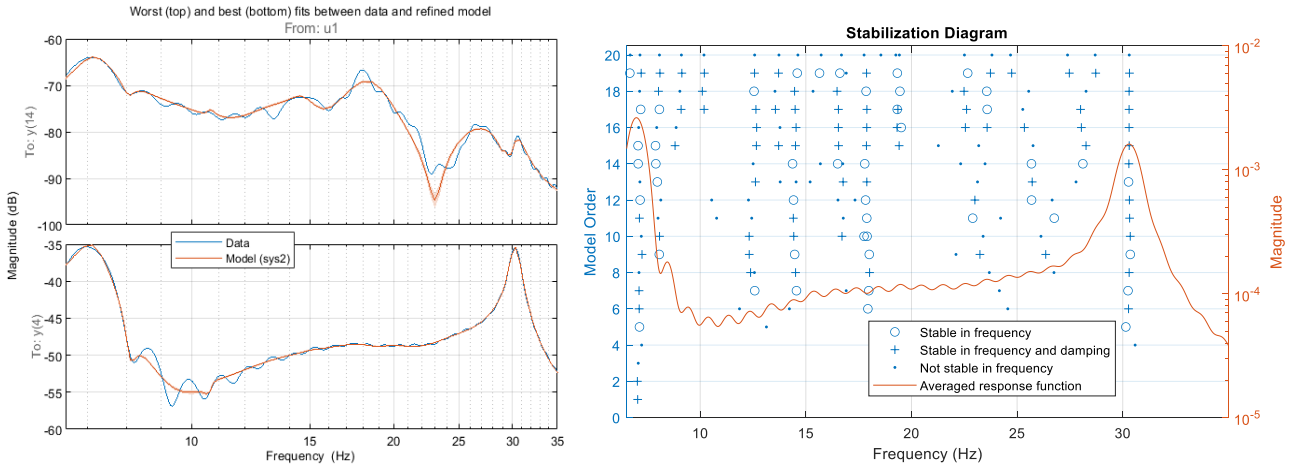


Figure 4. 28: Curve fitted FRF and Stabilization Diagrams of the Side Extension-1st CLT Floor

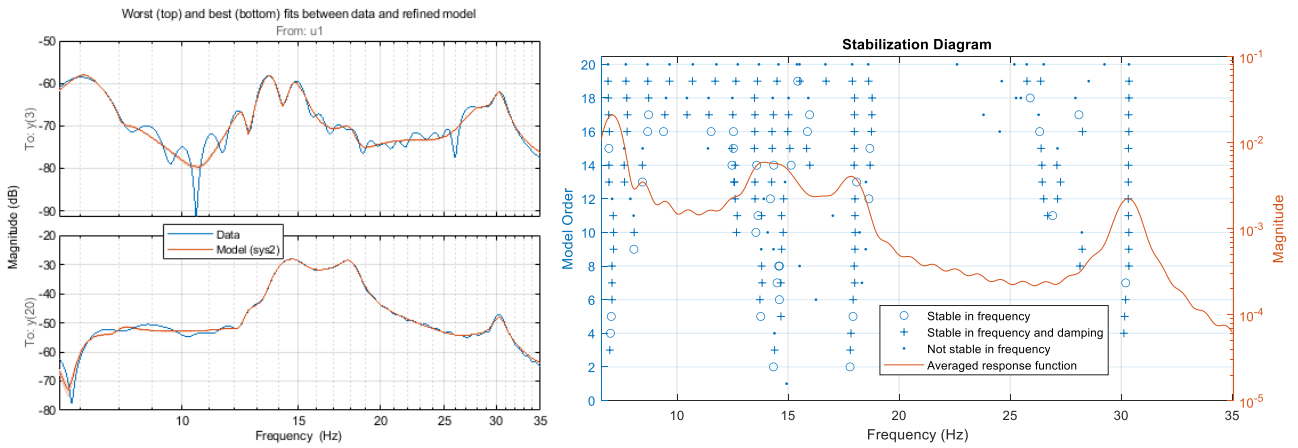


Figure 4. 29: Curve fitted FRF and Stabilization Diagrams of the Side Extension-2nd CLT Floor

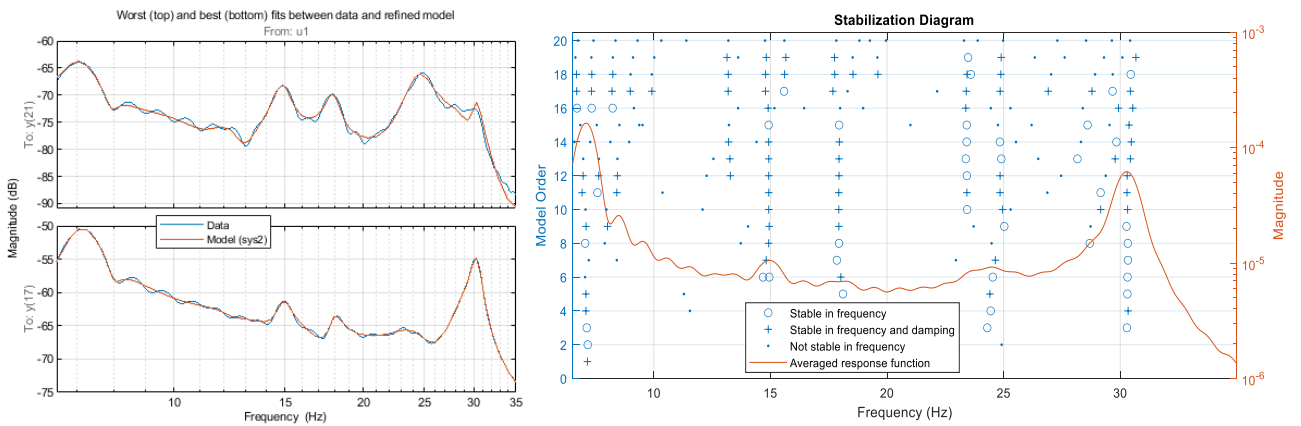


Figure 4. 30: Curve fitted FRF and Diagrams of the Side Extension-3rd CLT Floor

4.4.3 Heel drop results of frequency and damping

An Impact Test (Heel-drop) was conducted after the shaker testing to further verify the accuracy of the frequency and damping results. In heel-drop testing, where the input force is unknown, damping

properties were extracted from the FFT plots of the output data. The time-domain identification Complex Exponential (CE) Method were employed to estimate the modal parameters.

4.4.3.1 Site 1

The Fast Fourier Transform (FFT) analysis, as illustrated in Figure 4.31, indicates that the first natural frequency of the small bare floor is 9.20 Hz, while that of the small raised access floor is 7.60 Hz. The reduction in natural frequency for the raised access floor can be attributed to the additional mass introduced by the raised floor system. Smaller floors typically exhibit greater structural stiffness, resulting in higher natural frequencies, as smaller spans limit the degree of flexion within the structure. This is evident when comparing the small bare floor to the large bare floor. Furthermore, the raised access floor exhibits a higher damping ratio, which can be attributed to the increased mass and flexibility of the floor system, enabling more effective dissipation of external forces.

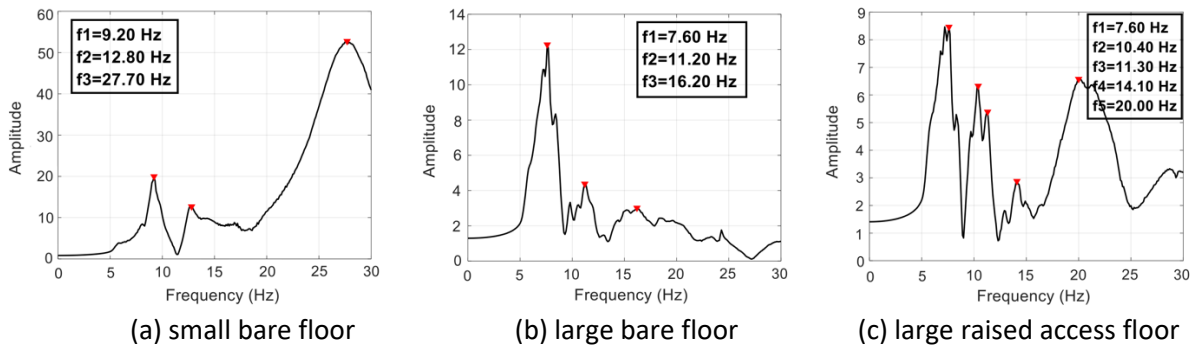


Figure 4. 31: FFT results of Heel-drop Test on Site 1

Following the FFT analysis, additional verification of these findings was conducted using the heel-drop test. The results of the heel-drop test for Site 1 were identified using the Complex Exponential (CE) method in MATLAB, a technique frequently used to extract modal parameters from structures. These results are presented in Table 4.6.

Table 4. 6: Comparison between Heel Drop Results on Site 1

Mode	Small bare floor		Large bare floor		Large raised access floor	
	frequency	damping	frequency	damping	frequency	damping
1	9.28	5.70%	7.74	9.05%	7.75	11.58%
2	12.42	5.11%	10.74	9.39%	10.23	9.97%
3	18.31	7.38%	14.98	10.64%	13.09	8.95%
4	27.73	11.42%	21.03	16.60%	19.36	12.82%
5	31.93	3.15%	23.31	11.07%	23.97	9.94%
6	34.98	7.87%	30.25	9.21%	29.22	4.70%
7					34.03	20.22%

4.4.3.2 Site 2

The small floor, which consists of two spans, underwent two heel-drop tests. The FFT results from these tests, depicted in Figure 4.32, reveal closely aligned fundamental frequencies of 8.7 Hz and 8.9 Hz. Similarly, the large floor, consisting of three spans, was subjected to three heel-drop tests, with one test conducted at the center of each span. The fundamental frequency for the large floor was consistently identified at approximately 9 Hz, as shown in the FFT plots in Figure 4.33. The detailed identification results of frequency and damping ratio, providing further insight into the modal properties of both floors, are presented in Table 4.7.

It is important to note that both FFT results and the CE method may yield erroneous results due to factors such as noise or inadequate signal processing.

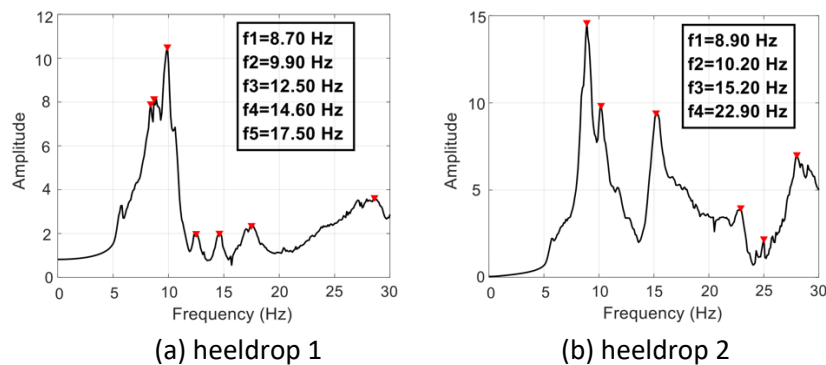


Figure 4. 32: FFT results of Heel Drop Test on the Small floor (Site 2)

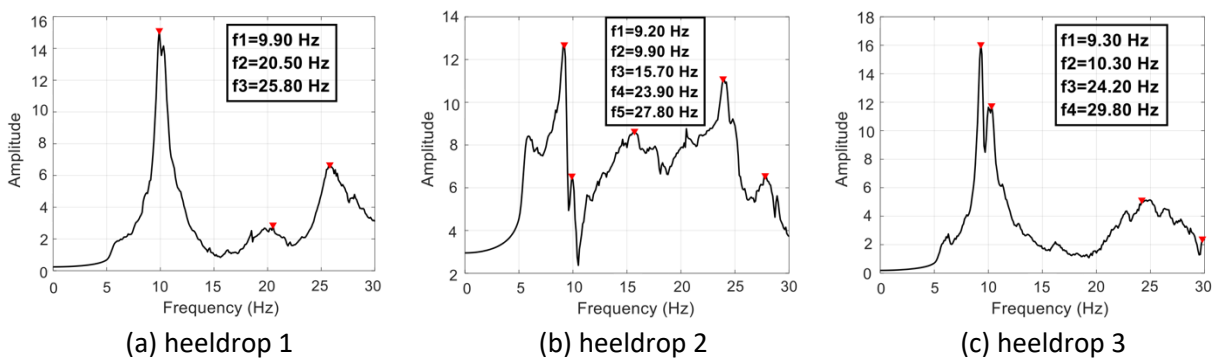


Figure 4. 33: FFT results of Heel Drop Test on the Large floor (Site 2)

Table 4. 7: Comparison between Heel Drop Results on Site 2

Mo de	Small floor				Large floor					
	Heel drop 1		Heel drop 2		Heel drop 1		Heel drop 2		Heel drop 3	
	Frequen cy(Hz)	Dampi ng(%)								
1	9.27	13.13	8.87	6.25%	10.08	4.69	9.38	4.22	9.30	6.05
2	10.83	10.05	14.87	4.98%	11.89	13.95	18.64	8.24	10.72	17.00
3	17.07	5.34	23.19	2.53%	20.15	9.00	24.65	4.24	18.81	14.75
4	29.61	11.30	27.89	3.97%	25.76	4.72	28.19	4.66	23.19	11.38

5	30.39	3.53	33.38	3.74	31.60	5.66	33.95	9.31	26.56	14.02
6	35.56	3.11	38.13	3.49	36.94	3.36	37.87	4.81	29.93	2.83
7									37.13	4.10

4.4.3.3 Site 3

Multiple heel-drop tests were conducted in various areas of the CLT third floor, as shown in Figure 4.34. Heel Drop 1, Heel Drop 2, and Heel Drop 3 were performed on Floors A, B, and C, respectively, to evaluate the orientation of the CLT floor panels. To assess the continuity of the CLT floor, Heel Drops 4, 5, and 6 were conducted on Floors D, E (the same as Floor B), and F, respectively. The same test was also performed on Floors G, H, and I, identified as Heel Drops 7, 8, and 9. The FFT results from these tests are presented in Figure 4.35.

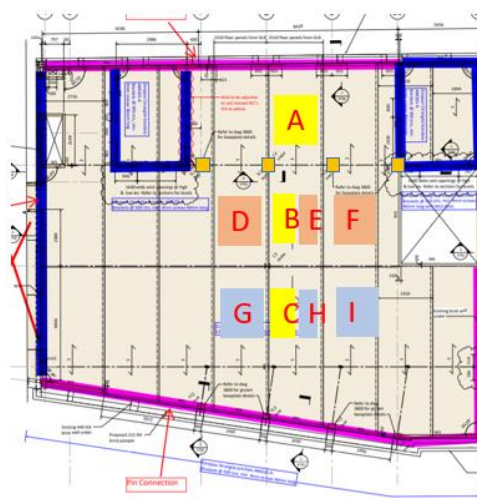
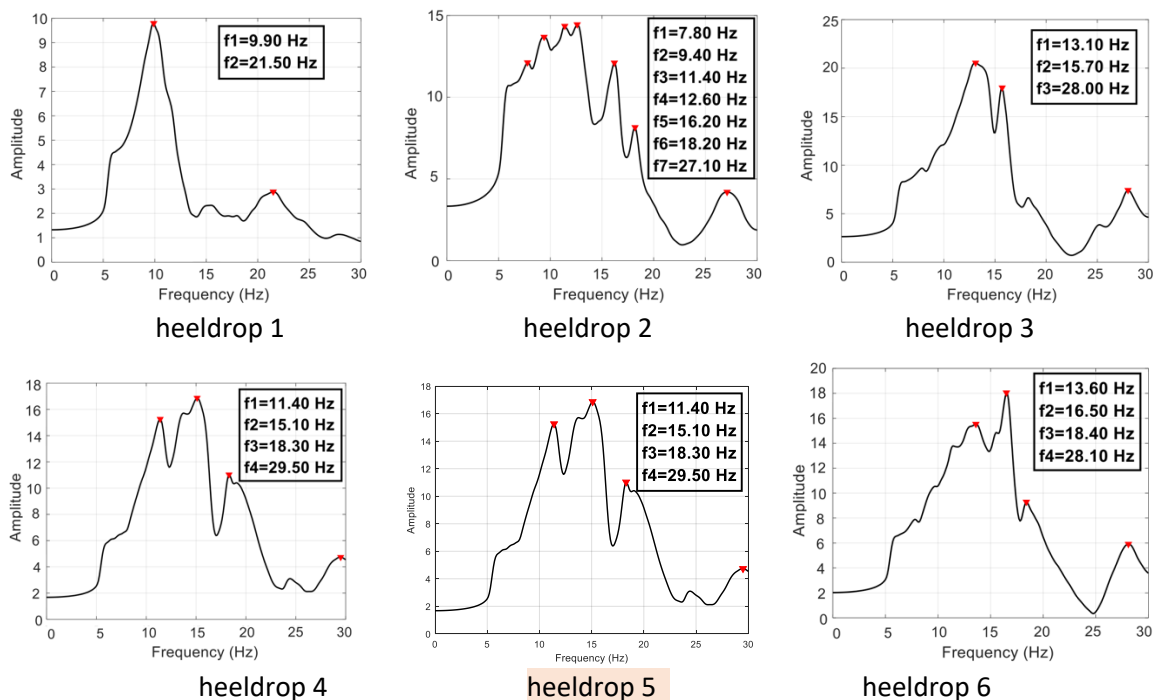


Figure 4. 34: Heel Drop Area on Site 3



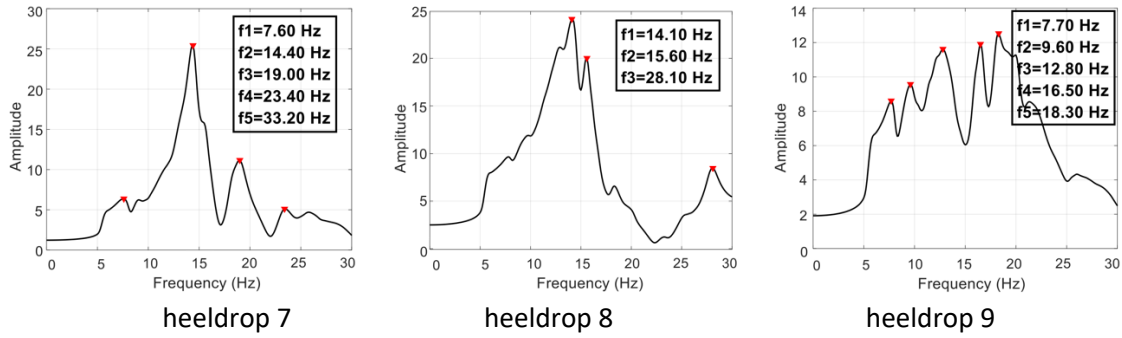


Figure 4. 35: FFT Results of Heel-drop 1-9 on HTS floors (Site 3)

The results of the natural frequencies and damping ratios, calculated using the Complex Exportation (CE) method, are summarized in Table 4.8. Despite Floors A and B belonging to the same floor panel, differences in frequencies and damping are observed. It is likely that this variance is attributable to the differing usage conditions. Floor A, for instance, accommodates a heavily equipped kitchen and tables, while Floor B is furnished with dining tables and movable chairs. These distinct usage scenarios likely contribute to the observed differences in natural frequencies and damping ratios.

Damping in higher-order modes presents significant complexity, and a reliable evaluation method has not yet been established. Existing research lacks consistent and reliable measured data for higher-order mode damping, aside from the first-order mode. Consequently, first-order damping is considered the most relevant and reliable for reference. Table 4.8 demonstrated that the first-order mode damping values for Floor A, Floor C, and Floor H were 10.13%, 10.05%, and 13.65%, respectively. These values were significantly higher than the typical damping range for wooden structures, which is between 1% and 3%. The higher values can be attributed to the fact that these areas were dining spaces containing heavy kitchen equipment, 9 dining tables, and nearly 70 chairs, all of which contributed to increased structural damping.

In contrast, the damping values for Floor B, Floor D, Floor F, Floor G, and Floor I were 6.18%, 5.42%, 7.22%, 4.19%, 5.53%, and 4.31%, respectively. These values fell within the acceptable range, as no additional equipment was placed in these test areas. However, it should be noted that during the actual on-site tests, factors such as floor decorations and the presence of dining occupants caused a slight increase in the original damping values, typically within the range of 1-2%.

Table 4. 8: Comparison between Heel-drop 1-9 on Area 1 and Area 2 (Site 3)

Mode	Heel drop 1 (Floor A)		Heel drop 2(Floor B)		Heel drop 3 (Floor C)	
	frequency	damping	frequency	damping	frequency	damping
1	9.96	10.13%	9.05	6.18%	13.45	10.05%
2	12.80	9.51%	13.48	12.95%	16.06	1.64%
3	20.80	7.76%	15.91	8.85%	27.69	2.18%
4	26.76	3.88%	17.85	2.06%	32.08	6.44%
5	32.15	2.34%	27.36	4.66%	38.63	2.98%
6	39.06	2.83%	31.73	13.74%		
			35.21	2.25%		
Mode	Heel drop 4 (Floor D)		Heel drop 5 (Floor E)		Heel drop 6 (Floor F)	
1	11.49	5.42%	9.36	7.22%	8.34	4.19%
2	16.20	15.31%	13.26	14.93%	13.12	6.12%
3	17.12	7.56%	16.79	2.75%	16.74	2.68%
4	22.77	8.47%	18.32	7.74%	21.46	5.90%
5	27.94	4.97%	27.71	4.36%	26.21	3.32%
6	33.55	9.07%	31.53	11.15%	34.27	5.43%
7	37.49	4.56%	34.33	3.85%		
Mode	Heel drop 7 (Floor G)		Heel drop 8 (Floor H)		Heel drop 9 (Floor I)	
1	8.23	5.53%	9.15	13.65%	8.41	4.31%
2	14.48	5.21%	13.82	9.93%	13.25	12.03%
3	18.24	5.70%	15.73	3.06%	16.52	7.42%
4	20.63	18.89%	19.42	12.55%	18.71	5.34%
5	23.34	7.62%	27.52	14.15%	23.60	4.90%
6	30.51	3.53%	27.76	2.22%	29.61	4.74%
7	37.83	1.82%	33.52	5.61%	35.49	2.87%

The new side extension, which includes three CLT floors, heel-drop tests were conducted on the first, second, and third CLT floors of the extension to assess the effect of inter-plate connections. The FFT results, as shown in Figure 4.36, indicate that the inter-plate connections are robust enough to allow the three panels to behave as a single, unified structure under load. Given that the panels function as a cohesive unit, conducting the heel-drop test at the center of the floor is preferred, as this helps to minimize the risk of mode loss during FFT analysis. The frequency and damping results, calculated using the CE method, are presented in Table 4.9. While the preliminary FFT analysis provided initial insights, the CE method was crucial for refining these measurements and ensuring greater accuracy.

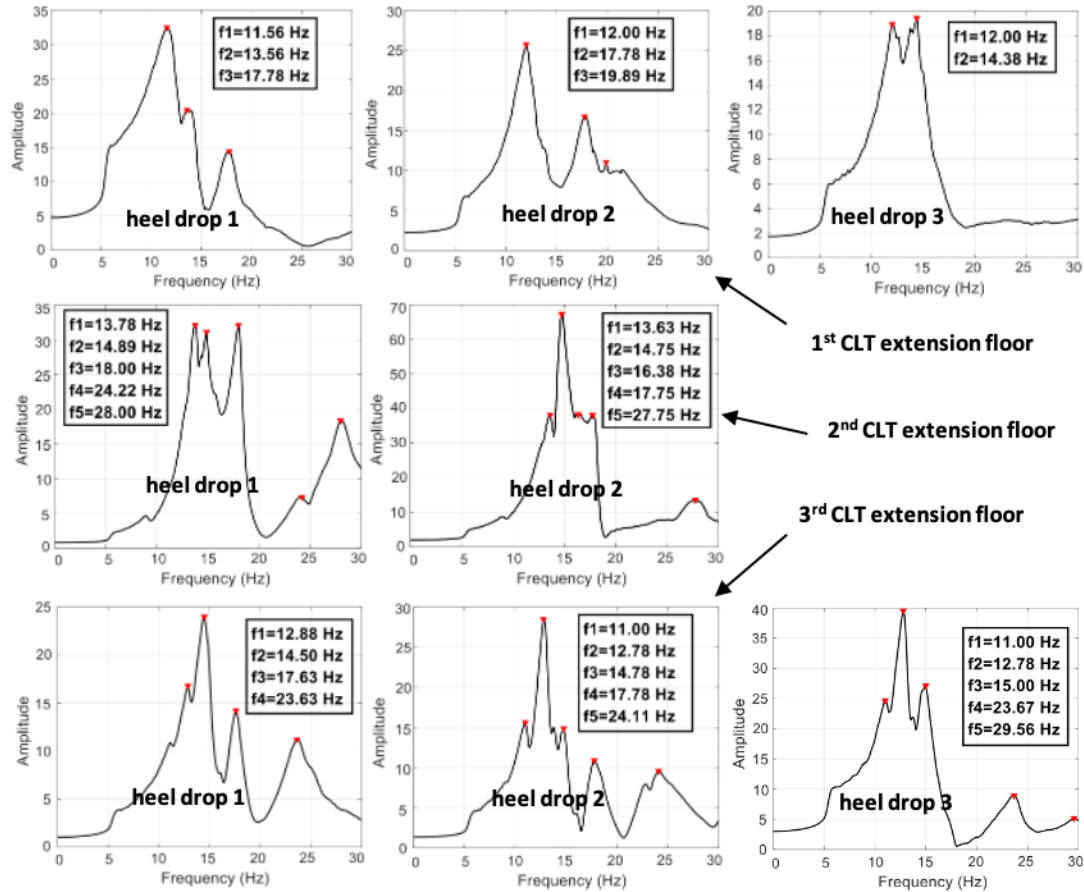


Figure 4.36: FFT Results of Heel-drops on the 1st, 2nd and 3rd CLT Extension Floor (Site 3)

Table 4.9 illustrated that the first-order structural damping of the three floors of the CLT Extension was significantly high. Heel-drop tests were conducted at three locations on each floor slab to reduce test errors. The average damping value of the first CLT extension floor was approximately 9.8%, while the second and third floors exhibited values of 16.5% and 14.8%, respectively. These damping values were notably high, and two primary factors contribute to these results. **First, the floors were primarily supported by CLT walls**, and the wooden structure significantly increased the damping of the test floors. Second, the areas tested were heel used as conference rooms, which **contain large furniture, including a long desk and nearly 20 chairs**. Given the relatively small size of the test floor (4.2 m wide by 8.4 m long), the presence of these equipment further increased the damping of the floor slabs.

Table 4. 9: Comparison between Heel-drops on the 1st, 2nd and 3rd CLT Extension Floor (Site 3)

1 st CLT Extension floor						
	Heel drop 1		Heel drop 2		Heel drop 3	
Mode	frequency	damping	frequency	damping	frequency	damping
1	12.16	10.26%	11.98	9.07%	12.27	9.97%
2	13.87	5.64%	17.78	5.73%	14.23	6.65%
3	17.62	5.68%	20.78	10.28%	18.92	18.42%
4	25.22	17.47%	29.11	8.26%	25.64	4.74%
5	31.98	6.11%			33.52	9.82%
2 nd CLT Extension floor						
Mode	Heel drop 1		Heel drop 2			
1	11.23	19.18%	10.16	13.91%		
2	14.04	8.82%	13.60	11.98%		
3	18.01	2.37%	14.88	3.32%		
4	23.78	9.27%	17.89	2.49%		
5	27.80	6.07%	27.60	10.84%		
6	30.28	8.56%	27.83	2.05%		
7	35.44	4.83%	34.25	3.81%		
3 rd CLT Extension floor						
Mode	Heel drop 1		Heel drop 2		Heel drop 3	
1	14.66	4.40%	12.35	12.31%	11.92	17.33%
2	17.73	3.61%	12.43	3.77%	12.77	3.02%
3	23.60	5.79%	17.22	4.59%	15.43	5.99%
4	30.17	15.52%	21.00	18.49%	23.62	4.11%
5	31.61	4.29%	23.84	11.10%	29.92	8.41%
6			29.88	3.92%	34.28	7.00%
7			35.56	7.59%		

4.4.4 Mode Shape and Modal Assurance Criteria (MAC) value

Measurements were conducted at 9 to 12 evenly distributed points across the plate, and the resulting data were used to generate Frequency Response Functions (FRFs) in a 3D mesh plot, allowing for visualization of the mode shapes. The imaginary component of the FRF was extracted using MATLAB to enable accurate mapping of the mode shapes.

The Modal Assurance Criterion (MAC) is a widely adopted method for quantifying the similarity between two mode shapes, commonly in structural analysis. MAC is frequently employed to compare experimental and theoretical mode shapes, but it can also be applied in Test-Test, FEA-FEA, and FEA-Test comparisons. A variant of MAC, AutoMAC, evaluates a set of mode shape vectors against themselves, which can help assess the sufficiency of the selected degrees of freedom (DOF) in identifying distinct modes. In test-test comparisons, AutoMAC is useful in highlighting potential issues in modal analysis, such as insufficient data points, which can make it difficult to differentiate between closely spaced modes.

The Modal Assurance Criterion (MAC) provides a measure of the least-squares deviation, or "scatter" of points from a straight-line correlation. Mathematically, the AutoMAC between two mode shapes, denoted as φ_r and φ_s , is the square of the correlation between two modal vectors, yielding a value between 0 and 1. A value of 1 indicates identical mode shapes, while values near zero indicate significant differences. This allows for an objective comparison of mode shapes in various analytical contexts.

$$MAC(\{\varphi_r\}, \{\varphi_s\}) = \frac{X}{F} = \frac{|\{\varphi_r\}^{*t} \{\varphi_s\}|^2}{(\{\varphi_r\}^{*t} \{\varphi_r\})(\{\varphi_s\}^{*t} \{\varphi_s\})} \quad (4.1)$$

4.4.4.1 Site 1

Figure 4.37 illustrated the mode shapes of the small floating floor. Most modes represented long bending along the X-axis, except for Mode 3 and Mode 4, which displayed torsional bending modes. These torsional modes indicated twisting motion along the floor, contrasting with the predominantly bending nature of the other modes.

For the large bare floor (Figure 4.38), Modes 1 through 4 depicted whole-span bending. In these modes, different sections of the floor vibrated either in unison or in opposition. Meanwhile, Modes 5 through 8 involved localized bending, where the plate vibrated in smaller, more defined areas.

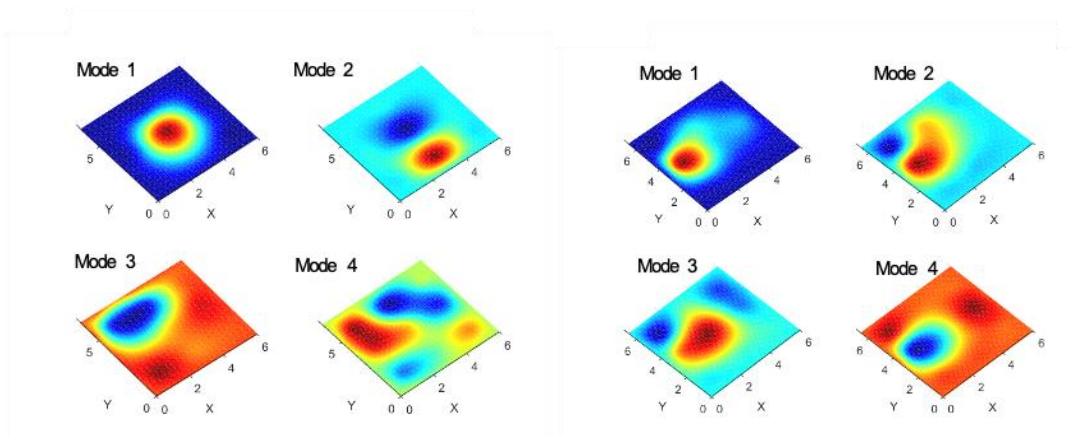


Figure 4. 37: Mode shapes of Small Bare floor and Small Raised Floor of Site 1

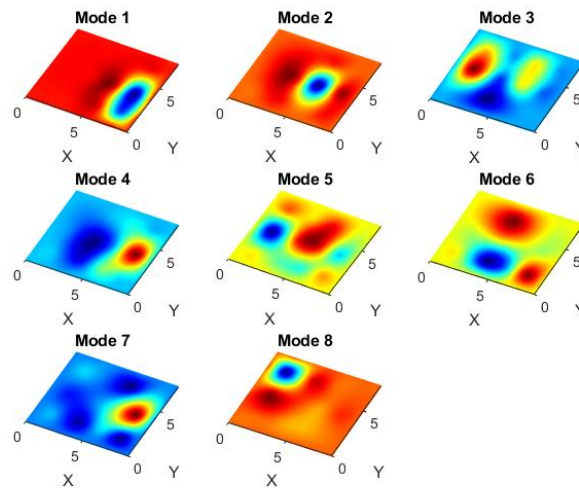


Figure 4. 38: Mode shapes of Large Bare Floor of Site 1

Insufficient measurement points often led to the incorrect identification of mode shapes. For instance, during the testing of the small bare floor at Site 1, several off-diagonal MAC values exceeded 0.8. This suggested that the measurement points were insufficient to capture the mode shapes with full accuracy. While the MAC data itself was not erroneous, these high off-diagonal values underscored the limitations in the data collection process.

In the specific case of Mode 4 for the small bare floor at Site 1, a MAC value of 0.78 indicated a strong similarity with Mode 3, as shown in Figure 4.39 (a). Similarly, the MAC analysis for the small raised access floor, shown in Figure 4.39 (b), revealed a strong correlation between Mode 2 and Mode 3, with a MAC value of 0.94. This level of correlation was comparable to the similarity observed between Modes 3 and 4 on the small bare floor.

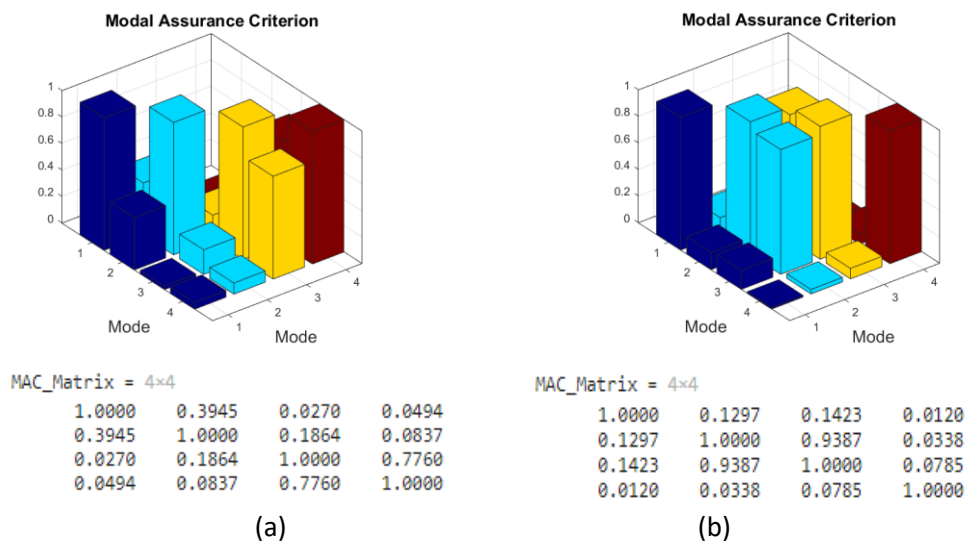


Figure 4. 39: MAC Values of Site 1: Small Bare floor and Small Raised Floor

The large bare floor provided more accurate identification of frequency and damping, resulting in more mode shapes and corresponding MAC values. As illustrated in Figure 4.40, one off-diagonal MAC value exceeded 0.8 (0.8165), indicating that Mode 4 and Mode 5 share a similar mode shape.

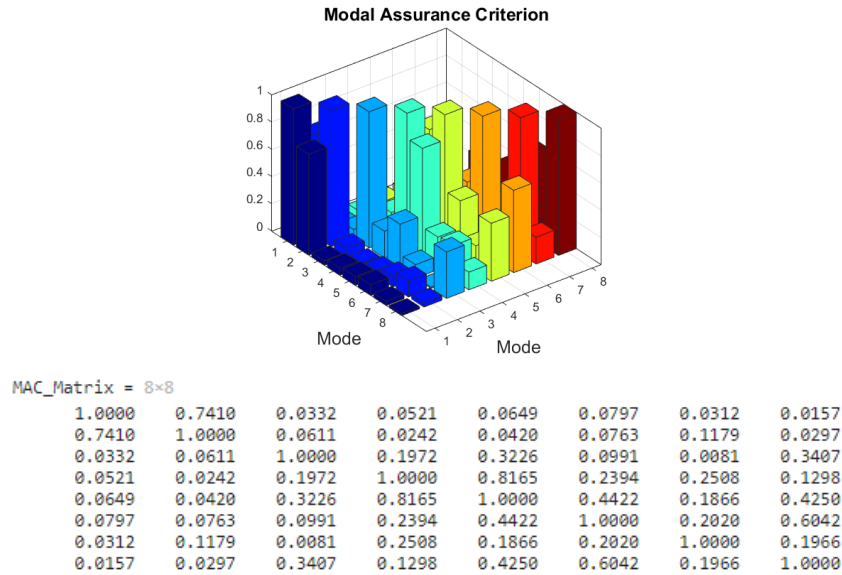


Figure 4. 40: MAC Values of Site 1: Large Bare Floor

4.4.4.2 Site 2

Modal testing was conducted at Site 2 on two distinct floor systems: a small floor with two bays and a large floor with three bays. For the small floor, 36 test points were used to capture the mode shapes, while 54 points were applied to the large floor.

As shown in Figure 4.41, the mode shapes for the small floor revealed different vibration patterns depending on the mode. In Modes 1 and 2, vibrations were concentrated in two main areas of the plate. By Modes 3 and 4, vibrations occurred in four distinct regions. As the modes increased, such as in Modes 5 and 6, the plate exhibited vibrations across eight areas. In the higher modes, from Mode 7 to Mode 9, the vibrations spread to twelve separate areas.

The accuracy of these measurements was confirmed by the MAC values. Diagonal MAC values were consistently 1, and all off-diagonal values were below 0.8. These results indicate that the mode shapes were well-identified, thanks to the sufficient number of measurement points.

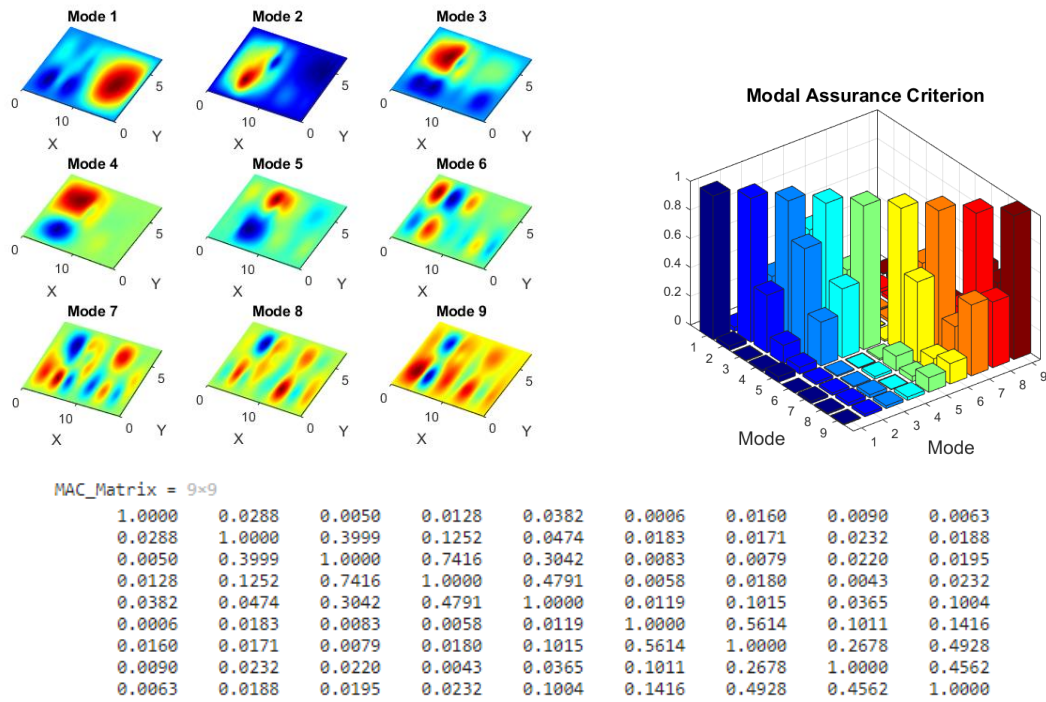


Figure 4. 41: Mode Shape and MAC Values of Small Floor (Site 2)

Similarly, the mode shapes of the large floor (Figure 4.42) displayed clear distinctions between modal orders, supported by an adequate number of test points and high-quality FRFs. As with the small floor, MAC values confirmed the distinctiveness of the modes, with off-diagonal values below 0.8 and diagonal values consistently at 1. These results provided strong evidence of distinct modes, ensuring that the mode shapes for both the small and large floors were accurately identified.

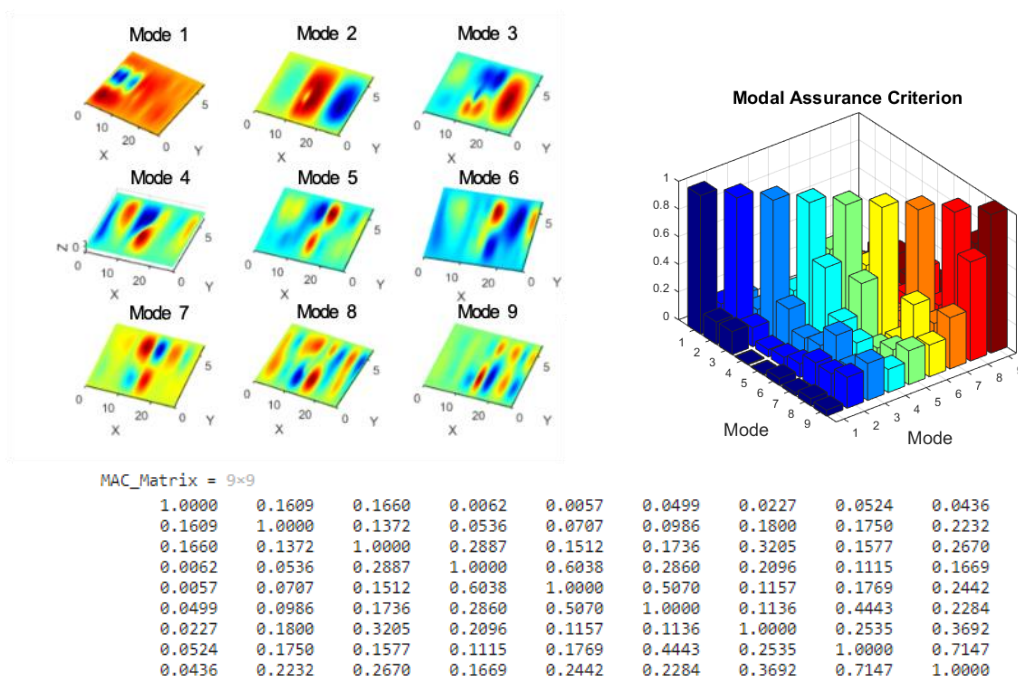


Figure 4. 42: Mode Shape and MAC Values of Large Floor (Site 2)

4.4.4.3 Site 3

For the modal testing conducted at Site 3, two areas of the third floor were tested using a modal shaker, while three extended CLT floors were assessed using an impact hammer. As illustrated in Figures 4.43 and 4.44, the mode shapes were clearly distinguishable. With increasing mode order, local vibration patterns became more pronounced. However, despite these visual distinctions, the calculated MAC values (0.7674) indicated similarities between mode 3 and mode 4, which are not easily discernible from the mode shapes alone.

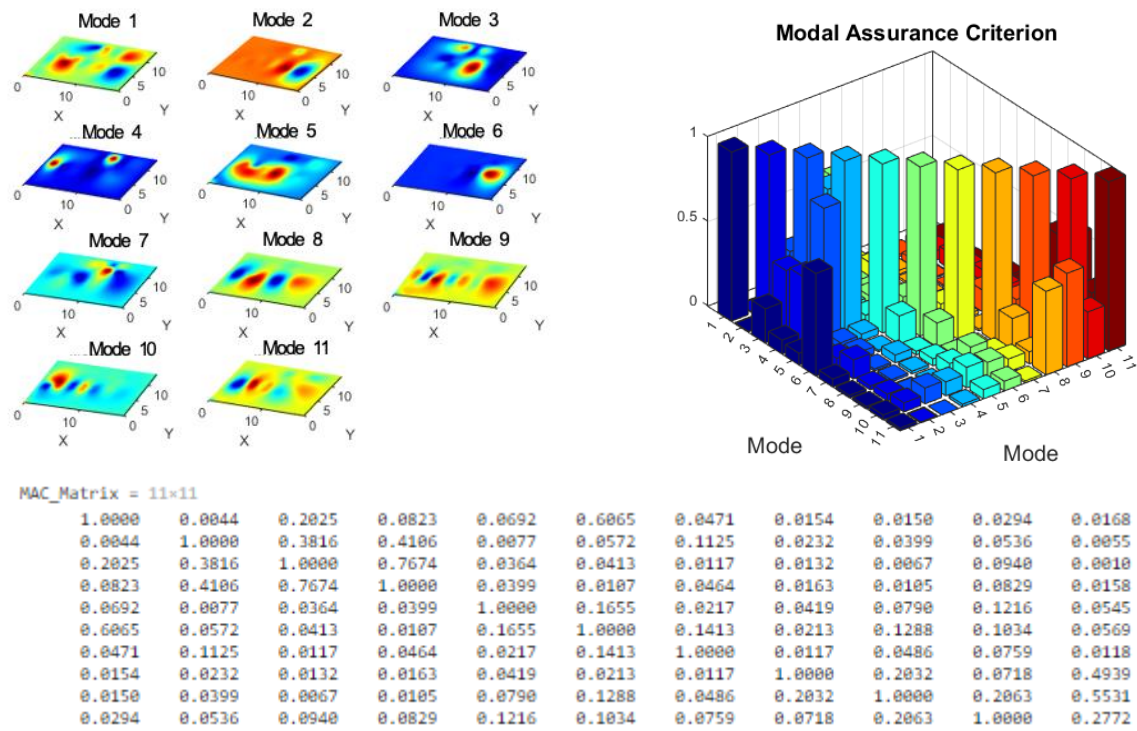
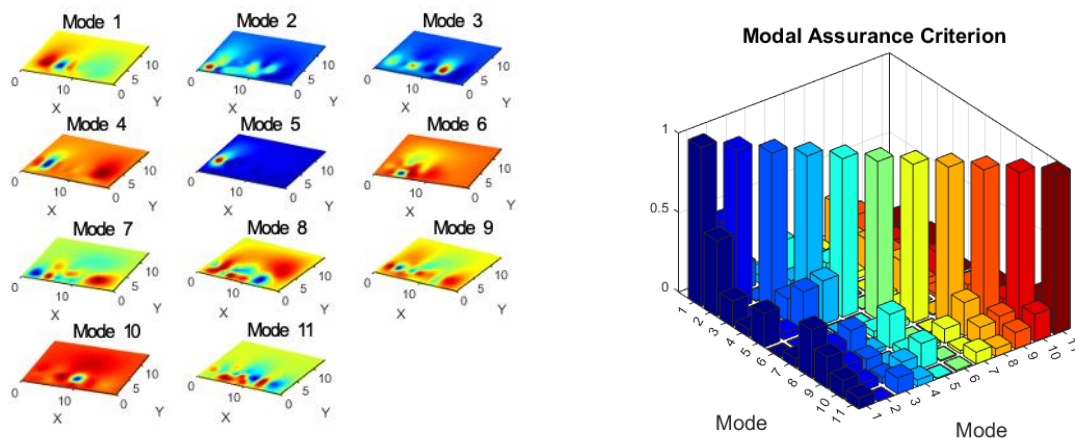


Figure 4.43: Mode Shape and MAC Values of Area 1 (Site 3)



MAC_Matrix = 11x11

1.0000	0.4773	0.1614	0.0485	0.2125	0.0042	0.0562	0.3048	0.1980	0.1156	0.0689
0.4773	1.0000	0.0046	0.0119	0.0433	0.0037	0.0038	0.1509	0.1021	0.0518	0.0039
0.1614	0.0046	1.0000	0.1470	0.2555	0.0124	0.0451	0.2057	0.0890	0.0406	0.1008
0.0485	0.0119	0.1470	1.0000	0.2758	0.0068	0.0035	0.0255	0.0075	0.0882	0.0411
0.2125	0.0433	0.2555	0.2758	1.0000	0.0064	0.0401	0.2124	0.0423	0.1585	0.0066
0.0042	0.0037	0.0124	0.0068	0.0064	1.0000	0.0365	0.0021	0.0200	0.0077	0.0089
0.0562	0.0038	0.0451	0.0035	0.0401	0.0365	1.0000	0.0074	0.0896	0.0191	0.0735
0.3048	0.1509	0.2057	0.0255	0.2124	0.0021	0.0074	1.0000	0.2096	0.1180	0.0496
0.1980	0.1021	0.0890	0.0075	0.0423	0.0200	0.0896	0.2096	1.0000	0.1413	0.1034
0.1156	0.0518	0.0406	0.0882	0.1585	0.0077	0.0191	0.1180	0.1413	1.0000	0.1715

Figure 4. 44: Mode Shape and MAC Values of Area 2 (Site 3)

In the Side Extension test area, the first three modes of the three CLT floors display a high degree of collinearity, as reflected in the MAC values. As seen in Figure 4.45, the MAC values for the first CLT extension floor reveal significant similarities between mode 1 and modes 2, 3, 8, 9, 11, and 12. Similar patterns were observed on the second and third CLT extension floors (Figures 4.46 and 4.47). These findings suggested that the impact hammer testing did not provide the most accurate modal parameter identification, and further updates to the FRFs are required to improve the results.

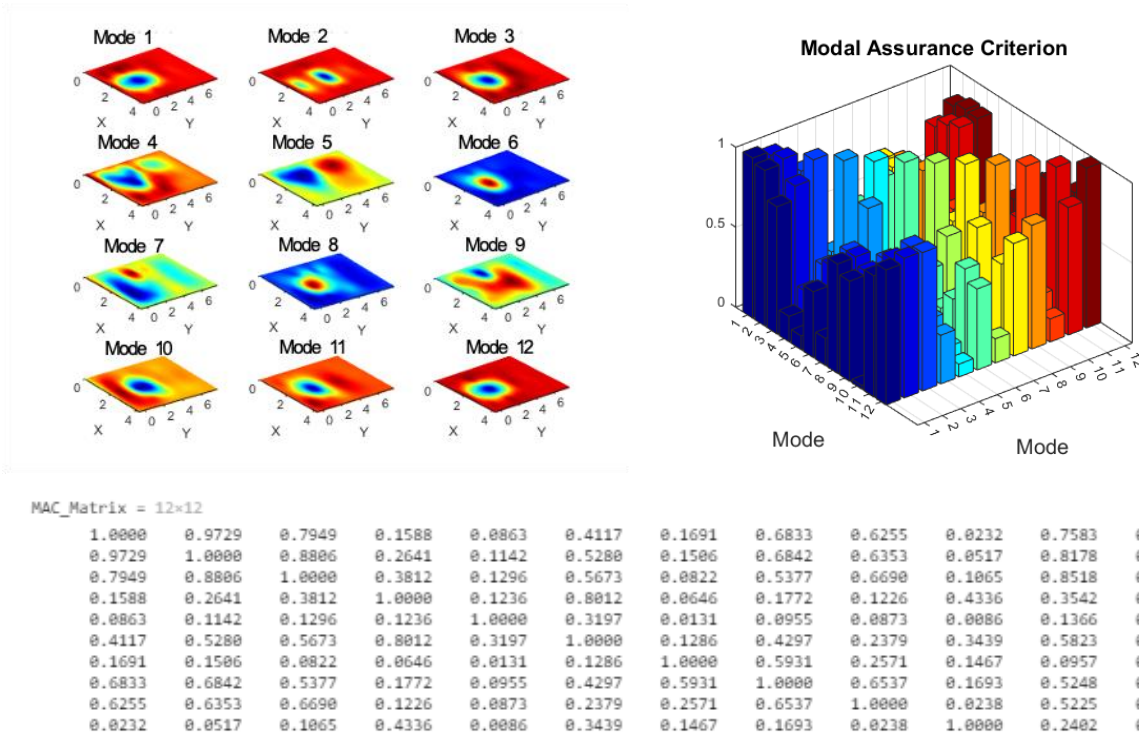


Figure 4. 45: Mode Shape and MAC Values of 1st CLT Extension (Site 3)

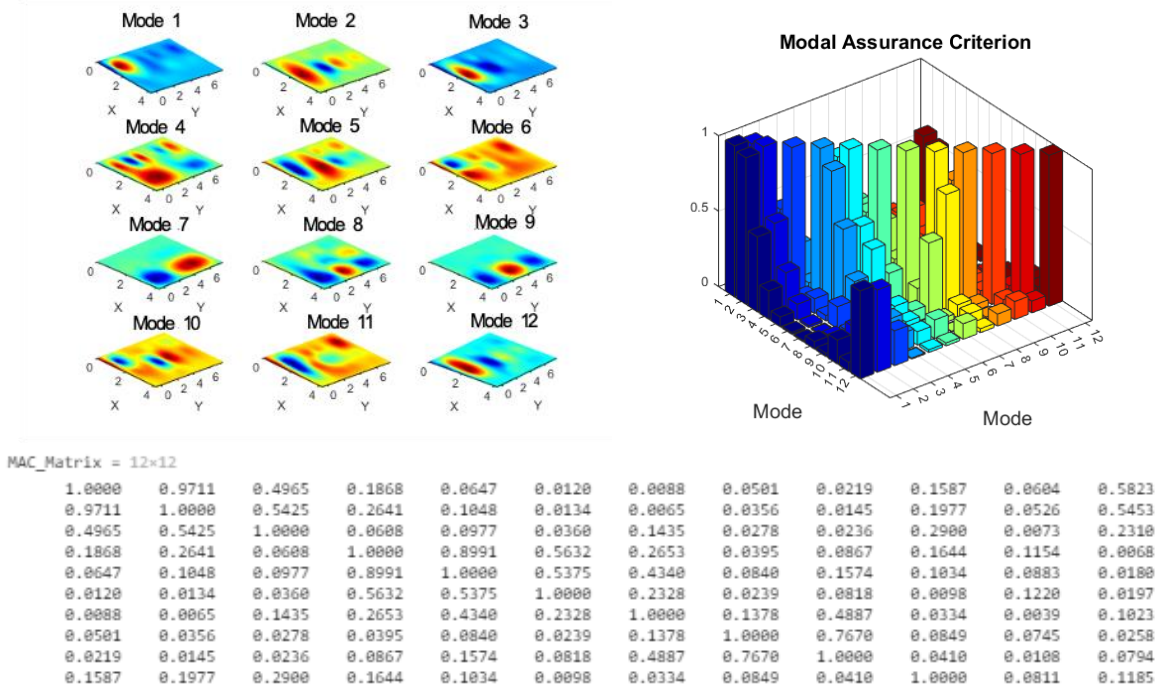


Figure 4.46: Mode Shape and MAC Values of 2nd CLT Extension (Site 3)

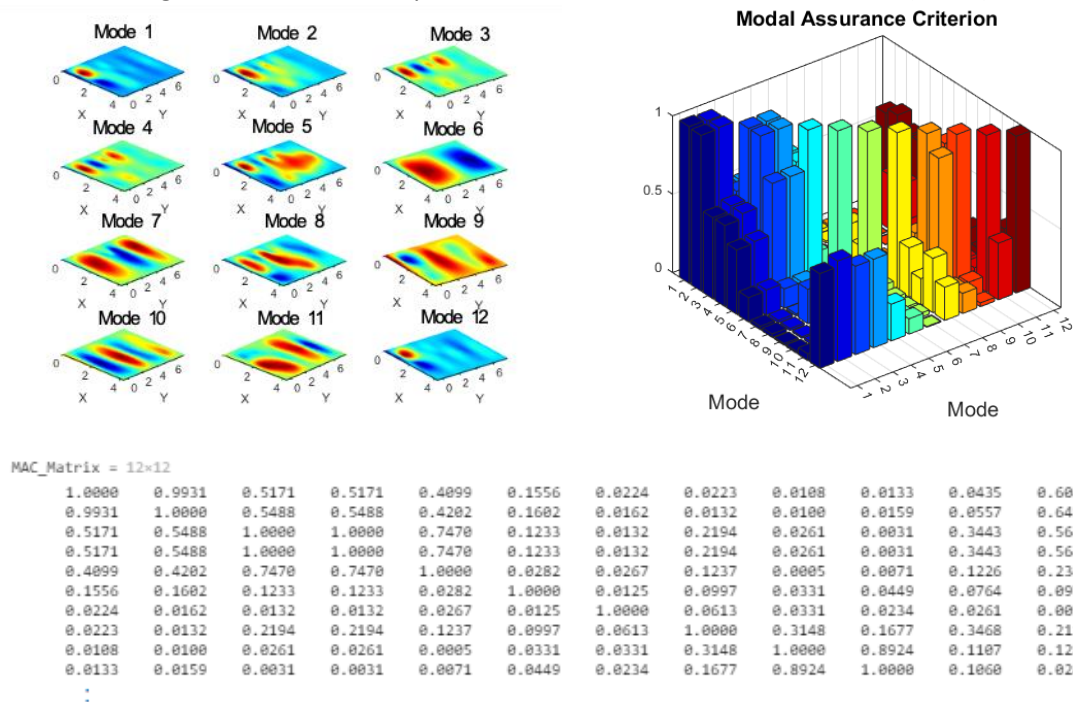


Figure 4.47: Mode Shape and MAC Values of 3rd CLT Extension (Site 3)

4.5 Acceleration and R-factor

The frequency-weighted root mean square (RMS) acceleration results for 10 floors were summarized in Table 4.10. **Running induces higher acceleration responses compared to walking, with increased step frequency raising the likelihood of discomfort.** The results for the running condition at 2.89 Hz were shown in Table 4.10, representing the maximum R-factor among the three tests: walking at 1.5 Hz, walking at 2 Hz, and running at 2 Hz. The R-factor for wooden floors is intuitive, with a widely

accepted range of 4 to 36. Lower R-factors are typically used for residential floors, while office floors generally fall within the range of 24 to 36. The calculation of the running R-factor can assist in quickly identifying whether the tested floor slab is within the conventional comfort design range.

Table 4. 10: The RMS Acceleration and R-factor Results from Walking and Running

Site 1 a_{rms} [m/s ²]								
Total	Storey	Size	Walking 1.5Hz	Walking 2Hz	Running 2.89 Hz	R-factor *	Level IV Pass/Fail	Level V Pass/Fail
3 floors	3 rd floor- CLT	Small bare floor 6x6.6m	0.012	0.024	0.11	22.77	✓	✓
		Large bare floor 9x7.8m	0.009	0.012	0.09	16.96	✓	✓
		Raised access floor 9x7.8m	0.020	0.026	0.15	30.35	✗	✓
Site 2 a_{rms} [m/s ²]								
Total	Storey	Size	Walking 1.5Hz	Walking 2Hz	Running 2.89 Hz	R-factor	Level IV Pass/Fail	Level V Pass/Fail
2 floors	4 th floor- CLT	Small floor (9+9) x6.6 m	0.013	0.023	0.29	47.49	✗	✗
		Large floor (9+9+9) x6m	0.012	0.021	0.21	42.46	✗	✗
Site 3 a_{rms} [m/s ²]								
Total	Storey	Size	Walking 1.5Hz	Walking 2Hz	Running 2.89 Hz	R-factor	Level IV Pass/Fail	Level V Pass/Fail
5	3 rd floor	Area 1: 9x4.5m	0.019	0.023	0.19	37.30	✗	✗
		Area 2: 9x4.5m	0.012	0.027	0.12	24.95	✗	✓
		Extension CLT floor: 4.2x 7.8m	0.027	0.050	0.14	27.01	✗	✓
	2 nd floor	Extension CLT floor: 4.2x 7.8m	0.060	0.047	0.22	44.95	✗	✗
	1 st floor	Extension CLT floor: 4.2x 7.8m	0.025	0.064	0.19	38.96	✗	✗

R-factor* is the running R-factor

The calculation results were provided without the Vibration Dose Value (VDV) results because the VDV method, as recommended by BS 6841 and BS 6471, presented challenges in practical application. For instance, BS 6472 required acceleration data to be collected over 16 or 8 hours to calculate VDV, complicating the process despite the provision of limit ranges. Other methods for calculating VDV also encountered challenges, often requiring users to estimate parameters and make assumptions, which could introduce inaccuracies.

The revised Eurocode 5 (rEC5) introduces a classification system for office and residential flooring designs, offering performance levels for vibration control. While the standard provides higher usability compared to other guidelines, concerns remain regarding its suitability for building types such as schools and hospitals.

In this analysis, the performance of office floors was assessed. Two performance levels were considered: Level IV, with a recommended response factor (R) of 24, and Level V, with an R-factor of 36. **The acceleration control threshold for both levels is defined as 0.005R.**

Figure 4.48 illustrated the relationship between the R-factor in rEC5 and the frequency-weighted root mean square (RMS) acceleration results for the 10 test floors listed in Table 4.10. Under

walking frequencies of 1.5 Hz and 2 Hz, all 10 floors met the standards for Level IV, the basic performance level for office floor designs. The floors also met the standards for Level V, which offers a more economical choice for office vibration control. However, when tested at a running frequency of 2.89 Hz, none of the floors met the standards for any performance level.

As discussed in Chapter 2, **the revised Eurocode 5 (rEC5) is designed for human-induced vibrations caused by walking, within the frequency range of 1.5 to 2.5 Hz. As a result, it excludes other common motions, such as running, which may lead to design inadequacies.** The R-factor recommendations in the design specification may be too low to account for vibrations at higher frequencies.

Although rEC5 draws on the design parameters of ISO 2631, it selectively applies these standards, focusing only on the 1.5 to 2.5 Hz range. ISO 2631, however, covers a broader frequency range of 1 to 80 Hz. **By limiting its scope to walking-induced frequencies, rEC5 overlooks other motions, such as running, which can occur frequently in building environments. This selective approach warrants further scrutiny regarding its applicability to real-world scenarios.**

Additionally, as shown in Figure 4.48, the natural frequencies of all the tested floors were above 7 Hz. This finding suggests that **further research is needed on low-frequency floors, particularly those with frequencies between 4.5 and 7 Hz, as current knowledge in this area remains limited.**

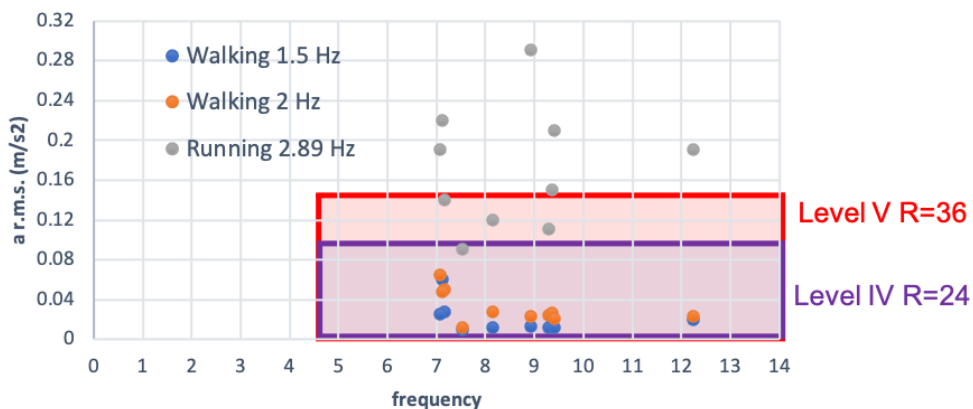


Figure 4. 48: Acceleration Compared with Criteria Response Factor R Recommended in Revised Eurocode 5

4.6 Summary of the Comparison between Sites and Various Test Methods

4.6.1 Investigated Buildings

Three office buildings were investigated, and six cross-laminated timber (CLT) floors of varying sizes and configurations were selected for testing. The dimensions of the test floors were depicted in Figure 4.49. The general information and support details of eight floors were summarized below:

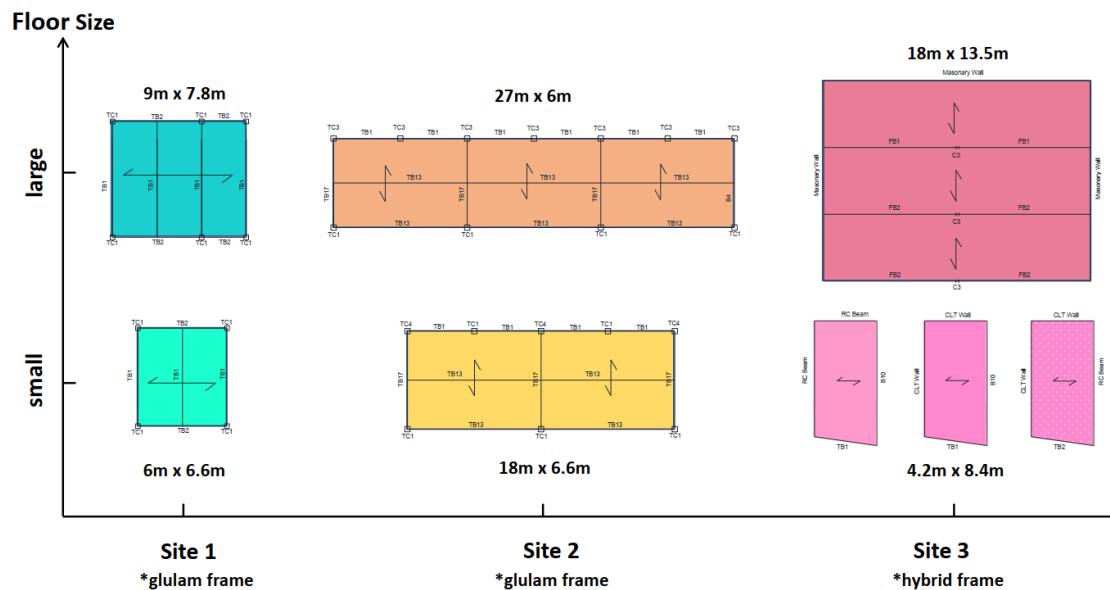


Figure 4. 49: The Layout of the Eight Tested Floors

Site 1 is a refurbished building constructed using CLT. Two areas on the third floor were selected for testing: a two-span small floor and a three-span large floor, both supported by glulam beams. Modal testing was conducted while the building was still under construction, allowing the raised access floor panels to be removed during testing.

Site 2 is a CLT and Glulam structured 6 story office building, as an extended part of the old existing building. Two areas on the fourth floor were selected, containing a two-bay small floor test area and a three-bay large floor test area. The whole floor area has finished with the raised access floor system which is ready for the occupied and therefore cannot be removed. The test area was clean and empty without any furnishings and equipment.

Site 3 is a redevelopment of an existing four-story masonry building, which was expanded with a new side extension. The third floor, constructed using a hybrid steel and CLT system, was selected

for testing. The raised access floor, with an 8 mm acoustic resin layer, was installed on top of the CLT flooring system. Additionally, three CLT floors in the side extension were selected, all predominantly constructed using CLT. Field tests were conducted on the in-service floor system, which had been occupied for over two months following the completion of construction.

4.6.2 Experiments

4.6.2.1 *The location of the exciter and sensors*

For shaker excitation, the shaker was positioned near the center of the single-span floor. When testing the continuous multi-span floor, the shaker was placed at modal antinodes to improve the quality of the measured response. For example, it was positioned at one-quarter of the span length to avoid placement directly above the support beams.

For impact hammer testing, the center of the single-span floor was chosen as the preferred location for the impact points. To ensure consistency in the test, the location was marked. However, if the center point was obstructed by heavy furniture or equipment, alternative points were considered to facilitate testing.

The criteria for the heel-drop test were similar to those for the impact hammer test. Using a timer to control the duration of each test is recommended.

The roving sensor method was adopted for the consideration of the limited sensor and the moving convenience. The 0.6m test grid was selected to help locating the sensors (shown in Figure 4.50). A wider grid can be divided when limited sensors are used, to achieve the time-saving goal while accepting the loss on the mode shape accuracy. One accelerometer was fixed as the reference point, the location of the exciter can be also used as the reference point. Considering the consistency of the measurement unit, another point (difference from exciter) was selected as the reference point. At each step of the test (shaker and hammer), six accelerometers No.2 through No.7 were moved along the marks on the grid to measure the structure response amplitude under the excitation.

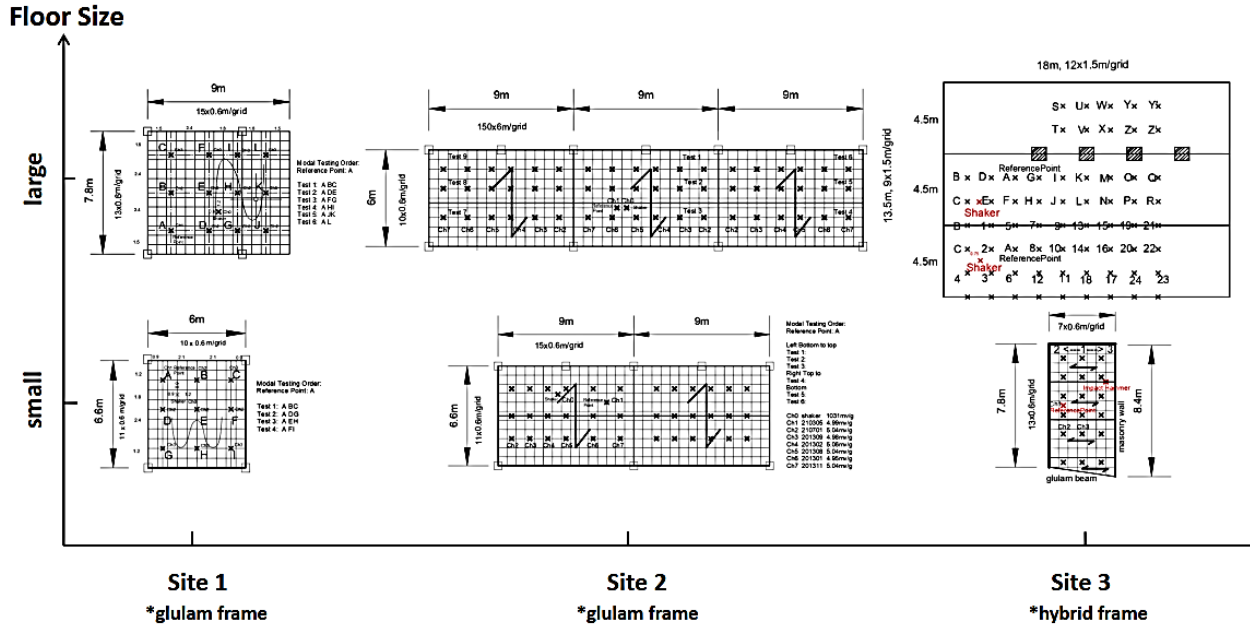


Figure 4.50: The Test Grid and Location of the Sensors and Exciter

For all dynamic tests, two four-channel WebDAQ 504 data loggers, connected to a laptop computer, were used to record the test measurements. An accelerometer was attached to the shaker armature to measure the acceleration and compute the input during the modal tests. The impact hammer used a sensor embedded in its tip.

4.6.2.2 The input signal of the field test

Modal testing using a shaker and impact hammer typically lasted 3-5 minutes to ensure that repeated inputs generate sufficient responses. During the impact hammer test, at least 10 seconds were allowed to pass after each hit, with heel drops repeated every 3 minutes. Figure 4.51 illustrated one of the output channels (top) and the input (bottom) time history raw data from the six tested floors.

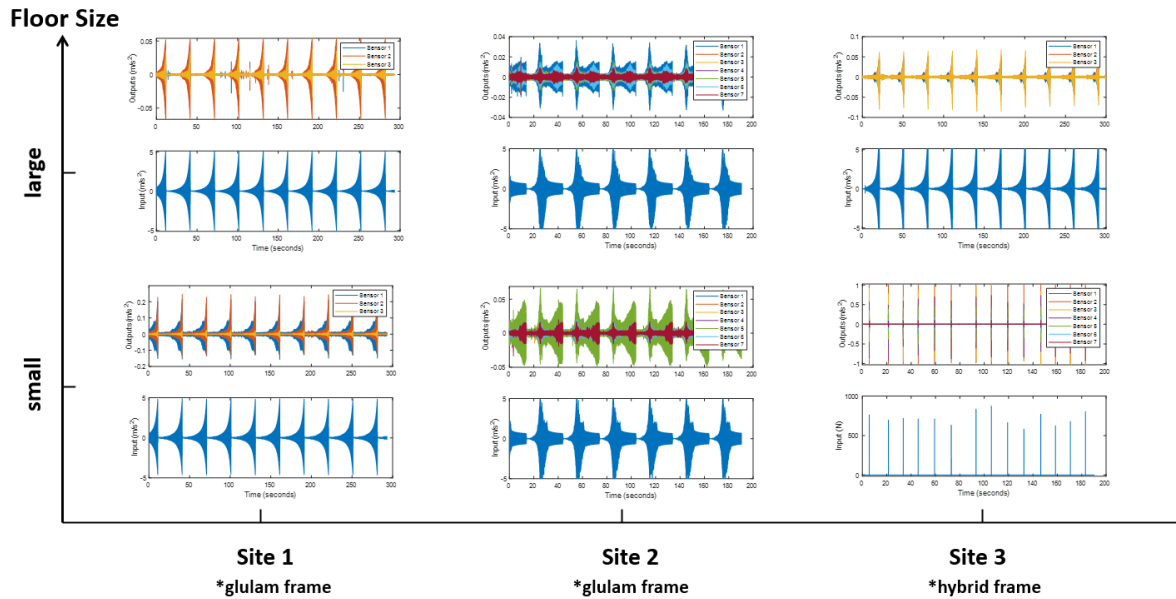


Figure 4.51: Output and Input Time History Data from the Field Test

In the impact hammer testing method, a harder tip was selected to excite the floor's response. For the modal shaker, a sweep sine input was provided by the controller. The primary advantage of these two methods lies in their measurable input signals, which can be further utilized to estimate the Frequency Response Function (FRF) curve, natural frequency, and damping ratio.

Figure 4.52 presents the Power Spectral Density (PSD) of the input signal in the frequency domain. This FFT-based time-frequency analysis visualizes how the frequency content of the signal changes over time. The small floor on Site 2 and the 1st CLT Extension floor on Site 3 are selected for explanation. The modal shaker testing clearly reveals a prominent peak at 12 Hz in the input signal compared to other frequency components. In contrast, the impact hammer yields a broader frequency response across the entire range.

The spectrogram provides additional insights, with colors encoding frequency power levels. Yellow indicates higher power frequency content, whereas blue signifies very low power. The plot from the modal shaker testing shows a linear sine-sweep signal ranging from 0 to 30 Hz, with the strongest signals appearing around 10 Hz and 25 Hz, as indicated by the brighter yellow colors. In contrast, the impact hammer results show a broadly distributed signal from 0-100 Hz for each hit, with significant noise below 10 Hz that persists over time.

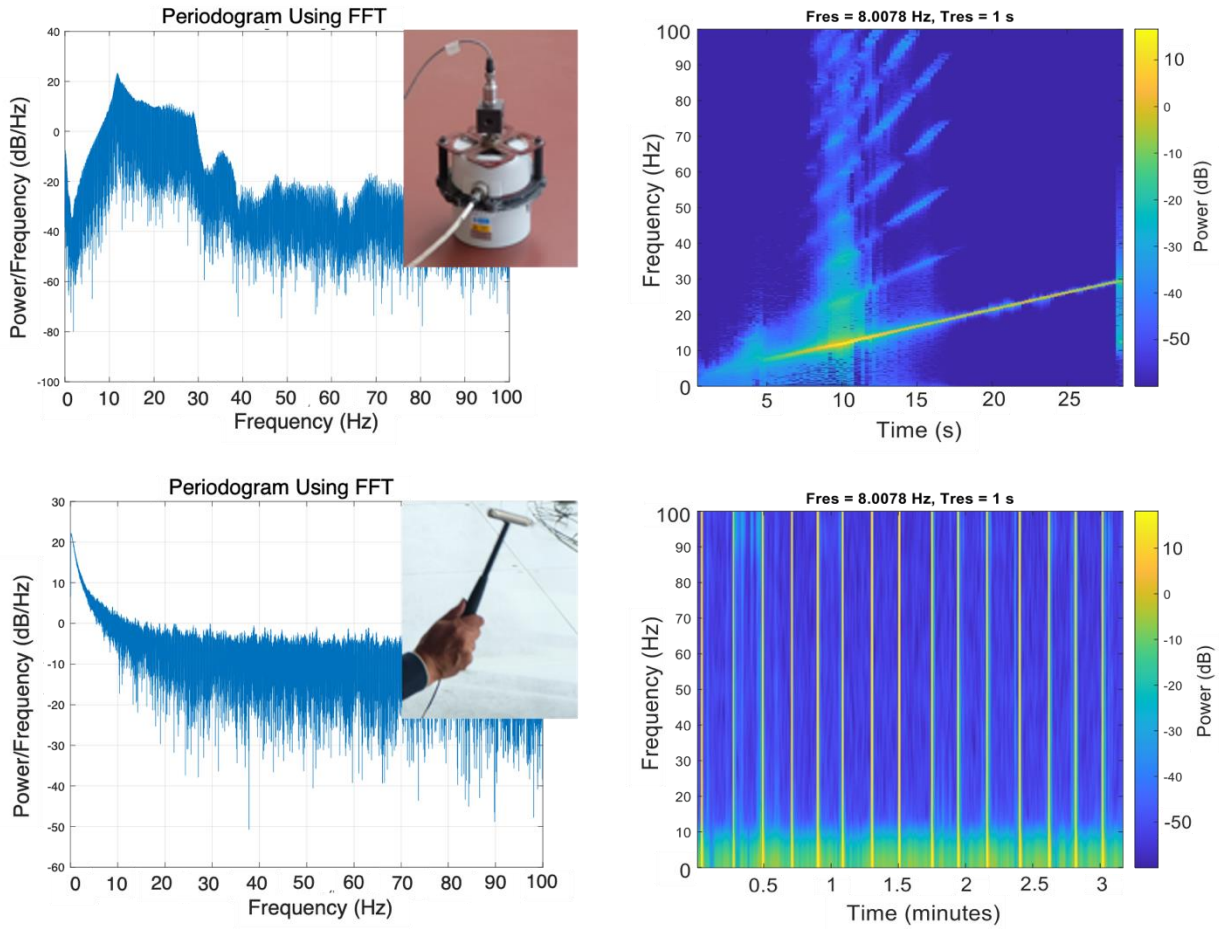


Figure 4.52: The Tested 6m×6m Floor and the Frequency Response

The key difference between the impact hammer and modal shaker lies in the excited frequencies. Generally, when the y-axis value exceeds 0.8, the coherence between input and output is strongest at that frequency. As illustrated in Figure 4.53, the best coherence found in shaker testing occurs roughly between 0-30 Hz. For the impact hammer, higher frequency components are primarily excited, with good coherence achieved after 8 Hz. Below this threshold, noise complicates the recognition of input frequencies, leading to a lower signal-to-noise ratio.

This finding leads to a critical conclusion: for floors with lower frequencies (<8 Hz), the modal shaker is a more effective choice than the impact hammer. The latter is more suitable for cases where the natural frequency exceeds 8 Hz, as lower modes may be missed with the impact hammer.

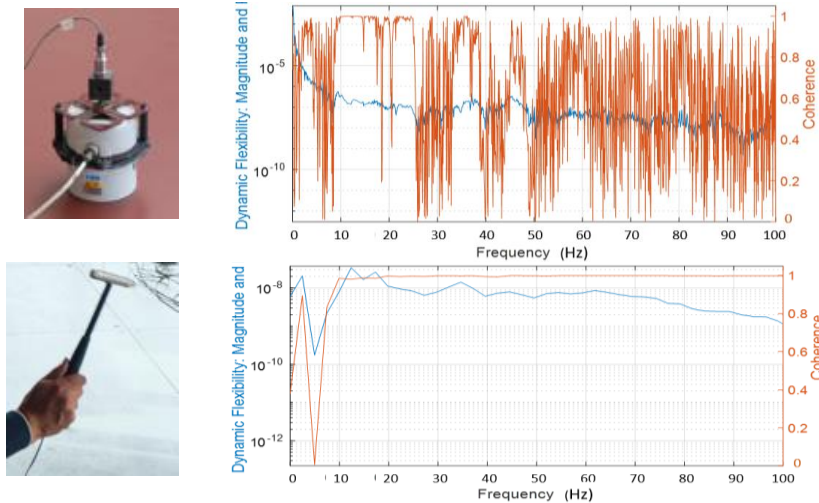


Figure 4. 53: The tested 6m×6m floor and Coherence Function

The heel drop test has been utilized for many years due to its simplicity and ease of understanding. However, it has a significant limitation: only the output is measured, which complicates the analysis due to unknown and variable input forces. Consequently, the FRF cannot be analyzed, and coherence diagrams cannot be constructed to assess test quality. An output-only analysis method must be adopted, heavily relying on the operator's engineering knowledge and experience. Blakeborough and Williams (2002) noted that the heel drop method is appropriate when the floor frequency is around 10 to 15 Hz, based on an understanding of the input force (see Figure 4.54). They also mentioned that the tester's weight has minimal influence on the PSD diagram in the frequency domain.

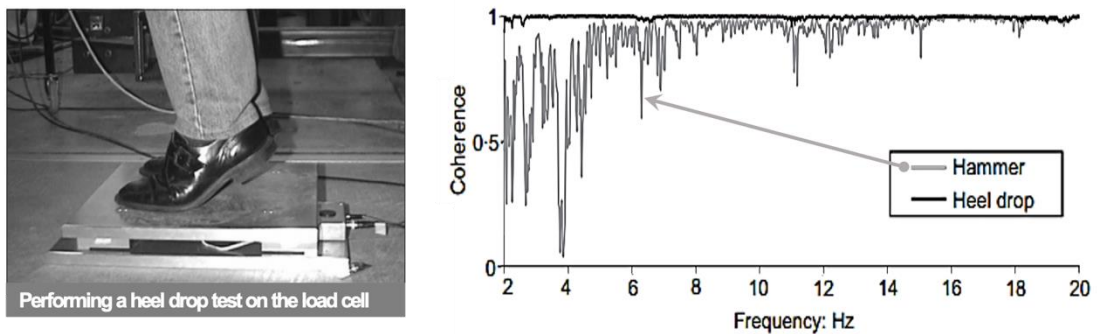


Figure 4. 54: Performing a Heel Drop Test on the Load Cell and the Coherence Determined by Instrumented Heel Drop Test (Blakeborough and Williams, 2003)

4.6.2.3 The analysis method

A curve-fitting method was adopted for the analysis, specifically through the creation of a state-space model for Frequency Response Function (FRF) modal fitting. The stability of the modal parameters was verified, and stable natural frequencies and damping ratios were identified using

the state-space model. Figure 4.55 illustrates the state-space model fit results for the large floor at Site 2.

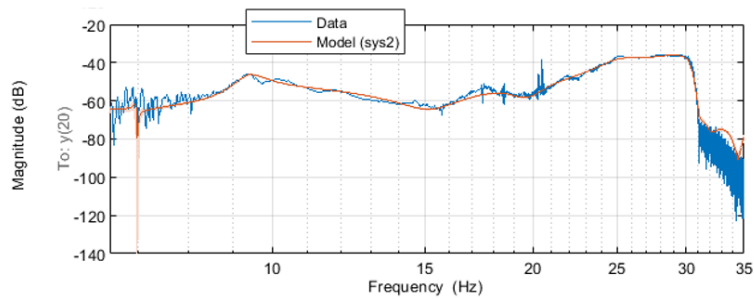


Figure 4. 55: The Fit between FRF Data and Refined Model of the Large Floor on Site 2

A similar approach was employed for the heel-drop test, utilizing the CE method in the time domain for identification. The shape and amplitude of the fitted orange line closely match the measured blue line, as depicted in Figure 4.56.

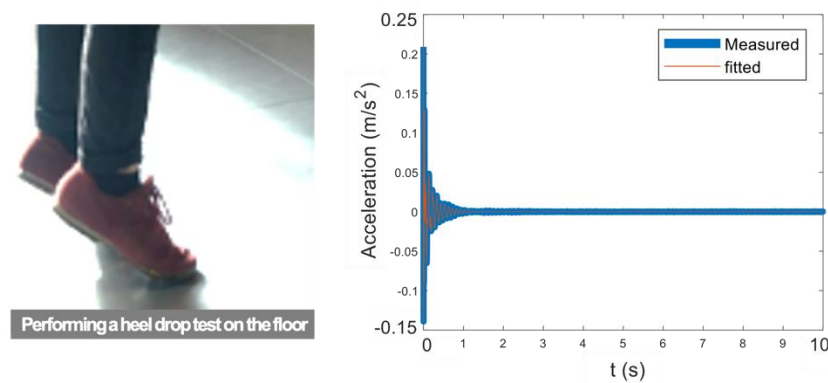


Figure 4. 56: CE Method in Time Domain for Identification

Following the modal parameter identification analysis, the natural frequencies and damping ratios were calculated. The natural frequencies were well separated; however, low-frequency modes may have been lost due to the uncontrollable field test environment. When comparing the damping ratios obtained from the modal shaker and impact hammer, the amplitudes were found to be acceptable based on the established criteria. In contrast, the heel-drop output-only test indicated that most damping ratios for the corresponding frequencies were excessively high, raising questions about their validity. Specific data will be tabulated and discussed in the next section.

4.6.3 Experimental Results and Conclusions

4.6.3.1 The natural frequency and damping ratio of Site 1

The data presented in Table 4.11 shows that the natural frequencies obtained from heel drop testing and modal shaker testing are closely aligned. The differences between the two methods range from

99.78% similarity to deviations of 94.04% and 115.86%. Regarding the damping results, modal shaker testing demonstrates a clear advantage, providing more precise values. Typically, the damping ratio for timber structures ranges from 1% to 3%, depending on construction conditions. Table 4.11 indicates that the modal shaker method produced damping ratios of 1.52% and 2.50% for the first natural frequency, while the heel drop test resulted in significantly higher damping ratios of 5.7% and 9.05%—which are 3.75 and 3.62 times higher, respectively.

Table 4. 11: Comparison between Heel Drop and Modal Shaker Results on Site 1

Site1: Small bare floor						
	Heel-drop		Modal Shaker		Ratio % (Heel-drop/Modal Shaker)	
Mode	frequency	damping	frequency	damping	frequency	damping
1	9.28	5.70%	9.30	1.52%	99.78%	375.00%
2	12.42	5.11%	12.97	1.93%	95.76%	264.77%
3	18.31	7.38%	17.89	3.30%	102.35%	223.64%
4	27.73	11.42%	24.62	4.83%	112.63%	236.44%
Site1: Large bare floor						
	Heel-drop		Modal Shaker		Ratio % (Heel-drop/Modal Shaker)	
Mode	frequency	damping	frequency	damping	frequency	damping
1	7.74	9.05%	7.81	2.50%	99.10%	362.00%
2	10.74	9.39%	11.00	6.96%	97.64%	134.91%
3	14.98	10.64%	15.93	19.90%	94.04%	53.47%
4	21.03	16.60%	19.91	7.73%	105.63%	214.75%
5	23.31	11.07%	22.33	7.17%	104.39%	154.39%
6	30.25	9.21%	26.11	5.70%	115.86%	161.58%

The trends in these results are illustrated in Figure 4.57. It is evident that the natural frequencies identified from both the modal shaker and heel drop tests are almost identical, with natural frequency increasing as the mode order rises. Furthermore, both methods reveal a similar trend for damping ratios, with values increasing alongside the mode order. However, the damping ratios from the heel drop test are consistently higher than those from the modal shaker test.

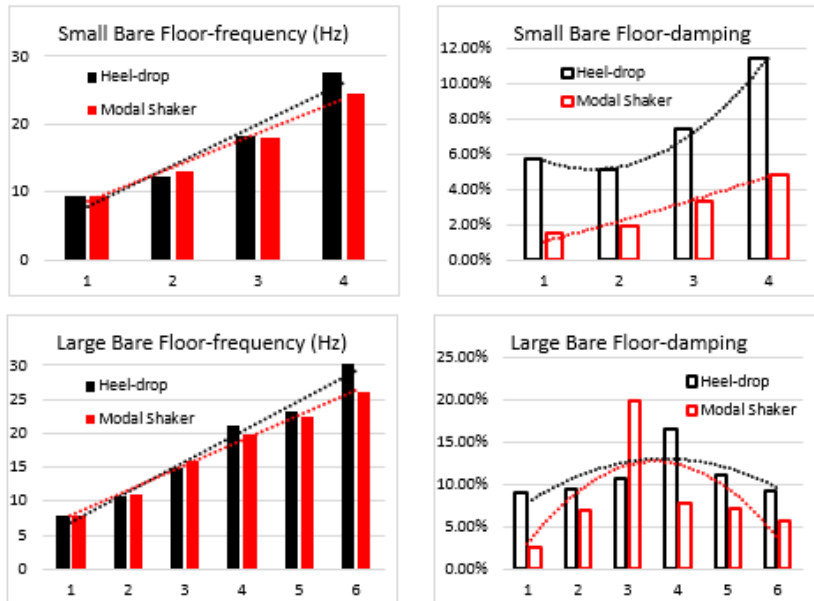


Figure 4.57: Illustrated Frequency and Damping Data of Table 1

4.6.3.2 The natural frequency and damping ratio of Site 2

The frequency and damping testing results for Site 2 were summarized in Table 4.12. The frequencies identified from both the modal shaker and heel drop testing methods were closely aligned, with the frequency ratio (heel drop/modal shaker) reaching 99.84% for the small floor and 99.79% for the large floor. In some modes, the frequencies were smaller or larger depending on the test method, with the ratios varying between 107.44% for the small floor and 102.10% for the large floor. These differences, which are within a 10% range, suggested that the natural frequencies identified from both methods are highly similar. This indicated that heel drop testing is comparable to modal shaker testing in terms of accuracy, even though the input signal is not accounted for in the calculation.

For ease of comparison, the data is illustrated in Figure 4.58, which clearly shows the trends in frequency and damping as the mode order increases. In both the small and large floors, the natural frequencies rise with higher mode orders. Additionally, the quality of coherence directly influences the stability of the identified frequency and damping, with more stable results observed in the modal shaker testing.

The damping ratio exhibits a similar "M-shaped" trend in both testing methods, increasing twice before decreasing across the identified modes. On the small floor, the heel drop test produced higher damping ratios than the modal shaker test for the first four modes but lower ratios for the higher modes. However, on the large floor, the modal shaker consistently provided higher damping ratios across all modes compared to the heel drop test. Due to the random variation in damping results,

drawing definitive conclusions on the accuracy of the damping values from the two methods is challenging.

Table 4. 12: Comparison between Heel drop and Modal shaker Results on Site 2

Site2: Small floor						
Mode	Heel-drop		Modal Shaker		Ratio % (Heel-drop/Modal Shaker)	
	frequency	damping	frequency	damping	frequency	damping
1	8.87	6.25%	8.93 Hz	2.02%	99.33%	309.41%
2	10.83	10.05%	10.08 Hz	8.53%	107.44%	117.82%
3	14.87	4.98%	14.68 Hz	2.23%	101.29%	223.32%
4	17.07	5.34%	17.40 Hz	3.78%	98.10%	141.27%
5	23.19	2.53%	24.13 Hz	3.40%	96.10%	74.41%
6	27.89	3.97%	27.83 Hz	7.76%	100.22%	51.16%
7	29.61	11.30%	29.80 Hz	15.90%	99.36%	71.07%
8	30.39	3.53%	30.44 Hz	3.58%	99.84%	98.60%

Site2: Large floor						
Mode	Heel-drop		Modal Shaker		Ratio % (Heel-drop/Modal Shaker)	
	frequency	damping	frequency	damping	frequency	damping
1	9.38	4.22%	9.4	3.48%	99.79%	121.26%
2	18.64	8.24%	19	10.00%	98.11%	82.40%
3	25.76	4.72%	25.23	5.37%	102.10%	87.90%
4	28.19	4.66%	28.7	9.48%	98.22%	49.16%
5	29.93	2.83%	30.46	1.35%	98.26%	209.63%

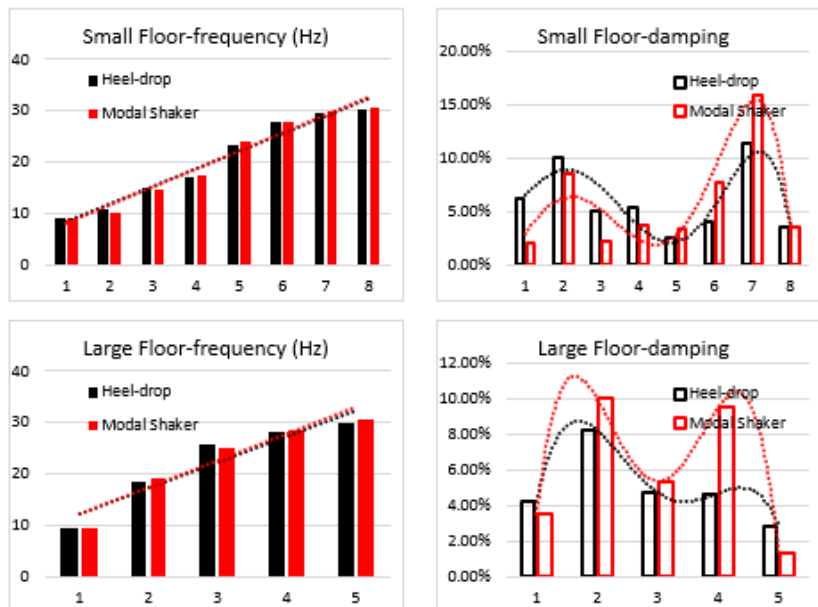


Figure 4. 58: Illustrated Frequency and Damping Data of Table 4.12

4.6.3.3 The natural frequency and damping ratio of Site 3- 3rd Floor and CLT Extension

Table 4.13 compared the identified frequency and damping results for Site 3, focusing on test Area 1 and Area 2 on the third floor. In general, the natural frequencies identified from the heel-drop test were slightly lower than those obtained from the modal shaker test. The frequency ratio (heel-

drop/modal shaker) ranged from 88.82% to 102.76% in Area 1, and from 94.55% to 99.87% in Area 2. The largest difference in identified natural frequency was 11.18%, which suggested that the two methods yield comparable results.

Most of the damping results obtained from the heel-drop test are higher than those from the modal shaker test. For the first mode, the damping ratio from the heel-drop test is 120.71% of the modal shaker result in Area 1, and 207.12% in Area 2. This means that if the first mode damping from the modal shaker test ranges from 3% to 5%, the heel-drop test could estimate damping ratios between 3.62% and 6.04% (120.71%) in Area 1, and between 6.21% and 10.36% (207.12%) in Area 2.

These elevated damping values could lead to inaccurate predictions of the floor's performance, particularly in cross-laminated timber (CLT) floors, where higher-than-expected damping may result in lower-than-anticipated dynamic responses. It is important to note that the heel-drop test, while convenient, may not provide reliable damping results for lower modes due to the challenges in controlling test conditions and ensuring consistent data quality.

Table 4. 13: Comparison between Heel Drop and Modal Shaker Results on Site 3 (Area 1 and Area 2)

Site3: Area 1						
	Heel-drop		Modal Shaker		Ratio % (Heel-drop/Modal Shaker)	
Mode	frequency	damping	frequency	damping	frequency	damping
1	11.49	5.42%	12.25	4.49%	93.80%	120.71%
2	13.12	6.12%	14.04	2.35%	93.45%	260.43%
3	16.74	2.68%	16.29	3.29%	102.76%	81.46%
4	21.46	5.90%	24.16	3.36%	88.82%	175.60%
5	27.71	4.36%	29.15	3.09%	95.06%	141.10%
Site3: Area 2						
	Heel-drop		Modal Shaker		Ratio % (Heel-drop/Modal Shaker)	
Mode	frequency	damping	frequency	damping	frequency	damping
1	8.23	5.53%	8.16	2.67%	100.86%	207.12%
2	10.50		10.77	1.19%	97.49%	
3	11.70		11.75	3.53%	99.57%	
4	14.48	5.21%	14.37	1.81%	100.77%	287.85%
5	15.73	3.06%	15.75	4.23%	99.87%	72.34%
6	18.71	5.34%	18.77	3.97%	99.68%	134.51%
7	23.60	4.90%	24.96	2.39%	94.55%	205.02%
8	27.69	2.18%	28.00	2.61%	98.89%	83.52%
9	30.51	3.53%	30.15	1.29%	101.19%	273.64%

Figure 4.59 highlights key trends in frequency and damping. As expected, the natural frequency increases with mode order in both test areas. The damping ratio exhibits a similar trend for both testing methods, although the pattern differs between the areas. In Area 1, an "M-shaped" trend is

observed, while in Area 2, only a partial "M-shape" is visible. Overall, the heel-drop test consistently produced higher damping values than the modal shaker test for Site 2.

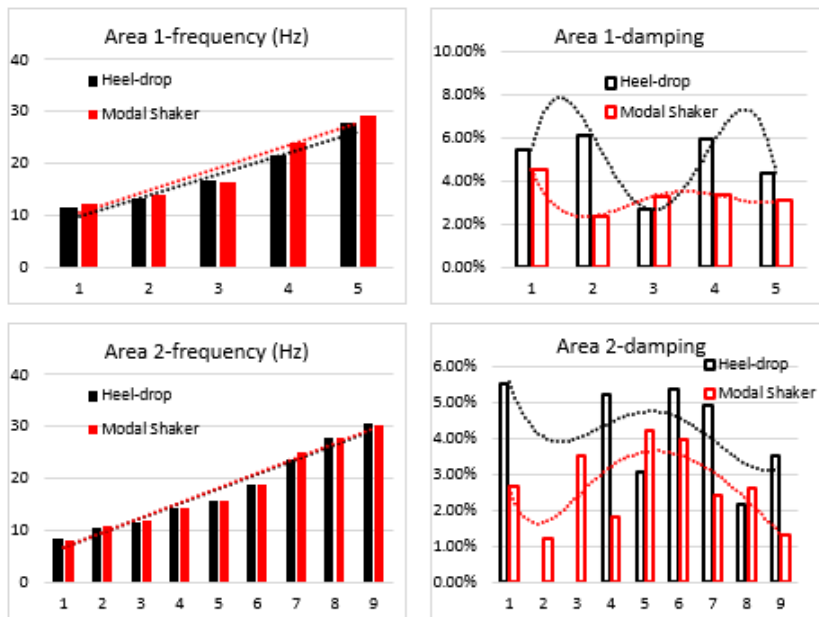


Figure 4.59: Illustrated Frequency and Damping Data of Table 4.13

For the CLT extensions, three floors were tested using an impact hammer, and the frequency and damping results were compared with those obtained from the heel-drop test (Table 4.14). These floors, located on different stories with varying support conditions, showed differences in natural frequency. The stiffness of the support frames ranked as follows: 1st storey CLT > 2nd storey CLT > 3rd storey CLT. As a result, the 1st storey CLT floor had the highest natural frequency. However, since the dimensions of the extension floor area were not large (7.8m x 4.2m), the boundary conditions had a limited effect on the frequency differences.

The frequency ratio between the modal shaker and heel-drop tests across the three CLT extension floors was close to 100%, indicating a high degree of similarity in the frequency estimates from both methods. For the 1st CLT extension, the two frequency results were as close as 97.80%, with 99.87% for the 2nd extension and 99.05% for the 3rd. The difference between the two results was within 5.47%, demonstrating a closer similarity between the heel-drop test and the impact hammer test compared to the heel-drop and modal shaker tests. However, as previously highlighted, the heel-drop test tended to miss lower frequency and damping results that are captured by the impact hammer.

Most of the damping results from the heel-drop test are higher than those from the impact hammer test. This difference can be explained by the smaller force amplitude generated by the impact

hammer, leading to a weaker response measured by the accelerometer and, consequently, a lower damping value (due to a lower signal-to-noise ratio). The first mode damping values were not identified by the heel-drop test; however, the impact hammer results show that the first mode damping is 6.80% for the 1st CLT extension, 6.77% for the 2nd, and 7.17% for the 3rd. These values suggest that the 1st and 2nd CLT extensions share similar raised floor materials, while the 3rd extension uses a resin raised flooring, unlike the fabricated metal-wood access flooring used in the 1st and 2nd floors.

Table 4. 14: Comparison between Heel Drop and Modal Shaker Results on Site 3- Extension

Site3: 1st CLT Extension						
	Heel-drop		Impact Hammer		Ratio % (Heel-drop/Modal Shaker)	
Mode	frequency	damping	frequency	damping	frequency	damping
1			7.16	6.80%		
2	14.23	6.65%	14.55	4.84%	97.80%	137.40%
3	17.78	5.73%	18.56	8.81%	95.80%	65.04%
4	31.98	6.11%	30.32	2.12%	105.47%	288.21%
Site3: 2nd CLT Extension						
	Heel-drop		Impact Hammer		Ratio % (Heel-drop/Modal Shaker)	
Mode	frequency	damping	frequency	damping	frequency	damping
1			7.12	6.77%		
2	14.88	3.32%	14.83	4.23%	100.34%	78.49%
3	18.01	2.37%	18.08	3.28%	99.61%	72.26%
4	27.80	6.07%	28.05	5.42%	99.11%	111.99%
5	30.28	8.56%	30.32	2.09%	99.87%	409.57%
Site3: 3rd CLT Extension						
	Heel-drop		Impact Hammer		Ratio % (Heel-drop/Modal Shaker)	
Mode	frequency	damping	frequency	damping	frequency	damping
1			7.08	7.17%		
2	14.66	4.40%	14.88	3.16%	98.52%	139.24%
3	17.73	3.61%	17.90	2.63%	99.05%	137.26%
4	23.60	5.79%	24.72	5.89%	95.47%	98.30%
5	29.88	3.92%	30.30	1.99%	98.61%	196.98%

As shown in Figure 4.60, the frequency of the three CLT extension floors increases with the mode order. The damping trend, however, lacks a consistent pattern across different modes. Nevertheless, both the impact hammer and heel-drop tests show similar damping trends for the same test floors.

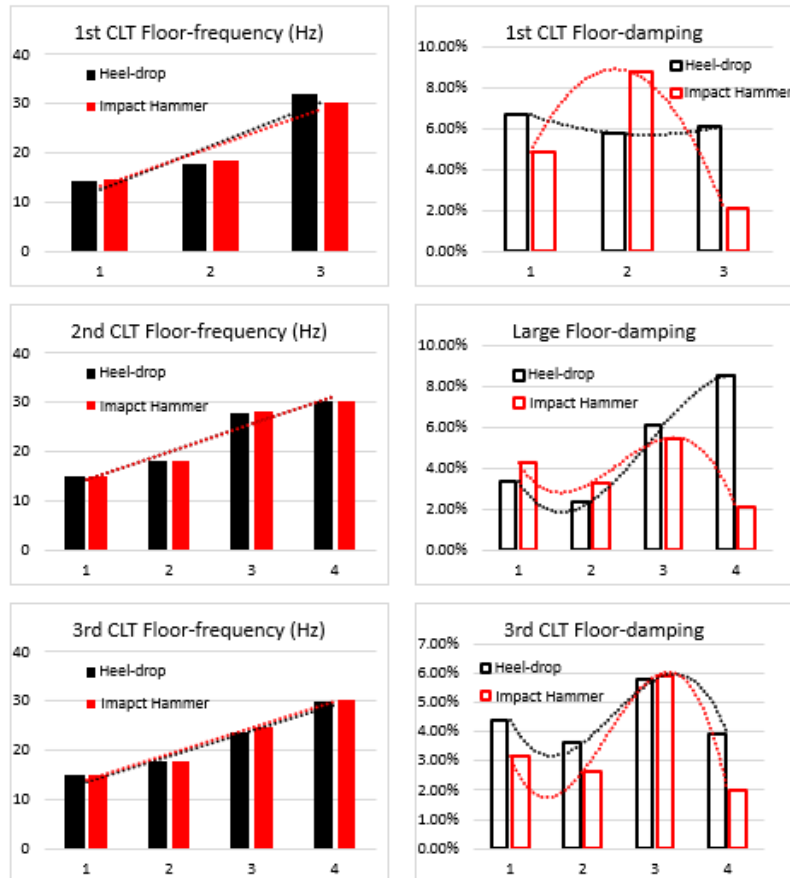


Figure 4.60: Illustrated Frequency and Damping Data of Table 4.14

4.6.4 Conclusions and Recommendations

This research relies on field test data, emphasizing the need for high-quality inputs. However, it is unrealistic to expect perfect data, especially in full-scale vibrational tests where noise is present throughout the procedure. The results demonstrate consistency in frequency, with higher modes corresponding to higher frequencies, and comparable outcomes were observed across different test methods. Nevertheless, certain methods, such as the heel-drop test, tend to underestimate frequencies below 8 Hz.

Regarding damping, the determination process is complex and highly dependent on test procedures and data analysis methods. Although consistent trends were observed across different modes using various methods, variations were noted between testing areas on the same storey. The heel-drop test, in particular, tends to overestimate damping values, often by two to four times compared to shaker or hammer tests. Therefore, it is recommended that the average damping across modes be used to avoid misleading conclusions.

Key findings on frequency and damping estimation include:

Frequency Estimation:

- The analysis revealed consistent frequency identification, with higher modes associated with higher frequencies.
- Results from various test methods produced similar findings, reinforcing the robustness of the outcomes.
- The first natural frequency serves as a reliable classification indicator.
- Notably, the heel-drop test underestimates frequencies below 8 Hz, making it unsuitable for low-frequency assessments.

Damping Estimation:

- Damping estimation is non-deterministic and complex, relying on test procedures and analytical methods.
- While trends are consistent across modes within a single test method, variations exist between different testing areas, even within the same structure.
- The heel-drop test typically yields damping values that are significantly larger (2-4 times) than those from shaker or hammer tests.
- The first damping value cannot be used to distinguish between different floors, as it is neither the lowest nor the highest value. Therefore, averaging damping across modes is recommended to avoid misleading conclusions.
- The heel-drop test, based on the findings of this research, may inaccurately estimate damping values within the frequency range of 10 to 12 Hz.

Testing Methods for Low-Frequency Floors:

For the estimation of natural frequencies below 10 modes, three methods—modal shaker, heel-drop, and impact hammer—can be equally adopted, depending on the desired accuracy of the damping ratio. Among these, the modal shaker provides the most accurate results, followed by the heel-drop, and finally the impact hammer, which is prone to greater variability due to difficulties in controlling input force.

- For low-frequency timber floors ($f_1 > 4.5$ Hz), the modal shaker is the most reliable method for frequency identification. The heel-drop method is less reliable, and the impact hammer introduces significant variability due to non-linearity.
- For floors with frequencies above 8 Hz, the heel-drop method is appropriate, though care must be taken to account for potential overestimation of damping.
- Both the heel-drop and impact hammer methods tend to yield higher damping ratios due to local non-linearity.

Recommendations:

Although the heel-drop method offers simplicity, it introduces significant inaccuracies, particularly in estimating lower natural frequencies. The modal shaker is the most reliable method, providing stable results in the frequency range of 10–30 Hz. For frequencies below 8 Hz, such as in CLT floors with frequencies between 4.5 and 8 Hz, improvements can be made by ensuring the input signal's energy aligns with the desired frequency range.

Considerations for Method Selection:

Each testing method has distinct advantages and disadvantages. The decision on which method to employ should balance accuracy with practical constraints such as equipment availability, space restrictions, and the required expertise.

In summary:

- The heel-drop test is recommended when equipment is limited or space is constrained.
- A more detailed testing code is required for situations where professional knowledge is lacking.
- The modal shaker remains the preferred method for achieving the highest accuracy across a broad frequency range.

5. Computational work

5.1 Introduction to the Computational Work

5.1.1 Mode Participation Factor and Effective Mass in ANSYS

For a realistic model, one may encounter thousands or even millions of degrees of freedom (DOFs), resulting in an equivalent number of natural frequencies. In many cases, high-frequency modes can be neglected, as not every mode contributes equally to the deformation of the structure under dynamic loads. To determine the sufficient number of modes for extraction and to identify the most significant natural frequencies, two key scalars in ANSYS are utilized: the mode participation factor and the effective mass.

The definitions of the participation factor and effective mass can be mathematically expressed as follows:

- **Mode participation factor:** This involves mode shapes $\{\varphi\}_i^T$, the mass matrix $[M]$, and an assumed unit displacement vector $\{D\}$, which depends on the direction of excitation and the rotation about each global axis.

$$\gamma_i = \{\varphi\}_i^T [M] \{D\} \quad (5.1)$$

- **Effective mass:** This is defined as the square of the participation factor.

$$M_{\text{eff},i} = \gamma_i^2 \quad (5.2)$$

Both the mode participation factor and effective mass quantify the amount of mass moving in each direction for each mode. The vector $\{D\}$ indicates the direction in which the participation factor is calculated. Consequently, a high value in a particular direction suggests that the mode will be excited by forces acting in that direction.

As illustrated by the mathematical formulas, the participation factor and effective mass serve similar roles in modal analysis. In this research, the effective mass scalar is employed to gain insights into the structural behavior of the model constructed in ANSYS.

5.1.2 Bonded Contact in ANSYS

Choosing the appropriate contact type is crucial and can be challenging depending on the specific problem being solved. ANSYS provides several contact types, including frictionless, rough, frictional,

and no separation. The **bonded contact** type is the default configuration and applies to all contact regions, such as surfaces, solids, lines, faces, and edges. When contact regions are bonded, no sliding or separation between faces or edges is permitted; the regions are effectively "glued." This type of contact allows for a linear solution, as the contact length or area remains constant during the application of a load.

In the mathematical model, bonded contact assumes that any gaps between surfaces will be closed and any initial penetration will be disregarded. This type of contact is particularly suitable for describing the connection between a cross-laminated timber (CLT) floor panel and its supporting beams. In practice, the connection between the floor panel and the beam is achieved using self-tapping screws, spaced at appropriate intervals to ensure the components move together as a unit.

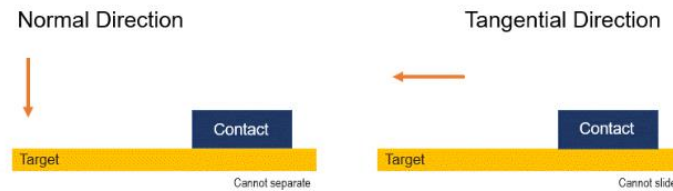


Figure 5. 1: Bonded Contact

5.2 Floor models of Site 1

5.2.1 Model 1- Small Floor

The layout of the third-floor level is illustrated in Figure 5.2, where two tested areas are highlighted with orange rectangles. The CLT floor panel is constructed from a 120mm thick (5 layers) C24 CLT slab, with the thickness of the layers indicated in Figure 5.2. The dimensions of the small test area are 6m x 6.25m, while the large test area measures 9m x 7.62m.

For the CLT flooring systems, the support boundaries for the small floor and the large test area are depicted in Figure 5.3. Specifically:

- Two TB1 beams, each measuring 440mm x 360mm (GL28c), support the long side of the floor.
- Two TB2 beams, each measuring 560mm x 320mm (GL28c), support the short side.
- TC1 columns, positioned under the four corners of the CLT flooring, each measure 320mm x 320mm (GL28h).



Figure 5. 2: Test Areas and CLT Panel Material (Site 1)

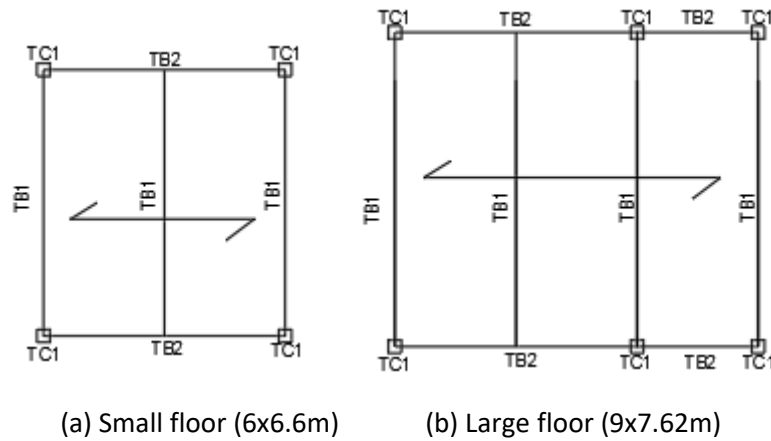


Figure 5. 3: Support conditions of floors (Site 1)

Early modeling efforts involved simulating the material properties of CLT multi-layer plywood through detailed multi-layer models, which were time-consuming. In this study, modeling each layer of CLT separately was deemed unnecessary; instead, a single-layer shell model was employed to simulate the CLT floor slab, enhancing both modeling and calculation efficiency.

According to EN 1995 and BS EN 14080, specimens of glue-laminated timber or glued solid timber should be tested using typical cross-sectional dimensions provided by the manufacturer. This indicates that the parameters in the manufacturer’s product manual are derived from full cross-section CLT test specimens. While CLT is recognized as a multi-layer structure, it is tested as a whole rather than layer by layer. Consequently, these parameters represent the overall performance of the composite panel, resulting in a single-layer shell model that is more consistent with actual test conditions compared to a detailed multi-layer model.

The material property parameters used in the computational analysis, as detailed in Table 5.1, were derived from the supplier's CLT product manual. Specific mechanical properties, including elastic modulus, shear modulus, and thermal conductivity, were selected based on data from major wood suppliers referenced in Chapter 2, ensuring alignment with the actual construction design on site.

Table 5. 1: The Material Properties of the CLT and Glulam (Site 1)

CLT Floor: C24 120-5s						
Density	Young's Modulus X direction	Young's Modulus Y direction	Young's Modulus X direction	Poisson's Ratio XY	Poisson's Ratio YZ	Shear Modulus XY
530 kg/m ³	12 Gpa	450 Mpa	200 Mpa	0.44	0.3	690Mpa
Glulam Beam: GL28c						
390 kg/m ³	12.5 Gpa	300 Mpa	300 Mpa	0.3	0.3	650Mpa
Glulam Column: GL28h						
425kg/m ³	12.6 Gpa	300 Mpa	300 Mpa	0.3	0.3	650Mpa

The model of the small floor is represented as a 3D frame model constructed using column, beam, and surface elements. The mesh size for all elements is set at 0.1m, satisfying sensitivity requirements without sacrificing accuracy. The contact between the plate surface and columns is modeled as bonded, with the top and bottom of the columns fixed to prevent movement. The plate is fixed at its four corners, as shown in Figure 5.4.

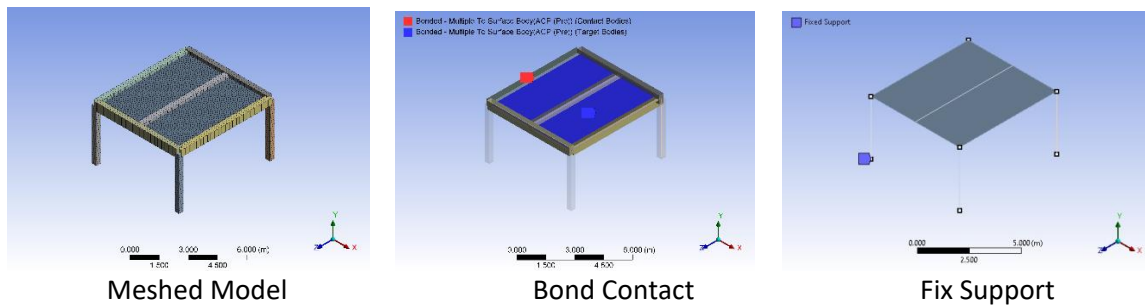


Figure 5. 4: Model Settings of the Small Floor (Site 1)

Damping is not considered in this finite element model; however, the damping ratio can be obtained from field testing. The results for natural frequency and the ratio of effective mass to total mass were summarized in Table 5.2. The total mass participation reached 56.74%, which is acceptable given that the fixed columns contribute no mass participation but add to the total model mass.

An additional model without the four columns was constructed to assess their effect. Results indicated minimal differences in natural frequencies and mode shapes, while modal mass participation improved significantly from 56.74% to 64.73% (an increase of 7.99%). When modeled solely with surface and nodal boundary constraints, modal mass participation rose to 72.28%, representing a 15.54% improvement compared to the column model.

A useful conclusion can be drawn: the wooden frame composed of beams and columns contributes 15.54% to the model mass, with columns contributing 7.99% and beams providing 7.55% in this small floor model. The beam-only model yields the same frequency and mode shape results as the column-

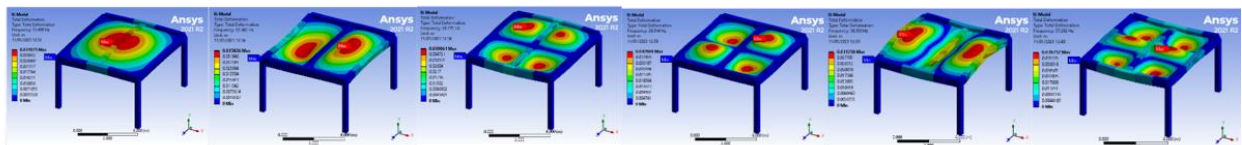
beam model; thus, the simplest model should include at least the beam and plate components. The plate model is not recommended due to the lack of necessary beam support locations, which may lead to inaccurate estimations of mode shapes. The co-movement between the beams and the plate cannot be simplified using line or nodal boundary conditions.

Table 5. 2: Frequency and Mass Participation (Site 1: Small Floor)

Mode	Column-beam-model		Beam-model		Plate-model	
	Frequency (Hz)	Mass Participation	Frequency (Hz)	Mass Participation	Frequency (Hz)	Mass Participation
1	13.50	46.42%	13.50	52.95%	5.57	60.82%
2	22.46	0.00%	22.46	0.00%	15.32	0.00%
3	26.78	0.00%	26.78	0.00%	20.07	0.00%
4	28.91	0.00%	28.91	0.00%	21.60	0.00%
5	30.99	6.37%	30.99	7.27%	28.60	11.46%
6	37.28	3.95%	37.28	4.51%	33.22	0.00%
Sum		56.74%		64.73%		72.28%

Corresponding to the frequency results, the mode shapes were presented in Figure 5.5. The first six modes correspond to bending modes. As the mode order increases, the bending mode transitions from the entire plate into different sections, typically delineated by the supported beams.

Column-beam-model



Beam-model

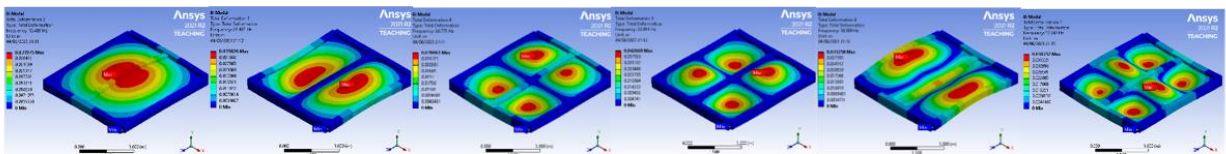


Plate-model

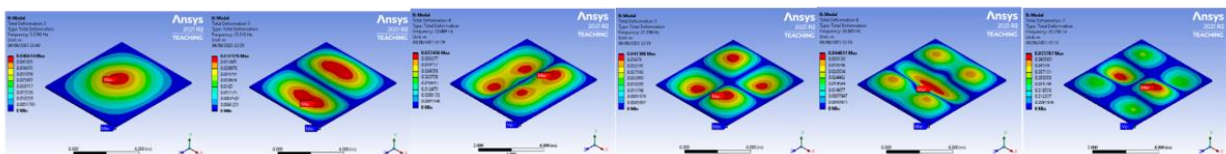


Figure 5. 5: Comparison between mode shapes of the Small Floor built in 3 models (Site 1)

5.2.2 Modal 2- Large Floor

The large floor model utilized the same material properties as Model 1, which featured three spans compared to the two spans of the small floor. The mesh size remained consistent at 0.1m, as

illustrated in Figure 5.6. Additionally, the model incorporated bonded surface contact and maintained the same fixed supports for the columns as in Model 1.

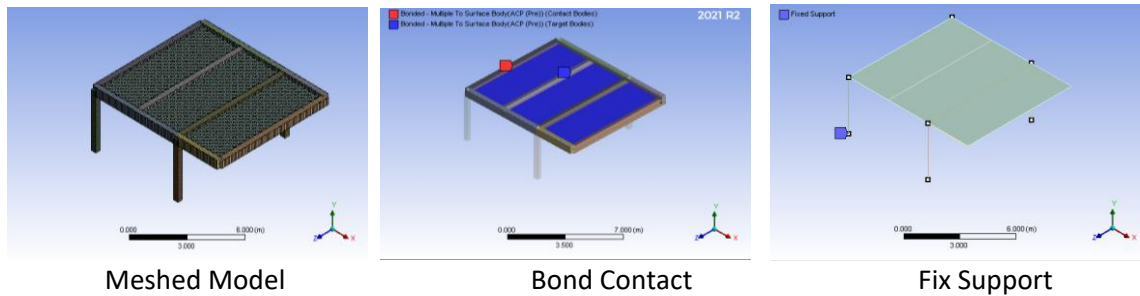


Figure 5. 6 Model Settings of the Large Floor (Site 1)

For the large floor, nine modes were extracted, covering the frequency range from 0 to 30 Hz. The data presented in Table 5.3 showed the natural frequencies and the ratio of effective mass to total mass. Modes 2, 5, and 7 significantly contributed to deformation in the y-direction and are easily excited by vibrations. In modal analysis, it is crucial to include significant modes, which necessitates extracting a sufficient number of modes to ensure accurate evaluation. In this model, nine modes were extracted, resulting in a ratio of effective mass to total mass of 63.4%.

Table 5. 3: Frequency and Mass Participation (Site 1: Large Floor)

Mode	Model: one and half bay		Model: two bays	
	Frequency (Hz)	Mass Participation	Frequency (Hz)	Mass Participation
1	10.17	0.19%	10.09	0.00%
2	10.69	54.83%	10.30	48.84%
3	16.96	0.06%	16.61	0.23%
4	20.92	0.00%	16.85	0.00%
5	21.82	6.20%	22.84	0.08%
6	23.03	0.00%	22.95	0.01%
7	25.62	2.04%	23.08	9.84%
8	25.81	0.11%	24.72	0.01%
9	30.33	0.00%	25.78	0.00%
10			29.20	0.09%
11			32.39	2.69%
Sum		63.43%		61.80%

The results of the mode shapes were illustrated in Figure 5.7. All identified modes were bending modes, which can occur in bays separated by columns or spans divided by beams. Mode 2 demonstrates the movement of a bay as a whole, while modes 5 and 7 illustrated how the plate vibrates across different spans. Other modes may occur but exhibit low mass participation. The total mass participation for the nine modes reached 63.43%, which is acceptable when excluding the mass of the columns without compromising stiffness.

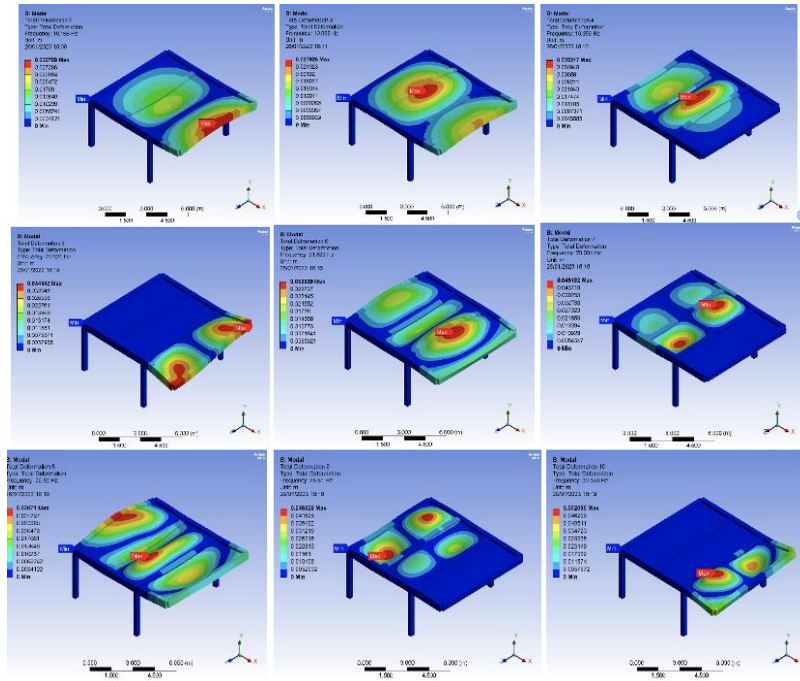


Figure 5. 7: The Mode Shape of the One and Half Bay Model

An additional model was developed that includes two bays, as shown in Figure 5.8. The frequency and mode shape results were provided below. Compared to the one-and-a-half bay model, the two-bay model yielded more accurate results for observing shape changes in another bay. The one-and-a-half bay model effectively created a cantilever beam condition for the half bay; even with boundary restrictions to limit edge movement, the true behavior cannot be represented as effectively as in the two-bay model.

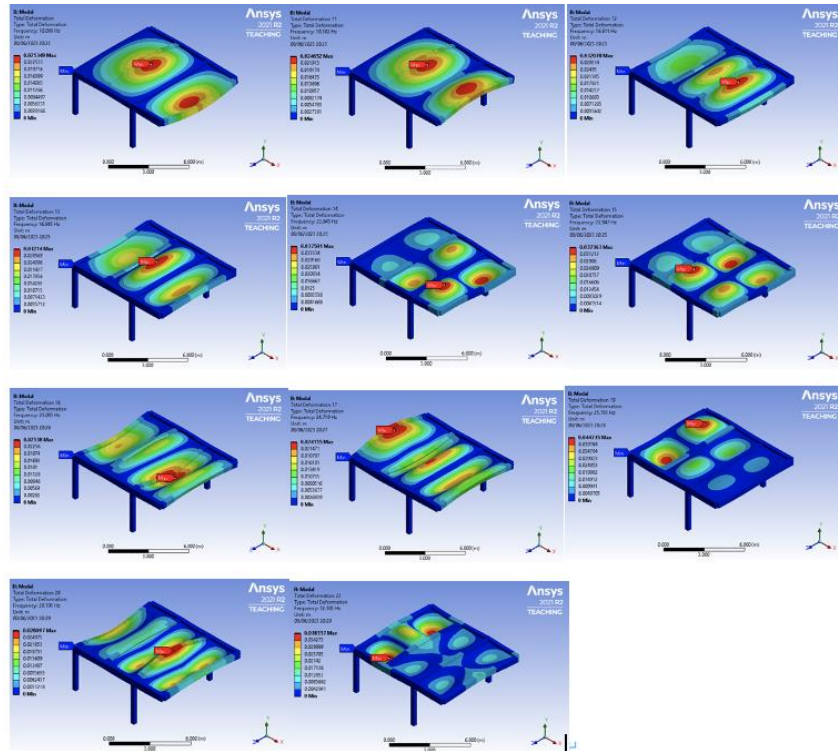


Figure 5. 8: The Mode Shape of the Two Bay Model

5.3 Floor models of Site 2

The fourth floor of the building was selected for testing, using a CLT flooring system as part of the refurbishment efforts. The areas chosen for testing were determined based on the space requirements of the test equipment and the layout of the test plan, as highlighted in Figure 5.9. The CLT flooring is constructed with a 140mm thick, 5-layer CLT slab. Two test areas were selected: the small floor area contains 2 bays, measuring 18m x 6.6m, while the large floor area has 3 bays, with dimensions of 27m x 6m.

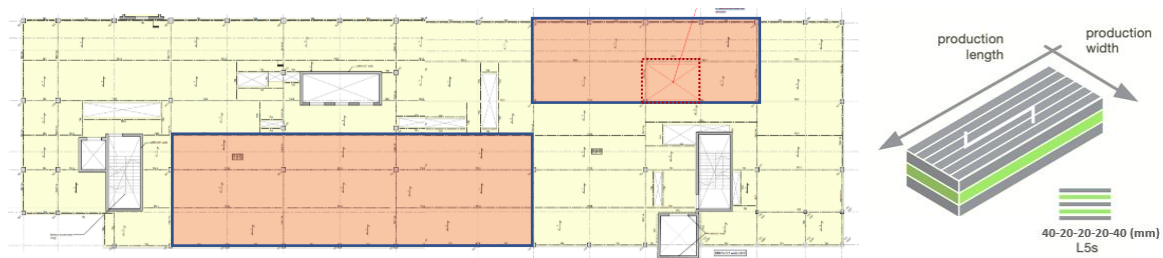
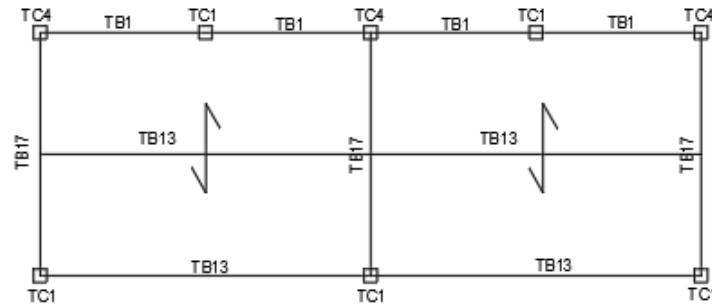


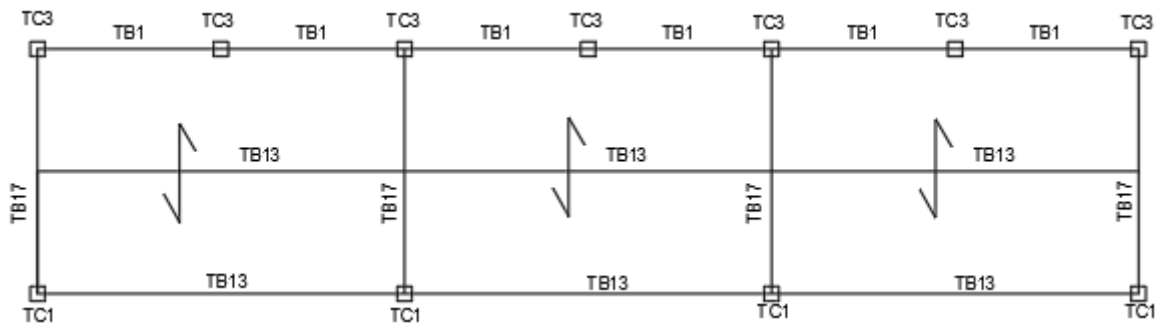
Figure 5. 9: Site 2 Test Areas and CLT Panel Material

Both test areas adopt a similar support framework layout; however, differences exist in the boundary support materials and dimensions. In the small floor area, as depicted in Figure 5.10, the CLT slabs in the two bays were supported by four TB1 beams and four TB13 beams along the short direction, as well as three TB17 beams along the long direction. The dimensions of these beams are as follows:

TB1 is 360mm x 240mm (GL28c), TB13 is 600mm x 400mm (GL28c), and TB17 is 720mm x 260mm (GL28c). Beneath the beams, there are five TC1 columns and three TC4 columns, where TC1 measures 320mm x 320mm (GL30c) and TC4 measures 360mm x 360mm (GL30c). The large floor, which consists of three bays, employs the same beam configuration as the small floor; however, it utilizes two types of columns beneath the beams: eight TC1 columns and seven TC3 columns (280mm x 280mm, GL30c).



(a) Small test floor (6x6.6m)



(b) Large floor (9x7.62m)

Figure 5. 10: Support Conditions of Floors (Site 2)

5.3.1 Model 3- Small Floor

Table 5.4 lists the three materials used in the small floor on Site 2, which include a 140mm thick (5-layer) CLT floor plate, glulam beams, and columns. A total of five cross-sections were created for the glulam frame structure, incorporating two sizes of columns and three sizes of beams, in accordance with real construction details.

Table 5. 4: The Material Properties of the CLT and Glulam (Site 2)

CLT Floor (140-5s)						
Density	Young's Modulus X direction	Young's Modulus Y direction	Young's Modulus X direction	Poisson's Ratio XY	Poisson's Ratio YZ	Shear Modulus XY
450 kg/m ³	11.8 Gpa	370 Mpa	250 Mpa	0.44	0.3	690Mpa
Glulam Beam: GL28c						
390 kg/m ³	12.5 Gpa	300 Mpa	300 Mpa	0.3	0.3	650Mpa
Glulam Beam: GL30c						
390 kg/m ³	13.0 Gpa	300 Mpa	300 Mpa	0.3	0.3	650Mpa

A consistent mesh size of 0.1m was applied to all elements, as shown in Figure 5.11. To facilitate accurate modeling, a bonded surface connection was established between the plate and beams, maintaining their relative motion (see Figure 5.11). Fixed boundary conditions were implemented for all columns to ensure stability during analysis, as illustrated in Figure 5.11.

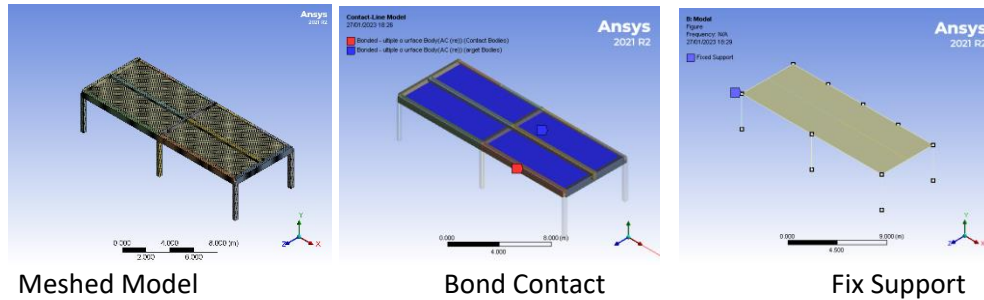


Figure 5. 11: Model Settings of the Small Floor (Site 2)

Twelve eigenvalues were generated to analyze the frequency range of interest, from 0 to 30 Hz. The mode shapes of the small floor were presented in Figure 5.12. By combining the mass participation information from Table 5.5, the dominant modes can be identified. The total mass participation for this model reached 66.88%, which is acceptable given that the columns are fixed. The first two modes were bending modes, with the second mode shape exhibiting a mass participation percentage of 56.33% of the total mass participation.

The third and fourth mode shapes divided the floor into four vibrating areas, while subsequent modes segment the total floor into six, eight, and ten distinct areas of vibration. It is important to note that a mass participation ratio of zero, such as the 1st mode having a mass participation ratio of 0%, does not imply that this mode is unimportant. Rather, it indicated that the mass participates in the height direction, allowing the vibrated mass to move in the opposite direction and cause dispersion. Therefore, caution should be exercised when interpreting the effective mass participation parameter.

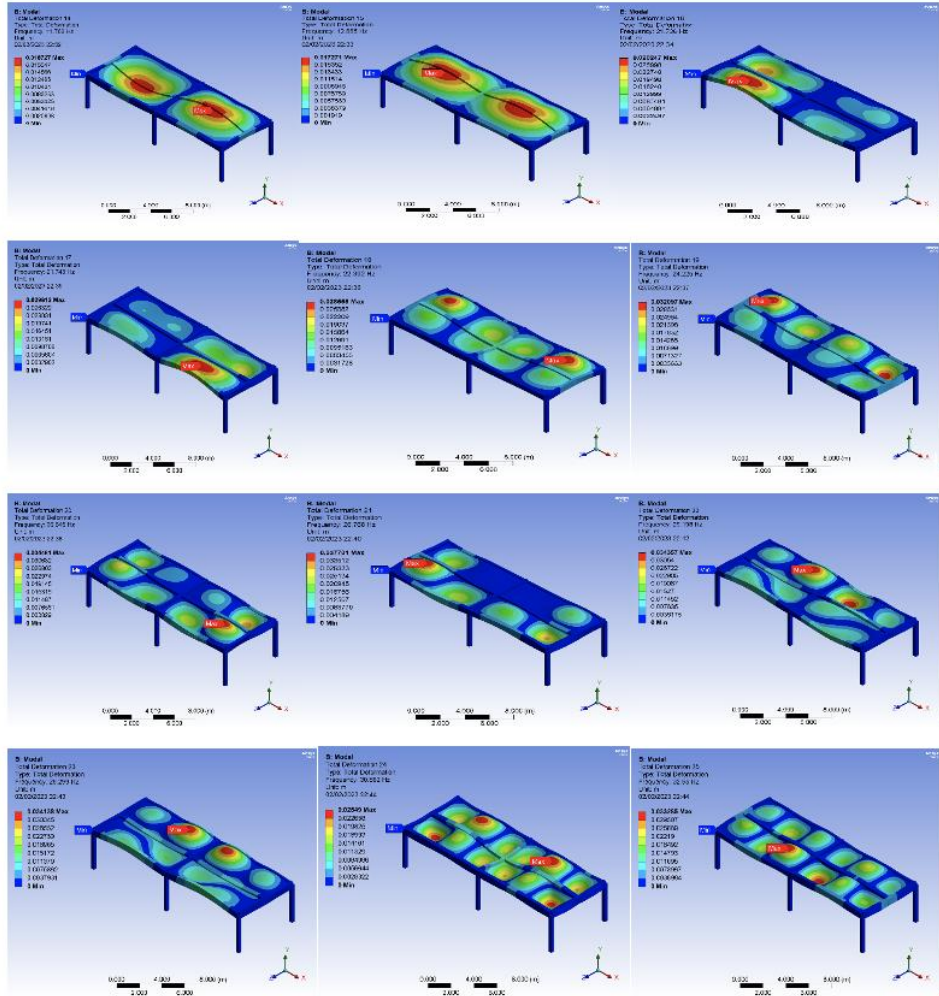


Figure 5. 12: Model Settings of the Small Floor (Site 2)

Table 5. 5: Frequency and Mass Participation (Site 2: Small Floor)

Mode	Frequency (Hz)	Mass Participation
1	11.76	0.00%
2	12.67	56.33%
3	21.74	0.22%
4	21.75	1.19%
5	22.39	0.15%
6	24.23	0.00%
7	26.65	1.18%
8	26.77	0.02%
9	29.20	0.00%
10	29.30	5.29%
11	30.88	2.50%
12	32.55	0.00%
Sum		66.88%

5.3.2 Model 4- Large Floor

The large floor shared the same material as the small floor (Model 3) on Site 2, as shown in Table 5.4. The only difference lies in the size of the column cross-sections. The small floor model utilized a 0.1 m grid. The floor panel was modeled using plate elements, bonded to the support beam elements beneath, as illustrated in Figure 5.13. As is typical, fixed supports were applied at both the top and bottom of the columns (Figure 5.13).

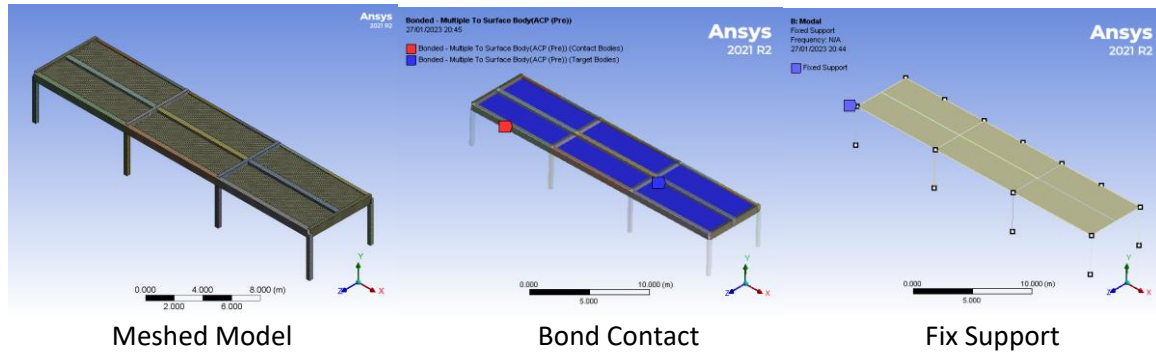


Figure 5. 13: Model Settings of the Small Floor (Site 2)

In terms of modal analysis, as the mode order increased, more complex mode shapes emerged in the higher modes, as shown in Figure 5.14. The total mass participation of the large floor, as shown in Table 5.6, reached 59.21%. Notably, the sum of the first three modes contributed 56.93%, representing a significant portion of the entire model, nearly 96.15%. However, the field test results for higher-order mode shapes may not perfectly match the computational results. Therefore, the principle for validating the finite element model should focus on matching the first three mode shapes, while other higher modes may be given lower priority.

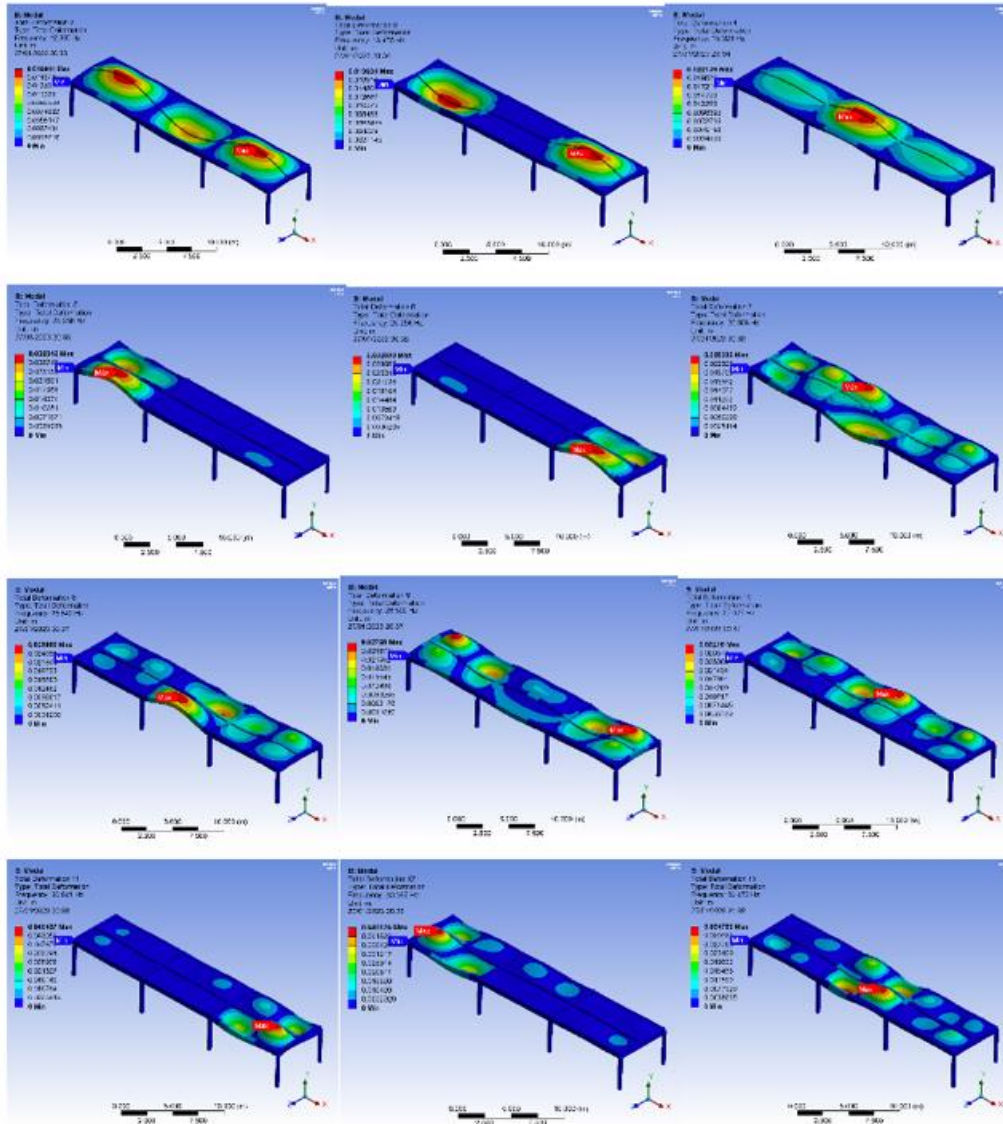


Figure 5. 14: Model Settings of the Small Floor (Site 2)

Table 5. 6: Frequency and Mass Participation (Site 2: Large Floor)

Mode	Frequency (Hz)	Mass Participation
1	12.81	8.75%
2	13.48	0.00%
3	15.02	48.18%
4	25.26	0.63%
5	25.26	0.38%
6	25.61	0.21%
7	25.64	0.24%
8	26.50	0.02%
9	27.98	0.00%
10	30.84	0.44%
11	30.97	0.33%
12	32.47	0.03%
Sum		59.21%

5.4 Floor Models of Site 3

5.4.1 Model 5- Area 1 and Area 2

The total testing area was located on the third floor of Site 3, measuring 15 m by 13.5 m. A 140 mm thick CLT floor panel was constructed with a steel support structure. This structure, shown in Figure 5.15, included a total of six I-steel beams: two FB1 beams and four FB2 beams, which support the entire CLT floor area. Three I-steel columns were positioned at the midpoint along the lateral direction beneath the six I-steel beams. Additionally, an RC beam was used on the left side, while angle steel beam B10 (L150x100x8) was employed to support the other three sides, which were then resin-fixed to the existing masonry walls.

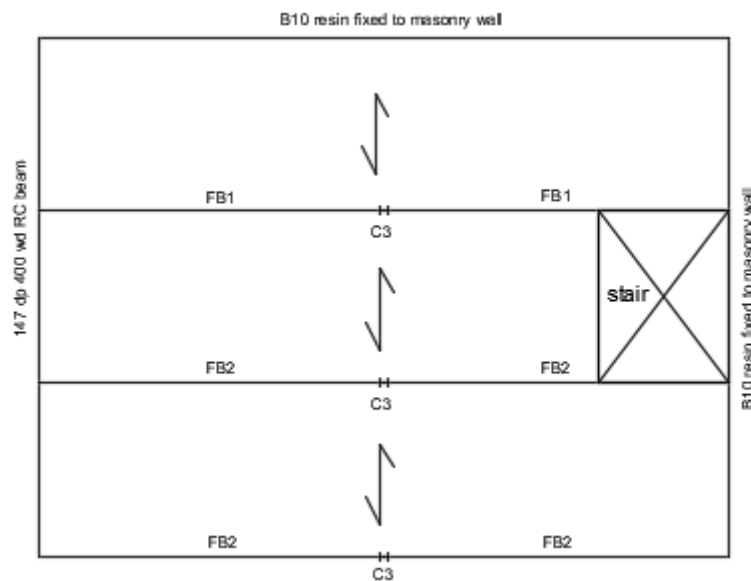


Figure 5. 15: Support Conditions of Floors (Site 3)

In addition to the structural components, the computational analysis incorporated a range of materials including CLT, glulam, steel, and reinforced concrete, consistent with those used on the actual construction site. Table 5.7 listed the specific parameters of these materials.

Table 5. 7: The Material Properties of the Model 5-8 (Site 3)

CLT Floor						
Density	Young's Modulus X direction	Young's Modulus Y direction	Young's Modulus X direction	Poisson's Ratio XY	Poisson's Ratio YZ	Shear Modulus XY
530 kg/m ³	11.8 Gpa	370 Mpa	250 Mpa	0.44	0.3	690 Mpa
Glulam Beam						
390 kg/m ³	12.5 Gpa	300 Mpa	300 Mpa	0.3	0.3	650 Mpa
RC Beam						
2300 kg/m ³	30 Gpa	-	-	0.18	-	12.7 GPa
I-steel Beam and B10 Steel Angle						

7850 kg/m ³	200 Gpa	-	-	0.3	-	76.9 Gpa
------------------------	---------	---	---	-----	---	----------

Due to limitations in the number of sensors and the length of the cable, the entire third floor cannot be tested in one experiment. Consequently, the CLT floor region was been partitioned into Area 1 and Area 2, as marked in Figure 5.16. Area 1 included the stair area to model the actual construction layout, while Areas 1 and 2 were built within the same model.



Figure 5. 16: The Partitioning of the Test Area on the Third Floor of Site 3

The final HTS model measured 18 m by 14.5 m, with a 3.4 m wide opening for stairs included in the computational model. However, the opening area could not be tested during field testing. To ensure that the mode shapes could be compared with field-testing results, a section plane operation in ANSYS was performed to match the testing area. The fixed support conditions were described as follows: the concrete beam support side and both sides of B10 were simply supported, while the columns were fixed at both the top and bottom (Figure 5.17).

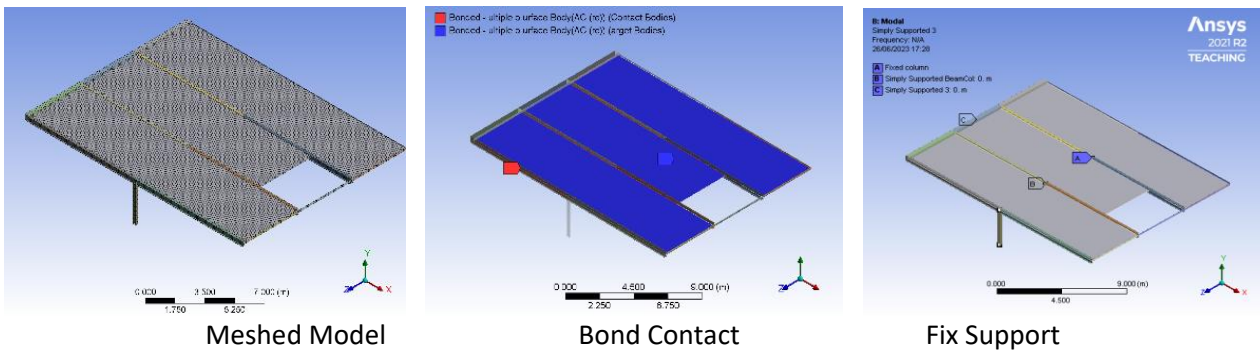


Figure 5. 17: Model Settings of Area 1 and Area 2 (Site 3)

To achieve the desired frequency range of 0 to 30 Hz, a total of 35 modes were identified in the analysis settings. As the model size increases, there is a greater occurrence of local mode shapes due to the substantial mass of the model, which makes it challenging for the entire structure to vibrate uniformly, leading to localized excitation. Notably, modes 4, 5, and 6 collectively accounted for 44.9% of the mass participation within the total of 65.27%, as shown in Table 5.8. This observation was

further substantiated by examining the mode shapes depicted in Figure 5.18, which highlighted conspicuous red areas in these three modes.

Table 5. 8: Frequency and Mass Participation of model 5 (Site 3)

Mode	Frequency (Hz)	Mass Participation
1	6.06	2.25%
2	7.75	1.41%
3	8.44	0.49%
4	9.48	31.39%
5	10.32	8.58%
6	11.09	4.97%
7	12.38	1.38%
8	12.66	0.12%
9	14.11	0.01%
10	14.37	2.96%
11	14.88	0.14%
12	16.12	0.06%
13	16.52	1.65%
14	17.23	0.14%
15	18.04	0.04%
16	18.15	0.18%
17	18.65	2.00%
18	19.15	1.02%
19	20.05	2.22%
20	20.66	0.61%
21	21.2	0.26%
22	22.97	0.36%
23	23.39	0.82%
24	23.94	0.45%
25	24.28	0.00%
26	25.03	0.76%
27	26.59	0.09%
28	26.65	0.03%
29	27.33	0.03%
30	27.62	0.51%
31	30.02	0.09%
32	30.8	0.18%
33	32.35	0.04%
34	33.32	0.00%
35	33.91	0.01%
Sum		65.27%

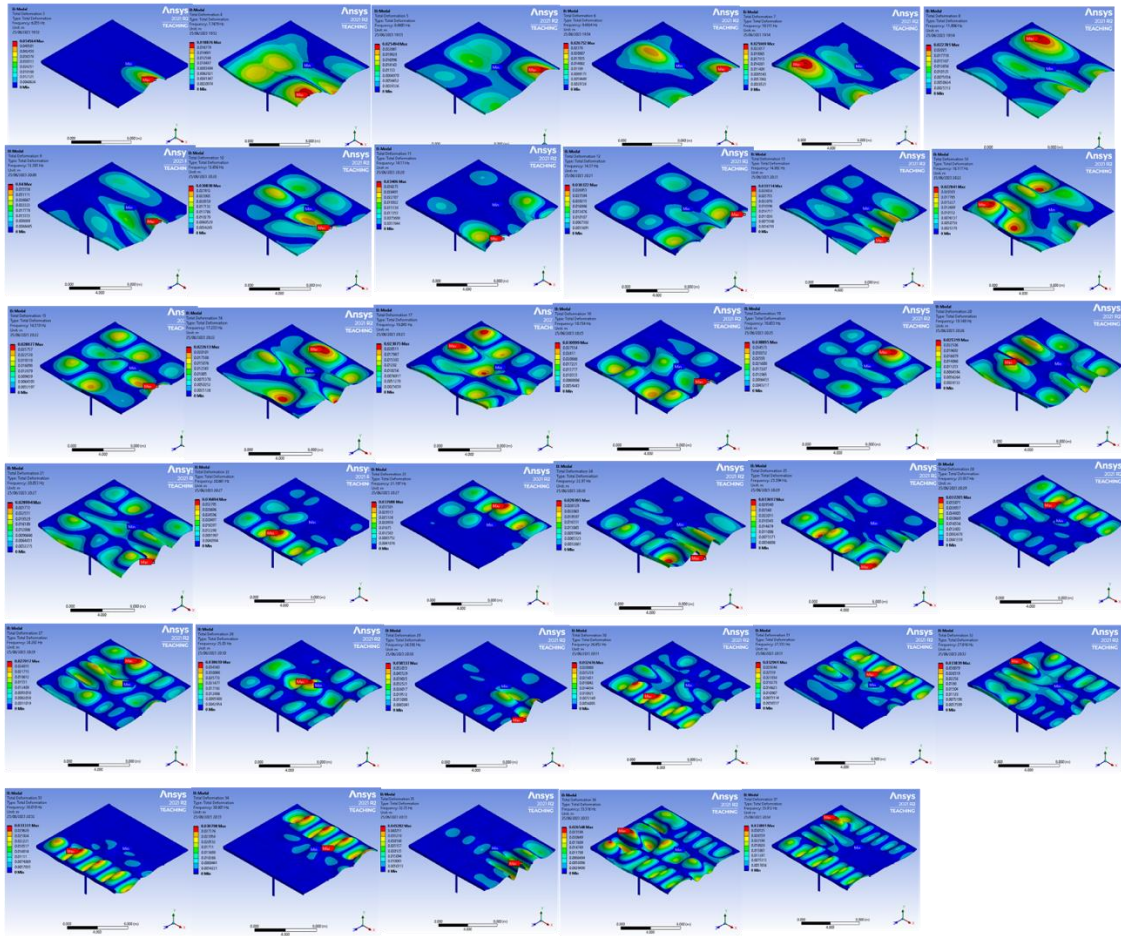


Figure 5. 18: Mode Shape of Model 5 (Site 3)

5.4.2 Model 6, Model 7 and Model 8- CLT Extensions

As shown in Figure 5.19, the side extension area has a trapezoidal shape with base lengths of 7.8 m and 8.4 m, and a height of 4.2 m. The support conditions for the side extension are illustrated in Figure 5.20. The first floor is supported by B10 (L150x100x8) beams fixed to the existing masonry wall with M16 bolts, along with a glulam beam TB1 (220 mm x 200 mm, GL28) and an RC beam (980 mm x 250 mm) at both sides of the masonry wall. The second and third floors are supported by CLT walls on two sides, with one side utilizing a glulam beam and the same L-steel angle (B10) for boundary conditions. An RC capping beam is placed at the head of the masonry wall specifically for the third CLT extension floor.

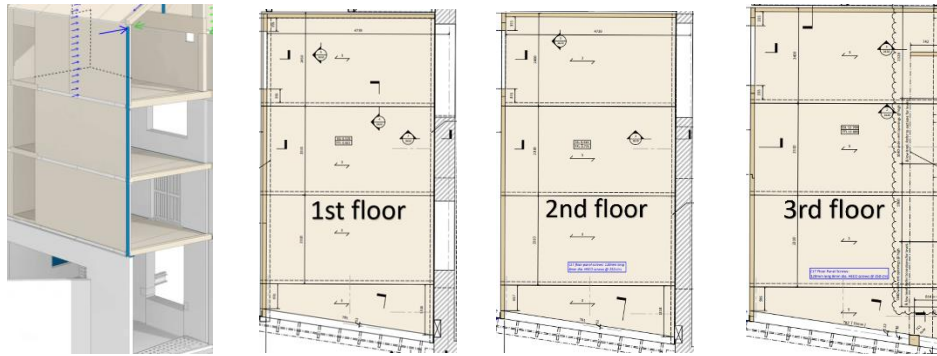


Figure 5. 19: Test Areas of Extension CLT Floors (Site 3)

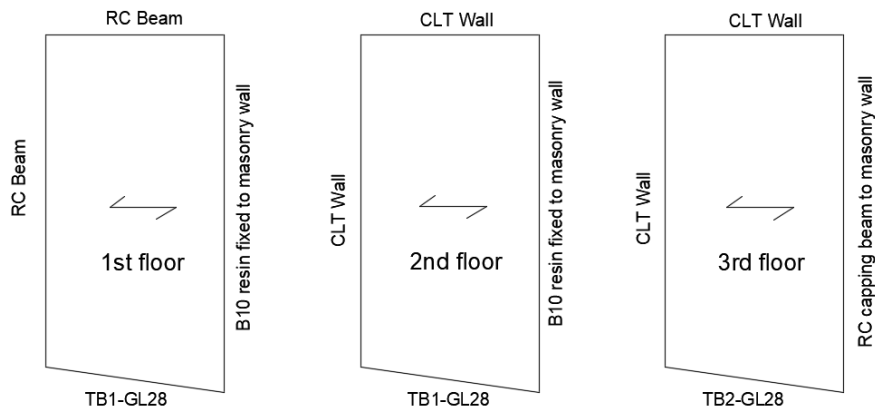


Figure 5. 20: Support Conditions of Extension CLT Floors (Site 3)

Three CLT extension floors are modeled as a 3D frame using beam and surface elements, with a grid size of 0.1 m for calculations (Figure 5.20). In terms of boundary conditions, the floor slabs and supporting beams are bonded. However, due to the asymmetrical stiffness of the supporting structure—where one side is notably weaker than the other—Model 6 for the first CLT extension floor is designated as simply supported on that particular side. The differences in support conditions between the first CLT extension floor and the second or third floors are clearly illustrated in the FE models displayed in Figure 5.21. Specifically, the first floor is supported on all four sides by beams, while the second and third floors are supported on two sides by CLT walls.

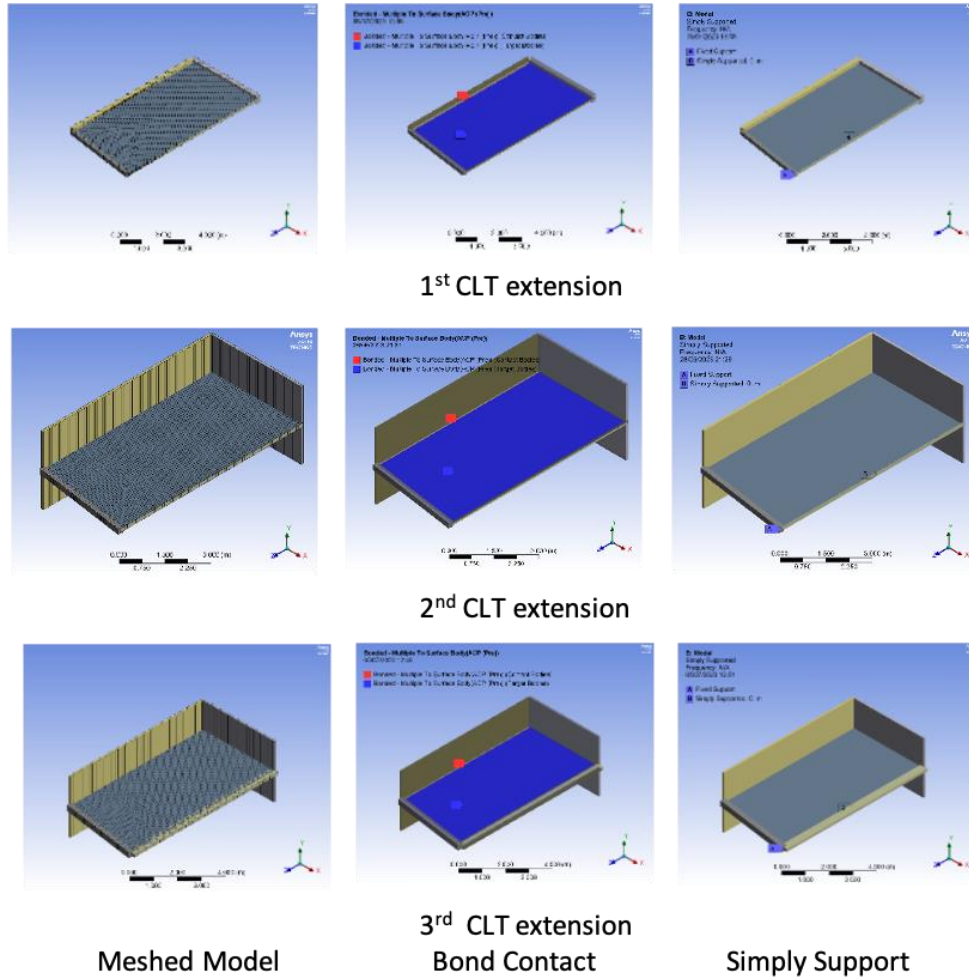


Figure 5. 21: Model Settings of CLT Extensions (Site 3)

Given the targeted frequency range of 0-30 Hz, six modes were extracted for the first CLT extension floor, resulting in a total mass participation rate of 56.25%, as shown in Table 5.9. This relatively low participation rate may arise from potential inaccuracies in the material strength settings compared to the actual structure. Such discrepancies can be further explored and refined in future model updates that incorporate field test data.

The mode shapes corresponding to these frequency outcomes are illustrated in Figure 5.22. Notably, the initial six modes primarily exhibit bending characteristics. As the modal order increases, these bending modes evolve from affecting the entire slab to influencing specific sections. This localized behavior can be attributed to the composite nature of the floor, which consists of three separate CLT panels.

For the second CLT extension floor (Model 7), 20 modes were extracted to meet the same frequency requirement of 0-30 Hz (Figure 5.23). This model achieves a total mass participation rate of 77.12%.

The first three modes contribute approximately 80% of the total modal participation, as indicated in Table 5.10. Additionally, higher-order modes, such as the 12th, 13th, and 14th modes, exhibit relatively high mass participation, suggesting an increased likelihood of causing floor vibration.

The third CLT extension floor shares the same boundary conditions as the second extension floor but has a smaller size. Its overall mass participation, with 20 modes (Figure 5.24), reaches 60.96%, with the first three modes contributing about 74%. This indicates a comparable level of participation. Furthermore, higher-order modes demonstrate a higher likelihood of excitation compared to lower-order modes; for instance, the mass participation coefficient of the 16th mode is as high as 7.36%.

Table 5. 9: Frequency and Mass Participation of Model 6 (Site 3)

Mode	Frequency (Hz)	Mass Participation
1	16.81	26.43%
2	20.38	4.20%
3	24.37	19.20%
4	25.97	5.06%
5	31.79	0.11%
6	41.72	1.25%
Sum		56.25%

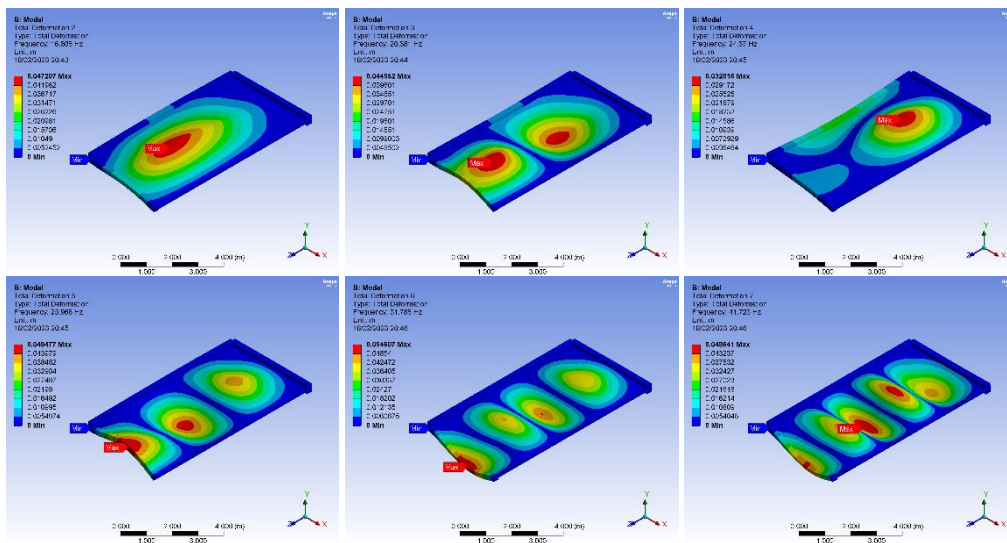


Figure 5. 22: Mode Shapes from Model 6 (Site 3)

Table 5. 10: Frequency and mass participation of model 7 (Site 3)

Mode	Frequency (Hz)	Mass Participation
1	9.71	33.87%
2	11.91	0.76%
3	16.21	21.12%
4	17.22	1.59%
5	21.14	0.26%
6	22.14	2.46%
7	23.52	4.00%

8	24.71	0.59%
9	25.56	0.69%
10	26.30	0.05%
11	27.26	0.03%
12	27.98	2.24%
13	28.81	2.47%
14	28.99	2.85%
15	30.14	0.25%
16	30.72	0.00%
17	31.37	0.00%
18	32.08	0.74%
19	32.27	3.15%
20	32.54	0.00%
Sum		77.12%

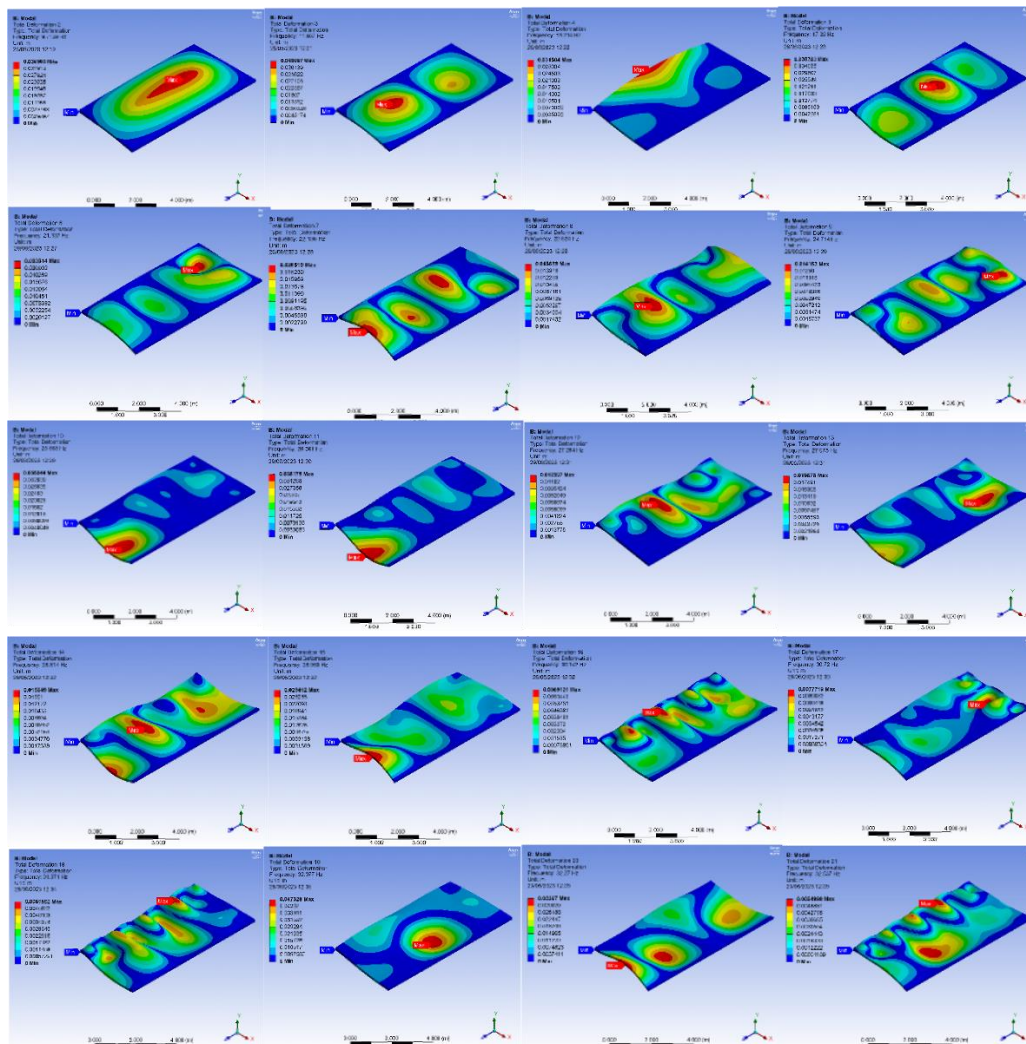


Figure 5. 23: Mode Shapes from Model 7 (Site 3)

Table 5. 11: Frequency and Mass Participation of Model 8 (Site 3)

Mode	Frequency (Hz)	Mass Participation
1	10.64	26.49%
2	13.69	0.39%
3	16.28	18.16 %
4	18.61	0.05%
5	21.62	0.01%
6	22.81	2.93%
7	23.78	1.95%
8	24.99	0.25%
9	25.99	0.14%
10	27.33	0.00%
11	27.72	0.38%
12	28.31	0.08%
13	28.90	0.31%
14	30.14	0.01%
15	30.69	1.09%
16	31.18	7.36%
17	31.38	0.07%
18	32.52	0.04%
19	32.73	1.20%
20	32.95	0.05%
Sum		60.96%

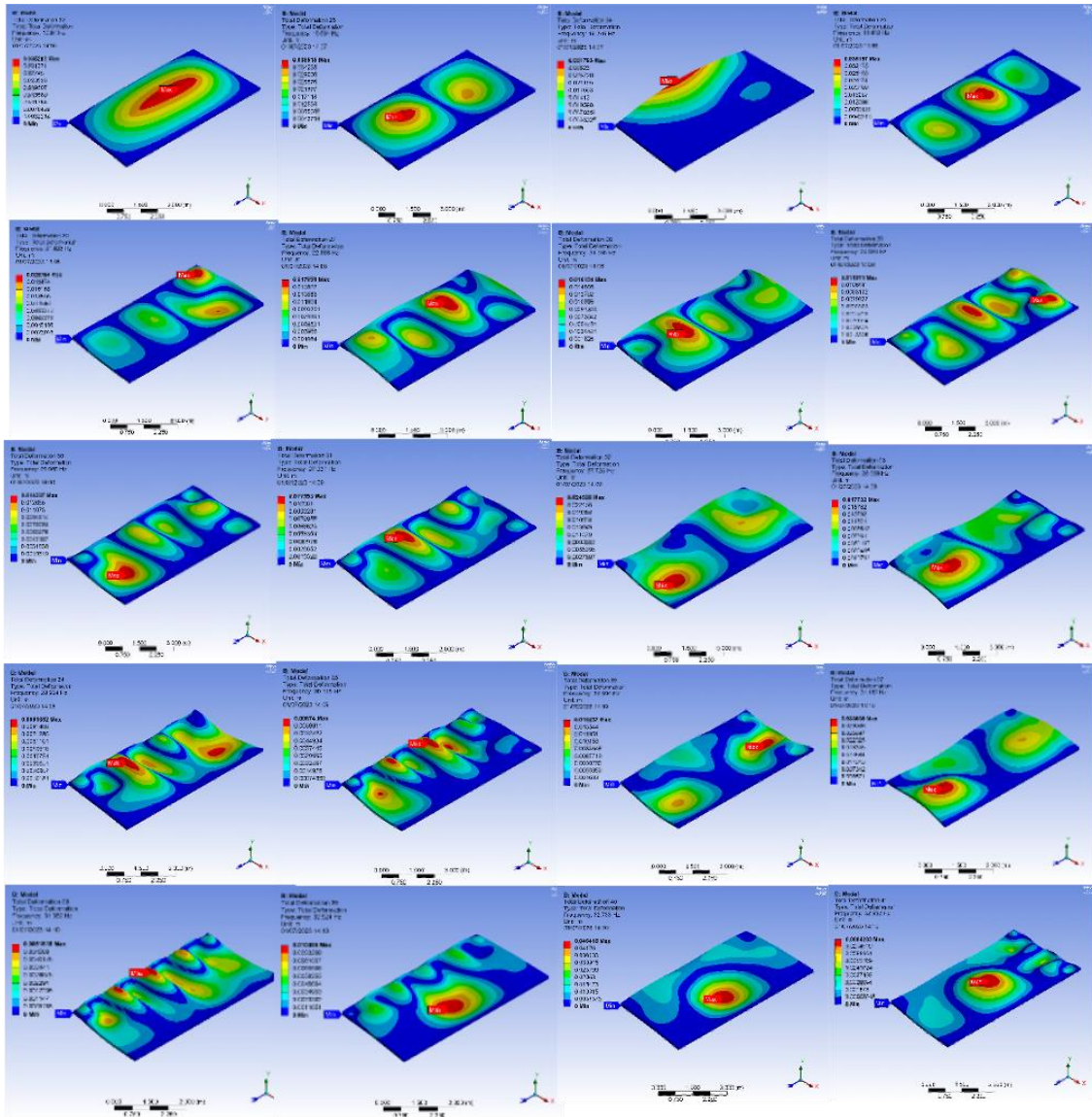


Figure 5.24: Mode Shapes from Model 8 (Site 3)

5.5 Comparison between the Experimental and Computational Results

5.5.1 Site 1- Small Floor and Large Floor

Experimental results for the small floors were obtained through shaker tests. However, the computational model only provided an estimate of the natural frequency, omitting any damping ratio settings. Although damping can be incorporated into finite element modeling, it was excluded from this study. The modal parameter results were summarized in Table 5.12, revealing a natural frequency difference exceeding 25%. This discrepancy suggested that adjustments are needed for the model's stiffness and mass in ANSYS. The first four calculated mode shapes were illustrated in Figure 5.25.

Table 5. 12: Comparison of Frequencies between Measurements and FE Results of Model 1

Mode	Shaker (Measurement)	ANSYS (FE)	Ratio % (Measurements/FE results)
	frequency (Hz)	frequency (Hz)	
1	9.30	13.50	68.89%
2	12.97	22.46	57.75%
3	17.89	26.78	66.80%
4	24.62	28.91	85.16%

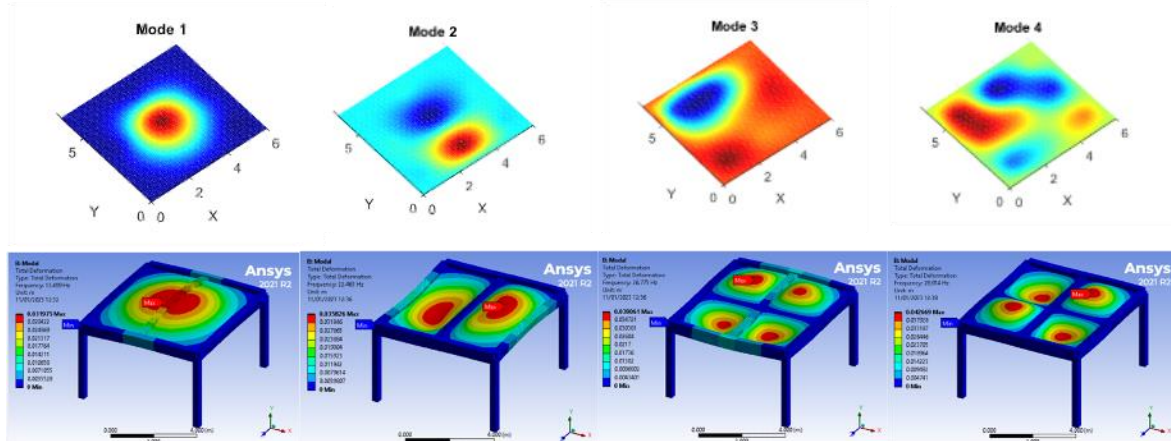


Figure 5. 25: Small Floor (Site 1) - Comparison of the Mode Shapes between Measurements and FE Results of Model 1

The natural frequency results from modal shaker testing and finite element modeling in ANSYS 2021 R2 were summarized in Table 5.13, with frequency differences ranging from 1% to 30%. By comparing the mode shapes identified from modal shaker testing (Figure 5.26) with those simulated by ANSYS, the accuracy of the computational model can be assessed. The similarity in deformation shapes suggested that the large floor model adequately represents the actual CLT floor structure.

Table 5. 13: Comparison of Frequencies between Measurements and FE Results of Model 2

Mode	Shaker (Measurement)	ANSYS (FE) One and half bay model	Ratio % (Measurements/FE results)	ANSYS (FE) two bay model	Ratio % (Measurements/FE results)
	frequency (Hz)	frequency (Hz)		frequency (Hz)	
1	7.54	10.17	74.14%	10.09	74.73%
2	7.81	10.69	73.06%	10.30	75.83%
3	11.00	16.96	64.86%	16.61	66.23%
4	15.93	21.82	73.01%	16.85	76.15%
5	16.85 (damping 32.02%)	21.82	77.22%	21.82	77.22%
6	19.91	23.03	86.45%	22.84	94.54%
7	22.33	25.62	87.16%	23.08	96.75%
8	26.11	25.81	101.16%	25.78	101.28%

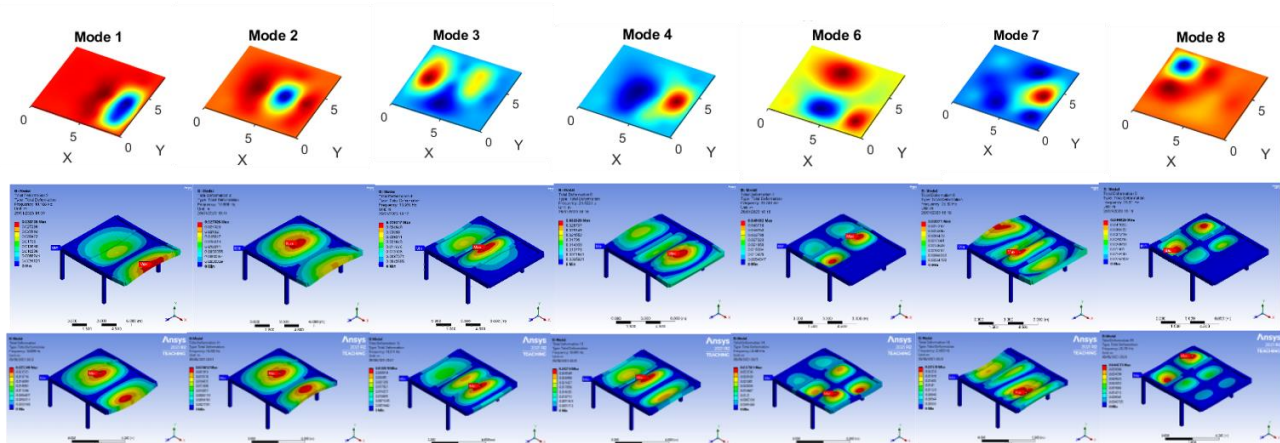


Figure 5. 26: Large Floor (Site 1) - Comparison of the Mode Shapes between Measurements and FE Results of Model 2

Upon comparing the two finite element models with the measurement results, it can be concluded that the two-bay model exhibits a closer ratio between the measured frequencies and simulation results. However, the one-and-a-half-bay model aligns more closely with the measured mode shapes. Consequently, the one-and-a-half-bay model was selected due to its principal mode shape's higher similarity to the experimental results compared to the natural frequency.

The lower similarity in mode shapes for the two-bay model can be attributed to the location of the sensors. Different sensor placements for collecting response data significantly influence the measured mode shape results. In this measurement, the sensors were positioned only within the one-and-a-half-bay section, making them more sensitive to mode shapes occurring in that area and less responsive to those influenced by the two-bay model.

A comparison of the mode shapes obtained from experimental data with those simulated in ANSYS indicates that the materials selected and the model established in ANSYS are valid, highlighting the potential for utilizing this computational model in further studies involving parameter updates.

5.5.3 Site 2-Small Floor and Large Floor

The comparison of small floors at Construction Site 2, as illustrated in Table 5.14, revealed that the predicted and measured frequencies closely align, with differences falling within 25%. However, it was noteworthy that all measured frequencies are lower than the simulated frequencies. This discrepancy may be attributed to the exclusion of the effects of raised floors in the structure. While

the frequencies align well and a correlation between the test mode shape and the simulated mode shape has been established (Figure 5.27), challenges remain in matching the local mode shapes.

Table 5. 14: Comparison of Frequencies between Measurements and FE Results of Model 3

	Shaker (Measurement)	ANSYS (FE)	Ratio % (Measurements/FE results)
Mode	frequency (Hz)	frequency (Hz)	
1	8.93	11.76	75.94%
2	10.08	12.67	79.56%
4	17.40	21.74	77.71%
5	24.13	24.23	99.59%
6	27.83	29.20	95.31%
7	29.80	30.88	96.50%
8	30.44	32.55	93.52%

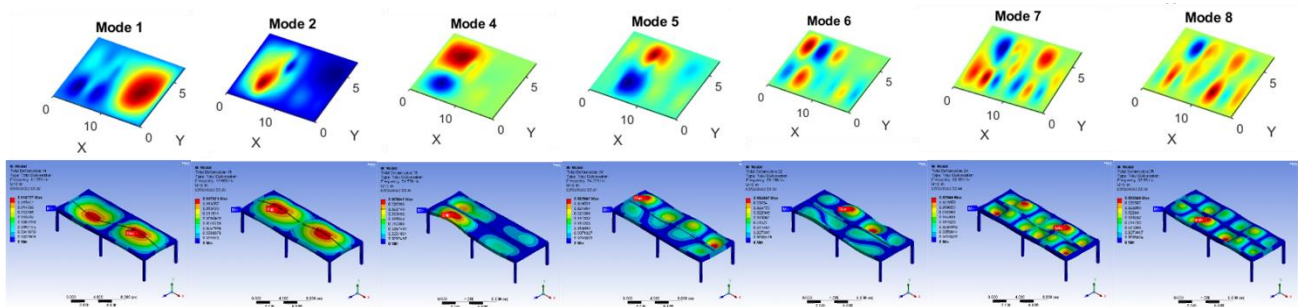


Figure 5. 27: Small Floor (Site 2) - Comparison of the Mode Shapes between Measurements and FE Results of Model 3

Similarly, the results for the large floor at Site 2, obtained from modal testing measurements and computational analysis in ANSYS, were summarized in Table 5.15. The difference between the testing and simulation predictions was approximately 25%, which is considered acceptable. Like the small floors, all tested frequencies were lower than the numerical simulation results, indicating that the stiffness and quality of the finite element model require further refinement. Future studies should consider simulating the composite nature of the actual raised access floor.

The mode shapes for different frequencies, illustrated in Figure 5.28, demonstrate relative consistency, with four modes from the shaker test and ANSYS simulation analysis exhibiting good correlation.

Table 5. 15: Comparison of Frequencies between Measurements and FE Results of Model 4

Mode	Shaker (Measurement) frequency (Hz)	ANSYS (FE) frequency (Hz)	Ratio % (Measurements/FE results)
1	9.40	12.81	73.38%
2	19.00	25.61	74.19%
3	25.23	27.98	90.17%
4	30.46	32.47	93.81%

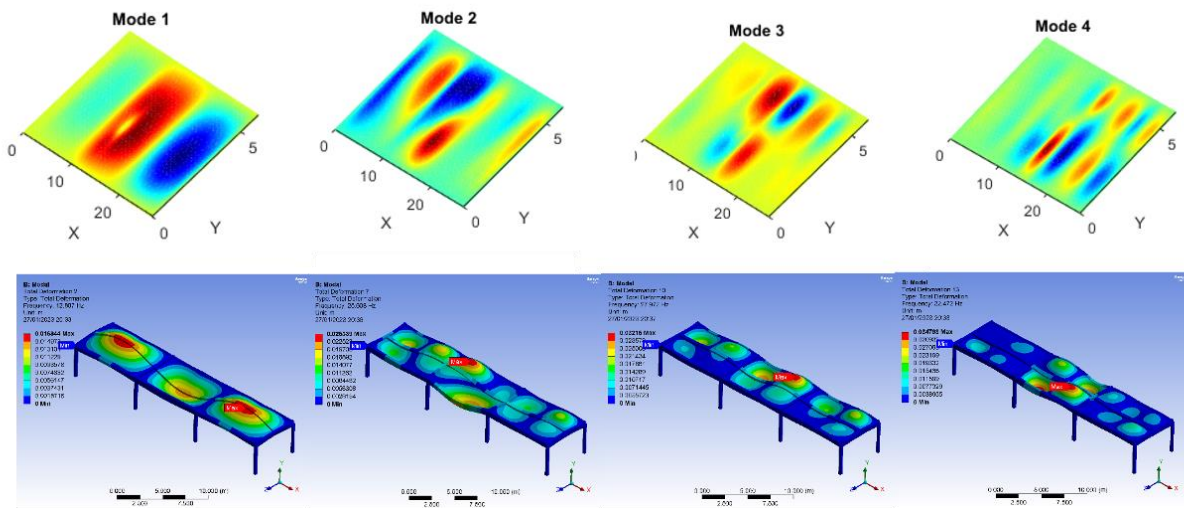


Figure 5. 28: Large Floor (Site 2) - Comparison of the Mode Shapes Measurements and FE Results of Model 4

5.5.4 Site 3- Area 1, Area 2 and CLT Extensions

Area 1 and Area 2 belong to different sections of the same floor, and their comparison assesses the consistency of test results across the structure. As shown in Table 5.16, the frequencies of five modes in Area 1 closely matched the shaker test data, with the fundamental frequency variance being less than 4% and other frequencies within a 20% difference from the test data. This alignment confirmed the reliability of the shaker test. However, significant differences in mode shapes were evident in Figure 5.29. While it is possible to discern finite element simulation results corresponding to the tests, this requires considerable effort due to the large modeling size, which results in numerous local modes.

Table 5. 16: Comparison between Measurements and FE Results of Site 3- Area 1

Mode	Shaker (Measurement) frequency (Hz)	ANSYS (FE) frequency (Hz)	Ratio % (Measurements/FE results)
1	12.25	12.66	96.76%
2	14.04	17.23	81.49%

3	16.29	18.04	90.30%
4	24.16	25.03	96.52%
5	29.15	33.32	87.48%

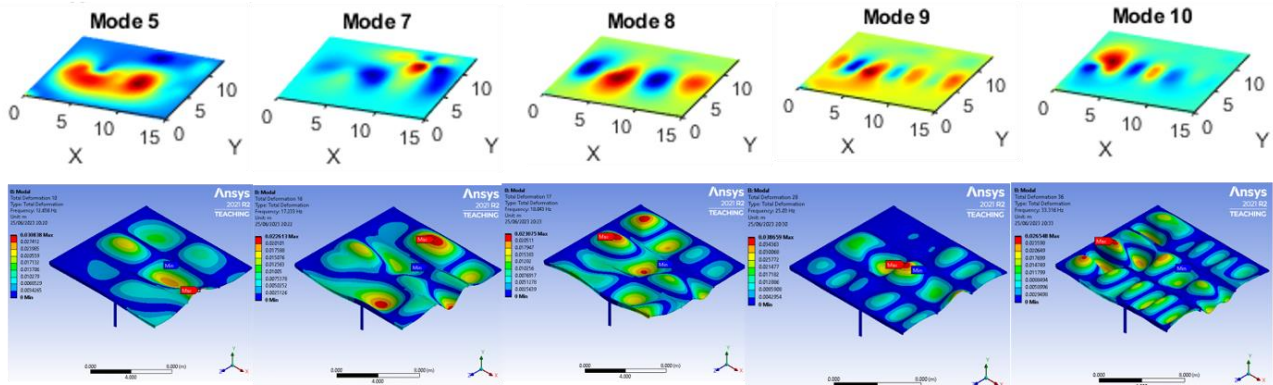


Figure 5. 29: Area 1 (Site 3) - Comparison of the Mode Shapes between the FE Model and Measurement

In Area 2, Table 5.17 indicated no comparison result for the third mode frequency. However, the difference between the test results and numerical simulations for nine modes was generally within 20%, with one outlier being considered acceptable. Additionally, comparing the mode shapes in Figure 5.30 from experiments and finite element analysis proved time-consuming due to the large-scale modeling, which spans more than three spans in both directions, resulting in many small local modes. A key indicator of these local modes was the narrow spacing between adjacent frequencies, which was less than 1 Hz.

Table 5. 17: Comparison of Frequencies between Measurements and FE Results of Site 3-Area 2

Mode	Shaker (Measurement) frequency (Hz)	ANSYS (FE) frequency (Hz)	Ratio % (Measurements/FE results)
1	8.16	10.32	79.07%
2	10.77	14.11	76.33%
3	11.75	-	-
4	14.37	16.12	89.14%
5	15.75	22.97	68.57%
6	18.77	23.39	80.25%
7	24.96	26.65	93.66%
8	28.00	30.02	93.27%
9	30.15	33.32	90.49%

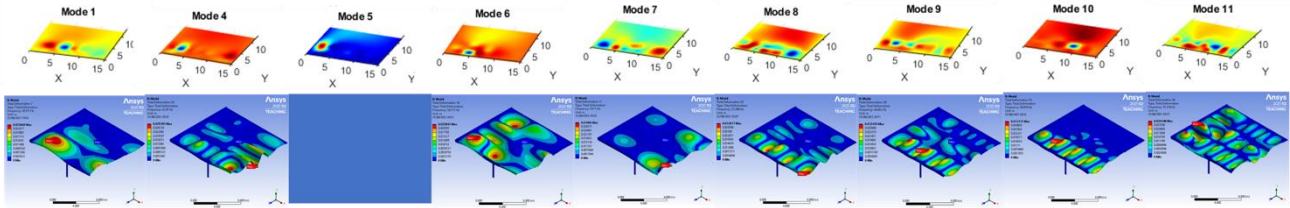


Figure 5. 30: Area 2 (Site 3) - Comparison of the Mode Shapes between the FE Model and Measurement

The comparison in Table 5.18 highlights significant differences between the modal parameters derived from the hammer test and the ANSYS numerical simulation. For the 1st CLT extension floor, the first-order natural frequency is only 42.59% of that obtained through numerical simulation, while for the 2nd CLT extension floor, it is 36.40%. In contrast, the first-order natural frequency for the 3rd CLT extension floor exceeds the simulated frequency, reaching 117.39%. These findings suggest that the ANSYS model requires further refinement to ensure that variations from the measured model remain within 20%.

Among the Site 3 extension CLT floors, only the simulation of the 3rd CLT extension floor was the most reliable, with differences between measurement and simulation for five modes falling within 20%. Notably, the simulated frequencies for the higher-order modes of the 1st and 2nd CLT extension floors were significantly better than those for the fundamental mode. This discrepancy may stem from a misjudgment of the first mode during impact hammer testing. Figure 5.31 illustrated that the mode shape of the 3rd CLT extension numerical simulation model exhibits the closest agreement with the test data. While the mode shapes of the 1st and 2nd CLT extension floors were generally similar to the numerical simulation results, they were insufficient compared to the correspondence observed in the mode shapes of the 3rd CLT extension.

Table 5. 18: Comparison between Measurements and FE Results of Site 3 - CLT Extensions

Site 3: 1st CLT extension			
Mode	Hammer(Measurement)	ANSYS (FE)	Ratio % (Measurements/FE results)
	frequency (Hz)	frequency (Hz)	
1	7.16	16.81	42.59%
2	14.55	20.38	71.39%
3	18.56	24.37	76.16%
4	28.12	25.97	108.28%
5	30.32	31.79	95.38%
Site 3: 2nd CLT extension			
1	8.06	22.14	36.40%

2	12.45	24.71	50.38%
3	13.58	27.26	49.82%
4	14.83	27.98	53.00%
5	18.08	28.81	62.76%
6	28.05	30.14	93.07%
7	30.32	32.27	93.96%
Site 3: 3rd CLT extension			
1	12.49	10.64	117.39%
2	14.88	13.69	108.69%
3	17.90	18.61	96.18%
4	24.48	24.99	97.96%
5	30.30	28.31	107.03%

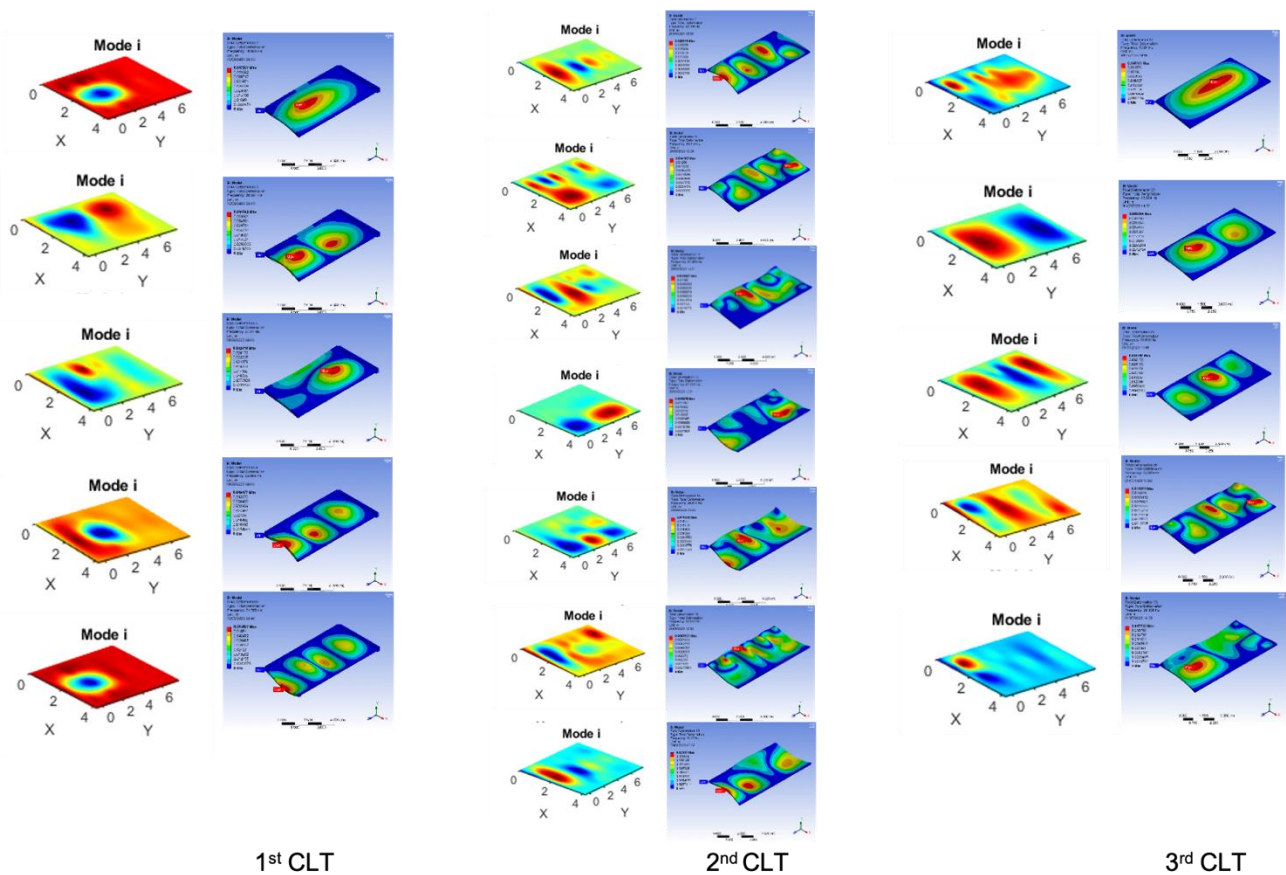


Figure 5.31: CLT Extensions (Site 3) - Comparison of the Mode Shapes between the FE Model and c Measurement

5.6 Summary of Conclusions from FE Analysis

This chapter explores the feasibility of employing a simplified model to verify modal parameters. Although complex models are essential in some studies, they do not provide meaningful value within the scope of this research. Specifically, the composite slab modeling method, while detailed, is overly intricate for the level of accuracy it offers and lacks the efficiency required for automation.

The primary objective of this modeling approach was to verify the reliability of the modal parameters derived from the test data, with a focus on the accuracy of the mode shapes obtained using the MATLAB analysis program developed by the authors. Mode shapes generated experimentally are often imprecise, particularly when identifying higher-order modes, making it even more challenging to achieve distinct and independent modes at each stage of the experiment.

Finite Element Analysis (FEA) played a crucial role in addressing these challenges by simulating higher-order modes. Its application allowed for the validation of the experimental results, offering a more robust method for assessing the reliability of the modal parameters. This chapter dedicated substantial effort to matching the mode shapes, ultimately achieving a frequency matching difference of each mode within 20%. This level of accuracy, while difficult to attain, underscores the advantages of the chosen modeling approach, particularly in improving the precision of high-order mode identification.

Looking ahead, future research will incorporate the raised access floor into the model. Furthermore, the development of more refined finite element models is expected to further reduce the frequency matching differences, enhancing both accuracy and reliability. This refinement represents a key focus of ongoing research efforts.

Modeling Recommendations:

1. The wooden frame, comprising beams and columns, contributed 15.54% to the model's mass, with columns at 7.99% and beams at 7.55% in the small floor model. The beam-only model yielded identical frequency and mode shape results as the column-beam model. Therefore, the simplest model should include at least beams and plates. However, a plate-only model is not recommended, as it lacks necessary beam support locations, which can lead to erroneous mode shape estimations. Simplifying the co-movement between beams and plates using line or nodal boundary conditions is also not feasible.
2. The one-and-a-half-bay model created a cantilever beam effect for the half bay. While boundary restrictions limit edge movement, it cannot represent actual behavior as effectively as the two-bay model.
3. The position of the support beam significantly influences vibration and divides the mode shape into distinct regions. Excessive local vibration from large-scale modeling can complicate the identification of adjacent frequencies.

4. Although simulations using bonded contacts can provide guidance for computational predictions, the simulation of connections between the CLT floor panel and supported beams may not accurately reflect real conditions. This indicates a need for further refinement in finite element simulations.

Reducing Disparities between Measurements and FEA Results:

1. Typically, the first three modes contributed approximately 80% of the total mode participation. However, there were instances where higher-order modes may exhibit a greater likelihood of excitation than lower-order modes. Consequently, validating the FE model should prioritize matching the first three mode shapes, with higher modes being of lower priority.
2. Closely spaced adjacent modes may be indistinguishable from experimental test data alone. Evaluating frequency accuracy through experimental analysis is inherently less precise than finite methods; therefore, it is crucial to assess the differences between the two approaches appropriately.
3. A considerable amount of time was dedicated to comparing mode shapes, with the primary focus on achieving a match. The ratio between measured frequencies and FE results serves as a useful indicator, with a 20% difference commonly accepted. In this study, the frequency differences between shake testing and FE results were 30% at Site 1, 25% at Site 2, and 20% at Site 3. Additionally, Site 3 experienced a maximum frequency difference of 60% when the measured frequency was obtained from a hammer test.

6. Conclusions and Related Further Work

6.1 Conclusions

The number of case studies involving on-site cross-laminated timber (CLT) laminate flooring is limited, and the quality of measurements is often questionable. This limitation arises from the scarcity of opportunities to test large-scale systems in environments free from occupants, building materials, and office furniture. Additionally, even fewer studies utilize equipment capable of capturing high-quality modal measurements in the field.

This study emphasizes the experimental testing of relatively 'clean' flooring systems, which serve as valuable specimens for developing effective finite element (FE) computational models. By creating computationally efficient yet accurate FE models that predict floor vibration parameters, designers will gain improved tools to evaluate proposed floor designs and address potential vibration issues.

Three test sites with nine designated test areas were involved in this study. Field tests conducted on CLT floor slabs within these areas facilitated the acquisition of dynamic properties and performance data through various test methods. The applicability of design codes and evaluation standards for CLT floors was then assessed based on the acquired parameters.

This research offered a comprehensive modal testing methodology and analysis framework, particularly suited for individuals seeking cost-effective testing protocols for timber floor structures and the establishment of non-commercial testing setups. Specifically:

- 1) A review of ISO 18324 (2016) and BS EN 16929 (2018) standards enabled the determination of test requirements, test data, and methodologies, ensuring that all critical testing details were addressed.
- 2) The modal testing analysis was conducted exclusively using MATLAB, without requiring additional software.

A finite element model was established, and modal shapes obtained from this model were compared with those derived from MATLAB's modal calculations based on test data. The comparison showed consistency between the modal shapes, and the frequency discrepancies between the modes fell within an acceptable range of 10% to 30%. This indicates that the finite element model is effective and holds promise for application in structural dynamic analysis, especially with further refinement.

6.1.1 Field Test Results of CLT Flooring Systems

Field tests were conducted on three buildings at different phases of construction and occupancy. At Site 1, the building was still under construction, while at Site 2, it was ready for occupancy. Site 3, in contrast, had been occupied for over two months at the time of testing. Consequently, the tests at **Sites 1 and 2 did not account for the influence of personnel or equipment, whereas Site 3 included the effects of furnishings and equipment, which contributed to increased damping.** This was confirmed by the test results.

The floor slabs at Sites 1 and 2 were supported by glulam beams, while those at Site 3 rested on steel beams. Additionally, the floor at Site 3 featured a hybrid boundary, including CLT walls, reinforced concrete beams, and angle steel. **Across all three sites, the slabs incorporated raised access floors atop the CLT.**

Regarding dynamic properties, the fundamental natural frequencies of the two test floors at Site 1 were measured at 9.3 Hz and 7.8 Hz, with damping values of 1.5% and 2.5%, respectively. At Site 2, the natural frequencies were 8.9 Hz and 9.4 Hz, with dampings of 2.02% and 3.48%. Site 3 showed a natural frequency of 8.2 Hz for the test area with steel supports, accompanied by a damping value of 2.67%. Another area at Site 3, supported by CLT walls and glulam beams, exhibited a natural frequency of 7.1 Hz and a higher damping of 6.8%. **These results suggest that timber structural components provide significant damping, although they are typically associated with lower natural frequencies.**

Structural frequencies and damping values were measured up to the 5th order for all test data. The results showed a clear increase in frequency with higher modes, demonstrating good order correlation. Hence, the fundamental frequency can serve as a limiting factor in design codes. However, changes in damping values were not consistently related to mode order, with lower-order modes sometimes exhibiting higher damping values. Damping is difficult to predict accurately, and Eurocode 5 recommends a 1% damping value for wooden structures. The British national annex suggests a higher value of 2% for residential joisted timber floors. **The findings from this study suggest that a 2% damping value is appropriate for combined structures, but for CLT-CLT wall support systems, a higher value, closer to 5%, may be more reasonable.** The recommendations in rEC 5 are considered reliable, particularly the 4% damping ratio for CLT floors with floating floor layers.

6.1.2 Guidelines and Standards Check Results

The response of floor slabs to human-induced loads was investigated through walking and running tests. Two timber structure design codes, Eurocode 5 (EC5) and the revised Eurocode 5 (rEC5), were used to evaluate whether the test results met the serviceability design requirements. Three human comfort vibration evaluation standards were also employed to assess the severity of human annoyance.

The results show that higher walking frequencies led to a more pronounced floor response. **The acceleration caused by running was found to be 10 times higher than that caused by walking.** When evaluated under Eurocode 5, 40% of the tested floor slabs failed to meet the design requirements, largely due to the 8 Hz frequency limit set by the code. However, when the revised rEC5 was used, all tested floors passed the design requirements, provided that the frequency exceeded 4.5 Hz.

Further examination of the acceleration criteria, known as the R-factor in rEC5, revealed that at a higher performance level IV (intended for office spaces), only floors under walking conditions passed the design requirements. Almost no floors met the design criteria under running conditions. Even at the lowest performance level V, 17% of the floor slabs failed to meet the acceleration criteria. These results suggest that **the R-factor, which is used to inspect rEC5-designed floors, may need further refinement to be effectively applied to measured floor slabs.**

The severity of human annoyance was evaluated using three standards: ISO 2632:1997, BS 6841:1987, and BS 6472:2028. Although **the estimated vibration dose value (eVDV)** could be easily calculated using ISO 2632:1997, **it lacks a clear reference range for interpretation.** BS 6841:1987 provides a reference line for eVDV values but does not account for accelerations below 1 m/s². Therefore, it cannot be directly compared with the vibration dose value (VDV) range specified in BS 6472:2028, which is used to determine the probability of adverse human reactions.

6.1.3 Different Test Methods for Measuring Design Parameters

Heel Drop Test:

The heel drop test was conducted following parameters set by previous research. In this test, the participant weighs 66 kg and drops their heel at the midpoint of the floor. The test is repeated eight times, with a 10-second interval between each drop to allow sufficient time for the floor's response to decay. This waiting period ensures accurate measurement of the floor's dynamic response.

Walking and Running Test:

Participants used a metronome app to maintain the desired walking frequency during the walking and running tests. Slow walking was conducted at 1.5 Hz, while fast walking was measured at 2 Hz. For safety reasons, the running frequency was not predetermined, and was analyzed post-test using Fast Fourier Transform (FFT). Testers were required to complete at least one round trip of the test area. To improve accuracy, multiple tests were conducted, and the results were averaged.

Impact Hammer Test:

Before conducting the impact hammer test, a pre-test was performed to determine the appropriate hammer size and head type. **A soft hammer tip was preferred over a hard tip**, particularly for timber floors, due to the focus on frequencies below 30 Hz. Using a hard tip could compromise the accuracy of low-frequency modal parameter identification. Care was taken to avoid the "double-hit" phenomenon, which would cause multiple peaks in the data. The hammer impact force was monitored to ensure that only one peak value appeared within each time interval.

Shaker Test:

The shaker test involved an excitation system comprising a shaker, amplifier, and signal generator. A pre-test was performed to ensure the system could generate the necessary excitation signals. Sine swept excitation was used to quickly assess the floor's frequency response. Ensuring even distribution of energy across the entire test area was critical for obtaining reliable input-output data. **A sampling frequency of at least 1024 Hz** was used to meet the BS EN 16929:2018 specification and prevent data overflow. The shaker was positioned at the center of the floor to maximize excitation for all modes.

Additional Test Considerations:

When using the roving sensor method, the most time-consuming part of the test involved moving cables over long distances, especially when the measurement range exceeded 6 meters. On-site measures were taken to prevent cable tangling and ensure smooth test operation.

Method Selection:

Among the test methods, **the shaker test system provides the highest data quality**, making it the preferred option for precise and controlled low-frequency measurements of timber floors, especially when floor frequencies exceed 4.5 Hz. While the **heel-drop method is more suitable for testing high-frequency floors (above 8 Hz)**, it is not reliable for low-frequency floors, as it may lead to

underestimation of the natural frequencies and overestimation of the damping values. The impact hammer method offers a middle ground, providing an affordable and time-efficient alternative. However, it should only be used when the structure can be adequately stimulated by the hammer.

6.1.4 Post-processing in MATLAB

Modal Parameter Estimation Using MATLAB

In the post-processing stage, modal parameters were extracted from test data using MATLAB. The data was first classified and packaged to allow for efficient model estimation with batch data. The process began with operating modal analysis to identify characteristic frequencies and damping properties. The 'etfe' command was used to estimate the transfer function, with the model order set to 24, a value chosen after experimenting with various orders and evaluating the fit of the model to the Frequency Response Function (FRF).

A critical part of this process was refining the model using the 'ssest' command, which applies the non-linear least-squares (NLLS) Curve-Fit method. This approach requires selecting an appropriate frequency band for model identification and constructing a modal formulation model. The NLLS method fits the measured data and iteratively minimizes the sum of square errors until the error falls below a predetermined threshold, ensuring accuracy in parameter estimation.

Damping Extraction from Heel Drop Tests

For extracting frequency damping parameters from heel drop tests, the complex exponential method was employed. This method has the advantage of not requiring an initial estimate of modal parameters, making it useful in situations where such parameters are difficult to predict. However, it requires multiple hypotheses and modal order identifications, which can make the process labor-intensive.

Although the frequency range of interest in this study typically fell between 0-30 Hz, it was necessary during debugging to set the mode order to 100 Hz. This adjustment ensured more accurate estimation results, even though the modal frequencies of interest remained within the lower range.

6.2 Recommendations for Future Research

Recommended directions for future research focus on testing and simulating the vibration characteristics of CLT floor slab. This includes additional in-situ testing to evaluate dynamic performance under various conditions, as well as improvements in finite element modeling

techniques for predicting frequency and damping behavior. Future studies should also aim to calibrate frequency and damping anomalies, especially in models incorporating raised access floors, to enhance the accuracy of the simulations.

1. Low-Frequency CLT Flooring Data Collection:

The fundamental natural frequency of the tested floors falls within the 7-13 Hz range, coinciding with the boundary of human activity influence (4-8 Hz). However, for CLT flooring systems with lower frequencies, the acceleration response to human-induced loads is higher. This highlights the need for stricter requirements on the R-factor proposed in the revised Eurocode 5. In light of this, increasing the collection of low-frequency CLT flooring test data within the 4.5-8 Hz range is crucial for enhancing vibration serviceability in future designs.

2. Impact of Raised Access Floors on Dynamic Properties:

All current test results incorporate the effects of raised access floors. To isolate the dynamic response of the pure CLT surface floor, it is essential to conduct tests before the installation of raised access floors during construction. This would allow for an examination of dynamic parameter changes when pure wooden floors are attached to topping floor structures, thus facilitating the refinement of design specifications. This investigation could also provide suggested values for frequency and damping. Additionally, the research of Reynolds (doctoral thesis) on the vibrational performance of long-span concrete floors with raised access systems can serve as a valuable reference for future studies on the effects of raised access flooring.

3. Finite Element Model Updates:

While a finite element model has been established, further research is required to refine the model using measured data. These updates are critical for improving finite element analyses of resonant structures responding to human-induced vibrations. Sehgal's review on structural dynamic model updating techniques in engineering (2016) offers valuable insights into this area and can be used as a reference for further advancements in the field of model updating.

References

- Agreement, P., 2015, December. Paris agreement. In report of the conference of the parties to the United Nations framework convention on climate change (21st session, 2015: Paris). Retrived December (Vol. 4, No. 2017, p. 2). Getzville, NY, USA: HeinOnline.
- Allen, D.E. and Hassay, T.M., 1993. Design criterion for vibrations due to walking. *Engineering Journal*, 30(4), pp.117-129.
- Allen, D.E. and Rainer, J.H., 1976. Vibration criteria for long-span floors. *Canadian Journal of Civil Engineering*, 3(2), pp.165-173.
- Allen, D.L., 1974. Vibrational behavior of long-span floor slabs. *Canadian journal of civil engineering*, 1(1), pp.108-115.
- Aloisio, A., Pasca, D.P., De Santis, Y., Hillberger, T., Giordano, P.F., Rosso, M.M., Tomasi, R., Limongelli, M.P. and Bedon, C., 2023. Vibration issues in timber structures: A state-of-the-art review. *Journal of Building Engineering*, p.107098.
- Azaman, N.M., Abd Ghafar, N.H., Azhar, A.F., Fauzi, A.A., Ismail, H.A., Idrus, S.S., Mokhjar, S.S. and Abd Hamid, F.F., 2018, April. Investigation of concrete floor vibration using heel-drop test. In *Journal of Physics: Conference Series* (Vol. 995, No. 1, p. 012027). IOP Publishing.
- Bachmann, H., 1995. *Vibration problems in structures: practical guidelines*. Springer Science & Business Media.
- Barrett, A.R., 2006. Dynamic testing of in-situ composite floors and evaluation of vibration serviceability using the finite element method.
- Blakeborough, A. and Williams, M.S., 2003. Measurement of floor vibrations using a heel drop test. *Proceedings of the Institution of Civil Engineers-Structures and Buildings*, 156(4), pp.367-371.
- Brandner, R., Flatscher, G., Ringhofer, A., Schickhofer, G. and Thiel, A., 2016. Cross laminated timber (CLT): overview and development. *European journal of wood and wood products*, 74, pp.331-351.
- Brownjohn, J.M., Pavic, A. and Omenzetter, P., 2004. A spectral density approach for modelling continuous vertical forces on pedestrian structures due to walking. *Canadian Journal of Civil Engineering*, 31(1), pp.65-77.
- BS 6472-1:2008. Guide to evaluation of human exposure to vibration in buildings – Part 1: Vibration sources other than blasting. British Standard.
- BS 6841:1987. Guide to measurement and evaluation of human exposure to whole-body mechanical vibration and repeated shock. British Standards Institution.
- BS EN 16929:2018. Test methods – Timber floors – Determination of vibration properties. British Standard.

Butz, C., Sedlacek, G., Heinemeyer, C., 2006. Generalisation of criteria for floor vibrations for industrial, office, residential and public building and gymnastic halls. European Commission, Directorate-General for Research and Innovation.

Casagrande, D., Giongo, I., Pederzoli, F., Franciosi, A. and Piazza, M., 2018. Analytical, numerical and experimental assessment of vibration performance in timber floors. *Engineering Structures*, 168, pp.748-758.

Chen, J., Wang, H.Q. and Peng, Y.X., 2014. Experimental investigation on Fourier-series model of walking load and its coefficients. *J. Vib. Shock*, 33(8), pp.11-15.

Dackermann, U., Li, J., Rijal, R. and Crews, K., 2016. A dynamic-based method for the assessment of connection systems of timber composite structures. *Construction and Building Materials*, 102, pp.999-1008.

De Araujo, V., Aguiar, F., Jardim, P., Mascarenhas, F., Marini, L., Aquino, V., Santos, H., Panzera, T., Lahr, F. and Christoforo, A., 2023. Is cross-laminated timber (CLT) a wood panel, a building, or a construction system? A systematic review on its functions, characteristics, performances, and applications. *Forests*, 14(2), p.264.

Ebrahimpour, A., Hamam, A., Sack, R.L. and Patten, W.N., 1996. Measuring and modeling dynamic loads imposed by moving crowds. *Journal of Structural Engineering*, 122(12), pp.1468-1474.

Ekhaese, E.N. and Ndimako, O.O., 2023. Eco-friendly construction materials and health benefits in the design of an all-inclusive health resorts, Nigeria. *Frontiers in Built Environment*, 9.

Ellingwood, B. and Tallin, A., 1984. Structural serviceability: floor vibrations. *Journal of Structural engineering*, 110(2), pp.401-418.

Ellis, B.R., 2000. On the response of long-span floors to walking loads generated by individuals and crowds. *Structural Engineer*, 78(10), pp.17-25.

Ellis, B.R., 2003. The influence of crowd size on floor vibrations induced by walking. *Structural Engineer*, 81(6), pp.20-27.

EN 1995-1-1:2004. Eurocode 5: Design of timber structures – Part 1-1: General – Common rules and rules for buildings. European Committee for Standardisation CEN: Brussels.

European Commission, 2019. New Rules for Greener and Smarter Buildings Will Increase Quality of Life for All Europeans.

Ewins, D.J., 2009. *Modal testing: theory, practice and application*. John Wiley & Sons.

Feldmann, M., Heinemeyer, C., Butz, C., Caetano, E., Cunha, A., Galanti, F., Goldack, A., Hechler, O., Hicks, S., Keil, A. and Lukic, M., 2009. Design of floor structures for human induced vibrations. JRC–ECCS joint report, 45.

Fu, Z.F. and He, J., 2001. *Modal analysis*. Elsevier.

Glisovic, I. and Stevanovic, B., 2010, June. Vibrational behaviour of timber floors. In *World Conference on Timber Engineering*.

- Griffin, M.J., 2012. Handbook of human vibration. Academic press.
- Guignard, J.C., 1971. Human sensitivity to vibration. *Journal of sound and vibration*, 15(1), pp.11-16.
- Hamm, P., Richter, A. and Winter, S., 2010, June. Floor vibrations–new results. In *Proceedings of 11th World Conference on Timber Engineering (WCTE2010)*, Riva del Garda.
- Hanagan, L.M. and Murray, T.M., 1997. Active control approach for reducing floor vibrations. *Journal of structural engineering*, 123(11), pp.1497-1505.
- Hassanieh, A., Chiniforush, A.A., Valipour, H.R. and Bradford, M.A., 2019. Vibration behaviour of steel-timber composite floors, part (2): evaluation of human-induced vibrations. *Journal of Constructional Steel Research*, 158, pp.156-170.
- Hassanieh, A., Valipour, H.R. and Bradford, M.A., 2017. Experimental and numerical investigation of short-term behaviour of CLT-steel composite beams. *Engineering Structures*, 144, pp.43-57.
- Hassay, T.M., Allen, D.E., Ungar, E.E. and Davis, D.B., 2016. Design guide 11: Vibrations of steel-framed structural systems due to human activity. American Institute of Steel Construction AISC, Chicago.
- Hicks, S., 2004. Vibration characteristics of steel–concrete composite floor systems. *Progress in Structural Engineering and Materials*, 6(1), pp.21-38.
- Hicks, S.J. and Smith, A.L., 2011. Design of floor structures against human-induced vibrations. *Steel Construction*, 4(2), pp.114-120.
- Hu, L. and Gagnon, S., 2012, July. Controlling cross-laminated timber (clt) floor vibrations: fundamentals and method. In *World Conference on Timber Engineering* (pp. 269-275).
- Hu, L., 2013. Serviceability of next generation wood buildings: laboratory study of vibration performance of cross-laminated-timber (CLT) floors. Québec, Québec.
- Hu, L.J., Chui, Y.H. and Onysko, D.M., 2001. Vibration serviceability of timber floors in residential construction. *Progress in Structural Engineering and Materials*, 3(3), pp.228-237.
- Huang, H., Gao, Y. and Chang, W.S., 2020. Human-induced vibration of cross-laminated timber (CLT) floor under different boundary conditions. *Engineering Structures*, 204, p.110016.
- Irvine, T., 2013. Effective modal mass and modal participation factors. Available on the web on site: <http://www.vibrationdata.com/tutorials2/ModalMass.pdf>.(last access on march 7 2007).
- ISO 10137:2007, Bases for design of structures – Serviceability of buildings and walkways against vibration, International Organization for Standardization.
- ISO 18324:2016. Timber structures – Test methods – Floor vibration performance. International Organization for Standardization, Geneva, Switzerland.
- ISO 2631-1:1997. Mechanical vibration and shock – Evaluation of human exposure to whole-body vibration – Part 1: General Requirements. International Organization for Standardization, Geneva, Switzerland.

- ISO 2631-2:2003. Mechanical vibration and shock – Evaluation of human exposure to whole-body vibration – Part 2: Vibration in buildings (1 Hz to 80 Hz). International Organization for Standardization, Geneva, Switzerland.
- Jarnerö, K., Brandt, A. and Olsson, A., 2015. Vibration properties of a timber floor assessed in laboratory and during construction. *Engineering structures*, 82, pp.44-54.
- Ji, T. and Ellis, B.R., 1994. Floor vibration induced by dance-type loads: theory. *Structural Engineer*, 72, pp.37-37.
- Jiang, Y. and Crocetti, R., 2019. CLT-concrete composite floors with notched shear connectors. *Construction and Building Materials*, 195, pp.127-139.
- Karacabeyli, E. and Douglas, B., 2013. CLT handbook-US edition. FPIInnovations and Binational Softwood Lumber Council, Point-Claire, Quebec.
- Karampour, H., Piran, F., Faircloth, A., Talebian, N. and Miller, D., 2023. Vibration of timber and hybrid floors: A review of methods of measurement, analysis, and design. *Buildings*, 13(7), p.1756.
- Karjalainen, M., Ilgin, H.E., Metsäranta, L. and Norvasuo, M., 2021. Suburban residents' preferences for livable residential area in Finland. *Sustainability*, 13(21), p.11841.
- Kerr, S.C., 1999. Human induced loading on staircases. Doctoral dissertation, University of London, University College London (United Kingdom).
- Lehmann, S., 2012. Sustainable construction for urban infill development using engineered massive wood panel systems. *Sustainability*, 4(10), pp.2707-2742.
- Leicester, R.H. and Beresford, F.D., 1977. A probability model for serviceability specifications. In *Proc., 6th Australian Conf. on the Mech. of Struct. and Mat* (pp. 407-413).
- Liu, C., Wang, H., Wang, Z., Liu, Z., Tang, Y. and Yang, S., 2022. Research on life cycle low carbon optimization method of multi-energy complementary distributed energy system: A review. *Journal of Cleaner Production*, 336, p.130380.
- Ljunggren, F., 2006. Floor vibration: dynamic properties and subjective perception (Doctoral dissertation, Luleå tekniska universitet).
- Loss, C. and Frangi, A., 2017. Experimental investigation on in-plane stiffness and strength of innovative steel-timber hybrid floor diaphragms. *Engineering Structures*, 138, pp.229-244.
- Loss, C., Piazza, M. and Zandonini, R., 2014, August. Experimental tests of cross-laminated timber floors to be used in timber-steel hybrid structures. In *Proceedings of WCTE 2014 conference*. Quebec, Canada, August.
- Loss, C., Piazza, M. and Zandonini, R., 2016a. Connections for steel–timber hybrid prefabricated buildings. Part I: Experimental tests. *Construction and Building Materials*, 122, pp.781-795.
- Loss, C., Piazza, M. and Zandonini, R., 2016b. Connections for steel–timber hybrid prefabricated buildings. Part II: Innovative modular structures. *Construction and Building Materials*, 122, pp.796-808.

- Mai, K.Q., Park, A., Nguyen, K.T. and Lee, K., 2018. Full-scale static and dynamic experiments of hybrid CLT–concrete composite floor. *Construction and Building Materials*, 170, pp.55-65.
- Mohammed, A.S., Pavic, A. and Racic, V., 2018. Improved model for human induced vibrations of high-frequency floors. *Engineering Structures*, 168, pp.950-966.
- Muhammad, Z., Reynolds, P., Avci, O. and Hussein, M., 2018. Review of pedestrian load models for vibration serviceability assessment of floor structures. *Vibration*, 2(1), pp.1-24.
- Murray, T.M., 1975. Design to prevent floor vibrations. *Engineering Journal*, 12(3).
- NA to BS EN 1995-1-1:2004+A2:2014. UK National annex to Eurocode 5: Design of timber structures. General- common rules and rules for buildings, British Standards Institution.
- Negrão, J.H.J.D.O., Maia de Oliveira, F.M., Leitão de Oliveira, C.A. and Cachim, P.B., 2010. Glued composite timber-concrete beams. II: Analysis and tests of beam specimens. *Journal of Structural Engineering*, 136(10), pp.1246-1254.
- Ohlsson, S.V., 1982. Floor vibrations and human discomfort. (Doctoral dissertation, Chalmers University of Technology).
- Onysko, D., 1986. Serviceability criteria for residential floors based on a field study of consumer response.
- Pavic, A. and Reynolds, P., 2002. Vibration serviceability of long-span concrete building floors. Part 1: Review of background information. *Shock and Vibration Digest*, 34(3), pp.191-211. Leicester, R.H., 1993. Serviceability criteria for building codes. IABSE REPORTS, pp.69-69.
- Pavic, A., 1999. Vibration serviceability of long-span cast in-situ concrete floors (Doctoral dissertation, University of Sheffield).
- Pavic, A., Reynolds, P. and Waldron, P., 2002. Modal testing and FE model correlation and updating of a long-span prestressed concrete floor. *Proceedings of the Institution of Civil Engineers-Structures and Buildings*, 152(2), pp.97-109.
- Pavic, A., Reynolds, P., Waldron, P. and Bennett, K., 2001. Dynamic modelling of post-tensioned concrete floors using finite element analysis. *Finite elements in analysis and design*, 37(4), pp.305-323.
- Pernica, G., 1990. Dynamic load factors for pedestrian movements and rhythmic exercises. *Canadian Acoustics*, 18(2), pp.3-3.
- Racic, V. and Brownjohn, J.M.W., 2011. Stochastic model of near-periodic vertical loads due to humans walking. *Advanced Engineering Informatics*, 25(2), pp.259-275.
- Racic, V., Pavic, A. and Brownjohn, J.M.W., 2009. Experimental identification and analytical modelling of human walking forces: Literature review. *Journal of Sound and Vibration*, 326(1-2), pp.1-49.
- Rainer, J.H., Pernica, G. and Allen, D.E., 1988. Dynamic loading and response of footbridges. *Canadian Journal of Civil Engineering*, 15(1), pp.66-71.

- Reyes, J.C., Riaño, A.C., Kalkan, E. and Arango, C.M., 2015. Extending modal pushover-based scaling procedure for nonlinear response history analysis of multi-story unsymmetric-plan buildings. *Engineering Structures*, 88, pp.125-137.
- Reynolds, P. and Pavic, A., 2003. Effects of false floors on vibration serviceability of building floors. II: Response to pedestrian excitation. *Journal of performance of constructed facilities*, 17(2), pp.87-96.
- Reynolds, P., 2000. The effects of raised access flooring on the vibrational performance of long-span concrete floors (Doctoral dissertation, University of Sheffield).
- Schirén, W. and Swahn, T., 2019. Vibrations in residential timber floors: A comparison between the current and the revised Eurocode 5.
- Sehgal, S. and Kumar, H., 2016. Structural dynamic model updating techniques: A state of the art review. *Archives of Computational Methods in Engineering*, 23, pp.515-533.
- Setragian, Z.B. and Chandra Kusuma, C., 2018. Moisture Safety Evaluation of CLT-Concrete Composite Slab.
- Siddika, A., Al Mamun, M.A., Aslani, F., Zhuge, Y., Alyousef, R. and Hajimohammadi, A., 2021. Cross-laminated timber–concrete composite structural floor system: A state-of-the-art review. *Engineering Failure Analysis*, 130, p.105766.
- Sikkema, R., Styles, D., Jonsson, R., Tobin, B. and Byrne, K.A., 2023. A market inventory of construction wood for residential building in Europe—in the light of the Green Deal and new circular economy ambitions. *Sustainable cities and society*, 90, p.104370.
- Singh, T., Arpanaei, A., Elustondo, D., Wang, Y., Stocchero, A., West, T.A. and Fu, Q., 2022. Emerging technologies for the development of wood products towards extended carbon storage and CO₂ capture. *Carbon Capture Science & Technology*, 4, p.100057.
- Smith, A.L., Hicks, S.J. and Devine, P.J., 2009. *Design of floors for vibration: A new approach*. Ascot, Berkshire, UK: Steel Construction Institute.
- Smith, I., and Chui, Y.H., 1988. Design of lightweight wooden floors to avoid human discomfort. *Canadian Journal of Civil Engineering*, 15(2), pp.254-262.
- Thelandersson, S. and Larsen, H.J. eds., 2003. *Timber engineering*. John Wiley & Sons.
- Toratti, T. and Talja, A., 2006. Classification of human induced floor vibrations. *Building acoustics*, 13(3), pp.211-221.
- Ussher, E., Arjomandi, K., Weckendorf, J. and Smith, I., 2017, August. Prediction of motion responses of cross-laminated-timber slabs. In *Structures* (Vol. 11, pp. 49-61). Elsevier.
- Ussher, E., Sadeghi, M., Weckendorf, J. and Smith, I., 2014, August. Vibration serviceability design analysis of cross-laminated-timber floor systems. In *World Conference on Timber Engineering*.
- Weckendorf, J., 2009. *Dynamic response of structural timber flooring systems* (Doctoral dissertation, Edinburgh Napier University).

Weckendorf, J., Toratti, T., Smith, I. and Tannert, T., 2016. Vibration serviceability performance of timber floors. *European Journal of Wood and Wood Products*, 74, pp.353-367.

Willford, M.R., Young, P. and CEng, M., 2006. A design guide for footfall induced vibration of structures. London, UK: Concrete Society for The Concrete Centre.

Yeoh, D., Fragiaco, M., De Franceschi, M. and Heng Boon, K., 2011. State of the art on timber-concrete composite structures: Literature review. *Journal of structural engineering*, 137(10), pp.1085-1095.

Young, P., 2001, October. Improved floor vibration prediction methodologies. In ARUP vibration seminar (Vol. 4).

Zhao, C., Zhou, J. and Liu, Y., 2023. Financial inclusion and low-carbon architectural design strategies: Solutions for architectural climate conditions and architectural temperature on new buildings. *Environmental Science and Pollution Research*, 30(32), pp.79497-79511.

Zhao, Q., Gao, W., Su, Y. and Wang, T., 2023. Carbon emissions trajectory and driving force from the construction industry with a city-scale: A case study of Hangzhou, China. *Sustainable Cities and Society*, 88, p.104283.

Zhou, X., Cao, L., Chen, Y.F., Liu, J. and Li, J., 2016. Acceleration response of prestressed cable RC truss floor system subjected to heel-drop loading. *Journal of Performance of Constructed Facilities*, 30(5), p.04016014.

Živanović, S., 2006. Probability-based estimation of vibration for pedestrian structures due to walking. (Doctoral dissertation, University of Sheffield).

Živanović, S., Pavić, A. and Reynolds, P., 2007. Probability-based prediction of multi-mode vibration response to walking excitation. *Engineering structures*, 29(6), pp.942-954.

Živanović, S., Pavić, A.L.E.K.S.A.N.D.A.R. and Reynolds, P., 2005. Vibration serviceability of footbridges under human-induced excitation: a literature review. *Journal of sound and vibration*, 279(1-2), pp.1-74.